DINOFLAGELLATE BLOOMS AND PHYSICAL SYSTEMS IN THE GULF OF MAINE

by

Peter John Selwyn Franks

B.Sc. Queen's University (1981)
M.Sc. Dalhousie University (1984)

SUBMITTED IN PARTIAL FULFILLMENT OF THE
REQUIREMENTS FOR THE DEGREE OF

DOCTOR OF PHILOSOPHY

at the

MASSACHUSETTS INSTITUTE OF TECHNOLOGY

and the

WOODS HOLE OCEANOGRAPHIC INSTITUTION

May 1990

Signature of Author _____
Joint Program in Oceanography,
Massachusetts Institute of Technology/
Woods Hole Oceanographic Institution

Certified by _____
Donald M. Anderson
Thesis Supervisor

Accepted by _____
John Stegeman
Chairman, Joint Committee for Biological Oceanography
Massachusetts Institute of Technology/
Woods Hole Oceanographic Institution

DINOFLAGELLATE BLOOMS AND PHYSICAL SYSTEMS
IN THE GULF OF MAINE

by

PETER JOHN SELWYN FRANKS

submitted in partial fulfillment of the requirements for the degree of
Doctor of Philosophy

ABSTRACT

Numerous studies have shown dinoflagellate blooms to be closely related to density discontinuities and fronts in the ocean. The spatial and temporal patterns of the dinoflagellate population depend on the predominant mode of physical forcing, and its scales of variability. The present study combined field sampling of hydrographic and biological variables to examine the relationship of dinoflagellate population distributions to physical factors along the southwestern cost of the Gulf of Maine.

A bloom of *Ceratium longipes* occurred along this coast during the month of June, 1987. A simple model which coupled along-isopycnal diffusion with the logistic growth equation suggested that the cells had a growth rate of about 0.1 d^{-1}, and had reached a steady horizontal across-shelf distribution within about 10 d. Further variations in population density appeared to be related to fluctuations of light with periods of ~10 d. To our knowledge, this was the first use of this simple diffusion model as a diagnostic tool for quantifying parameters describing the growth and movement of a specific phytoplankton population.

Blooms of the toxic dinoflagellate, *Alexandrium tamarense* have been nearly annual features along the coasts of southern Maine, New Hampshire and Massachusetts since 1972; however the mechanisms controlling the distribution of cells and concomitant shellfish toxicity are relatively poorly understood. Analysis of field data gathered from April to September, 1987-1989, showed that in two years when toxicity was detected in the southern part of this region, *A. tamarense* cells were apparently transported into the study area between Portsmouth and Cape Ann, Massachusetts, in a coastally trapped buoyant plume. This plume appears to have been formed off Maine by the outflow from the Androscoggin and

Kennebec Rivers. Flow rates of these rivers, hydrographic sections, and satellite images suggest that the plume had a duration of about a month, and extended alongshore for several hundred kilometers. The distribution of cells followed the position of the plume as it was influenced by wind and topography. Thus when winds were downwelling-favourable, cells were moved alongshore to the south, and were held to the coast; when winds were upwelling-favourable, the plume sometimes separated from the coast, advecting the cells offshore.

The alongshore advection of toxic cells within a coastally trapped buoyant plume can explain the temporal and spatial patterns of shellfish toxicity along the coast. The general observation of a north-to-south temporal trend of toxicity is consistent with the southward advection of the plume. In 1987 when no plume was present, *Alexandrium tamarense* cells were scarce, and no toxicity was recorded at the southern stations. A hypothesis was formulated explaining the development and spread of toxic dinoflagellate blooms in this region. This plume-advection hypothesis included: source *A. tamarense* populations in the north, possibly associated with the Androscoggin and Kennebec estuaries; a relationship between toxicity patterns and river flow volume and timing of flow peaks; and a relationship between wind stresses and the distribution of low salinity water and cells.

Predictions of the plume-advection hypothesis were tested with historical records of shellfish toxicity, wind speed and direction, and river flow. The predictions tested included the north-south progression of toxic outbreaks, the occurrence of a peak in river flow prior to the PSP events, the relationship of transit time of PSP toxicity along the coast with river flow volume, and the influence of surface wind stress on the timing and location of shellfish toxicity. All the predictions tested were supported by the historical records. In addition it was found that the plume-advection hypothesis explains many details of the timing and spread of shellfish toxicity, including the sporadic nature of toxic outbreaks south of Massachusetts Bay, and the apparently rare occurrence of toxicity well offshore on Nantucket Shoals and Georges Bank.

Thesis Supervisor: Donald M. Anderson, WHOI

This thesis is dedicated
to
my wonderful brother

Timothy Christian Selwyn Franks

TABLE OF CONTENTS

ACKNOWLEDGEMENTS

During my stay in Woods Hole, I have had the help and encouragement of so many people, it is difficult to know where to start. And even when I have finished, I know I will have forgotten some whose names deserve to be here; to you I offer my apologies and implicit thanks.

Of the multitude of wonderful people with whom I have shared my time in Woods Hole, Adria Elskus and Noellette Conway deserve special mention. These two women helped create some of my brightest and best memories of Woods Hole. They kept me sane, happy, drunk, well-fed, tired, physically fit and otherwise normal, although perhaps not all at the same time. Thank you both.

I must also thank Chris Scholin, who designed a rigorous program to help me keep my sea legs during the summer, Hagen Schempf whose warm heart and Teutonic humour kept us all actually quite amused, and Laela Sayigh and Alex Bocconcelli for their wonderful parties, food, and G 'n' T's. Mary Athanis was a ray of sunshine in a potentially dreary existence. Merryl Alber was a comfortable presence during times of stress and indecision. Abbie Jackson ensured that all my visits to the Education Office were cheery as well as productive, and the warmth and hospitality of Jake and Anna Maria Peirson will never be forgotten. A special thanks to the Frickes; Rob, Marianne, Emma and Jacob, whose art decorated my office, and whose leftovers decorated my stomach.

To my advisor, Don Anderson, I owe a great deal of thanks for guidance, advice, and example during a formative and maturing time of my scientific career. My committee members Ken Brink, Wendell Brown, John Cullen, Cabell Davis and Glenn Flierl deserve medals for sitting through my marathon meetings, and for being some of the few people who will actually read this whole document. Dan Kelley was, as always, an inspiration. Thank you all for your time, criticisms, ideas and insights during the course of this work.

I cannot thank Bruce Keafer enough for his help during the field seasons. The quiet competence and good humour of Paul Pelletier, captain of the R/V Jere A. Chase, made the cruises enjoyable and instructive. Thanks also to Mike Goodridge, captain of the C/V Unity, for bearing with our bizarre scheduling procedure. Special thanks to Wendell Brown's group at UNH: Jim Irish, Karen

Garrison, Jon Woods, and the amazing supply of volunteers who helped during the field seasons.

John Hurst and Sally Sherman-Caswell of the Maine Department of Marine Resources, and Mike Hickey and Frank Germano of the Massachusetts Department of Marine Fisheries were very generous with their time and data. Without their contribution this work would not have been complete. Thanks also to Dave McCartney and Gail Abend of the United States Geological Survey for making the river flow data available to me.

I would like to thank the other members of the Anderson lab: Dave Kulis, Cathy Cetta, John Kokinos and Greg Doucette, for their help, encouragement, companionship, and unfailing ability to be somewhere nearby when I had a new plot. My "Beds for Blondes" friends, Rebecca Schudlich, Susan Wijffels and Cecelie Mauritzen provided warm friendship and companionship. And thanks to Joe Adelstein and "Gas, Food and Lodging" who provided humour and great music for our parties. Diane Herbst entered some of the data found buried in this tome (not tomb), and Raffaella Casotti slaved with Adria to provide assistance in the final exhausting days of preparing this thesis. Thank you.

My parents, Ned and Daphne Franks, have always given me love, support and encouragement. I apologize for the irreversible "repairs" performed on certain household appliances (and parts of the household!) when I was younger, but look where it got me! Thank you for all you do to help me through endeavours such as theses, and life.

And now the important stuff: This research was supported by ONR contract N00014-87-K-0007 and ONR grant N00014-89-J-111 to Donald M. Anderson, and NOAA Office of Sea Grant contract NA86AA-D-SG090. Additional financial support during my stay in the WHOI/MIT Joint Program in Oceanography was made available through the Center for Analysis of Marine Systems, and the WHOI Education Office.

BIOGRAPHICAL NOTES

Peter J.S. Franks was born, to his surprise, in the Toronto General Hospital on May 26, 1959. Attempts at educating him spanned two continents and several decades. With the unique qualifications of being 5'6" tall, just over 118 lbs and freckled, Peter entered Queen's University, Kingston, from which he was graduated with a B.Sc. (hons) in 1981. Now weighing over 125 lbs, Peter put his experience in ornithology to good use and entered the Department of Oceanography at Dalhousie University, Halifax, in 1982. There he formulated a coupled physical/biological model of a warm-core ring under the tutelage of Dr. J.S. Wroblewski. He was graduated with an M.Sc. in September of 1984. After several hours holiday, he began his journey in the MIT/WHOI Joint Program in Oceanography. In 1986, he joined Dr. D.M. Anderson's lab, and began a study of the physical mediation of toxic phytoplankton blooms in the coastal Gulf of Maine. Weighing in, now, at about 128 lbs, Peter's interests lie in studying the modes of coupling of primary production and physical systems.

CHAPTER 1

INTRODUCTION

"Hallo!" said Piglet, "what are you *doing?"*

"Hunting," said Pooh.

"Hunting what?"

"Tracking something," said Winnie-the-Pooh very mysteriously.

"Tracking what?" said Piglet, coming closer.

"That's just what I ask myself. I ask myself, What?"

"What do you think you'll answer?"

"I shall have to wait until I catch up with it," said Winnie-the-Pooh.

A.A. Milne
Winnie-the-Pooh

One of the most spectacular manifestations of phytoplankton growth in the sea is the formation of "red tides". These unusually dense accumulations of single phytoplankton species can visibly discolour the water, and often cause widespread economic damage. In spite of the moniker, red tides are often not red, and are seldom associated with tides. In fact, identification of the physical processes which influence the development of red tides, and phytoplankton blooms in general, is a major field of study in oceanography.

Not all phytoplankton blooms result in red tides; indeed the concept of a "bloom" can be quite subjective. The term bloom is often reserved for conditions of high biomass, such as the spring bloom (Parker and Tett, 1987). Tett (1987) suggests that the term be used only when the chlorophyll concentrations exceed 10 mg m^{-3}, or when there is visible discolouration of the sea surface (a red tide). However, this definition excludes species which occur in relatively low numbers, but which may be ecologically or economically significant. The dinoflagellate *Alexandrium tamarense*[1] has been known to form red tides; however, in concentrations as low as 1,000 cells l^{-1}, populations of this organism have been responsible for widespread closures of shellfish beds along the coast of the Gulf of Maine (Chapter 4).

In the chapters which follow, studies which examined the factors controlling the distribution of two species of dinoflagellate are described. Neither of these dinoflagellate populations visibly coloured the water. One species, *Ceratium longipes*, is not known to be an economically important, or nuisance species. While the population of *C. longipes* described in Chapter 3 dominated the

---

[1] *Alexandrium tamarense* and *Alexandrium fundyense* were formerly included in the genera *Protogonyaulax* or *Gonyaulax* but are now accepted as *Alexandrium* (Steidinger and Moestrup, 1990). Both species bloom in the Gulf of Maine (Anderson, unpub. data), but since discrimination between them is impossible for large-scale field programs or when referring to shellfish toxicity, only the more familiar name *Alexandrium tamarense* will be used here.

phytoplankton community, it went unnoticed by the general public. The second species, *Alexandrium tamarense*, is a toxic dinoflagellate known to cause red tides, and is responsible for recurrent paralytic shellfish poisoning (PSP) outbreaks along the coast of the Gulf of Maine. The populations of *A. tamarense* described in Chapter 4 were often so sparse as to be noticeable under a microscope only to trained personnel, yet they caused widespread closures of shellfish beds, and considerable economic damage. Thus neither of these dinoflagellate blooms constituted a red tide; however, understanding of the factors controlling the distribution and abundance of these species can lead to a better understanding of the causes of red tides, and nuisance phytoplankton blooms in general.

Initiation and Regulation of Red Tides

The theories formulated to account for red tides generally fall into two groups, with a broad overlap: those which espouse a biological causation, and those which invoke physical mechanisms. Ingle and Martin (1971) advocated prediction of red tides by the iron index, i.e. the amount of iron introduced to the bloom area by river outflow. They felt that iron, or some chelating agent, was limiting dinoflagellate growth, except when delivered to the bloom area in large quantities. They also noted that the iron index may, in fact, be a measure of humic acid levels which have been shown to stimulate the growth of dinoflagellates (Prakash and Rashid, 1968). What they do not acknowledge, however, is that the iron index may indirectly measure water column stability: the iron is delivered with a fresh water outflow, creating a sharp pycnocline between the saline waters of the bloom area and the fresh waters containing the iron. As will be discussed below, this may be the more important factor in determining dinoflagellate blooms.

Provasoli (1979) has summarized the studies of the stimulatory and inhibitory effects of coexisting phytoplankton on dinoflagellate blooms. The stimulatory effects could arise through the complexing of toxic ions (e.g. Cu, Fe) by algal secretions, while

the inhibitory effects could arise through reduction of available nutrients, or complexing of necessary growth factors (e.g. vitamin B_{12}). Further evidence for this is given by Takahashi and Fukazawa (1982) who showed stimulation of red tide algal growth on the addition of Fe, Mn, and vitamin B_{12}. Provasoli (Ibid.) also suggests the possibility of dinoflagellate inhibition of phytoplankton which coexist with, or follow them in the seasonal succession.

In his discussion of the effects of coexisting phytoplankton, Provasoli (1979) notes the possibility of blooms caused by dinoflagellates taking up limiting nutrients faster than competitors. MacIsaac (1978) and MacIsaac et al. (1979) used the stable isotope ^{15}N to examine this possibility with *Gonyaulax polyedra* and *G. excavata*, and found no evidence that the light- or nutrient-controlled uptake of nitrate and ammonium was any different than that measured in diatoms or other dinoflagellates. However, the ^{15}N technique requires addition of relatively large amounts of tracer, so that *in situ* uptake rates were not accurately measured.

Wyatt and Horwood (1973), Holligan et al. (1984a), and Kishi and Ikeda (1986) have suggested that a reduction in grazing pressure can allow dinoflagellates to bloom. Wyatt and Horwood (1973) show that if the dinoflagellates were concentrated in a narrow band due to migration to the pycnocline, and the grazing pressure were distributed evenly over the water column, the loss due to grazing would be low enough to allow a bloom. This mechanism invokes the ability of the dinoflagellates to maintain a particular depth in the water column, yet does not credit the zooplankton with the ability to adjust to this. Kishi and Ikeda (1986) indicate that a bloom could occur if the zooplankton and the dinoflagellates had vertical migration patterns which were 180° out of phase. It is unlikely, however, that this situation would persist for the length of time necessary for bloom formation.

Rather than invoking a phase shift in the migration patterns of dinoflagellates and zooplankton, Holligan et al. (1984b) suggest an

inhibition of grazing through production of toxic substances. That this may occur has been demonstrated by Ives (1985), who showed a reduction of grazing by *Acartia hudsonica* and *Pseudocalanus* spp. on toxic forms of *Gonyaulax tamarensis*. This reduction in grazing was proportional to the toxicity of the clone offered as food. Huntley (1982) noted that *Calanus pacificus* did not graze on the dinoflagellate *Gymnodinium flavum* in a La Jolla Bay bloom, and concluded that this lack of grazing was an important factor in the persistence of the bloom.

The reduction of grazing pressure on dinoflagellates will not explain the extremely high concentrations of nutrients seen in blooms. If the dinoflagellates bloomed only because of a lack of grazing control, or because of stimulation by micronutrients, then the bloom would terminate when the concentration of nutrients (for instance nitrogen) in the cells equalled that of the parent water mass. However, it has been shown (Ketchum and Keen, 1948; Holligan, 1985) that the amount of phosphorus or nitrogen sequestered in a dinoflagellate bloom can be up to 10 times that which was originally in the water. Thus we must look for some mechanism whereby nutrients may be accumulated independent of the water motions.

The obvious candidate for this mechanism is the ability of dinoflagellates to swim. This may manifest itself as a vertical migration, or simply a maintenance of depth in the face of vertical currents. Slobodkin (1953) noted that the vertical migration of *Gonyaulax monilata* could account for the 10 fold increase of phosphorus in the bloom versus outside the bloom. He states that invoking "upwelling or other purely marine phenomena are superfluous assumptions" (pg. 153), and that the factor limiting the bloom is the rate of diffusion of the water mass containing the bloom. Ryther (1955) described several scenarios by which dinoflagellates maintaining their position at the water surface could accumulate passively at convergence zones set up by wind-driven coastal downwelling, frontal circulations, and Langmuir circulations,

causing a corresponding increase in particulate nutrients. Pomeroy et al. (1956) confirmed these ideas in a study of dinoflagellate blooms in Delaware Bay, where they found that the positive phototaxis of the cells allowed accumulation in the weak convergence zones. Additional supporting evidence has been supplied in the studies of Seliger et al. (1970; 1971; 1979) and Tyler and Seliger (1978).

Numerous studies have since noted the accumulation of dinoflagellates in Langmuir circulations, and theoretical treatments have elucidated the mechanisms by which this might occur (Stommel, 1949; Evans and Taylor, 1980; Watanabe and Harashima, 1986). As first noted by Stommel (Ibid), active swimming is not a necessity for accumulation in Langmuir cells; mere passive sinking will ensure retention at the convergence zone. Surprisingly, the retention of dinoflagellates at convergences created by tidal fronts has not been examined theoretically, although the idea is often included in conceptual models of bloom formation (Pomeroy et al., 1956; Wyatt, 1975; Carreto et al., 1986).

Margalef et al. (1979) and Holligan (1985) note that a common condition for the formation of red tides appears to be either well developed stratification or a water column stability that is commensurate with the swimming speed of the organisms. Margalef et al. (1979) suggested that red tides require the relatively rare combination of low turbulence and high nutrient concentrations. Any increase in turbulence leads to a dominance by diatoms. The conceptual models do not indicate the mechanism whereby dinoflagellate growth is suppressed relative to diatom growth in well-mixed isothermal waters. The effect of biotic factors in bloom formation is considered secondary to environmental factors. Carreto et al. (1986) inferred that the red tide in the Argentine Sea which they studied was limited by turbulence on the well-mixed side of the front, but no measurements of turbulence were made.

Eppley et al. (1968) suggested that downward migration of dinoflagellates at night into the nutrient-rich layers afforded them the opportunity of increased uptake of nitrate. MacIsaac (1978), and more recently Cullen et al. (1985) examined this hypothesis, and showed that dark uptake of nitrate by *Gonyaulax excavata* and *Heterocapsa niei* did occur, but mainly in nitrogen-starved cells and at a rate similar to that of diatoms. However, MacIsaac (Ibid.) noted that dark uptake coupled with vertical migration could account for the *persistence* of dinoflagellate blooms. Cullen and Horrigan (1981) found that the migratory behaviour of *Gymnodinium splendens* showed adaptations suitable for exploitation of a nutricline below a nutrient-poor layer. Thus carbohydrate was stored during the day while the cells were in the well-lit, nutrient-depleted surface waters, and was metabolized at night to support uptake of nitrate in the nitracline. Work on *Heterocapsa niei*, however, did not demonstrate the behaviour patterns necessary to coordinate nocturnal nitrate assimilation and diel vertical migration (Cullen et al., 1985). Rasmussen and Richardson (1989) examined *Alexandrium tamarense* in stratified artificial water columns and found complex behaviour dependent on the degree of stratification, light attenuation, and the nutrient regime. In particular, they found that low nutrient conditions caused the organism to lose its phototactic response and accumulate at the pycnocline. Paasche et al. (1984) studied seven different species of dinoflagellate representing three major orders (Gymnodiniales, Peridiniales, and Prorocentrales) in nutrient-sufficient batch cultures. They found that three of the species took up ammonium or nitrate equally well in the light or dark, while the other four had reduced uptake capacity in the dark. They did not examine the dinoflagellate behaviour in relation to the nutrient regime.

A common feature of many bloom-forming dinoflagellates is the ability to form resting cysts. This has been shown to be an important factor in the timing of estuarine bloom formation (Anderson and Wall, 1978; Anderson and Morel, 1979). In some coastal environments, the phytoplankton community contains

members of bloom-forming species throughout the year, the relative dominance of species changing continuously with the season and consequent physical dynamics. In harsher climates, the bloom-forming species often form an overwintering cyst, which can explain the absence of the species from the water during certain times, as well as its subsequent reappearance prior to blooms. In general, cyst populations influence the initiation, timing and location of some dinoflagellate blooms, however the growth and accumulation of the motile vegetative cells in response to physical and environmental factors determines the magnitude and duration of bloom events.

The theories regarding coastal dinoflagellate blooms, then, are
1) stimulation of dinoflagellate growth due to the addition of a micronutrient through physical processes or the growth of other phytoplankton;
2) inhibition of growth of other phytoplankton by secretion of toxic substances by dinoflagellates;
3) suppression of grazing pressure by a) vertical migrations or b) production of toxic substances;
4) diel vertical migration combined with dark uptake of nitrate in the nitracline;
5) accumulation in convergence zones due to diel vertical migration, or positive phototaxis;
6) stimulation of growth due to increased water column stability, combined with 3) and/or 4) and/or 5); and
7) initiation of blooms through benthic cyst germination.

Almost any combination of the above hypotheses may be found in the literature in descriptions of the dynamics of dinoflagellate blooms. That this is so is an indication of how poorly we understand the relative contributions of each process to the initiation, persistence, and decline of a bloom. This lack of understanding stems mainly from the difficulty in obtaining synoptic samples of a sufficient number of processes in a bloom, over a sufficiently long timescale. Seliger and Holligan (1985) have noted five criteria which are felt essential to a sampling program

directed at the understanding of dinoflagellate blooms. These are: i) determination of hydrographic features concurrently with biological samples, ii) on-line *in vivo* fluorescence for vertical and horizontal transects, combined with enumeration of dominant species, iii) two-dimensional measurements of nutrients, iv) remote sensing of sea surface temperatures, and v) flexibility in the timing of cruises. The studies described in the following chapters have incorporated these five criteria into a sampling program designed to elucidate the factors controlling the distribution and abundance of *Alexandrium tamarense* in the Gulf of Maine.

ALEXANDRIUM TAMARENSE IN THE GULF OF MAINE: A BRIEF HISTORY

The earliest reports of paralytic shellfish poisoning (PSP) in the Gulf of Maine are from the early 1800's (Medcof, 1960), from the shores of the Bay of Fundy. PSP poisonings in that area in 1936, and 1945 led to systematic testing of commercial mussels (*Mytilus edulis*) by the Canadian government (Medcof et al., 1947). A three-year study from 1943-1945 (Medcof et al., Ibid.) showed that the occurrence of PSP toxins in mussels and soft-shelled clams (*Mya arenaria*) was an annual event, with peak levels of toxicity during the months of August and September. It was not until the work of Needler (1949), however, that the connection was made between populations of the toxic dinoflagellate *Alexandrium tamarense*, and PSP outbreaks.

Until 1972, outbreaks of PSP in the Gulf of Maine were confined to the Bay of Fundy. In early September of 1972, however, Hurricane Carrie passed over the region from Massachusetts to New Brunswick, Canada, leaving up to 10 cm of rain, with 30 kt winds. During August, prior to the hurricane, Mulligan (1973) had recorded concentrations of *Alexandrium tamarense* of 1,000-2,000 cells l^{-1} in the area of Cape Ann, MA. By mid September, the cell concentrations were up to 100,000 cells l^{-1} in the same region, and severe PSP toxicity was recorded along the coast from Massachusetts to Canada. Since that episode, PSP outbreaks have been approximately annual

occurrences along the coasts of Massachusetts, New Hampshire and Maine.

Mulligan (1973, 1975) explained the occurrence of the 1972 outbreak through the interaction of local, offshore populations of *Alexandrium tamarense* with wind-driven upwelling systems. Mulligan (1975) cites his earlier work, summarizing, "Mulligan (1973) suggested that an upwelling which was noted on August 9 at Annisquam was perhaps the necessary additional ingredient for the development of the red tide to the north of Cape Ann." Thus the passing of the hurricane was not thought to be a causative factor for the PSP outbreak, except in delivering nutrients to the coastal waters via runoff from the land. The offshore flux of freshwater also caused onshore movement of *A. tamarense*-containing waters, which led to development of the bloom in the estuaries. The unusual event in this scenario was not the winds of the hurricane, but the earlier upwelling-favourable winds during an unusually dry August, followed by a heavy rainfall.

The first suggestion that the 1972 bloom may not have been caused by local populations, but by advection of an established population from an external source was given by Hartwell (1975), who speculated that the strong northeast winds associated with Hurricane Carrie forced a bloom from the waters of eastern Maine to the Cape Ann region to create a seed population. Contrary to Mulligan (1973, 1975), the unusual event leading to the first PSP outbreak in Hartwell's (1975) scenario was the occurrence of the hurricane over northeastern Maine during a bloom of *Alexandrium tamarense* in that region. Subsequent outbreaks of PSP in the fall were hypothesized to follow wind-driven upwelling events. The lack of a PSP outbreak in the fall of 1973 was thought to be due to the lack of upwelling-favourable winds at that time.

Seliger et al. (1979) reiterated the ideas of Mulligan (1973, 1975) and Hartwell (1975), suggesting that blooms of *Alexandrium tamarense* were caused by local populations responding to wind-

driven upwelling. The initial introduction of *A. tamarense* cells into the coastal embayments in 1972 was thought to have allowed seeding of the sediments with cysts, which germinated to cause subsequent blooms. Seliger et al. (Ibid.) suggested that since *A. tamarense* had not been a permanent or autochthonous resident of the embayments, and the combination of events which led to the 1972 bloom was relatively rare, then the toxicity would gradually decline from these areas. Unfortunately, this has been the case only in the far south of the region on Cape Cod.

Anderson et al. (1982) concur with the authors cited above, concluding that the *Alexandrium tamarense* populations were local, originating from cyst beds offshore, but close to the Cape Ann region. In addition, they suggested that the general trend of PSP outbreaks was from south to north for a given year. The occurrence of PSP toxicity between Cape Ann and Cape Cod was thought to be due to advection of cells from Cape Ann or offshore, but not from local populations since no cysts were found in the estuaries of this region. They note that toxicity to the south of Cape Ann occurred about one week after it was detected at Cape Ann.

Martin and Main (1981) performed one of the first detailed studies of the spatial and temporal distribution of *Alexandrium tamarense* in the embayments to the north of Cape Ann. Their work, performed almost a decade after the initial PSP outbreak at Cape Ann, led to the conclusion "that the toxic dinoflagellate *Gonyaulax tamarensis* [=*Alexandrium tamarense*] moved into Massachusetts coastal waters as a direct result of the southward movement of prevailing currents... It is, further, our opinion that earlier reports of minimal increases in shellfish toxicity observed in Gloucester and Essex and our own observation of *G. tamarensis v. excavata* in Ipswich Bay as early as March represent totally independent occurrences and cannot have been precursors for the [toxicity outbreaks] in late June and early July of [1981]." Thus they make a clear distinction between local populations of *Alexandrium tamarense* and the exogenous populations which caused the

widespread toxicity outbreaks. The southward advection of an established population alongshore could explain the observation of Anderson et al. (1982) that toxicity in shellfish showed a one week lag from Cape Ann to coast south of Boston. Martin and Main (Ibid.) do not, however, go so far as to identify the vehicle which advected the cells alongshore from the north.

There are numerous mechanisms which could generate currents along the coast of the Gulf of Maine. Graham (1970) and Yentsch and Garfield (1981), suggest that the western coast is strongly affected by winds which tend to drive surface waters along- or offshore, and bottom waters onshore. Butman (1976), Graham (1970) and Sigaev (1977) indicate that freshwater runoff may strongly affect the stability and circulation of nearshore waters. Loder and Greenberg (1986) predicted extensive coastal tidal fronts, including a band of well-mixed water along the western coast at depths less than 27m. Each of these mechanisms could create a frontal zone at which cells could accumulate, while the currents set up by the balance of forces could cause alongshore or onshore advection of populations.

The studies described in the following chapters were designed to elucidate the physical mechanisms which influence dinoflagellate distribution and abundance in the Gulf of Maine. One of the main hypotheses which resulted from this work is the "plume-advection hypothesis". This hypothesis, which is formulated in Chapter 4 and tested in Chapter 5, states that the spring PSP outbreaks along the coasts of Maine, New Hampshire, and Massachusetts, result from alongshore advection of established populations of *Alexandrium tamarense* in a coastally trapped buoyant plume. The plume forms through the discharge of the Androscoggin and Kennebec Rivers in southwestern Maine in response to rainfall, and flows southwestward along the coast at a rate determined by the flow volume and the prevailing winds. It is demonstrated that advection of an established population of *A. tamarense* in a buoyant plume can

explain many of the details of the spatial and temporal distribution of PSP outbreaks.

In 1960, J.C. Medcof, who was then the head of the Molluscan Shellfish Investigations of the Fisheries Research Board of Canada, wrote,

> "If we could discover (1) the conditions which permit the development and maintenance of a population of [*Alexandrium tamarense*] and (2) the conditions which determine the density of that population, once it establishes itself, then we would have everything we have been looking for as a basis for a long-range forecasting system.
>
> I think there is a reasonable chance of discovering these. Furthermore, I think it would be cheaper, in the long run, to monitor these conditions and do the necessary forecasting than to maintain our present complex [shellfish monitoring] system that may break down sometime in the next 25 years when we need it most."

It is ironic that 30 years after Medcof published that quote, we still rely on the state-run shellfish monitoring program to protect us from PSP poisoning (e.g. Shumway et al., 1988), and have no prospects for any long-range forecasting of toxic outbreaks. The plume-advection hypothesis described in Chapters 4 and 5 gives us a testable model for bloom occurrence. However, it also indicates that the timing of bloom initiation along the coast is strongly dependent on the rain and wind, which can be forecasted only insofar as we can predict the weather. Thus, in spite of Medcof's optimistic tone, it is likely that the best means of protecting the public from toxic shellfish are the current state-run shellfish monitoring programs.

LITERATURE CITED

Anderson, D.M., D. Kulis, J. Orphanos and A. Cuervels. 1982. Distribution of the toxic dinoflagellate *Gonyaulax tamarensis* in the southern New England region. Estuar. Coastal Mar. Sci. 14:447-458.

Anderson, D.M. and F. Morel. 1979. The seeding of two red tide blooms by the germination of benthic *Gonyaulax tamarensis* hypnocysts. Estuar. Coastal Mar. Sci. 8:279-293.

Anderson, D.M. and D. Wall. 1978. Potential importance of benthic cysts of *Gonyaulax tamarensis* and *G. excavata* in intiating toxic dinoflagellate blooms. J. Phycol. 14:224-234.

Butman, B. 1976. Hydrography and low-frequency currents associated with the spring runoff in Massachusetts Bay. Mem. Soc. R. Sci. Liege 6(X):247-275.

Carreto, J., H. Benavides, R. Negri and P. Glorioso. 1986. Toxic red-tide in the Argentine Sea. Phytoplankton distribution and survival of the toxic dinoflagellate *Gonyaulax excavata* in a frontal area. J. Plankton Res. 8:15-28.

Cullen, J.J. and S.G. Horrigan. 1981. Effects of nitrate on the diurnal vertical migration, carbon to nitrogen ratio, and the photosynthetic capacity of the dinoflagellate *Gymnodinium splendens*. Mar. Biol. 62:81-89.

Cullen, J.J., M. Zhu, R.F. Davis and D.C. Pierson. 1985. Vertical migration, carbohydrate synthesis, and nocturna; nitrate uptake during growth of *Heterocapsa niei* in a laboratory water column. In, "Toxic Dinoflagellates", D.M. Anderson, A.W. White and D.G. Baden (eds). Elsevier. 189-194.

Eppley, R.W., O. Holm-Hansen, and J.D.H. Strickland. 1968. Some observations on the vertical migration of dinoflagellates. J. Phycol. 4:333-340.

Evans, G.T. and F. Taylor. 1980. Phytoplankton accumulation in Langmuir cells. Limnol. Oceanogr. 25:840-845.

Graham, J.J. 1970. Coastal currents of the western Gulf of Maine, ICNAF Res. Bull 7:19-31.

Hartwell, A.D. 1975. Hydrographic factors affecting the distribution and movement of toxic dinoflagellates in the western Gulf of Maine. In, "Proceedings of the First International Conference on Toxic Dinoflagellate Blooms", V.R. LoCicero (ed.) Massachusetts Science and Technology Foundation, Wakefield, MA. 47-68.

Holligan, P.M. 1985. Marine dinoflagellate blooms - growth strategies and environmental exploitation. In, "Toxic Dinoflagellates", D.M. Anderson, A.W. White and D.G. Baden (eds). Elsevier. 133-140.

Holligan, P.M., W.M. Balch and C.M. Yentsch.1984a. The significance of subsurface chlorophyll, nitrite and ammonium maxima in relation to nitrogen for phytoplankton growth in stratified waters of the Gulf of Maine. J. Mar. Res. 42:1051-1073.

Holligan, P.M., P. LeB. Williams, D. Purdee and R. Harris. 1984b. Photosynthesis, respiration and nitrogen supply of plankton populations in stratified, frontal and tidally mixed shelf waters. Mar. Ecol. Prog. Ser. 17:201-213.

Huntley, M. 1982. Yellow water in La Jolla Bay, California, July 1980. II. Suppression of zooplankton grazing. J. Exp. Mar. Biol. Ecol. 63:81-91.

Ingle, R.M. and D.F. Martin. 1971. Prediction of the Florida red tide by means of the iron index. Env. Lett. 1:69-74.

Ives, J.D. 1985. The relationship between *Gonyaulax tamarensis* cell toxin levels and copepod ingestion rates. In, "Toxic Dinoflagellates", D.M. Anderson, A.W. White and D.G. Baden (eds). Elsevier. pp413-418.

Ketchum, B.H. and J. Keen. 1948. Unusual phosphorus concentrations in the Florida "red tide" seawater. J. Mar. Res. 7:17-21.

Kishi, M. and S. Ikeda. 1986. Population dynamics of 'red tide' organisms in eutrophicated coastal waters - numerical

experiment of phytoplankton bloom in the East Seto Inland Sea, Japan. Ecol. Modelling 31:145-174.

Loder, J.W. and D.A. Greenberg. 1986. Predicted positions of tidal fronts in the Gulf of Maine region. Cont. Shelf Res. 6:397-414.

MacIsaac, J.J. 1978. Diel cycles of inorganic nitrogen uptake in a natural phytoplankton population dominated by *Gonyaulax polyedra*. Limnol. Oceanogr. 23:1-9.

MacIsaac, J.J., G.S. Grunseich, H.E. Glover and C.M. Yentsch. 1979. Light and nutrient limitation in *Gonyaulax excavata* : nitrogen and carbon trace results. In, "Toxic Dinoflagellate Blooms", D.L. Taylor, H.H. Seliger C.M. Lewis (eds.). Elsevier, Amsterdam. 107-110.

Margalef, R., M. Estrada and D. Blasco. 1979. Functional morphology of organisms involved in red tides, as adapted to decaying turbulence. In, "Toxic Dinoflagellate Blooms", Taylor, Seliger (eds.). Elsevier, Amsterdam. 89-94.

Martin, C. and J.M. Main. 1981. Toxic dinoflagellate blooms (red tides) and shellfish resources in Plum Island Sound and adjacent Massachusetts waters. Final report to the Town of Ipswich, MA, under UMass/Amherst OGCA Contract No. 80A613.

Medcof, J.C. 1960. Shellfish poisoning - another North American ghost. Canad. M.A.J. 82:87-90.

Medcof, J.C., A.H. Leim, A.B. Needler, A.W.H. Needler, J. Gibbard and J. Naubert. 1947. Paralytic shellfish poisoning on the Canadian Atlantic coast. Bull. Fish. Res. Bd. Can. 75:1-32.

Mulligan, H. 1973. Probable causes for the 1972 red tide in the Cape Ann region of the Gulf of Maine. J. Fish. Res. Bd. Can. 30:1363-1366.

Mulligan, H. 1975. Oceanographic factors associated with New England red tide blooms. In, "Proceedings of the First International Conference on Toxic Dinoflagellate Blooms", V.R. LoCicero (ed.) Massachusetts Science and Technology Foundation, Wakefield, MA. 23-40.

Needler, A.B. 1949. Paralytic shellfish poisoning and *Gonyaulax tamarensis*. J. Fish. Res. Bd. Can. 24:1589-1606.

Paasche, E., I. Bryceson and Karl Tangen. 1984. Interspecific variation in dark nitrogen uptake by dinoflagellates. J. Phycol. 20:394-401.

Parker, M. and P. Tett. 1987. Special meeting on the causes, dynamics, and effects of exceptional marine blooms and related events. Rapp. P.-v. Réun. Cons. int. Explor. Mer 187:5-8.

Pomeroy, L, H. Haskin and R. Ragotzkie. 1956. Observations on dinoflagellate blooms. Limnol. Oceanogr. 1:54-60.

Prakash, A. and M.A. Rashid. 1968. Influence of humic substances on the growth of marine phytoplankton: dinoflagellates. Limnol. Oceanogr. 13:598-606.

Provasoli, L. 1979. Recent progress, an overview. In, "Toxic Dinoflagellate Blooms", D.L. Taylor, H.H. Seliger C.M. Lewis (eds.). Elsevier, Amsterdam. 1-14.

Rasmussen, J. and K. Richardson. 1989. Response of *Gonyaulax tamarensis* to the presence of a pycnocline in an artificial water column. J. Plankton Res. 11:747-762.

Ryther, J.H. 1955. Ecology of autotrophic marine dinoflagellates with reference to red water conditions. In,"The Luminescence of Biological Systems", F.H. Johnson (ed.). A.A.A.S., Washington. 387-413.

Seliger, H.H., J.H. Carpenter, M. Loftus and W.D. McElroy. 1970. Mechanisms for the accumulation of high concentrations of dinoflagellates in a bioluminescent bay. Limnol. Oceanogr. 15:234-245.

Seliger, H.H., J.H. Carpenter, M. Loftus and W.D. McElroy. 1971. Bioluminescence and phytoplankton successions in Bahia Fosforescente, Puerto Rico. Limnol. Oceanogr. 16:608-622.

Seliger, H. and P.M. Holligan. 1985. Sampling criteria in natural phytoplankton populations. In, "Toxic Dinoflagellates", D.M. Anderson, A. White and D. Baden (eds.). Elsevier, New York. Pg 240.

Seliger, H.H., M.A. Tyler and K.R. McKinley. 1979. Phytoplankton distributions and red tides resulting from frontal circulation patterns. In, "Toxic Dinoflagellate Blooms", D.L. Taylor, H.H. Seliger C.M. Lewis (eds.). Elsevier, Amsterdam. 239-248.

Shumway, S., S. Sherman-Caswell and J.W. Hurst. 1988. Paralytic shellfish poisoning in Maine: monitoring a monster. J. Shellfish Res. 7:643-652.

Sigaev, I.K. 1977. Intra-year variability of geostrophic circulation on the continental shelf off New England and Nova Scotia.

Slobodkin, L.B. 1953. A possible initial condition for red tides on the coast of Florida. J. Mar. Res. 12:148-155.

Steidinger, K.A. and Ø. Moestrup. 1990. The taxonomy of *Gonyaulax, Pyrodinium, Alexandrium, Gessnerium, Protogonyaulax* and *Goniiodoma*. In, "Toxic Marine Phytoplankton", E. Graneli, B. Sundstrom, L. Edler and D. Anderson (eds.) Elsevier, New York. 522-523.

Stommel, H. 1949. Trajectories of small bodies sinking slowly through convection cells. J. Mar. Res. 8:25-29.

Takahashi, M. and N. Fukazawa. 1982. A mechanism of "red tide" formation. II. Effect of selective nutrient stimulation on the growth of different phytoplankton species in natural water. Mar. Biol. 70:267-273.

Tett, P. 1987. The ecophysiology of exceptional blooms. Rapp. P.-v. Réun. Cons. int. Explor. Mer 187:47-60.

Tyler, M.A. and H.H. Seliger. 1978. Annual subsurface transport of a red tide dinoflagellate to its bloom area: water circulation patterns and organism distributions in the Chesapeake Bay. Limnol. Oceanogr. 23:227-246.

Watanabe, M. and A. Harashima. 1986. Interaction between motile phytoplankton and Langmuir circulation. Ecol. Modelling 31:175-183.

Wyatt, T. 1975. The limitations of physical models for red tides. In, "Proceedings of the First International Conference on Toxic Dinoflagellate Blooms", V.R. LoCicero (ed.). Mass. Sci. Tech. Found. Wakefield, MA. 81-94.

Wyatt, T. and J. Horwood. 1973. Model which generates red tides. Nature 244:238-240.

Yentsch, C.S. and N. Garfield. 1981. Principal areas of vertical mixing in the waters of the Gulf of Maine, with references to the total productivity of the area. In, "Oceanography from Space", J.F.N. Gower (ed.). Plenum Press. NY. 303-312.

CHAPTER 2

DINOFLAGELLATE BLOOMS AT FRONTS: PATTERNS, SCALES AND FORCING MECHANISMS

"I saw one once," said Piglet. "At least, I think I did," he said. "Only perhaps it wasn't."

"So did I," said Pooh, wondering what a Heffalump was like.

"You don't often see them," said Christopher Robin carelessly.

"Not now," said Piglet.

"Not at this time of year," said Pooh.

A.A. Milne
Winnie-the-Pooh

ABSTRACT

Numerous studies have shown dinoflagellate blooms to be closely related to fronts in the ocean. The spatial and temporal patterns of the dinoflagellate population depend on the predominant mode of physical forcing, and its scales of variability. Four types of fronts were examined here: wind-driven upwelling, water mass/ buoyancy, tidal, and topographic. The phytoplankton pattern commonly found at each type of front is described. Finally, using published data, the scales of phytoplankton patchiness and the associated front are compared. It was found that there was no correlation between the scale of the front and the scale of its associated phytoplankton patch. This implies either that processes are acting to decorrelate the two fields, or that the forces mediating the enhanced production are not correlated with the length scale of the front. These possibilities are explored in some detail.

INTRODUCTION

Of the variety of forms of primary production in the ocean, perhaps the most spectacular is the formation of red tides. These massive blooms of single phytoplankton species have been seen the world over for centuries. Only now are we beginning to understand the mechanisms which cause and maintain red tides, but our knowledge is far from complete. However, one property which appears to be common to most, if not all, red tides is their association with water mass discontinuities such as pycnoclines or fronts.

Not all dinoflagellate populations at fronts reach red tide levels. Fronts are, however, typically the site of enhanced phytoplankton biomass. The present chapter will explore the associations of phytoplankton with fronts, looking first at the qualitative features of the phytoplankton patchiness, and then examining the causes of the enhanced production. This exploration will be done by comparing the length scales of phytoplankton patches to the length scales of their fronts. Before examining particular fronts in detail, however, the concepts of fronts and length scales will be introduced.

FRONTS

Fronts are regions of strong horizontal temperature and/or salinity contrast. They may occur in the atmosphere, lakes, rivers, and oceans. Here I will consider only a limited set of coastal oceanic fronts: wind-driven upwelling fronts, water mass or buoyancy fronts, tidally-generated fronts and topographically-formed fronts.

Figure 2-1 shows a typical density pattern for a front. The upward bending of the pycnocline separating the lighter surface

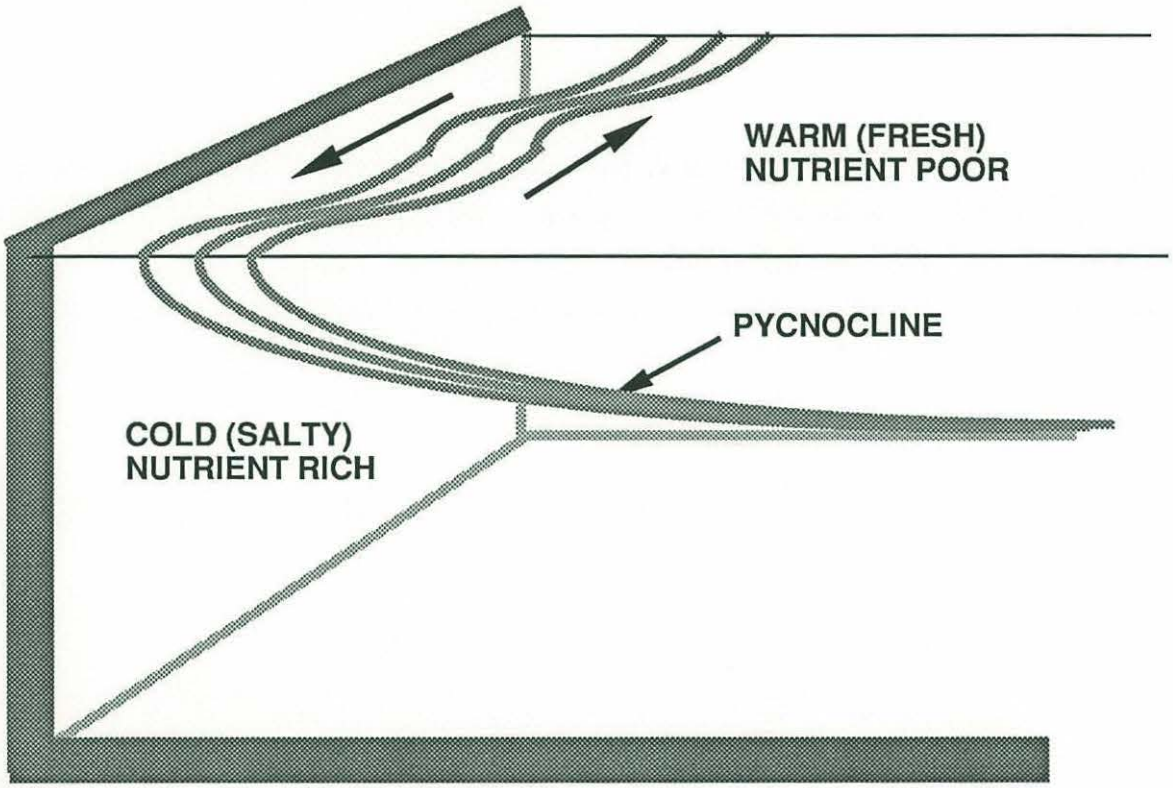

Figure 2-1. Typical density distribution at a front. The curved pycnocline forms the front, and is the region of strongest along-front shear.

water from the dense deep water creates the front. The front need not always break through to the surface; subsurface fronts are also frequently seen. The pycnocline may also bow downwards to intersect the bottom, creating a bottom front (Mooers *et al.*, 1978). In the present chapter, the width of the "frontal region" refers to the zone in which the pycnocline slopes upward or downward from the horizontal; the width of the "front" itself refers to the horizontal extent of the density contrast at the surface or bottom. Thus the frontal region will normally be wider than the front itself.

The balance of forces across the front (a strong pressure gradient vs. the Coriolis force) is associated with along-front jets, with the front being the zone of strongest shear. This jet can become unstable, forming cusps and eddies in the front (Pingree *et al.*, 1974; James, 1988). The strength of the along-front jets, and the general characteristics of the front depend on the mechanisms which cause and maintain the front. Thus fronts formed by a surface wind stress will have a different character from ones formed by tidally-induced mixing. However, certain generalities which can be made about fronts lead to insights into the mechanisms causing enhanced phytoplankton production there.

THE ROSSBY RADIUS

The present chapter examines the relationship of phytoplankton patches with a variety of different types of fronts. In order to make generalizations about these relationships, it would be useful to have a common basis with which to compare the different physical systems. The internal Rossby radius of deformation provides such a basis, giving the theoretical width scale of many kinds of frontal regions in the ocean.

When a front is formed, the pycnocline separating the two water masses becomes sloped, leading to a strong horizontal density contrast. The lighter water will always tend to flow over the more dense water to return the pycnocline to the horizontal. On a rotating

earth, however, this flow tendency becomes balanced by the Coriolis force, which causes the flow to turn to its right in the northern hemisphere. Thus, rather than relaxing to the horizontal, the pycnocline remains sloped. The curvature of this slope (and thus the width of the frontal region) depends on the density contrast of the two water masses, their thicknesses, and the strength of the Coriolis force (i.e. latitude). This length scale is given by the Rossby radius of deformation, and is shown in Figure 2-2.

If we consider two water masses of densities ρ and ρ', and thicknesses h and h', we can define two parameters: the "reduced gravity", and the "effective depth". With g the gravitational acceleration, the reduced gravity, g' (units of m s^{-2}), is given by:

$$g' = \frac{g(\rho'-\rho)}{\rho'} . \qquad (2\text{-}1)$$

This is the buoyancy of one water mass relative to the other. The effective depth, h_e, is defined as:

$$h_e = \frac{h h'}{h+h'} . \qquad (2\text{-}2)$$

With the reduced gravity, this equation allows the pycnocline in a two-layered system to be viewed as the free surface of a one-layered system, characterized by the effective depth, h_e. The baroclinic Rossby radius of deformation, R_{b1}, is a combination of these parameters:

$$R_{b1} = \frac{\sqrt{g' h_e}}{f} \qquad (2\text{-}3)$$

where f is the Coriolis frequency. This formulation of the Rossby radius is applicable to fronts which have a pycnocline that becomes horizontal at some distance from the front. However, some fronts extend from the surface to the bottom (see discussion of

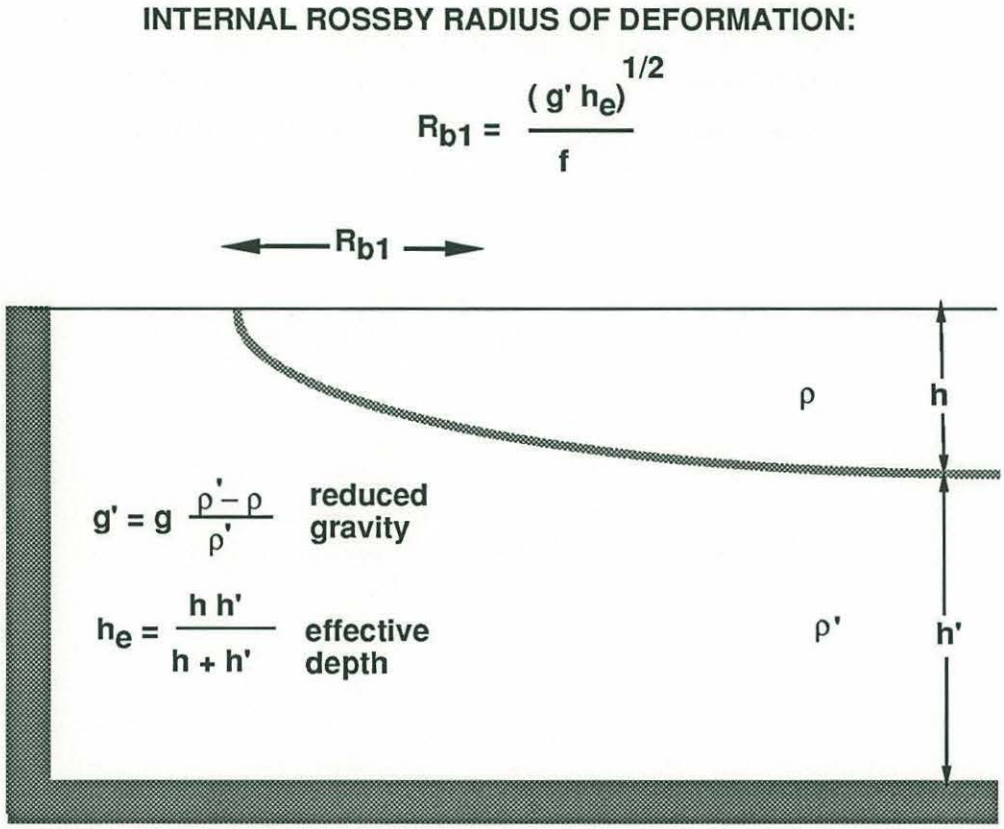

Figure 2-2. Calculation of the internal Rossby radius of deformation.

water mass/buoyancy fronts below), in which case another baroclinic Rossby radius of deformation, R_{b2}, is the appropriate length scale:

$$R_{b2} = \frac{\sqrt{g'(h+h')}}{f}. \qquad (2\text{-}4)$$

Notice that this formulation uses the total depth of the water column rather than the equivalent depth. The R_{b2} scale is often applicable to water mass fronts, particularly river plume fronts, as described below.

In many cases, the lower layer depth, h', is large relative to the surface layer thickness, h, so that $h_e \sim h$. In this instance it is convenient to calculate the Rossby radius from

$$R_b = \frac{\sqrt{g'h}}{f}. \qquad (2\text{-}5)$$

The Rossby radius scaling of the width of the frontal region is a useful theoretical tool for understanding the balance of forces at fronts. The Rossby radius of deformation gives the natural scale of pycnocline bending in the ocean. The assumptions inherent in its formulation, such as a sharp pycnocline, may render its application invalid. In more practical terms, it is often difficult to apply a calculated Rossby radius due to topography, external forces or mixing. Thus we must use some caution in applying a theoretically-calculated Rossby radius to a field situation.

QUALITATIVE ASPECTS

In this section four common types of fronts will be described: wind-driven upwelling fronts, water mass or buoyancy fronts, tidally-generated fronts and topographically-formed fronts. The

mechanisms of formation of each front will be outlined, and the typical Rossby radius given. Finally, the patterns of phytoplankton production which are commonly seen at these fronts will be described.

WIND-DRIVEN COASTAL UPWELLING

Fronts created by alongshore winds are common features along much of the world's most productive coastlines. These upwelling fronts have been intensively studied off the west coast of the United States (Mooers *et al.*, 1976; Halpern, 1976), the Northwest African coast (Barton *et al.*, 1977), and the South African coast (Shannon, 1985). A persistent upwelling system off the coast of Peru did not show an associated front (Brink *et al.*, 1983). Areas of persistent wind-driven coastal upwelling are some of the most productive oceanic zones; in particular, the upwelling region off Peru supported one of the most productive anchovy fisheries in the world (Rojas de Mendiola, 1981).

Wind-driven coastal upwelling (Figure 2-3) is generated by an alongshore wind stress at the water's surface. For a north-south oriented coastline on the east side of an ocean basin, an equatorward wind stress will generate upwelling, while a poleward wind stress generates downwelling. An upwelling-favourable wind stress creates an offshore Ekman flux within the surface layer. This offshore flux must be balanced by an onshore flow of deeper water, which causes the pycnocline to bend upwards near the coast. For particularly strong or persistent winds, the pycnocline may intersect the surface and move offshore, creating a strong surface thermal front (Csanady, 1982).

The hydrographic signature of a wind-driven upwelling front is usually seen most strongly in the temperature field. A relatively well-mixed region inshore is composed of cold, nutrient-rich waters of deep origin. A narrow region of strong horizontal thermal gradient (the front), separates the cold, well-mixed inshore waters

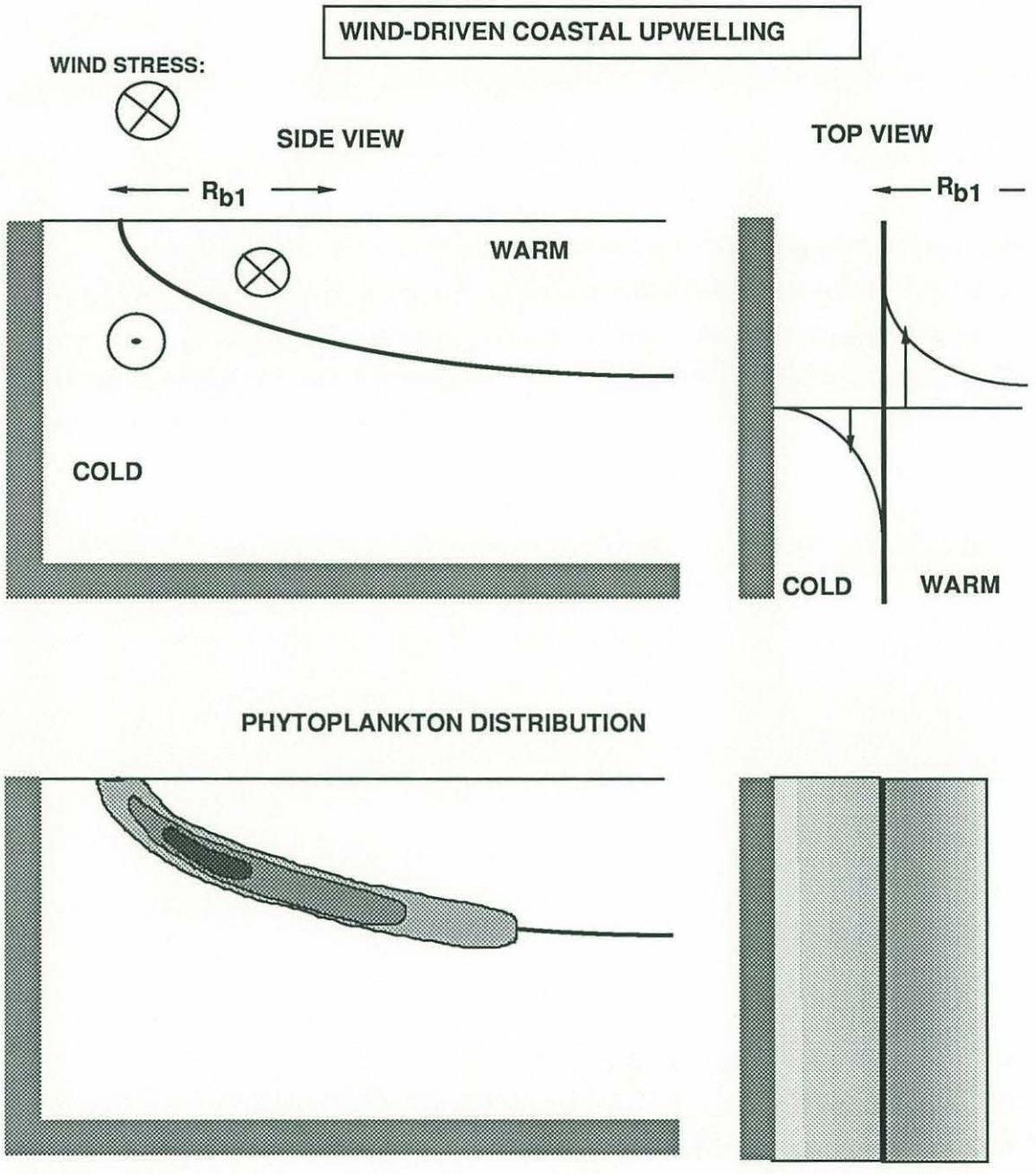

Figure 2-3. Upper panels show the hydrographic distributions at a wind-driven upwelling front. The lower panels indicate the distribution of chlorophyll commonly found at these fronts.

from the thermally-stratified offshore region (Brink, 1983; 1985). The salinity contrasts across the front are generally small, with temperature contributing the major part of the density difference.

The pycnocline which forms the front curves downward and offshore until it becomes horizontal. The length scale which governs this curvature is the baroclinic Rossby radius of deformation, R_b or R_{b1}. Typically the value of R_{b1} is on the order of ten kilometers, while in regions of steep bathymetry, the R_b scaling will be only approximately valid. It is also important to note that R_{b1} gives the scale of the curvature of the pycnocline, not the distance of the front from the shore (Brink, 1987).

A prominent chlorophyll maximum layer (measured as chlorophyll m^{-3}) is usually found just offshore of the front, within or slightly above the pycnocline (Jones and Halpern, 1981; Dengler, 1985; Traganza *et al.*, 1987). The chlorophyll concentrations decrease rapidly towards the nearshore side of the front, and more gradually towards the offshore (stratified) side. The peak of the distribution generally follows the pycnocline as it curves downward, leading to a marked subsurface band of chlorophyll within the curved pycnocline. Satellite images of surface chlorophyll distributions show strong surface signature in a banded structure oriented parallel to the isobaths (Abbott and Zion, 1985). This banding can extend for tens to hundreds of kilometers alongshore (Small and Menzies, 1981). Because of the curvature of the pycnocline, and the subsurface peak in chlorophyll, the surface signature does not always reflect the subsurface distribution of chlorophyll. This can create difficulties when trying to interpret satellite images of pigment concentration.

The phytoplankton species making up the chlorophyll maximum layer vary depending on location and time of year. Diatoms of the genera *Thalassiosira*, *Nitzschia* and *Chaetoceros* and dinoflagellates of the genera *Prorocentrum*, *Ceratium*, *Gyrodinium* and *Gymnodinium* have been found in upwelling areas (Rojas de

Mendiola, 1981; Blasco et al., 1981, Vincent et al., 1989). Dinoflagellates, in particular, have been found to reach red tide concentrations on occasion. A bloom of *Gymnodinium splendens* devastated the Peruvian fishery in 1976, when it reached concentrations of 2000 cells per ml (Rojas de Mendiola, 1979).

WATER MASS/ BUOYANCY FRONTS

Water mass, or buoyancy fronts (Figure 2-4) are created at the abutment of two dissimilar water masses. This may occur on a small scale at the mouth of an estuary (Garvine and Monk, 1974; Chao, 1987), or on a larger scale such as the Norwegian Current (Mork, 1981; Dundas *et al.*, 1989), or the shelf-slope front off eastern North America (Houghton and Marra, 1983). These fronts often run parallel to a coast due to the nature of the formation of the inshore water mass, but this is certainly not always the case. In the Skagerrak/ Kattegat areas, a strong water mass front was seen by Richardson (1985), the front being oriented perpendicular to the Danish coast.

The density contrast at a water mass front is often caused by a salinity difference between the two water masses. The lighter water mass will tend to flow over the heavier water mass, until the pressure gradient is balanced by the Coriolis force, creating an approximately geostrophic balance (Bowman and Iverson, 1978). Depending on the size and densities of the two water masses, and the bottom topography, the front may extend from the surface to the bottom, or from the surface to some equilibrium depth where the pycnocline becomes horizontal (Csanady, 1971). In either case, the pycnocline will slope downwards from the surface, away from the more dense water mass. Thus the front formed by estuarine outflow will always slope downwards toward the coast, unless the plume has separated from the coast.

The water mass/ buoyancy front will often have an ∫-shape in a vertical cross-section, due to the flow of light water over the

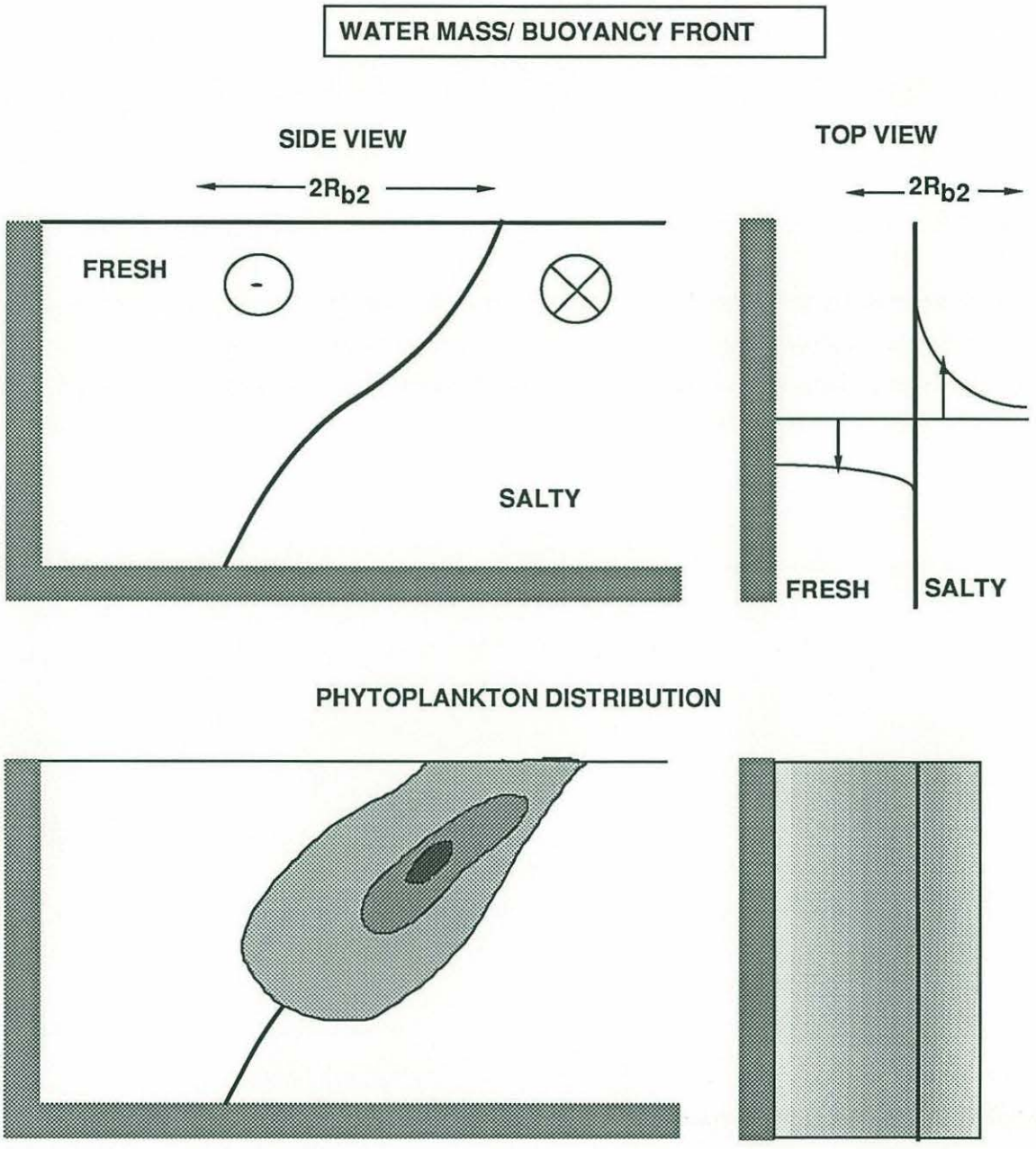

Figure 2-4. The hydrographic and dynamic signatures of water mass, or buoyancy fronts are shown in the upper panels. The distribution of chlorophyll at these fronts is shown in the lower panels.

deeper heavy water (Figure 2-4). The width of the front is usually scaled by the baroclinic Rossby radius of deformation, R_{b2}. The horizontal distance from the surface of the front to the intersection of the front with the bottom is roughly $2R_{b2}$. The width is usually a few kilometers, but may reach tens of kilometers in deep regions of high density contrast. The actual width of the frontal region is strongly influenced by the wind, which may increase it (flatten the front), or decrease it (steepen the front) (Csanady, 1971; 1978; Hsueh and Cushman-Roisin, 1983; Ou, 1984).

In general, the maximum chlorophyll value is found subsurface, within the front. The chlorophyll peak in vertical profiles is usually found in the pycnocline, giving a chlorophyll distribution which follows the isopycnals (Marra *et al.*, 1982; Richardson, 1985). This is not always the case, though, since water mass fronts vary considerably in the depth, and horizontal extent of the pycnocline. In regions where the pycnocline becomes deeper than the euphotic zone, and depending on the source of the density contrast, the peak chlorophyll values may be found within the lighter (less saline) water, rather than the front itself (e.g. Bowman and Iverson, 1979).

The distribution of dinoflagellates in water mass/buoyancy fronts is not always coincident with the chlorophyll distribution. In Chapter 4 a bloom of *Alexandrium tamarense* within a buoyancy front is described, while the chlorophyll peak, created by a bloom of the diatom *Eucampia*, was offshore of the front. However, Blasco (1977) found a bloom of *Gonyaulax polyedra* to correlate well with the chlorophyll field in the California Current. In this case the dinoflagellates composed up to 40% of the total phytoplankton numbers, whereas diatoms were only about 1%.

TIDAL FRONTS

Tidal fronts (Figure 2-5) are formed in shallow seas which have strong tidal currents and sloping bathymetry. Such areas are

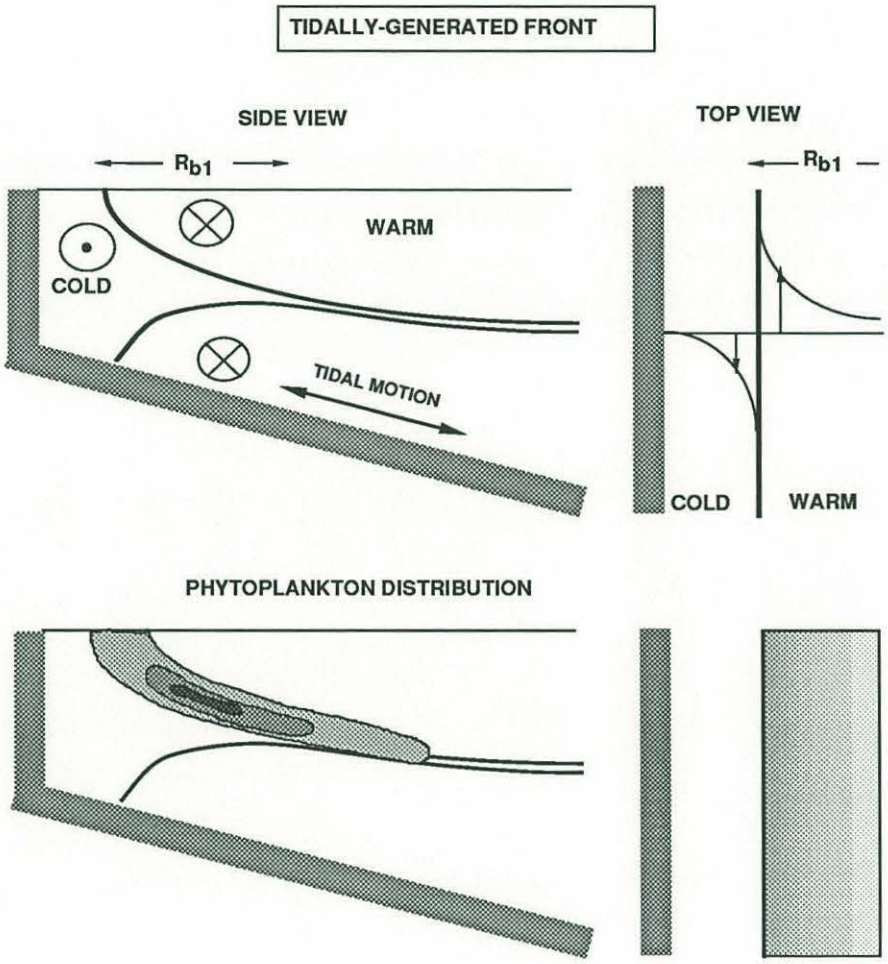

Figure 2-5. The hydrographic and dynamic signatures of tidally-generated fronts are shown in the upper panels. The distribution of chlorophyll at these front is shown below.

found around the British Isles (Pingree and Griffiths, 1978), the islands of Japan (Kishi and Ikeda, 1986), the northern areas of the Gulf of Maine (Yentsch and Garfield, 1981), and many other shallow seas. These fronts are often the site of intense dinoflagellate blooms.

The motion of water over the bottom generates turbulence, much the same way as a wind stress at the surface. Tidally-forced motions of the water are ubiquitous, although the local strength of the tidal currents is a function of basin shape and topography. In shallow waters, a sufficiently strong tidal current can generate turbulence that can mix the overlying waters. In deeper waters, the same turbulence may not mix high enough into the water column to affect the pycnocline. The region separating the well-mixed zone inshore from the stratified offshore waters is the tidal front.

The location of tidal fronts has been shown to be predictable through the H/u^3 criterion of Simpson and Hunter (1974). This criterion uses H, the depth of the water column, and u, the tidal velocity, to identify regions which should be either well mixed or stratified. A critical value of H/u^3 can often be found which will give the location of tidal fronts. This value varies geographically depending on local heat input, and wind stress (Garrett *et al.*, 1978; Loder and Greenberg, 1986). Heating will tend to move tidal fronts inshore, as it will oppose the mixing from below, while wind stress may move tidal fronts offshore by increasing the total turbulent kinetic energy, or inshore by advection due to downwelling.

The front created between the well-mixed inshore waters and the stratified offshore waters is usually seen most clearly in the temperature profiles. The mixing inshore creates an approximately isothermal water mass, giving a strong thermal contrast across the surface of a tidal front. The pycnocline generally surfaces, curving downwards and offshore; however, the lower part of the pycnocline may intersect the bottom if the inshore water mass has the same density as the water forming the pycnocline. The formation of this bifurcated pycnocline is dependent on the initial densities and

volumes of the two water masses (surface and deep) (van Heijst, 1986). The curvature of the pycnocline, i.e. the length scale of the front, is given by R_{b1}, the baroclinic Rossby radius of deformation. This length scale is usually less than 5 km, indicating a rather narrow frontal zone.

A marked chlorophyll maximum layer is often found within the pycnocline forming the tidal front (Holligan, 1981). The peak chlorophyll values are normally subsurface, slightly offshore of the front (i.e. on the stratified side) (Savidge, 1976; Pingree *et al.*, 1978; Simpson *et al.*, 1979; Holligan *et al.*, 1983). The chlorophyll contours follow the pycnocline, decreasing as the pycnocline becomes more horizontal. The inshore waters, although often nutrient rich, generally have a low concentration of phytoplankton due, perhaps, to light limitation caused by enhanced vertical mixing. Tidal fronts are often the site of intense dinoflagellate blooms (Pingree *et al.*, 1975; Holligan, 1981). Local concentrations of *Gyrodinium aureolum* reached 1.7×10^6 cells/l in tidal fronts around the British Isles, giving integrated chlorophyll concentrations 40 times higher than the surrounding waters (Pingree *et al.*, 1975). Simpson *et al.* (1979) found a ten-fold increase of *Peridinium trochoideum* within a tidal front compared to surrounding waters.

The phytoplankton community structure within tidal fronts is often predictable: the inshore waters are dominated by diatoms, the surface waters on the stratified side usually contain mainly small flagellates, while the front and pycnocline are the site of dinoflagellates and diatoms (Pingree *et al.*, 1978). This follows Margalef's (1978) description of the ontogeny of phytoplankton communities in response to physical forcings (see also Legendre *et al.*, 1986).

TOPOGRAPHIC FRONTS

Topographic fronts (Figure 2-6) are formed in the lee of stationary objects embedded in a flow. Thus they are found near

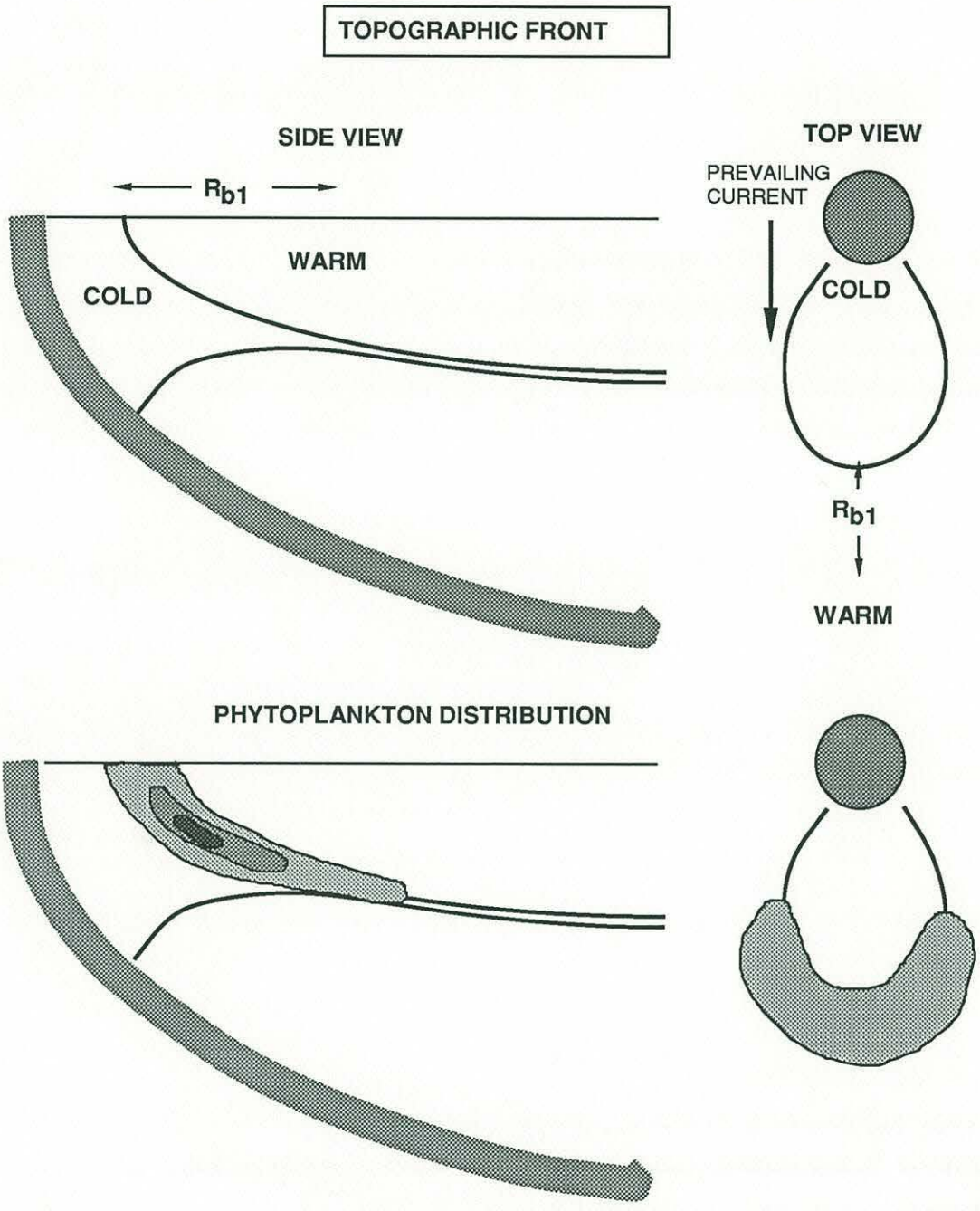

Figure 2-6. The hydrographic signature of topographically-generated fronts is shown in the upper panels. The chlorophyll distribution commonly found at these fronts is shown below.

islands and headlands in areas of strong currents (Pingree and Griffiths, 1978; Pingree and Maddock, 1979). If the current is normally from one direction, the topographic front may be stationary relative to the object, giving a predictable hydrographic signature. In areas dominated by tidal flows, two topographic fronts are formed around the flanks of an island, perpendicular to the main axis of the tidal ellipse (Wolanski *et al.*, 1984).

As a stratified fluid flows past a stationary object, mixing will take place in the lee of the object. As with the tidal front, this mixing generates a third water mass, with temperatures and salinities some average of the surface and deep water masses. The boundary between the well-mixed water in the lee of the topographic feature and the stratified water farther away is the topographic front.

The pycnocline of a topographic front slopes down from the surface, and away from the topographic feature which generated the front. It can also bifurcate in the same manner as a tidal front, creating both surface and bottom fronts (Simpson *et al.*, 1982; Wolanski *et al.*, 1984). The length scale which governs the steepness (and thus the width) of the front, is the baroclinic Rossby radius of deformation, R_{b1}. As with tidal fronts, this length is often less than 5 km.

The front is usually seen most strongly in the horizontal temperature contrast. Cold water near the topographic feature indicates the region of intense mixing, while the warmer, stratified waters farther away reflect the influence of solar heating (Pingree and Griffiths, 1978). In plan view, the front tends to be curved, either surrounding the topographic feature, or forming a tear-drop shape intersecting the topographic feature at its narrow end (Simpson *et al.*, 1982; Simpson and Tett, 1986). This is in contrast to the fronts described above, which tend to form long, relatively straight fronts extending for considerable distances (10's-100's km). In many cases the front is formed by an eddy in the lee of the topographic feature. Wolanski *et al.* (1984) present a simple model

for eddy formation, and suggest some basic criteria for the size of the eddy, and circumstances under which it will form. Unfortunately, calculation of these parameters requires a knowledge of values such as the vertical velocities and vertical eddy diffusion coefficient, both of which are extremely difficult to measure.

The distribution of chlorophyll within topographically-formed fronts is similar to that of tidally-generated fronts. A subsurface chlorophyll maximum is found just offshore of the front, while the chlorophyll maximum layer follows the sloping pycnocline. This puts the chlorophyll maximum on the side of the front away from the topographic feature (Pingree and Griffiths, 1978; Townsend *et al.*, 1983). Although these fronts have not been shown to have the same distribution of phytoplankton classes as tidal fronts, the similarity of hydrography suggests that this may be the case. Indeed, high concentrations of the dinoflagellate *Gyrodinium aureolum* were found within a topographic front near the British Isles (Simpson *et al.*, 1982).

QUANTITATIVE ASPECTS

One obvious question which arises from the preceding discussion is:

Is the phytoplankton distribution at a front scaled by the Rossby radius of deformation?

To answer this, we must calculate the length scale of the chlorophyll maximum within the front, and the appropriate Rossby radius for that front.

The length scale of phytoplankton distributions from published data were calculated using the method shown in Figure 2-7. First the horizontal axis zero was set at the location of the phytoplankton maximum. The distance from this zero to each of the contours within the pycnocline (i.e. not necessarily at the same depth) was measured. With these data the phytoplankton (chlorophyll, cell counts, etc.) could be plotted versus x, the horizontal distance along the pycnocline. The model

$$Chl(x) = Chl_{\infty} + Chl_{max} \exp(-x/L) \qquad (2\text{-}6)$$

was then fit to the data. Here Chl_{max} is the chlorophyll (or cell count) at x=0, i.e. the chlorophyll maximum, and Chl(x) is the predicted chlorophyll (cell count) distribution. Chl_{∞} is the concentration of chlorophyll in the pycnocline far away from the front (Chl(x) as $x \rightarrow \infty$). The parameter L, which is given by the regression, is the length scale of the phytoplankton patch. It is important to note that this length scale does not give the width of the patch at a given depth, but the width of the patch along an isopycnal. In doing this, we calculate a patch length scale which can be compared to the physical length scale.

Normalizing the chlorophyll data by Chl_{max}, and the length scales by the calculated Rossby radius allows comparison of the data from a variety of fronts. This will give us two non-dimensional

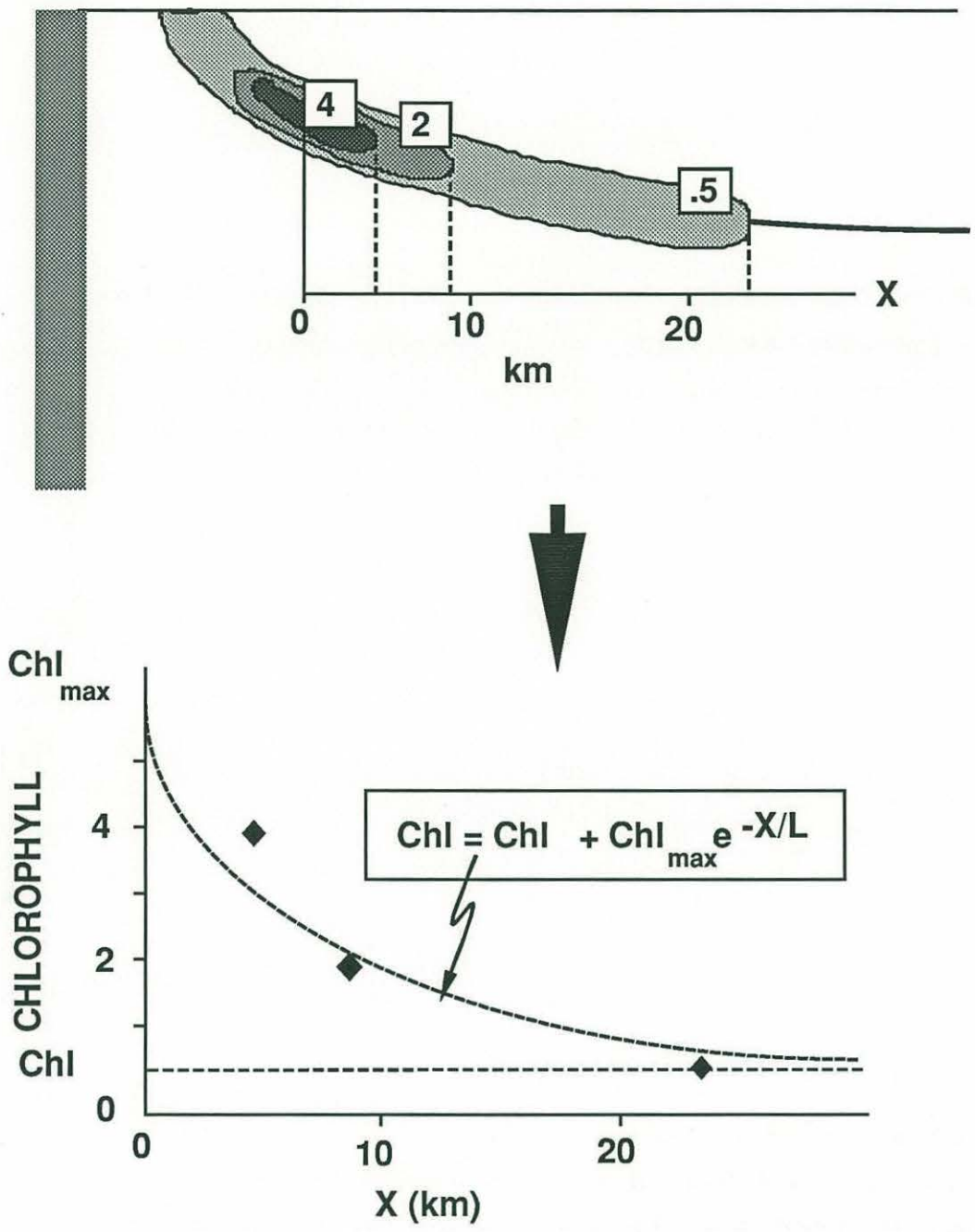

Figure 2-7. The method for calculating the phytoplankton patch length scale is illustrated here. The parameter L, given by the regression, is the patch length scale.

numbers to plot: $(Chl(x)-Chl_\infty)/(Chl_{max}-Chl_\infty)$ versus x/R_{bi}. If $L=R_{bi}$ (patch length = Rossby radius), all the points will lie along the line $y=\exp(-x)$. If $L>R_{bi}$ (patch length > Rossby radius), the points will lie above this line, and vice versa.

Eight data sets were utilized for this analysis, shown in Table 2-1. These data sets include a variety of fronts over a wide geographic range. The results are plotted in Figure 2-8, which shows quite clearly that the phytoplankton patch length scales are not equal to the theoretical Rossby radius of deformation. However, it also indicates that the patch length is always greater than or equal to the Rossby radius; generally 5-10 times greater. Thus, rather than a phytoplankton patch being on the order of 5 km in cross-frontal width, the patches are normally 25-100 km in width.

Having shown that the phytoplankton patch length scale is not equal to the Rossby radius, it is appropriate to ask,

Is the measured physical frontal length scale equal to the theoretically-calculated Rossby radius?

To answer this question, we take a similar approach to that above, but trace the depth, h(x), of an isopycnal from the front (h(0)=0) to its equilibrium depth, h_o, the depth at which the pycnocline becomes horizontal. Plotting $h_o-h(x)$ versus the horizontal distance, x, will give a horizontal profile of the depth of the isopycnal. However, we can normalize the axes in the same manner as above, by dividing $(h_o-h(x))$ by h_o, and x by R_b. This nondimensionalization will allow us to plot all the fronts on one set of axes. If the calculated frontal length scale is equal to its Rossby radius, all the points will lie along the curve $y=\exp(-x)$. Fronts with length scales longer than the Rossby radius will lie above this curve, and vice versa.

Figure 2-9 shows that the frontal length scale is not equal to the theoretically-calculated Rossby radius. In fact, it appears that the frontal scale is always larger than the Rossby radius, indicating that the front is

Table 2-1

DATA SETS USED IN ANALYSIS

Data Set	Type of Front	Frontal Scale (km)	Rossby Radius (km)
Simpson *et al.* (1982)	TOPOGRAPHIC	6.25	4.3
Chapter 4	BUOYANCY	1.2	6.5
Richardson *et al.* (1985)	WATER MASS	4.5	2.5
Richardson (1985)	WATER MASS	1.9	7.5
Holligan (1981)	TIDAL	37.0	4.5
Tett (1981)	TIDAL	3.4	1.5
Jones *et al.* (1986)	UPWELLING	20	7.5
Small and Menzies (1981)	UPWELLING	7.5	7.0

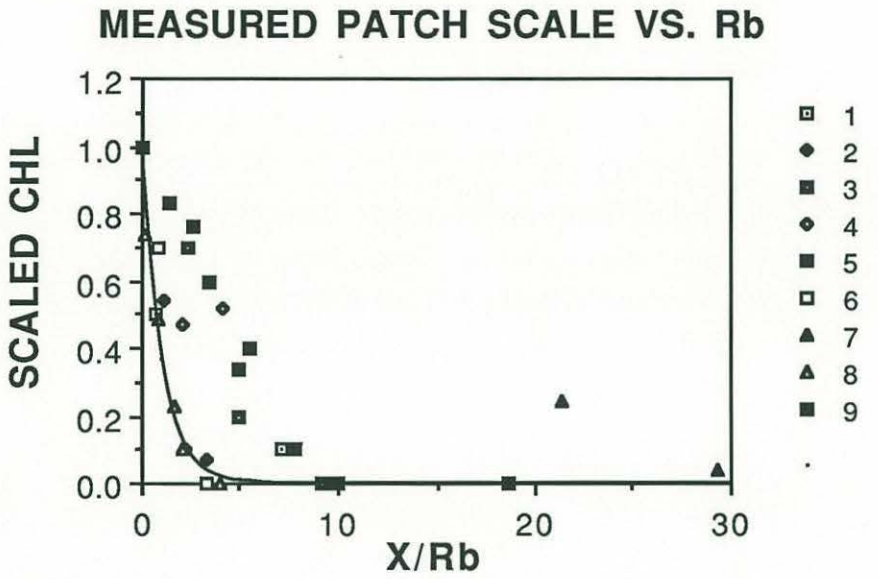

Figure 2-8. A plot of chlorophyll (cell count, etc.) vs. horizontal distance, x. The vertical axis has been scaled by Chl_{max}, the maximum chlorophyll (cell count, etc.) for a given data set, while the horizontal axis has been scaled by the Rossby radius. The solid line is y=exp(-x). The data sets indicated are 1: Simpson *et al.* (1982), 2: Chapter 4 data, 3: Richardson *et al.* (1985), 4: Richardson (1985; April 6), 5: Richardson (1985; April 8), 6: Holligan (1981), 7: Tett (1981), 8: Jones *et al.* (1986), 9: Small and Menzies (1981).

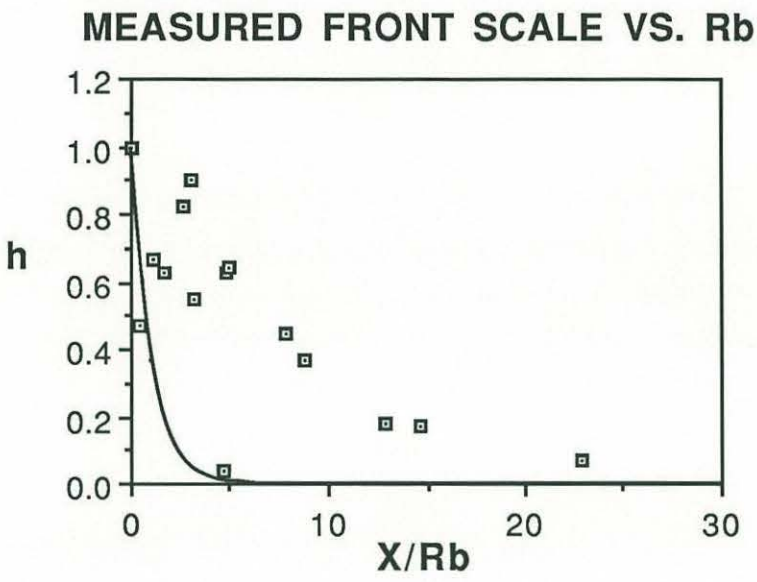

Figure 2-9. Here the scaled pycnocline depth is plotted vs. scaled horizontal distance. The pycnocline depth, h, has been scaled by the equilibrium pycnocline depth, h_o, and the horizontal distance scaled by the Rossby radius. The solid line is y=exp(-x).

more relaxed (less steep) than would be predicted on the basis of the Rossby radius alone. This is not too surprising, given the number of mechanisms which can relax the front. These include friction within the front, alongshore processes such as wind stress or bottom friction, nonzero vorticity, instabilities along the front, and eddy formation across the front.

Since both the phytoplankton patch length scale and the frontal length scale are greater than the theoretical Rossby radius of deformation, perhaps they are equal to each other. Thus we ask,

Are the phytoplankton patch and frontal length scales equal?

In this case we can plot the phytoplankton patch length scales versus the frontal length scales calculated above. If they are equal, the points should lie along the 1:1 line on the plot. Such a plot is shown in Figure 2-10. From this plot it is obvious that there is no relation between the patch size and the frontal scale, i.e. the points are scattered, and do not lie near the 1:1 line. Why might this be?

To try to solve this problem, we should explore two possibilities:

1) the length scales should be correlated
2) the length scales should not be correlated.

If we assume (1), we seek mechanisms which would decorrelate the patch and frontal length scales. If we assume (2), we must look for processes which would enhance phytoplankton growth at a front, but which do not have a length scale dependent on the front. By exploring each of the two possibilities, we should gain insight into the mechanisms driving the enhanced phytoplankton production at fronts.

A number of processes exist which would decorrelate phytoplankton patch and frontal length scales. The most obvious of these is a mismatch of the timescales of frontal development and phytoplankton growth. Walsh *et al.* (1977) suggest that the "event" timescale for wind-driven upwelling is about 3 days. This includes

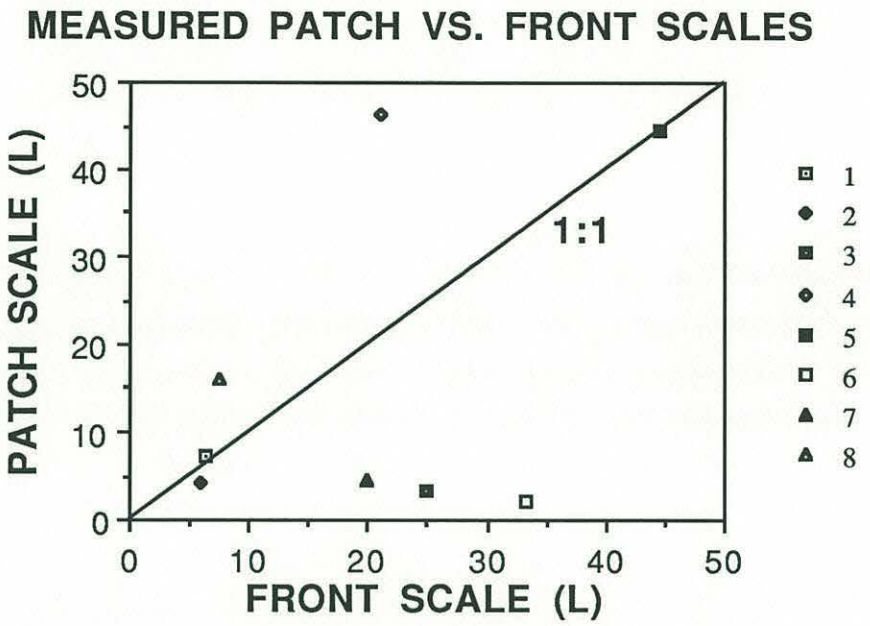

Figure 2-10. Here, the measured phytoplankton patch scale is plotted against the measured frontal scale. The solid line represents a 1:1 relationship. The data sets indicated are 1: Simpson *et al.* (1982), 2: Chapter 4 data, 3: Richardson *et al.* (1985), 4: Richardson (1985), 5: Holligan (1981), 6: Tett (1981), 7: Jones *et al.* (1986), 8: Small and Menzies (1981).

spin-up, frontal formation, and spin-down. With a specific growth rate of 1 per day, the phytoplankton would take at least one day, and probably closer to five days, to show a significant response to such an event. Thus the front could have formed and relaxed before the phytoplankton population could "catch up". This has been demonstrated by Jones and Halpern (1981), who found the primary productivity to peak about 5 days after the maximum in nitrate, and about 10 days after the onset of upwelling. Dugdale and Wilkerson (1989) give evidence to support the model of Wilkerson and Dugdale (1987), suggesting that the timescale to complete nutrient depletion following an upwelling event is about ten days. Small and Menzies (1981) examined historical data from the western coast of the United States, looking for situations in which the wind-driven upwelling should have reached and maintained a steady state over several days. Their data show that the frontal and patch length scales are equal under these conditions. This suggests that a mismatch of timescales could be an important decorrelation mechanism for wind-driven upwelling.

Tidal fronts show predominantly semi-diurnal, diurnal and fortnightly variations, driven by the M_2 and K_1. The M_2 tide not only creates and maintains the tidal front, but it also advects it back and forth along the long axis of the tidal ellipse. Superimposed on this semi-diurnal variation, is the fortnightly spring-neap tidal cycle. The variation in tidal velocity associated with these two components will alter the strength of the front, and the light, temperature and nutrient regime of the phytoplankton (Demers *et al.*, 1986). The fortnightly variation is slow enough that the phytoplankton may respond to this forcing (Balch, 1981), but the diel variation may keep the phytoplankton from reaching a steady state within the front. On the other hand, the predictable regularity of the tides may create a niche which certain phytoplankton species can exploit, aiding the formation of the high production seen at tidal fronts (Margalef, 1978; Legendre *et al.*, 1986).

The formation of topographic fronts may be dependent on tidal flows, or seasonal flows such as the gyre in the Gulf of Maine. Similarly, water mass or buoyancy fronts are often strongly seasonally variable, but show relatively small variations over days. Since the timescale of variation of these fronts is long relative to the generation time of phytoplankton, we would expect the phytoplankton to correlate well with the physical system.

Thus it would appear that, except for wind-forced flows and the semi-diurnal tide, the phytoplankton at most fronts should be able to track the variations in the physical system, and so should be closely correlated with the front. It seems, then, that a mismatch of timescales of variation may not be a sufficient explanation for the lack of a relationship between phytoplankton patch scales and frontal scales.

If we make the assumption that the patch and frontal length scales should not, *a priori*, be correlated, we must look for physical forcings which could enhance phytoplankton production at fronts, but which have a length scale independent of the front. One such process is diffusion.

Diffusion acts to smooth gradients of a property, by mixing adjacent parcels. As such, it has no inherent length scale, although the magnitude of the mixing may depend on the distance over which the mixing takes place (Okubo, 1971). Fronts are very dynamic regions, and have been predicted to have correspondingly strong mixing (e.g. Mooers *et al.*, 1978). The few measurements which have been made to test this, however, do not indicate any systematic enhancement of vertical mixing within or around the front (The Coastal Transition Zone Group, 1988). This suggests that the diffusion scales should be independent of the frontal scales.

There are three main ways by which diffusion can affect the phytoplankton distributions. The first is by altering phytoplankton residence time in the water column. Pingree *et al.* (1975) calculated

timescales for diffusion within a tidal front, and suggested that phytoplankton in the well-mixed waters below the thermocline should be quickly dispersed, negating any accumulation of chlorophyll in this area. Similar arguments may apply to the surface mixed layer, although the vagaries of the wind make this a difficult calculation. Within the thermocline, however, the stratification reduces the mixing, giving a phytoplankton residence time which is long compared to their growth rate.

Vertical mixing will also affect the photoadaptation of the cells (Marra, 1978; Lewis *et al.*, 1984) by mixing the cells through a light gradient. This may adversely affect certain species of phytoplankton which cannot respond to high frequency light fluctuations (Harris, 1980). In addition, vertical mixing may cause light limitation if the mixing layer is deeper than the euphotic zone (Sverdrup, 1953). Thus phytoplankton growth may be reduced in regions of enhanced vertical mixing, such as the unstratified waters near a front, or the surface waters on the stratified side of a front. This reduced growth may enhance the vertical and horizontal contrast of phytoplankton biomass in the various water masses. However, such processes will not explain the enhanced biomass generally seen at fronts.

The second influence of diffusion takes place through mixing of nutrients. Most fronts form a boundary separating a pool of dense, well-mixed, nutrient-rich water from more stratified nutrient-poor waters. Mixing of the two water masses will bring some of the nutrient-rich water into the euphotic zone on the stratified side of the front. This can be a significant source of nutrients for phytoplankton production at fronts (Loder and Platt, 1985).

Tett (1981), and Traganza *et al.* (1987) used one-dimensional (vertical) models to try to evaluate the contribution of various processes to the phytoplankton at tidal and wind-driven fronts, respectively. In both cases, vertical diffusion and entrainment was found to account for the bulk of the production. Smith *et al.* (1983)

employed a two-dimensional (cross-front) Lagrangian tracer model which suggested that vertical diffusion was more important than cross-frontal advection in supplying phytoplankton and nutrients to the frontal zone.

The third mode of influence of diffusion on phytoplankton is through the physical act of mixing. It well known that dinoflagellates are very sensitive to mixing. They are normally found in stratified waters in the field, and do not tolerate mixing in laboratory cultures (e.g. White, 1976). The reasons for this are not well understood. Based on evidence from the field, however, it is possible to predict the conditions which favour dinoflagellate growth (e.g. Margalef, 1978; Legendre *et al.*, 1986). In general, dinoflagellates are not found in well-mixed water columns, such as those seen on the non-stratified side of fronts. This does not present a mechanism by which phytoplankton production could be enhanced at fronts, however. Rather, it gives a mechanism whereby certain species may be reduced in regions surrounding the front.

The modes of diffusion most likely to enhance phytoplankton production at fronts are the effects on the phytoplankter's light environment, and the transport of nutrients. This is the same conclusion arrived at by Yentsch (1974) and Loder and Platt (1985), through quite different reasoning. The effects of these processes will be expressed at, and near, the front. Here the mixed layer becomes very shallow, and the nutrient-rich water is near the surface, in close proximity to the stratified waters. This may explain the association of the phytoplankton maximum with the pycnocline, on the stratified side of the front. Such arguments suggest that the enhanced phytoplankton production should be similarly restricted; as can be seen from Figure 2-10, however, this is not necessarily the case. It is possible that some mechanism, such as cross-frontal circulation, is acting to spread the cells along the pycnocline, away from the front.

Cross-frontal circulations are thought to be vertical circulation cells with either one closed loop (e.g. Csanady, 1975; Allen, 1980; Tang, 1983), or more commonly, two-closed loops such as described by Simpson *et al.* (1978) and Garrett and Loder (1981) for tidal fronts, or Foo (1981) and de Szoeke and Richman (1984) for wind-driven fronts. Such two-celled circulation patterns usually show a convergence zone at the front, with downwelling along the pycnocline. The upwelling from the deep water mass, followed by convergence at the front and downwelling within the pycnocline, may supply the phytoplankton within the pycnocline with nutrients otherwise unavailable to them. Although the cross-frontal flows should have the same length scales as the front itself, the advection within the pycnocline could act to decorrelate the phytoplankton populations from the frontal scales. This is supported by the model of Wilkerson and Dugdale (1987), which describes the "conveyor-belt" hypothesis for phytoplankton production in a wind-driven upwelling zone. Thus the peak in production should be physically removed from the main upwelling region due to cross-frontal advection coupled with the delayed response of phytoplankton to new nutrients ("shift-up"). This hypothesis appears to be supported by the extensive observations of Dugdale and Wilkerson (1989) in the Point Conception region of California. Garrett and Loder (1981) used scaling arguments to suggest that frictionally-induced cross-frontal flows within tidal fronts may be the predominant mode of cross-frontal transfer of properties at these types of fronts. Loder and Platt (1985), however, calculate that only about 6% of the nitrate flux to the phytoplankton on Georges Bank was due to cross-frontal circulations.

A secondary effect of the cross-frontal circulations is the possibility of enhanced vertical mixing due to shear within the frontal zone. Halpern (1976) showed the shear to increase, and the stratification to decrease during a wind event, suggesting vertical mixing within the pycnocline. Winant (1980) found a similar situation, and noted that the zone of maximal shear was found just below the thermocline. This observation may explain the

measurements of Pingree *et al.* (1978), who found that the chlorophyll maximum layer was in the deeper portion of the pycnocline, but above the nitracline. Thus a vertical supply of nitrate to these cells could take place by mixing only across the nitracline rather than the pycnocline. Such mixing should lead to a higher local chlorophyll concentration, and may increase the vertically integrated chlorophyll, depending on the rate of supply of new nutrients below the pycnocline.

The models of Foo (1981) and de Szoeke and Richman (1984) both indicate that localized regions of enhanced turbulence form within the frontal zone. In the model of Foo (*op. cit.*) in particular, the nonuniform vertical diffusion of density acts to generate upwelling from below the pycnocline. A further effect of this vertical mixing is to vary the effective local Rossby radius of deformation. Thus, such shear-induced mixing may influence the phytoplankton production through the vertical advection of phytoplankton and nutrient-rich water, while decorrelating the physical and biological scales.

DISCUSSION

The strong association of enhanced phytoplankton biomass with fronts has been described for a variety of cases. Qualitatively, the chlorophyll maximum is usually associated with the pycnocline forming the front, and is found subsurface on the stratified side of the front. Quantitatively, the scale of the phytoplankton patch was not found to be related to the theoretical scale of the front, or the actual scale of the front. The implications of this were discussed in terms of the processes mediating phytoplankton dynamics at fronts.

From the arguments presented above, it appears that the scale of enhanced phytoplankton production at fronts is uncorrelated with the scale of the front itself. This implies either that there are processes decorrelating the patch and front scales, or the processes generating the phytoplankton patch are uncorrelated with the scale of the front. There appears to be more evidence from the literature to support the latter conclusion, except in very variable systems such as wind-driven upwelling. It is suggested that diffusion is a major contributor to the phytoplankton production at fronts.

The effects of diffusion should be manifested in both the biomass of phytoplankton, and their growth rates. Thus the front should be the location of enhanced phytoplankton productivity, as well as growth. This inference is supported by a variety of studies at fronts. Traganza *et al.* (1987) and Dengler (1985) both found the highest productivity just offshore of a wind-driven upwelling front. Jones and Halpern (1981) corroborate this finding, and note that enhancement of productivity may show a lag of several days from the formation of the front. Holligan *et al.* (1984) and Videau (1987) showed primary productivity to peak within a tidal front off Ushant. However, when normalized to the amount of pigment present, Holligan *et al.* (*op. cit.*) showed the phytoplankton in the front to have a lower specific production rate than those in the surrounding waters. This finding is contradicted by that of Videau (*op. cit.*), who

found the highest specific production rates to occur within the front. Richardson (1985) found an enhancement of primary production at a water mass front in the North Sea, giving daily production rates up to 25 times those of surrounding waters.

There are certain limitations to the methods used above which deserve some mention. From a theoretical point of view, the calculation of a Rossby radius is often problematic. The actual bottom topography may render the calculated radius invalid, or require the use of a spatially-varying radius of deformation. Thus our rather simple-minded approach of estimating the Rossby radius may not always apply.

As was mentioned above, many physical processes will alter the structure of a front, so that the Rossby radius no longer scales with the width of the front. These processes include internal friction which will tend to relax (flatten out) a front, wind stresses which can steepen or flatten a front, heat exchange which can alter the buoyancy distribution, and a host of other processes operating on a variety of temporal and spatial scales.

From a more practical point of view, the data used to estimate patch and frontal scales may be insufficient for the purpose. If the theoretical Rossby radius is only a few kilometers, then the station spacing should be of the same order or less for the calculation of scales. In most cases, however, the station spacing is considerably larger. This means that the front may be much steeper than indicated in the data, and the scale which we are measuring is not the internal Rossby radius of deformation. A comparison of the fronts off Oregon shown in Brink (1983; pg. 235) to those of Halpern (1976) clearly demonstrates the difference station spacing makes in interpreting frontal scales. The pycnocline in Brink (*op. cit.*) is extremely steep near the surface, implying a short Rossby radius. The wider station spacing in Halpern (*op. cit.*) suggests a much more relaxed pycnocline, with a length scale on the order of 20 km. In fact

the pycnocline may have been as steep as in Brink (*op. cit.*), but the widely-spaced stations obscure this.

The same caveats apply to the calculation of the phytoplankton patch scales. Phytoplankton concentrations are known to fluctuate over a range of scales (Platt,1972); the scales measured here include just one band of the frequency range of patchiness. Thus we would expect some variance about the values chosen as representative of a particular point in time and space. It is assumed, however, that this variance is relatively constant about a spatially varying mean; it is the shape of this mean which defines the phytoplankton "patch".

With these limitations in mind, it is clear that the methods used above still provide us with some clues to the processes mediating enhanced phytoplankton production at fronts. To understand better the processes hypothesized to be important, we must continue to make measurements on a variety of scales within frontal systems. In doing so, we may eventually learn how processes occurring on small scales can affect production over much larger scales, and gain a better understanding of the dynamics of red tides.

LITERATURE CITED

Abbott, M. and P. Zion.
1985 Satellite observations of phytoplankton variability during an upwelling event. Cont. Shelf Res. 4:661-680.

Allen, J.S.
1980 Models of wind-driven currents on the continental shelf. Ann. Rev. Fluid Mech. 12:389-433.

Balch, W.M.
1981 An apparent lunar tidal cycle of phytoplankton blooming and community succession in the Gulf of Maine. J. exp. mar. Biol. Ecol., 55:65-77.

Barton, E.D., A. Huyer and R.L. Smith
1977 Temporal variation observed in the hydrographic regime near Cabo Corveiro in the northwest African upwelling region, February to April 1974. Deep-Sea Res., 24:7-23.

Blasco, D.
1977 Red tide in the upwelling region of Baja California. Limnol. Oceanogr., 22:255-263.

Blasco, D., M. Estrada and B.H. Jones
1981 Short-time variability of phytoplankton populations in upwelling regions - the example of northwest Africa. In: Richards, F.A. (ed.), Coastal Upwelling. American Geophysical Union, Washington, D.C. p. 339-347.

Bowman, M.J. and R.L. Iverson
1978 Estuarine and plume fronts. In: M. Bowman, W. Esaias (eds.), Oceanic Fronts in Coastal Processes. Springer- Verlag, New York, p. 87-104

Brink, K.H.
1983 The near-surface dynamics of coastal upwelling. Prog. Oceanogr., 12:223-257.

Brink, K.H.
1985 Some aspects of the physical processes in coastal upwelling. Int. Symp. Upw. W Afr., Inst. Inv. Pesq., Barcelona, 1:5-14.

Brink, K.H.
1987 Upwelling fronts: implications and unknowns. In: Payne, A.I.L., Gulland, J.A. and K.H. Brink (eds.), The Benguela and Comparable Ecosystems. S. Afr. J. mar. Sci., 5:3-9.

Brink, K.H., H. Halpern, D. Huyer and R.L. Smith
1983 The physical environment of the Peruvian upwelling system. Prog. Oceanogr., 12:223-257.

Chao, S.-Y.
1987 Wind-driven motion near inner shelf fronts. J. Geophys. Res., 92:3849-3860.

Csanady, G.T.
1971 On the equilibrium shape of the thermocline in a shore zone. J. Phys. Oceanogr., 1:263-270.

Csanady, G.T.
1973 Wind-induced baroclinic motions at the edge of the continental shelf. J. Phys. Oceanogr. 3:274-279.

Csanady, G.T.
1975 Lateral momentum flux in boundary currents. J. Phys. Oceanogr. 5:705-717.

Csanady, G.T.
1978 Wind effects on surface to bottom fronts. J. Geophys. Res., 83:4633-4640.

Csanady, G.T.
1982 Circulation in the coastal ocean. Reidel Publishing Co., Boston, 280 p.

Demers, S., L. Legendre and J.-C. Therriault
1986 Phytoplankton responses to vertical tidal mixing. In: Bowman, M.J., C.M. Yentsch and W.T. Peterson (eds.), Lecture Notes on Coastal and Estuarine Studies 17: Tidal Mixing and Plankton Dynamics. Springer-Verlag, Berlin, p. 1-40.

Dengler, A.T.
1985. Relationship between physical and biological processes at an upwelling front off Peru, 15°S. Deep-Sea Res., 32:1301-1315.

de Szoeke, R.A. and J.G. Richman
1984 On wind-driven mixed layers with strong horizontal gradients - a theory with application to coastal upwelling. J. Phys. Oceanogr., 14:364-377.

Dugdale, R.C. and F.P. Wilkerson
1989 New production in the upwelling center at Point Conception, California: temporal and spatial scales. Deep-Sea Res. 36:985-1007.

Dundas, I., O.M. Johannessen, G. Berge and B. Heimdal
1989 Toxic algal bloom in Scandinavian waters, May-June 1988. Oceanography, 2:9-14.

Foo, E.-C.
1981 A two-dimensional diabatic isopycnal model - simulating the coastal upwelling front. J. Phys. Oceanogr., 11:604-626.

Garrett, C., J. Keeley and D. Greenberg
1978 Tidal mixing versus thermal stratification in the Bay of Fundy and Gulf of Maine. Atm-Oc., 16:403-423.

Garrett, C.J.R. and J.W. Loder
1981 Dynamical aspects of shallow sea fronts. Phil. Trans. R. Soc. Lond. A302:563-581.

Garvine, R.W. and J.D. Monk
1974 Frontal structure of a river plume. J. Geophys. Res., 79:2251-2259.

Halpern, D.
1976 Structure of a coastal upwelling event observed off Oregon during July 1973. Deep-Sea Res., 23:495-508.

Harris, G.P.
1980 The relationship between chlorophyll a fluorescence, diffuse attenuation changes and photosynthesis in natural phytoplankton populations. J. Plankton Res., 2:109-127.

Holligan, P.M.
1981 Biological implications of fronts on the northwest European continental shelf. Phil. Trans. R. Soc. Lond., A302:547-562.

Holligan, P.M., P. LeB. Williams, D. Purdee and R. Harris

1984 Photosynthesis, respiration and nitrogen supply of plankton populations in stratified, frontal and tidally mixed shelf waters. Mar. Ecol. Prog. Ser., 17:201-213.

Holligan, P.M., M. Viollier, C. Dupouy and J. Aikens
1983 Satellite studies on the distributions of chlorophyll and dinoflagellate blooms in the western English Channel. Cont. Shelf Res., 2:81-96.

Houghton, R.W. and J. Marra
1983 Physical/biological structure and exchange across the thermohaline shelf/slope front in the New York Bight. J. Geophys., Res. 88:4467-4481.

Hsueh, Y. and B. Cushman-Roisin
1983 On the formation of surface to bottom fronts over steep topography. J. Geophys. Res., 88:743-750.

James, I.D.
1988 Experiments with a numerical model of coastal currents and tidal mixing fronts. Cont. Shelf Res., 8:1275-1297

Jones, B.H., L.P Atkinson, D. Blasco, K.H. Brink and S.L. Smith
1988 The asymmetric distribution of chlorophyll associated with a coastal upwelling center. Cont. Shelf Res., 8:1155-1170.

Jones, B.H. and D. Halpern
1981 Biological and physical aspects of a coastal upwelling event observed during March-April 1974 off northwest Africa. Deep-Sea Res., 28A:71-81.

Kishi, M. and S. Ikeda
1986 Population dynamics of 'red tide' organisms in eutrophicated coastal waters - numerical experiment of phytoplankton bloom in the East Seto Inland Sea, Japan. Ecol. Modelling, 31:145-174.

Legendre, L., S. Demers and D. LeFaivre
1986 Biological production at marine ergoclines. In: Nihoul, J.C. (ed.), Marine Interfaces Ecohydrodynamics. Elsevier, Amsterdam, p. 1-30.

Lewis, M.R., E.P.W. Horne, J.J. Cullen, N.S. Oakey and T. Platt
1984 Turbulent motions may control phytoplankton photosynthesis in the upper ocean. Nat., 311:49-50.

Loder, J.W. and D.A. Greenberg
1986 Predicted positions of tidal fronts in the Gulf of Maine region. Cont. Shelf Res., 6:397-414.

Loder, J. and T. Platt
1985 Physical controls on phytoplankton production at tidal fronts. In: Gibbs, P.E. (ed.), Proceedings of the 19th European Marine Biology Symposium. Cambridge University Press, Cambridge. p. 3-22.

Marra, J.
1978 Phytoplankton photosynthetic response to vertical movement in a mixed layer. Mar. Biol., 46:203- 208.

Marra, J., R.W. Houghton, D.C. Broadman, and P.T. Neale.
1982 Distributions of chlorophyll *a* and temperature at a shelf-break front. J. Mar. Res., 40:575-591.

Margalef, R.
1978 Life forms of phytoplankton as survival alternatives in an unstable environment. Oceanologica Acta., 1:493-509.

Mooers, C.N.K., C.A. Collins and R.L. Smith
1976 The dynamic structure of the frontal zone in the coastal upwelling region off Oregon. J. Phys. Oceanogr., 6:3-21

Mooers, C.N.K., C.N. Flagg and W.C. Boicourt
1978 Prograde and retrograde fronts. In: M. Bowman, W. Esaias (eds.), Oceanic Fronts in Coastal Processes. Springer- Verlag, New York, p. 43-58

Mork, M.
1981 Circulation phenomena and frontal dynamics of the Norwegian coastal current. Phil. Trans. R. Soc. Lond., A302:635-647.

Okubo, A.
1971 Oceanic diffusion diagrams. Deep-Sea Res., 18:789-802.

Ou, H.W.
1984 Wind-driven motion near a shelf-slope front. J. Phys. Oceanogr., 14:985-993.

Pingree, R., M.J. Bowman and W.E. Esaias

1978 Headland fronts. In: M. Bowman, W. Esaias (eds.), Oceanic Fronts in Coastal Processes. Springer- Verlag, New York, p. 78-86

Pingree, R., G. Forster and G. Morrison
1974 Turbulent convergent tidal fronts. J. mar. biol. Ass. U.K., 54:469-479.

Pingree, R. and D.K. Griffiths
1978 Tidal fronts around the British Isles. J. Geophys. Res., 83:4615-4621.

Pingree, R.D., P.M. Holligan and G.T. Mardell
1978 The effects of vertical stability on phytoplankton distributions in the summer on the northeast European shelf. Deep-Sea Res., 25:1011-1028.

Pingree, R.D. and L. Maddock
1979 Tidal flow around an island with a regularly sloping bottom topography. J. mar. biol. Ass. U.K., 59:699-710.

Pingree, R., P. Pugh, P. Holligan and G. Forster
1975 Summer phytoplankton blooms and red tides in the approaches to the English Channel. Nature, 258:672-677.

Platt, T.
1972 Local phytoplankton abundance and turbulence. Deep Sea Res., 19:183-187.

Richardson, K.
1985 Plankton distribution and activity in the North Sea/Skaggerak-Kattegat frontal area in April 1984. Mar. Ecol. Prog. Ser., 26:233-244.

Richardson, K., M.F. Lavin-Peregrina, E.G. Mitchelson and J.H. Simpson
1985 Seasonal distribution of chlorophyll a in relation to physical structure in the western Irish Sea. Oceanol. Acta, 8:77-86.

Rojas de Mendiola, B.
1979 Red tide along the Peruvian coast. In: Taylor, D.L. and H.H. Seliger (eds.), Toxic Dinoflagellate Blooms. Elsevier, Amsterdam, p.183-190.

Rojas de Mendiola, B.

1981 Seasonal phytoplankton distribution along the Peruvian coast. In: Richards, F.A. (ed.), Coastal Upwelling. American Geophysical Union, Washington, D.C. p. 348-356.

Savidge, G.
1976 A preliminary study of the distribution of Chlorophyll a in the vicinity of fronts in the Celtic and Western Irish Seas. Estuar. Coastal Mar. Sci., 4:617-625.

Shannon, L.V.
1985 The Benguela ecosystem. 1. Evolution of the Benguela, physical features and processes. In: Barnes, M. (ed.), Oceanography and Marine Biology. An Annual Review 23. University Press, Aberdeen. p. 105-182.

Simpson, J., C. Allen and N. Morris
1978 Fronts on the continental shelf. J. Geophys. Res. 83:4607-4614.

Simpson, J.H., D.J. Edlestein, A. Edwards, N.C.G. Morris and P.B. Tett
1979 The Islay Front: physical structure and phytoplankton distribution. Estuar. Coast. Mar. Sci., 9:713-726.

Simpson, J.H. and J.R. Hunter
1974 Fronts in the Irish Sea. Nature, 250:404.

Simpson, J.H. and P. Tett
1986 Island stirring effects on phytoplankton growth. In: Bowman, M.J., C.M. Yentsch and W.T. Peterson (eds.), Lecture Notes on Coastal and Estuarine Studies 17: Tidal Mixing and Plankton Dynamics. Springer-Verlag, Berlin, p. 41-76.

Simpson, J.H., P. Tett, M.L. Argotte-Espinoza, A. Edwards, K.J. Jones and G. Savidge
1982 Mixing and phytoplankton growth around an island in a stratified sea. Cont. Shelf Res., 1:15-31.

Small, L.F. and D.W. Menzies
1981 Patterns of primary productivity and biomass in a coastal upwelling zone. Deep-Sea Res., 28A:123-149.

Smith, W.O., G.W. Heburn, R.T. Barber and J.J. O'Brien
1983 Regulation of phytoplankton communities by physical processes in upwelling systems. J. Mar. Res., 41:539-556.

Sverdrup, H.U.
1953 On conditions for the vernal blooming of phytoplankton. J. Cons. Int. Explor. Mer., 18:287- 295.

Tang, C.L.
1983 Cross-front mixing and frontal upwelling in a controlled quasi-permanent density front in the Gulf of St. Lawrence. J. Phys. Oceanogr., 13:1468-1481.

Tett, P.
1981 Modelling phytoplankton production at shelf- sea fronts. Phil. Trans. R. Soc. Lond., A302:605.

The Coastal Transition Zone Group
1988 The coastal transition zone program. Eos, 69:698-699,704,707.

Townsend, D.W., C.M. Yentsch, C.E. Parker, W.M. Balch and E.D. True
1983 An island mixing effect in the coastal Gulf of Maine. Helgoländer Meeresunters., 36:347-356.

Traganza, E.D., D.G. Redalje and R.W. Garwood
1987 Chemical flux, mixed layer entrainment and phytoplankton blooms at upwelling fronts in the California coastal zone. Cont. Shelf Res., 7:89-105.

van Heijst, G.J.F.
1986 On the dynamics of a tidal mixing front. In: Nihoul, J.C. (ed.), Marine Interfaces Ecohydrodynamics. Elsevier, Amsterdam, p.165-194.

Videau, C.
1987 Primary production and physiological state of phytoplankton at the Ushant tidal front (west coast of Brittany, France). Mar. Ecol. Prog. Ser., 35:141-151.

Vincent, W.F., F.H. Chang, A. Cole, M.T. Downes, M.R. James, L. May, M. Moore and P.H. Woods
1989 Short-term changes in planktonic community structure and nitrogen transfers in a coastal upwelling system. Estuar. Coastal and Shelf Sci. 29:131-150.

Walsh, J.E., T.E. Whitledge, J.C. Kelley, S.A. Huntsman and R.D. Pillsbury

1977 Further transition states of the Baja California upwelling ecosystem. Limnol. Oceanogr., 22:264-280.

White, A.W.
1976 Growth inhibition caused by turbulence in the toxic marine dinoflagellate *Gonyaulax excavata*. J. Fish. Res. Bd. Can. 33:2598-2602.

Wilkerson, F.P. and R.C. Dugdale
1987 The use of large shipboard barrels and drifters to study the effects of coastal upwelling on phytoplankton nutrient dynamics. Limnol. Oceanogr. 32:368-382.

Winant, C.D.
1980 Downwelling over the Southern California shelf. J. Phys. Oceanogr., 10:791-799.

Wolanski, E., J. Imberger and M.L. Heron.
1984 Island wakes in shallow coastal waters. J. Geophys. Res., 89:10553-10569.

Yentsch, C.S.
1974 The influence of geostrophy on primary production. Tethys 6:111-117.

Yentsch, C.S. and N. Garfield
1981 Principal areas of vertical mixing in the waters of the Gulf of Maine, with references to the total productivity of the area. In: Gower, J.F.N. (ed.), Oceanography from Space. Plenum Press, NY. p. 303-312.

CHAPTER 3

Growth and Diffusion of a Phytoplankton Bloom: A Simple Model of *Ceratium longipes* in the Gulf of Maine

"I ought to say," explained Pooh as they walked down to the shore of the island, "that it isn't just an ordinary sort of boat. Sometimes it's a Boat, and sometimes it's more of an Accident. It all depends."

A.A. Milne
Winnie-the-Pooh

ABSTRACT

A bloom of *Ceratium longipes* occurred in the southwestern Gulf of Maine during the month of June, 1987. The bloom was first seen offshore in late May. By early June it extended inshore, where it remained until July. The peak cell densities reached at least 5000 cells l^{-1}, and followed the deepest portion of the seasonal pycnocline. A simple model coupling horizontal diffusion with the logistic growth equation was formulated to examine the population distributions. The model described the data well, suggesting that the cells had a growth rate of about 0.1 d^{-1}, and had reached a steady horizontal across-shelf distribution within about 10 d. Further variations in population density appear to be related to fluctuations of light with periods of ~10 d. To our knowledge, this is the first use of this simple diffusion model as a diagnostic tool for quantifying parameters describing the growth and movement of a specific phytoplankton population.

INTRODUCTION

Dinoflagellate blooms are often associated with strong hydrographic features, e.g.: *Gyrodinium aureolum* with tidal fronts around the British Isles (Holligan et al., 1984b; Pingree et al., 1978), *Alexandrium excavatum* with fronts in the Argentine Sea (Carreto et al., 1986), *Prorocentrum mariae-lebouriae* with buoyancy currents (Tyler, 1984), and *Gymnodinium splendens* with internal waves (Kamykowski, 1981). The dinoflagellates' exploitation of such regimes appears to be dependent on their ability to swim, and their preference for strong density gradients.

The southwestern coast of the Gulf of Maine has traditionally been regarded as a highly dynamic environment. Alongshore currents associated with the counter-clockwise circulation of the gulf are a predominant factor along this coast. Strong tidal currents can cause tidally-generated fronts along the northern regions of the gulf coast (Garrett et al., 1978). Wind mixing has been implicated in forming fronts in areas of relatively weak tidal currents (Yentsch and Garfield, 1981), and freshwater runoff can create strong buoyant plumes alongshore (Butman, 1976; Chapter 4).

During the spring and summer of 1987, however, the Gulf of Maine experienced a period of unusual calm. The record freshwater runoff in April of 1987 appeared to disrupt the normal spring/summer circulation patterns of the gulf, reducing the alongshore flows (Brown and Irish, unpub. ms.). Winds were weak, and precipitation low during the months of May, June and July. This summer was the only summer from 1973 to 1989 that a bloom of the toxic dinoflagellate *Alexandrium tamarense* (formerly *Gonyaulax tamarensis*) did *not* occur along the northern shore of Massachusetts. However, an extensive bloom of *Ceratium longipes* Gran was seen along this coast.

The present chapter examines the development of that bloom of *Ceratium longipes*. Through numerous cruises we trace its movement inshore and its association with specific hydrographic features. Finally, a model based on horizontal diffusion and the logistic equation is applied to the data. From this model we infer growth rates and environmental forcings of the *Ceratium* population. To our knowledge, this is the first use of this simple diffusion model as a diagnostic tool for quantifying parameters describing the growth and movement of a specific phytoplankton population.

METHODS

Five stations were sampled along a transect extending from Portsmouth, New Hampshire, 30 km into the Gulf of Maine (Figure 3-1). The stations were approximately 7 km apart, with bottom depths of 15 m at Station 1 to 175 m at Station 5. The ship used was the 45' vessel R/V Jere A. Chase. Nine cruises were taken during 1987, four of which will be described below: May 26, June 5, June 18 and July 2, 1987.

A submersible pump brought water through 40 m of 2 cm i.d. garden hose which was raised from 40 m depth to the surface at 2 m min^{-1}. Water flowing at a rate of about 2.0 l min^{-1} passed through a bubble trap, and through the flow cell of a Turner Designs fluorometer. The fluorometer was linked to a portable computer which plotted and recorded the fluorescence every two seconds. From the fluorometer, the water passed into buckets which integrated samples over 5 m depth. The buckets were subsampled as follows: one litre was filtered through 20 μm mesh, backwashed and preserved in 10% formaldehyde for cell counts, while 500 ml was filtered through GF/A filters for chlorophyll analysis, and the filtrate frozen for nutrient analyses. Irradiance was measured with a Biospherical 4π collector.

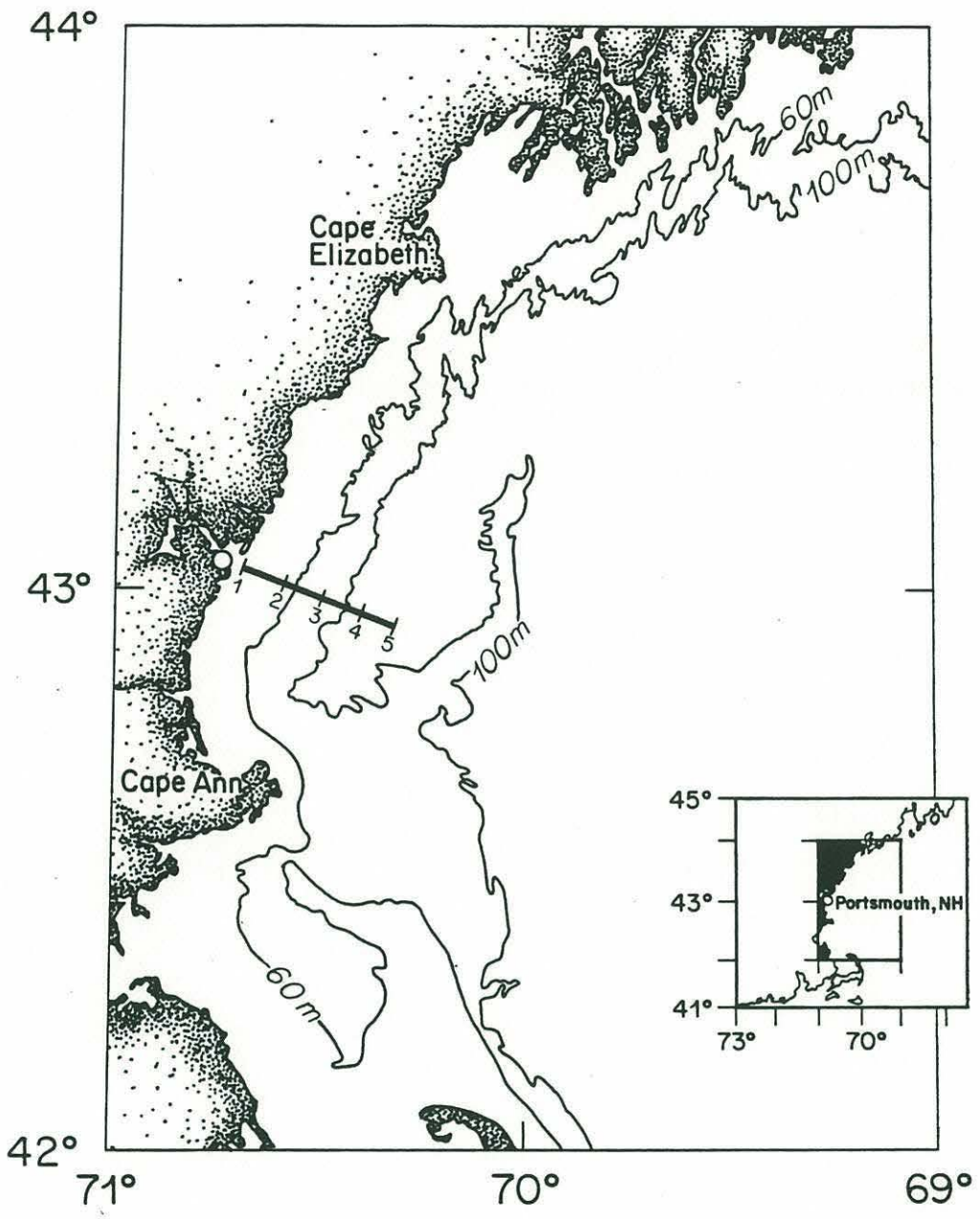

Figure 3-1. The cruise transect, Stations 1 (inshore) to 5 (offshore), are shown in relation to the coastline in this region. The transect is approximately 30 km long, with stations 7 km apart. The depth at Station 1 is ~15 m, while at Station 5 is ~175 m. The bottom is fairly smoothly sloping.

Samples for cell counts were settled in 50 ml settling chambers, and counted on a Zeiss inverted microscope. Half a slide was counted if there were less than 200 cells, otherwise 20 fields were counted at 160X. Fluorometric analysis of chlorophyll followed the Strickland and Parsons method (1972), corrected for phaeopigments. Nitrate+nitrite concentrations were measured on a Technicon AutoAnalyser II, using their protocol (Method No. 158-71W/B). Duplicate measurements were made, followed by a seawater wash prior to the introduction of the next sample.

A CTD (Sea Cat Profiler, Sea-Bird Electronics) was attached below the hose inlet. The sensors were oriented upward in order to take the upcast data. This was necessary as the hose had to be completely submerged to prime the pump. The CTD data were smoothed using an objective mapping routine (after Levy and Brown, 1986) to remove salinity spikes. Knowing the transit time of the water in the hose (1.8 min), the fluorescence vs. time could be converted to fluorescence vs. depth. These data could then be merged with the CTD data to examine the relationship of fluorescence with temperature and salinity.

Nine cruises were taken during 1987, from late March to early September. Four cruises which spanned the *Ceratium longipes* bloom will be described below: those taken on May 26, June 5, June 18 and July 2, 1987.

OBSERVATIONS

The density anomaly (σ_T), *in vivo* fluorescence, and cell concentrations from cruises on May 26, June 5, June 18 and July 2 are shown in Figure 3-2. Here the vertical data from the five stations have been contoured into cross-shore sections. The bottom profile is shown at the lower left of each panel.

The upper row of sections shows the density profiles from the four cruises. Between the May 26 and June 5 cruises, the pycnocline was established at about 10 m depth. The formation of the pycnocline was due to heating and rainfall. A storm on June 1 delivered ~5 cm of rain, enough to lower the salinity of the upper 5 m by 0.5 psu and create an enhanced density gradient at 5 m depth. A small surface feature on June 5 at Station 3 is suggestive of upwelling: cold salty water is found in the upper few metres. This feature is probably the result of an internal wave, or patchiness of the freshwater input a few days earlier. Given the wind field at that time (Figure 3-3), it is unlikely that it is a result of wind-driven upwelling, contrary to the speculation of Franks et al. (1989). Continued warming, combined with sporadic wind mixing, led to a very strong pycnocline by July 2 with some upwelling inshore on that date.

The middle panels of Figure 3-2 show that the fluorescence follows the density contours very closely. We know from earlier cruises that the fluorescence peak at 20 m at Station 3 on May 26 was a remnant of the spring diatom bloom, and was composed mainly of the genera *Thalassiosira* and *Chaetoceros*. One of the organisms contributing to the fluorescence patterns of the later cruises was the large dinoflagellate *Ceratium longipes*, as shown in the bottom panels. The maximal chlorophyll values seen were about 1.2 $\mu g\ l^{-1}$ at Station 3 on June 5. The cell concentration contours are more spread out vertically than the fluorescence contours. This is a result of the sampling methods: fluorescence is measured continuously, whereas the cell counts are integrated over 5 m vertically. Thus a narrow band of high cell densities will be smeared over 5 m.

The bloom of *Ceratium longipes* was first seen at Station 5 (offshore) on May 26. By June 5 it extended inshore to Station 3, forming a narrow band at 10 m. The cell density in this band increased over time, and followed the pycnocline as it deepened.

Figure 3-2. The density (upper panels, σ_T), *in vivo* fluorescence (middle panels, relative units), and *Ceratium longipes* concentrations (bottom panels, cells l^{-1}) are contoured for May 26, June 5, June 18, and July 2, 1987. The data extend only to 40 m depth (the length of the hose). The bottom profile is shown by the heavy line in the lower left corner of each panel. Station locations are given in Figure 3-1. The heavy line on the *Ceratium longipes* panels is the 0.5 µg-at l^{-1} contour of nitrate+nitrite.

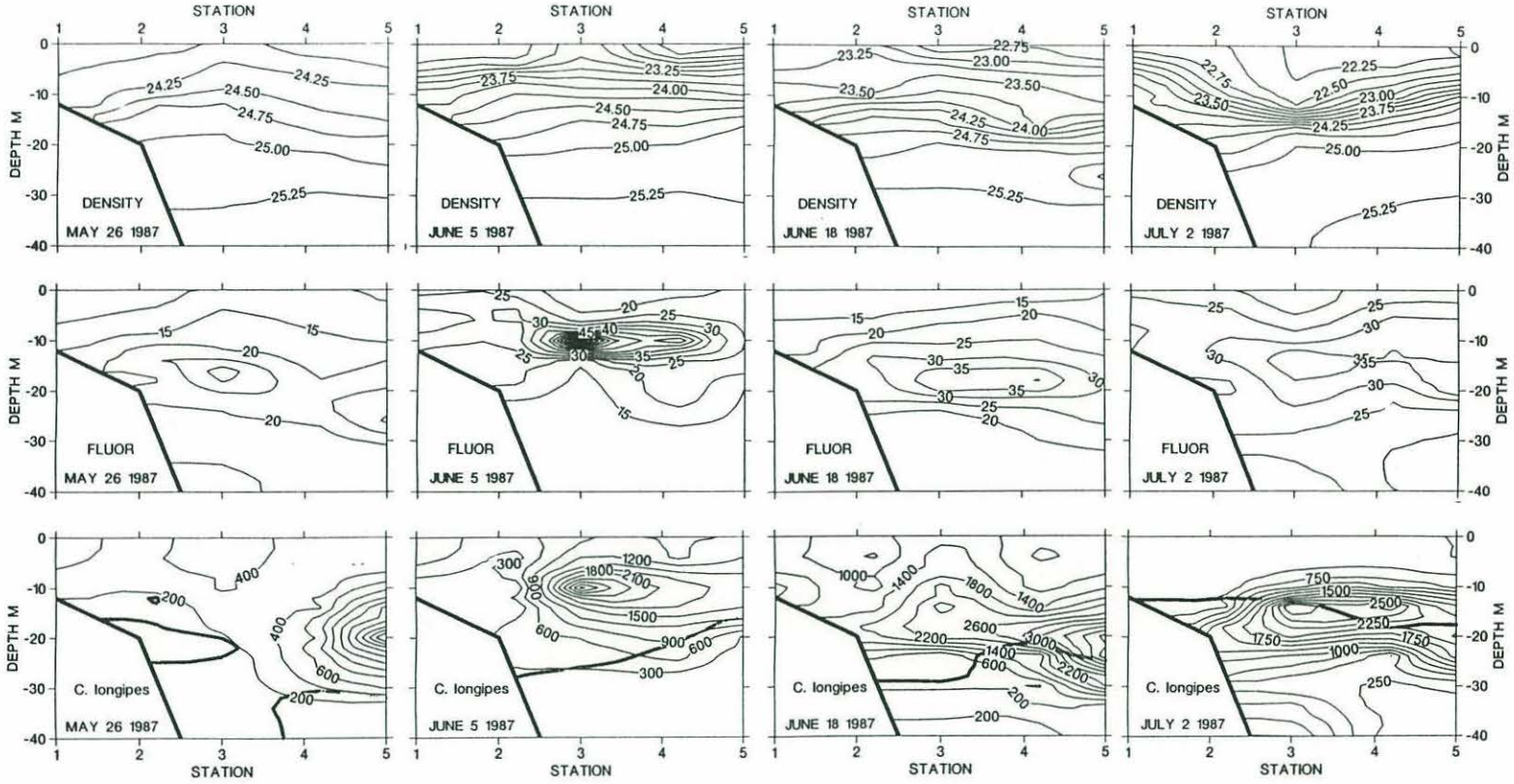
STATION
DEPTH M
DENSITY
MAY 26 1987
DENSITY
JUNE 5 1987
DENSITY
JUNE 18 1987
DENSITY
JULY 2 1987
FLUOR
MAY 26 1987
FLUOR
JUNE 5 1987
FLUOR
JUNE 18 1987
FLUOR
JULY 2 1987
C. longipes
MAY 26 1987
C. longipes
JUNE 5 1987
C. longipes
JUNE 18 1987
C. longipes
JULY 2 1987

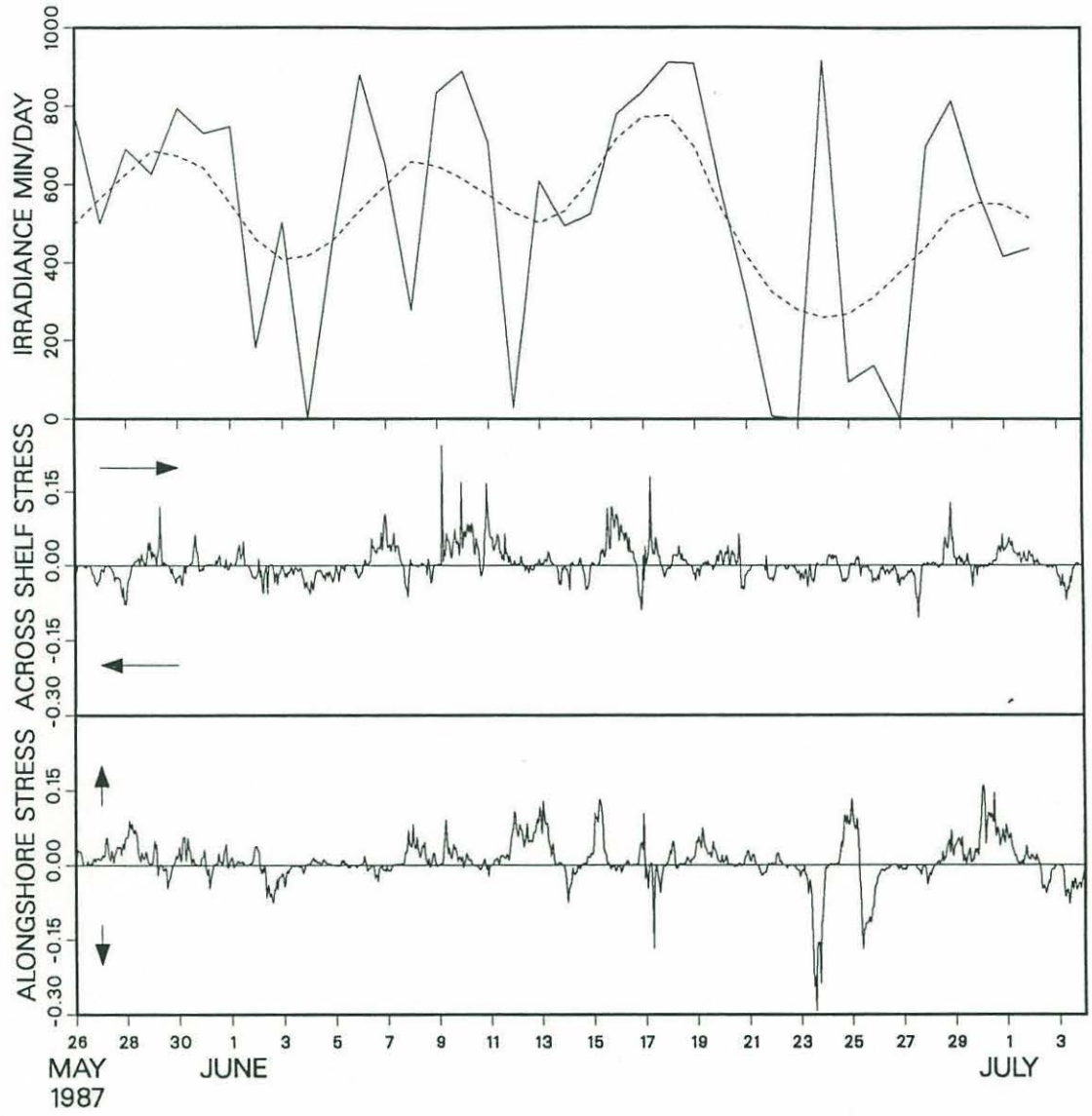

Figure 3-3. The top panel shows the number of minutes of clear sunlight measured each day at Boston (solid line), and the same data smoothed using objective analysis (dashed line), for the dates shown on the bottom axis. The middle and bottom panels show the wind stress at the Isles of Shoals (near Station 2). The stresses have been decomposed into cross-shore stress (middle panel, Pa), and long-shore stress (bottom panel, Pa). The arrows at the left of the stress plots show the direction the stress would act, given a straight coastline along the vertical axis. The data are courtesy of NOAA.

The cell concentrations were always much lower inshore at Stations 1 and 2 than the offshore stations, as will be discussed below. The maximal cell densities measured were about 5000 cells l^{-1}, at Station 5 on June 18. The cell densities were highest overall on June 18; June 5 and July 2 were approximately the same with maximal cell densities of about 3500 cells l^{-1} at Station 3. The heavy line on the cell concentration panels is the 0.5 µg-at N l^{-1} contour of nitrate+nitrite. This isopleth roughly indicates the location of the nitracline.

The greatest increase in cell density occurred at 10 m depth at Station 3 between May 26 and June 5. The average net population growth rate, r, can be calculated from the change in cell concentration, C, over a time interval Δt, from:

$$r = \frac{1}{\Delta t} \ln\left(\frac{C}{C_o}\right). \qquad (3\text{-}1)$$

If we attribute this increase solely to *in situ* growth of a stationary pattern, the average net population growth rate over this period was 0.19 d^{-1}. This calculation ignores any physical or biological factors other than exponential growth. As we discuss in the modelling section, however, it is likely that physical transport played a role in the increase in cell concentration.

For any given cruise, the cell density maximum at each station lay along the same isopycnal. For the May 26, June 18 and July 2 cruises, this was σ_T = 24.75. On June 5, the cells were found at a lower density, σ_T = 24.25. This change in density was due to freshening by rain on June 1. The cells show a strong association with the vertical gradient of density: on all cruises, the cell maximum was found within the near-surface maximum of N, the Brünt-Väisälä frequency. The Brünt-Väisälä frequency is a measure of the vertical gradient of density:

$$N = \left(-\frac{g}{\rho} \frac{\partial \rho}{\partial z} \right)^{\frac{1}{2}} \qquad (3\text{-}2)$$

where ρ is the density, and g the acceleration due to gravity. Where N is large, the water column is stable and resistant to vertical mixing. Thus the cells were found in the deepest stable region of the seasonal pycnocline. One example of this relation is shown in Figure 3-4, where the vertical profiles of N^2, fluorescence and *Ceratium longipes* of June 5 at Station 3 are plotted together. The strong relationship of fluorescence with N^2 is particularly apparent in this case. It is also apparent that the cells tended to be found near the 0.5 μgat l^{-1} isopleth of nitrate+nitrite (heavy line on the *C. longipes* panels in Figure 3-2). Thus the cells within the pycnocline were also in close proximity to the nitracline.

MODEL

One approach towards a better understanding of the physical and biological processes leading to the spatial and temporal distribution of *Ceratium longipes* is the formulation of a mathematical model. Such a model is a concise statement of a hypothesis including such processes as are deemed important, which can be tested against the field data. To formulate such a model, we must first decide which processes are to be included, and which data are to be used as a test.

Our approach is to use the simplest possible model which gives a reasonable fit to the data. This will minimize the number of parameters, and increase the robustness of the model. A simple model is also more easily solved and understood than a more detailed model. However, a simple model will not give information concerning processes which have been neglected or parameterized.

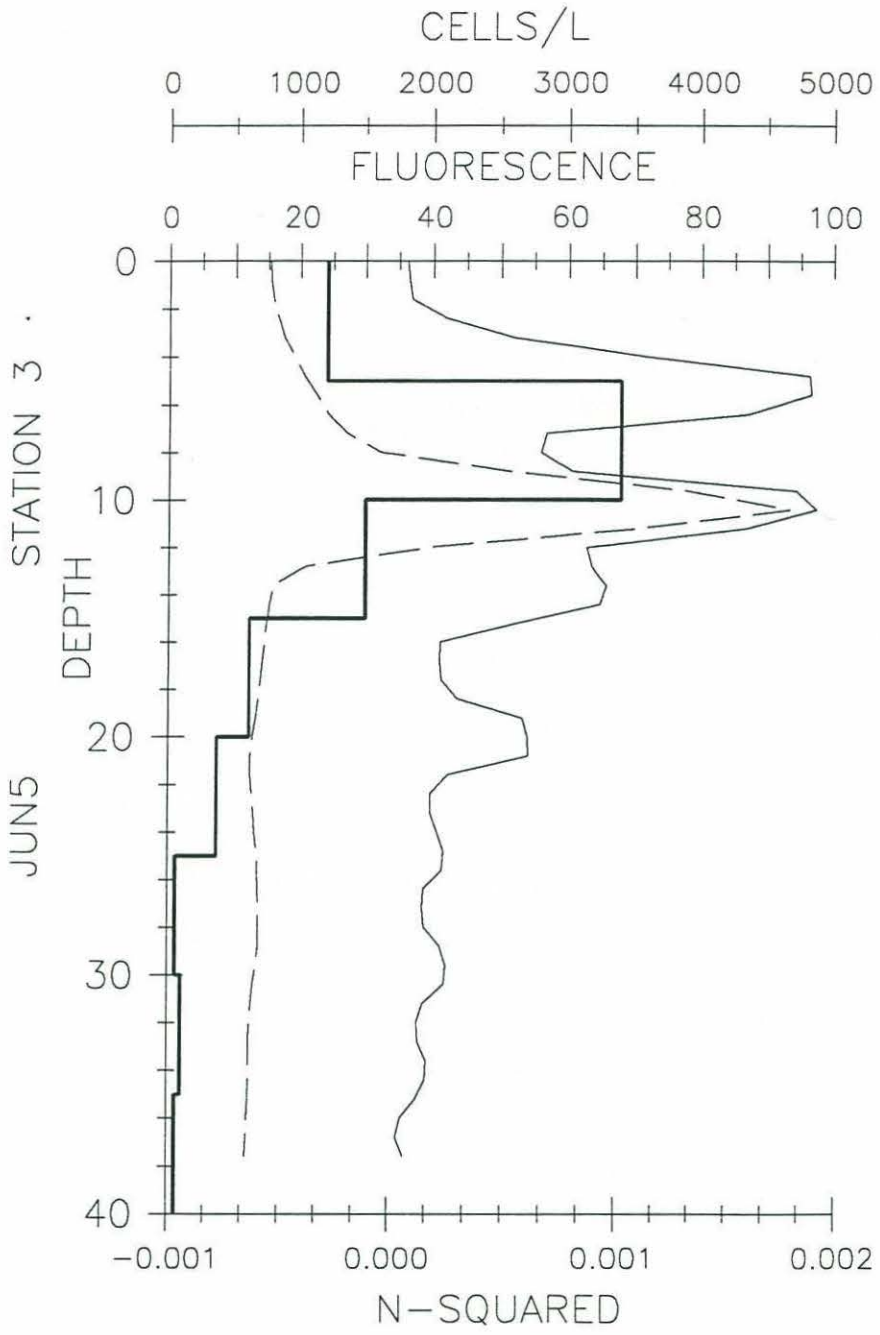

Figure 3-4. Vertical profiles of N^2 (thin solid line, s^{-2}), fluorescence (dashed line, relative units), and unsmoothed *Ceratium longipes* cell counts (thick line, cells l^{-1}) from Station 3, June 5 1987.

The physical processes which might be important in determining the phytoplankton distribution in the Gulf of Maine include advection, diffusion, tides, and wind. For a phytoplankton population of concentration C, an equation describing these processes is:

$$\frac{\partial C}{\partial t} + \mathbf{u}\cdot\nabla C - \kappa_h\left(\frac{\partial^2 C}{\partial x^2} + \frac{\partial^2 C}{\partial y^2}\right) - \kappa_v \frac{\partial^2 C}{\partial z^2} = \mu C - \beta C^2. \qquad (3\text{-}3)$$

(a) (b) (c) (d) (e) (f)

Here the local rate of change of the phytoplankton concentration (term (a)), is affected by physical forcings ((b) advection, (c) horizontal diffusion, (d) vertical diffusion) on the left hand side of the equation, and the biological terms ((e) and (f)) on the right hand side. We will now discuss each of these terms in some detail.

The biological processes to be included in the model can be diverse. The growth of the cells can be influenced by nutrients, light, temperature, and a host of other physical and biological phenomena. Cells are lost due to grazing, sinking, and physiological death. Rather than try to account for each of these processes explicitly, we use the logistic equation to describe the population growth, implicitly including processes such as nutrient limitation and grazing:

$$\frac{dC}{dt} = \mu C - \beta C^2 . \qquad (3\text{-}4)$$

The exponential growth rate of the cells is μ (time^{-1}), while βC^2 parameterizes the loss terms (grazing, death, etc.) This equation can be recast into the more familiar form:

$$\frac{dC}{dt} = \mu C \left(1 - \frac{\beta}{\mu} C\right). \qquad (3\text{-}5)$$

The "carrying capacity", i.e. the maximal number of cells which can be supported, is given by μ/β (units of cell concentration). The population grows until the carrying capacity is reached, at which point the cell concentration no longer increases. In this formulation the carrying capacity is not ascribed to any one process; indeed, it is likely to be the result of many different processes.

It appears that 1987 was an anomalous year in the Gulf of Maine: the usual counterclockwise circulation in the gulf was either weak or absent for most of May, June and July (Brown and Irish, unpub. ms.), perhaps due to a huge freshwater runoff during April. Thus alongshore advection was probably not as strong as in other years, and will be neglected as a component of term (b) in our model (equation (3-3)).

Advection due to tides is predominantly barotropic, and should not affect the cross-shore distribution of cells at lowest order. However, a shoaling bottom can increase the effects of tidally-induced bottom friction inshore. We have never observed tidally-generated fronts in this region; the tidal currents are too weak to effect significant mixing. Bottom friction may still be important to the cells, however. Rather than specify tidal currents explicitly, we will include bottom friction implicitly in our inshore boundary condition (see below), and simplify the model by neglecting tidal forcing.

Wind-driven flows can be extremely important in determining the distributions of phytoplankton and hydrographic variables in this region (Chapters 4 and 5). The alongshore wind stress has the greatest effect on the across-shelf water motions, and may have influenced the movement of the patch of *Ceratium longipes* from offshore to inshore. To assess the effects of the alongshore wind stress on the two-dimensional across-shelf phytoplankton distributions, we ran a simple two-layered model of wind-driven coastal upwelling and downwelling, similar to that of Csanady

(1973). Wind speed and direction measured at the Isles of Shoals (approximately Station 2), were converted to wind stresses (Figure 3-3) using the formula of Large and Pond (1981). The model was forced with a range of magnitudes and durations of steady wind stress.

The wind-forced model generated maximal horizontal velocities of ~10 cm s^{-1}, and vertical velocities of ~.0001 cm s^{-1} in response to a sustained 0.1 Pa wind stress. From Figure 3-3, it is apparent that the alongshore wind stress is seldom >0.1 Pa for more than a few hours, and is usually <0.05 Pa. For the upwelling-favourable wind event of June 9-13, the across-shore displacement of the surface layer was estimated to have been ~15 km in the offshore direction. This displacement is in the opposite direction than the movement of the *Ceratium longipes* population, and occurred after the population increase inshore. No strong wind events occurred between the May 26 and June 5 cruises, when the bulk of the inshore increase in *C. longipes* occurred. From this model we concluded that the vertical and horizontal currents generated by the alongshore wind stress were too weak to affect significantly the across-shelf distributions of *Ceratium longipes*. Based on these calculations, we will neglect wind forcing in the present model.

We are left with diffusion as the main physical process acting on the dinoflagellates. This is the same conclusion arrived at by Kierstead and Slobodkin (1953), who explored the balance of growth and diffusion in a model of phytoplankton patches. Vertical diffusion may cause some local variations in across-shelf cell density, but at large scales these should be smoothed by horizontal diffusion. We will assume vertical diffusion to be relatively unimportant in determining the across-shelf cell distributions, and specify only the horizontal component of diffusion.

Based on the above discussion, we will neglect advection, wind forcing, and vertical diffusion in this model. With the assumption of

a homogeneous alongshore distribution of cells, equation (3-3) becomes

$$\frac{\partial C}{\partial t} - \kappa \frac{\partial^2 C}{\partial x^2} = \mu C - \beta C^2. \qquad (3\text{-}6)$$

This describes the growth and diffusion of a limited population along a one-dimensional (across-shelf) domain. This equation is also used in genetics, where it is known as Fisher's equation (Levandowsky, 1979). Lande et al. (1989) used a very similar model to estimate phytoplankton population growth rates from vertical profiles of cell density and turbulence.

Two parameters are critical to the behaviour of this model: $\kappa/L^2\mu$, and μ/β. The first describes the balance between the diffusion, κ, over an across-shelf length scale L, and the growth. At steady state, growth will balance diffusion, and the cell concentrations will not vary. For a length scale, L, of 20 km (see below), a "typical" κ is 15 $m^2\ s^{-1}$ (Okubo, 1971). A growth rate, μ, of 0.1 d^{-1} gives $\kappa/L^2\mu$ of approximately 0.03. This low value indicates a growth-dominated system, i.e. diffusion should play a minor role in determining the cell distribution at large spatial scales.

The solution of equation (3-6), requires two boundary conditions. Since we have no information about the population density offshore of Station 5, we have made the assumption that the cell concentration beyond the boundary is equivalent to Station 5, i.e.

$$\frac{\partial C(L,t)}{\partial x} = 0. \qquad (3\text{-}7)$$

Further investigation showed the model to be relatively insensitive to the choice and location of this boundary condition, and to the initial cell concentrations beyond Station 5.

The inshore population of *Ceratium longipes* tended to be relatively low at Stations 1 and 2 (Figure 3-2). The isopycnals which harboured the peak cell concentrations always intersected the bottom between Stations 1 and 2. Following Kierstead and Slobodkin (1953), the model cell concentration was specified at Station 2 to be an arbitrarily low value, i.e.

$$C(0,t) = 2.5 \times 10^6 \text{ cells } m^{-2}. \qquad (3\text{-}8)$$

The domain of the model thus extends from Station 2 to Station 5, a distance of approximately 20 km (=L).

The choice of the boundary condition (3-8) is critical in determining the spatial structure of the steady-state solution. A reflecting, or no-flux boundary condition such as (3-7) would imply that the cells could grow over the whole domain. However, such a boundary condition would require a spatially-varying density dependence or growth rate to allow the model to fit the data (see below). The incorporation of either of these functional forms would require the specification of some relatively arbitrary and unknown parameters. We have no evidence that either of these assumptions is justified, and so use the simplest form which will allow a fit of the model to the data. Interpretation of this boundary condition (equation 3-8) in terms of the field situation will be explored in the discussion.

We must now specify the data to which the model is to be compared. Since we are using a one-dimensional (across-shelf) model, we must convert our two-dimensional cell concentrations to a one-dimensional form. The four methods used all gave similar results. The methods were to:

1) integrate the cell concentrations down to 30 m for each station, i.e. calculate the total number of cells in a column of water;

2)calculate the average cell concentration at each station;
3)use the maximum cell concentration at each station;
4)calculate the average cell concentration within a density interval which contained the population peak.

The results of method (1) should approximate the maximal number of cells which could be supported by the system at each station, and it is these values to which the model will be compared. The results of method (2) are slightly biased by deep (>30 m) samples which contained few cells. Methods (3) and (4) ignore the losses due to sinking or vertical mixing, and may have problems with variable layer thickness. The shape of the cross-shelf distributions from each method was practically identical. The first method was chosen, as explained above, but any of the methods could have been used, and would have given similar model results.

We estimated β from the growth rate and the maximum number of cells seen (a conservative estimate of the carrying capacity). The various methods used to calculate the one-dimensional cell concentrations would suggest different values for the carrying capacity. These differences arise through the different weightings of the water which is not occupied by *Ceratium longipes*. Since the cells are concentrated into a vertically narrow band, the best estimate for the actual carrying capacity might be to consider only the volume of water which the cells occupy (approximately method 4). This assumes that the rest of the water column is not a suitable habitat. However, the whole water column is involved in maintaining the population, through mixing of nutrients, light, etc., thus we consider the cell concentration supported by a column of water.

The initial condition for the model was a Gaussian function, fit by eye to the data of May 26, 1987 (Figure 3-5). Equations (3-6), (3-7), and (3-8) were solved numerically using a time step of 0.1 d, and a grid spacing of 0.42 km. A forward-time, centred-space scheme was used to solve the equation.

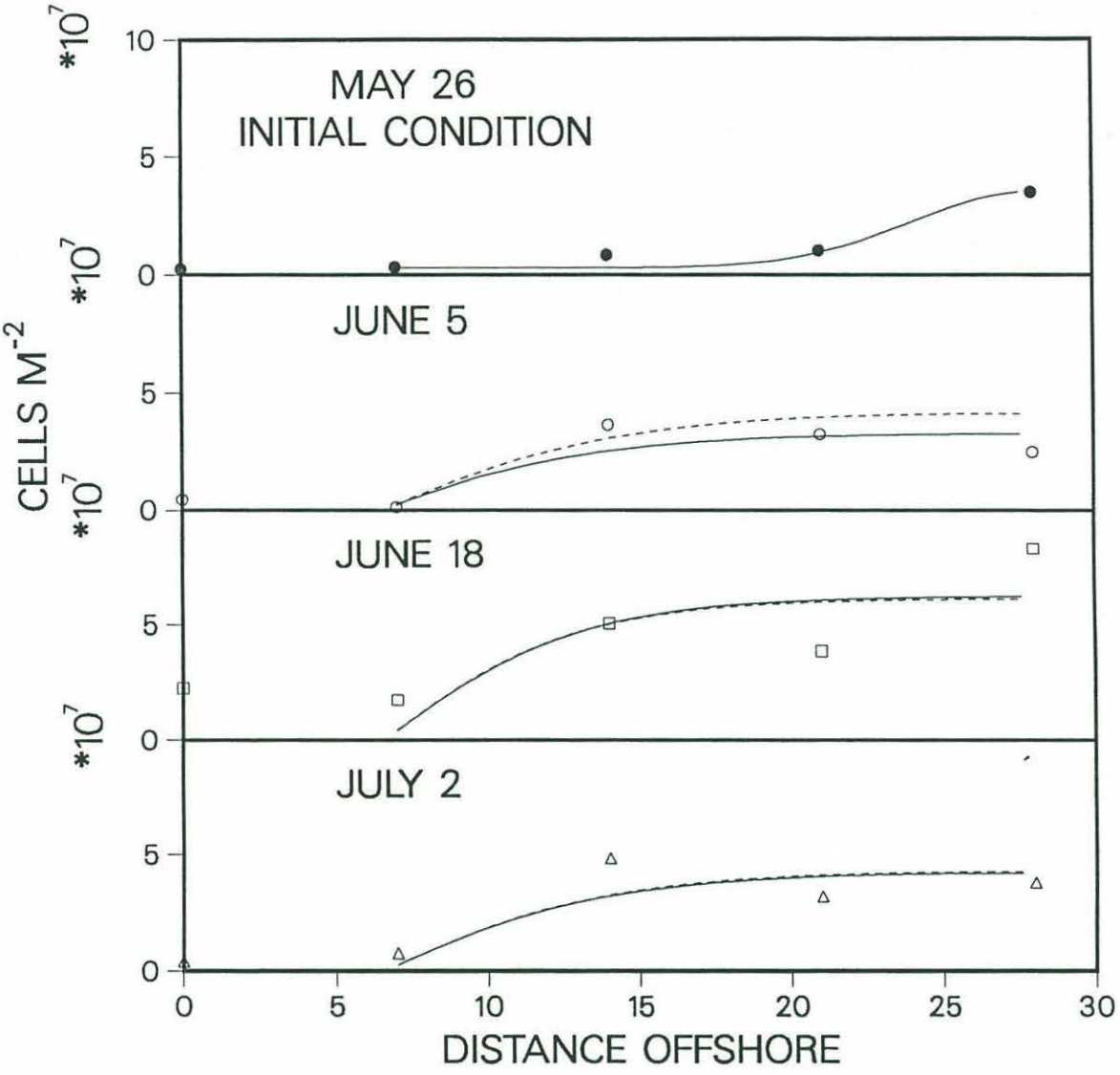

Figure 3-5. These graphs show the field data (points) and the model results (curves) for the dates shown in each panel. The field data have been obtained using method (1) as described in the text. The solid curves are the model solutions using the unsmoothed irradiance data of Figure 3-3, while the dashed curves are the solutions using the smoothed irradiance data. The initial condition for the model is shown in the top panel (May 26).

In initial runs of the model, it became apparent that steady state was reached in about 10 model days. Thus subsequent changes in the population density such as the increase from June 5 to June 18, and the decrease from June 18 to July 2 (Figure 3-5) could not be simulated without further time-dependence in the model. It was noted that the irradiance, measured as minutes of sunlight per day at Boston, showed considerable variability during the month of June (Figure 3-3). We used this as a forcing for the model as follows:

$$\mu(t) = \mu_{max} \frac{I(t)}{I_{max}}, \qquad (3\text{-}9)$$

where $\mu(t)$ is the time-dependent growth rate, μ_{max} is the maximum possible growth rate, I_{max} is the maximum possible number of minutes of sunlight, and $I(t)$ is the measured minutes of sunlight each day. Because of the form of the model, we could have chosen to have a time-dependent carrying capacity, i.e. $\beta(t)$ instead of $\mu(t)$, without changing the model results. This formulation does not necessarily imply that the growth rate is light-limited. Rather it indicates that variations in light may be responsible for some temporal variability of the population size through changes in growth rate or carrying capacity. Such changes may occur through, for example, temperature changes, stratification changes, light-dependence of grazing, light-dependence of growth, or light-dependent swimming behaviour of the *Ceratium* cells.

The parameters μ_{max} and β were found by fitting the model to the data from June 5. The model was then allowed to continue running until July 2, with all parameters fixed. The standard run is shown in Figure 3-5, along with the data to which the model was fit. The parameters for this run were $\mu_{max} = 0.17\ d^{-1}$, $\beta = 1 \times 10^{-5}$ $(cells/l)^{-1}\ d^{-1}$, $\kappa = 15\ m^2\ s^{-1}$, and $I_{max} = 920$ min. The model appears to describe the gross spatial variability of the cell concentrations for each cruise, and the long-term variability of the population density.

The model responds very quickly to changes in the light regime. Since it is unlikely that significant changes in the cell densities occur in the field over a day, the model was forced with the smoothed light regime shown in Figure 3-3. This irradiance time series has changes with a characteristic period of about 10 days. Using the standard parameter set and the smoothed irradiance, the model results were almost identical with the standard run (dashed curve in Figure 3-5). A time series of the cell concentrations at Station 3 (14 km offshore) is shown in Figure 3-6. It can be seen that the model forced with the smoothed irradiance data shows slow, smooth fluctuations in cell density. Smoothing the irradiance data over longer timescales caused the model to begin to depart from the field data. This indicates that the cells in the field may be responding to environmental changes on the time scale of about 10 days. Given the growth rates used in the model, this corresponds to approximately two generations of cells.

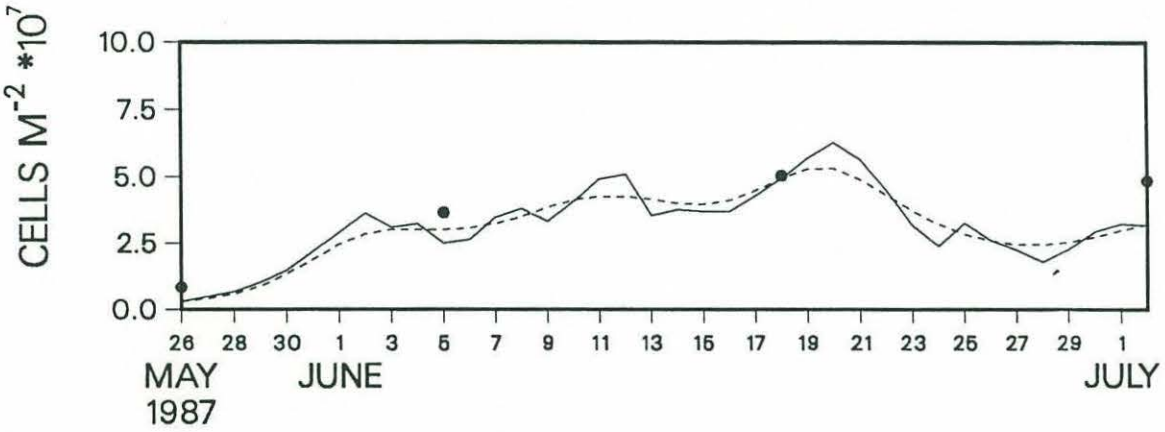

Figure 3-6. Here the model time series at Station 3 (14 km offshore) is plotted for unsmoothed (solid line) and smoothed (dashed line) irradiance data. The integrated field cell counts are shown by the dots.

DISCUSSION

A complex dinoflagellate bloom appears to be described by a simple modification of a model traditionally used to infer scales of phytoplankton patchiness (Kierstead and Slobodkin, 1953; Skellam, 1951). The main strength of the model presented is its ability to describe the movement of a phytoplankton bloom from offshore to inshore. This movement is consistent with horizontal diffusion of growing cells from an offshore patch. The behaviour of the model after about 10 days is dependent on the light forcing and the inshore boundary condition. The applicability of this model to a bloom in the Gulf of Maine was contingent on an unusually quiescent physical regime during the summer of 1987. Contrary to much of the literature describing dinoflagellate blooms, we can explain most of the bloom distribution without invoking swimming behaviour of the organisms.

Ceratium longipes is a common spring-summer constituent of the offshore waters of the Gulf of Maine. In one of the first detailed seasonal surveys of the phytoplankton species composition of the Gulf of Maine, Gran and Braarud (1935) found *C. longipes* to be the dominant phytoplankter in the offshore waters during May and June, in agreement with prior observations of Bigelow (1926, cited in Gran and Braarud, 1935). The maximum number of cells recorded in their survey was 4260 cells l^{-1}, at 40 m depth in June, in close agreement with the present data. The *Ceratium* population studied by Gran and Braarud (1935) was found at greater depths than those recorded in the present study; however, their vertical resolution was much less dense than the 5m sampling interval used in the present survey, and they may have missed the peak concentrations. Holligan et al. (1984a) found the distribution of *C. longipes* in the Gulf of Maine to follow the chlorophyll a patterns, with a maximum at about 20 m depth, in agreement with the present data. The cells were aggregated into a narrow layer, showing similar vertical

distributions to *C. tripos* during a catastrophic bloom in the New York Bight (Falkowski et al., 1980).

Much of the published literature concerning dinoflagellate blooms suggests that diel vertical migration of dinoflagellates is a key to their ecological success. However, Eppley et al. (1984) could not detect vertical motion of *Ceratium tripos* in a dense bloom off southern California, although diel migration of other dinoflagellates was seen. They suggest that the vertical ambit of *C. tripos* may have been so small as to be undetectable (~2 m). Heaney and Eppley (1981) have shown the migration patterns of *C. furca* to be disrupted in low nutrient conditions, such that the cells accumulated at the thermocline. This behaviour would allow them to receive adequate light, expend little energy in swimming since they are out of the mixing layer, and take advantage of whatever nutrient pulses occur from below. From Figure 3-2, it is apparent that the *C. longipes* cells in the present study tended to be found close to the 0.5 μgat l^{-1} contour of nitrate+nitrite, and within the pycnocline. This observation lends support to the hypothesis of Heaney and Eppley (1981) that the cells were optimizing the relative contributions of light, nutrients, and buoyancy. However, it is still not clear whether this response was an active depth-maintaining behaviour, or passive accumulation at the pycnocline.

The maximal specific growth rate, μ_{max}, specified for the model was 0.17 d^{-1}. However, the actual growth rate, $\mu(t)$, in the model was somewhat lower due to suboptimal irradiance. The average growth rate, $\bar{\mu}$, of the model phytoplankton can be calculated from:

$$\bar{\mu} = \frac{1}{n} \sum_{i=1}^{n} \mu_{max} \frac{I(n)}{I_{max}} \qquad (3\text{-}10)$$

where the sum is over n days. The average model growth rate using equation (3-10) was 0.1 d^{-1} from May 26 to June 5, 0.12 d^{-1} from June 5 to June 18, and 0.09 d^{-1} from June 18 to July 2. The maximal

net population growth rate, r, calculated from the field data using equation (3-1) was 0.19 d^{-1} for the period May 26-June 5 at Station 3. The net population growth rate, r, calculated from the model output using equation (3-1) was about 0.2 d^{-1} for the same period, in good agreement with the field data, but significantly higher than the modelled specific rate of growth, μ. These values for the net population growth rate do not take into account any physical factors such as diffusion which could enhance or reduce the local population density. Elbrächter (1973) calculated growth rates for *Ceratium longipes* in Kiel Bay to be between 0.05 d^{-1} and 0.14 d^{-1}, using the frequency of dividing cells. Weiler (1980), and Weiler and Chisholm (1976) also used this method, and found growth rates of 0.09 d^{-1} to 0.12 d^{-1} for various species of *Ceratium* in the open ocean. Eppley et al. (1984) found growth rates of 0.25 d^{-1} for *Ceratium tripos* in a bloom off the coast of southern California. These measured growth rates are equivalent to μ, the specific growth rate, rather than r, the net population growth rate. Thus the specific growth rates predicted by the model are reasonable.

The model depends on a proxy estimate of the amount of sunlight received during a day. As stated above, this dependence can be interpreted as acting through variations in the growth rate, carrying capacity, or both. Although this formulation does not give insight to the specific mechanisms controlling the population density, it does suggest that the cells are responding to variations in light, or processes correlated with the long-term light fluctuations.

We have assumed a constant diffusion coefficient of 15 $m^2 s^{-1}$. Although values of $\kappa/L^2\mu$ suggest that the system is growth-dominated, diffusion is critical in determining the shape of the bloom offshore of Station 2. A low value of κ will cause a sharp increase in cell density near Station 2, while a large κ will give a gradual increase in cell density offshore.

Without the inshore boundary condition, the model would tend toward a homogeneous across-shelf cell density. The number of cells lost through the inshore boundary in the model is very small: with such a low growth rate, a low loss rate of cells can still lead to large spatial variability. The inshore boundary condition used was the only one which would allow the model to fit the data, thus the model indicates the importance of processes which lower the cell concentrations inshore. Such processes may include reduction of growth due to enhanced turbulence generated by bottom friction, toxic substances leached from the sediments, a cline in some unmeasured property such as biologically-available iron, or restriction of the domain of optimum growth due to intersection of the pycnocline with the bottom. Unfortunately, at this stage we cannot distinguish between these possibilities.

The model was found to be relatively insensitive to the offshore boundary condition, or the initial condition offshore of Station 5. Although we have no information about the cell concentrations offshore of Station 5, the data of Gran and Braarud (1935) suggest that our assumption of no gradient in cell concentration offshore of Station 5 is valid. The cell concentrations recorded by Gran and Braarud (1935) well offshore of our Station 5 are approximately equal to those seen at Station 5, with a peak of just over 4000 cells l^{-1}.

The model appears to describe the gross spatial and temporal variability of the cell densities quite well. However, the smaller scale variability cannot be accounted for by such simple dynamics. Thus nutrient input due to internal waves, small-scale wind-driven upwelling, downwelling or mixing, advection and buoyancy effects are ignored. We suggest that these and other processes are not as important in generating the gross features of the *Ceratium* distribution as growth and along-isopycnal mixing. The results of the model were independent of the method used to calculate the one-dimensional *Ceratium longipes* distributions. This was due to

the fact that the cells were concentrated into a vertically narrow band; thus different methods of calculating the integrated cell concentrations all gave the same shape of distribution, but implied different weightings of the surface and deep waters.

The along-isopycnal diffusion of a growing dinoflagellate population described by the model is probably a common feature of the world's oceans. In many cases, however, the simple diffusive process is dominated by factors such as advection and shear, making application of the model impossible. In the present case, however, the model appears to be consistent with the anomalous physical regime of the Gulf of Maine during the summer of 1987.

The models of Kierstead and Slobodkin (1953), and Skellam (1951) (KISS models) were designed to examine the scales of phytoplankton patchiness due to growth and diffusion. We have modified the KISS model by adding a time-dependent growth rate and a carrying capacity, in order to fit the model to *Ceratium longipes* distributions in the Gulf of Maine. Lande et al. (1989) used a similar model without the carrying capacity to estimate net population growth rates, r, from vertical profiles of phytoplankton biomass. Including the carrying capacity in the present model has allowed us to estimate the specific species growth rate, μ (growth), as opposed to the net population growth rate, r (growth-mortality). It has given us considerable insight into the dynamics governing the population growth and distribution: we have inferred a growth rate for *Ceratium longipes*, and shown evidence for light-dependent fluctuations in population density. Because we have based the model structure on the data to which it was fit, we cannot perform a rigorous test of its validity. Thus, until we have another realization of the field data, we cannot reject the model as a hypothesis. However, it has proved a valuable diagnostic tool for understanding the dynamics of a bloom of *Ceratium longipes* in the Gulf of Maine.

LITERATURE CITED

Brown, W.S. and J.D. Irish. 1990. The annual evolution of geostrophic flow in the Gulf of Maine. Unpublished manuscript submitted to J. Geophys. Res.

Butman, B. 1976. Hydrography and low frequency currents associated with the spring runoff in Massachusetts Bay. Mem. Soc. R. Sci. Liège 6:247-275.

Carreto, J.I., H.R. Benavides, R.M. Negri and P.D. Glorioso. 1986. Toxic red-tide in the Argentine Sea. Phytoplankton distribution and survival of the toxic dinoflagellate *Gonyaulax excavata* in a frontal area. J. Plankton Res. 8:15-28.

Csanady, G.T. 1973. Wind-induced baroclinic motions at the edge of the continental shelf. J. Phys. Oceanogr. 3:274-279.

Elbrächter, M. 1973. Population dynamics of Ceratium in coastal waters of the Kiel Bay. Oikos Suppl. 15:43-48.

Eppley, R.W., F.M. Reid, J.J. Cullen, C.D. Winant and E. Stewart. 1984. Subsurface patch of a dinoflagellate (*Ceratium tripos*) off southern California: patch length, growth rate, associated vertical migrating species. Mar. Biol. 80:207-214.

Falkowski, P., T.S. Hopkins and J.J. Walsh. 1980. An analysis of factors affecting oxygen depletion in the New York Bight. J. Mar. Res. 38:479-506.

Franks, P.J.S., D.M. Anderson and B.A. Keafer. 1989. Fronts, upwelling and coastal circulation: spatial heterogeneity of *Ceratium* in the Gulf of Maine. In, "Red Tides: Biology, Environmental Science, and Toxicology", T. Okaichi, D.M. Anderson and T. Nemoto (eds.) Elsevier, New York. 153-156.

Garrett, C.J.R., J.R. Keeley and D.A. Greenberg. 1978. Tidal mixing versus thermal stratification in the Bay of Fundy and the Gulf of Maine. Atm. Oc. 16:403-423.

Gran, H.H. and T. Braarud. 1935. A quantitative study of the phytoplankton in the Bay of Fundy and the Gulf of Maine (including observations on hydrography, chemistry and turbidity). J. Biol. Bd. Can. 1:279-467.

Heaney, S.I. and R.W. Eppley. 1981. Light, temperature and nitrogen as interacting factors affecting diel vertical migrations of dinoflagellates in culture. J. Plankton Res. 3:331-344.

Holligan, P.M., W.M. Balch and C.M. Yentsch. 1984a. The significance of subsurface chlorophyll, nitrite and ammonium maxima in relation to nitrogen for phytoplankton growth in stratified waters of the Gulf of Maine. J. Mar. Res. 42:1051-1073.

Holligan, P.M., P.J.leB. Williams, D. Purdie and R.P. Harris. 1984b. Photosynthesis, respiration and nitrogen supply of plankton populations in stratified, frontal and tidally mixed shelf waters. Mar. Ecol. Prog. Ser. 17:201-213.

Kamykowski, D. 1981. The simulation of a Southern California red tide using characteristics of a simultaneously-measured internal wave field. Ecol. Modelling 12:253-265.

Kierstead, H. and L.B. Slobodkin. 1953. The size of water masses containing plankton blooms. J. Mar. Res. 12: 141-147.

Lande, R., W. Li, E. Horne and M. Wood. 1989. Phytoplankton growth rates estimated from depth profiles of cell concentration and turbulent diffusion. Deep-Sea Res. 36:1141-1159.

Large, W.S. and S. Pond. 1981. Open ocean momentum flux measurements in moderate to strong winds. J. Phys. Oceanogr. 11:324-336.

Levandowsky, M. 1979. On a class of mathematical models for Gymnodinium breve red tides. In, "Biochemistry and Physiology of Protozoa Vol. 1", M. Levandowsky and S.H. Hunter (eds.) Academic Press, New York. pp. 394-402.

Levy G. and R.A. Brown. 1986. A simple, objective analysis scheme for scatterometer data. J. Geophys. Res. 91:5153-5158.

Pingree, R.D., P.M. Holligan and G.T. Mardell. 1978. The effects of vertical stability on phytoplankton distributions in the summer on the northwest European Shelf. Deep-Sea Res. 25:1011-1028.

Okubo, A. 1971. Oceanic diffusion diagrams. Deep-Sea Res. 18: 789-802.

Skellam, J.G. 1951. Random dispersal in theoretical populations. Biometrika. 38:196-218.

Strickland, J.D.H. and T.R. Parsons. 1972. A practical handbook of seawater analysis. Fisheries Research Board of Canada. Ottawa. 310 pps.

Tyler, M.A. 1984. Dye tracing of a subsurface chlorophyll maximum of a red-tide dinoflagellate to surface frontal regions. Mar. Biol. 78:285-300.

Weiler, C.S. 1980. Population structure and in situ division rates of *Ceratium* in oligotrophic waters of the North Pacific central gyre. Limnol. Oceanogr. 25:610-619.

Weiler, C.S. and S.W. Chisholm. 1976. Phased cell division in natural populations of marine dinoflagellates from shipboard cultures. J. exp. mar. Biol. Ecol. 25:239-247.

Yentsch, C.S. and N. Garfield. 1981. Principal areas of vertical mixing in the waters of the Gulf of Maine, with reference to the total productivity of the area. In, "Oceanography From Space", J.F.R. Gower (ed). Plenum Press, NY. pp. 303-312.

CHAPTER 4

ALONGSHORE TRANSPORT OF A PHYTOPLANKTON BLOOM IN A BUOYANCY CURRENT: *Alexandrium tamarense* IN THE GULF OF MAINE

Pooh was very proud when he heard this, and he felt that the Heffalump was as good as caught already, but there was just one other thing which had to be thought about, and it was this. Where should they dig the Very Deep Pit?

Piglet said that the best place would be somewhere where a Heffalump was, just before he fell into it, only about a foot farther on.

A.A. Milne
Winnie-the-Pooh

ABSTRACT

Little is known about the mechanisms controlling blooms of the toxic dinoflagellate *Alexandrium tamarense*, and the concomitant patterns of shellfish toxicity in the southwestern Gulf of Maine. During a series of cruises over three years, various hydrographic parameters were measured to examine the physical factors affecting the distribution and abundance of dinoflagellates along this coast. In two years when toxicity was detected in the southern part of this region, *A. tamarense* cells were apparently transported into the study area between Portsmouth and Cape Ann, Massachusetts, in a coastally trapped buoyant plume. This plume appears to have been formed off Maine by the outflow from the Androscoggin and Kennebec Rivers. Flow rates of these rivers, hydrographic sections, and satellite images suggest that the plume had a duration of about a month, and extended alongshore for several hundred kilometers. The distribution of cells followed the position of the plume as it was influenced by wind and topography. Thus when winds were downwelling-favourable, cells were moved alongshore to the south, and were held to the coast; when winds were upwelling-favourable, the plume sometimes separated from the coast, advecting the cells offshore.

The alongshore advection of toxic cells within a coastally trapped buoyant plume can explain the details of the temporal and spatial patterns of shellfish toxicity along the coast. The general observation of a north-to-south temporal trend of toxicity is consistent with the southward advection of the plume. In 1987 when no plume was present, *Alexandrium tamarense* cells were scarce, and no toxicity was recorded at the southern stations. A testable hypothesis was formulated explaining the development and spread of toxic dinoflagellate blooms in this region. The hypothesis included: source *A. tamarense* populations in the north, possibly associated with the Androscoggin and Kennebec estuaries; a relationship between toxicity patterns and river flow volume and

timing of flow peaks; and a relationship between wind stresses and the distribution of low salinity water and cells. Local, *in situ* growth of dinoflagellates can be an important factor initiating toxic dinoflagellate blooms. However, these data demonstrate the significant role of alongshore transport of established populations of *Alexandrium tamarense* in controlling the location and timing of PSP outbreaks in May and June along the southwestern coast of the Gulf of Maine.

INTRODUCTION

Blooms of the toxic dinoflagellate *Alexandrium tamarense*[1] are a recurrent feature of the southwestern coast of the Gulf of Maine. Blooms of this dinoflagellate have occurred since 1958 between the months of May to October along the coast of Maine, and, with the exception of 1987, since 1972 along the north shore of Massachusetts. The economic importance of locating, and restricting the harvest of toxic shellfish has led to the development of regional monitoring programs (e.g. Shumway et al., 1988). These programs have demonstrated that toxicity in the mussel *Mytilus edulis* is a good indicator of the presence of *Alexandrium tamarense* populations. The toxic shellfish outbreaks typically show a north-to-south progression (Chapter 5); for example, a twenty-day lag is common between the first measurable toxicity at Lumbos Hole, Maine, and the first occurrence of toxicity at Cape Ann, Massachusetts.

This pattern, also described by Hurst and Yentsch (1981) and Shumway et al. (1988), has been assumed by some to reflect a southward sequence of local blooms of *Alexandrium tamarense*. Mulligan (1973, 1975), Hartwell (1975), and Seliger et al. (1979) have all suggested that nearshore, localized blooms of *A. tamarense* in the late summer are initiated by wind-driven upwelling. These studies were motivated by the first occurrence of PSP along the southern Maine, New Hampshire, and Massachusetts coasts in September, 1972. The origin of these blooms was linked to the passage of hurricane Carrie, which delivered up to 8.5 cm of rain with winds to the south of up to 15.5 m s^{-1}. Hartwell (1975)

---

[1] *Alexandrium tamarense* and *Alexandrium fundyense* were formerly included in the genera *Protogonyaulax* or *Gonyaulax* but are now accepted as *Alexandrium* (Steidinger and Moestrup, 1990). Both species bloom in the Gulf of Maine (Anderson, unpub. data), but since discrimination between them is impossible for large-scale field programs or when referring to shellfish toxicity, only the more familiar name *Alexandrium tamarense* will be used here.

suggested that an established bloom of *A. tamarense* was swept from the Bay of Fundy by the strong winds, and carried along the Massachusetts coast. It was further hypothesized that subsequent late-summer blooms of *A. tamarense* in the Cape Ann region were caused by germination of cysts in local waters, followed by growth and accumulation in response to wind-driven upwelling systems. These studies did not, however, directly address the question of the source of PSP toxicity in the spring (April-June).

The work of Martin and Main (1981) was one of the first studies designed to identify the source of the annual toxic outbreaks. Their field work just north of Cape Ann, performed almost a decade after the initial PSP outbreak at Cape Ann, led them to conclude that *Alexandrium tamarense* cells were advected into the study area from the north by the prevailing currents. This was the first suggestion that episodes of toxicity in the spring were related to alongshore advection of cells rather than local growth. They inferred a source of cells in Maine waters, but gave no further clues as to the vehicle for the alongshore advection.

Through drifter release experiments, Graham (1970) concluded that wind-driven upwelling and estuarine discharge are important forcings of alongshore currents in this region. Tidal forcing is also an important component of the physical dynamics of the coastal Gulf of Maine (Garrett et al., 1978; Greenberg, 1979; Loder and Greenberg, 1986). Balch (1986) noted a weak association of PSP outbreaks with the lunar cycle, and suggested that the cells may be controlled by the spring-neap tidal cycle. Yentsch et al. (1986) explored the possibility of the association of blooms of *A. tamarense* with tidal fronts as has been observed in other regions (e.g. Pingree et al., 1975), but presented no evidence of such an association for the coastal Gulf of Maine. Holligan et al. (1984) found enhanced concentrations of *A. tamarense* ~35 km offshore of the Maine coastline, but did not speculate on the causes of the horizontal patchiness.

Clearly, the coastal waters of the Gulf of Maine are subject to a variety of physical forcings, including wind-driven motions, estuarine discharge, and tidal mixing. Against this background is the observation that PSP toxicity progresses in a north-to-south pattern with time. The purpose of the present study was to elucidate the factors controlling the distribution of *Alexandrium tamarense* populations, and the concomitant shellfish toxicity, along the Massachusetts coast. Based on sampling over three bloom seasons, 1987-1989, we demonstrate that the blooms of *A. tamarense* seen in the Cape Ann area were not of local origin, but were advected alongshore in a coastally trapped buoyant plume created by enhanced river outflow in Maine.

METHODS

The majority of the sampling during 1987-1989 was along a six-station transect extending from Portsmouth, NH, 30 km into the Gulf of Maine (Figure 4-1, Stations 0-5). Stations were approximately 7 km apart, with depths of 10 m at Station 0 (in Portsmouth harbor) to 175 m at Station 5. The ship used was the 45' vessel R/V Jere A. Chase. In 1989, the charter vessel (C/V) Unity was used on three occasions (May 19, June 8, June 27) to perform more detailed horizontal mapping of the hydrography and cell concentrations. This vessel was capable of speeds of 18 kt, permitting surveys of the region from Cape Ann MA, to Portsmouth NH, in 8 hrs, covering 25 stations (Figure 4-1; Stations 0-4, and small circles).

Details of the sampling strategies and equipment are given in Appendix A. Briefly, when sampling from the R/V Jere A. Chase, a hose-pumping system was used. A "Li'l Giant" submersible pump brought water through 40 m of 2 cm i.d. garden hose which was raised from 40 m depth to the surface at 2 m min^{-1}. Water flowing at a rate of about 2.0 l min^{-1} passed through a bubble trap, and through the flow cell of a Turner Designs Model 10 fluorometer. The fluorometer was linked to a portable computer which plotted and

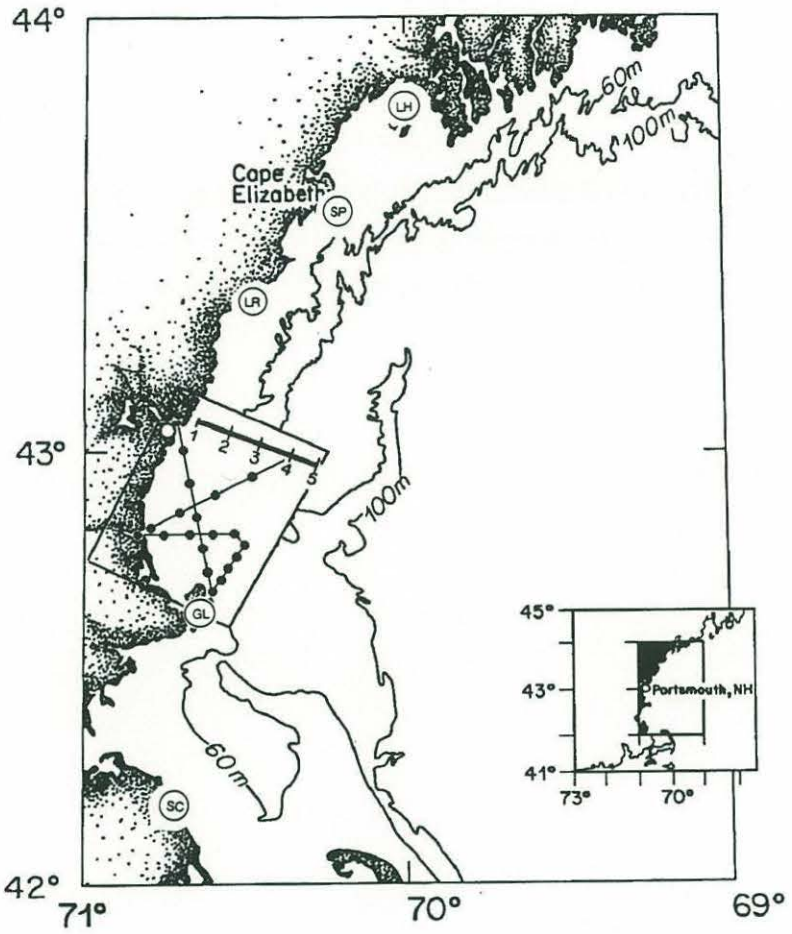

Figure 4-1. The coast of the Gulf of Maine is shown , from Casco Bay, south to Cape Cod Bay. Stations 0 to 5 comprise the regular cruise transect, sampled from 1987 to 1989. These stations are ~7 km apart. The additional stations are those sampled aboard the C/V Unity. The box indicates the region plotted in Figure 4-6. Toxicity sampling stations are LH=Lumbos Hole, SP=Spurwink River, LR=Little River, GL=Gloucester and SC=Scituate.

recorded the fluorescence every two seconds. From the fluorometer, the water passed into buckets used to integrate samples over 5 m depths. From each bucket one liter was filtered through 20 μm mesh, backwashed with 50 ml of filtered seawater, and preserved in 5% formaldehyde for cell counts, while 500 ml was filtered through GF/A filters for chlorophyll analysis. The filtrate was frozen for nutrient analyses.

Samples for cell counts were settled in 50 ml settling chambers, and counted on a Zeiss inverted microscope. Half a slide was counted if there were fewer than 200 cells, otherwise 20 fields were counted at 160X. Fluorometric chlorophyll analysis followed Strickland and Parsons method (1972), corrected for phaeopigment. Nitrate+nitrite concentrations were measured on a Technicon AutoAnalyser II, using the Technicon protocol (Method No. 158-71W/B). Measurements were in duplicate, followed by a seawater wash.

A CTD (Sea Cat Profiler, Sea-Bird Electronics) was attached below the hose inlet with sensors oriented upward in order to take the upcast data. This was necessary as the hose had to be completely submerged to prime the pump. The CTD data were smoothed using an objective mapping routine (after Levy and Brown, 1986) to remove salinity spikes. Using the transit time of the water in the hose (1.8 min), the fluorescence vs. time data were converted to fluorescence vs. depth. These data were then merged with the CTD data to examine the relationship of fluorescence with temperature and salinity. A SeaTech 25 cm path-length transmissometer was attached to the CTD during the 1988 and 1989 field seasons. The signal from this instrument was converted to beam attenuation (beam-c: m^{-1}) to facilitate comparison with the fluorescence profiles.

When sampling from the C/V Unity, vertical CTD/transmittance casts were made down to 40 m, but to minimize the time taken at each station, no hose-pumping system was

deployed. Surface (0.5 m) and 10 m water samples were taken using a 2 l Niskin bottle. Subsamples from the Niskin bottle were processed and preserved as above for cell counts.

Flow data for the Androscoggin, Kennebec and Merrimack Rivers were obtained through the United States Geological Survey. Data for station 01059000 on the Androscoggin near Auburn, ME, station 01049265 on the Kennebec River at North Sidney, ME, and station 01100000 at Lowell, MA, on the Merrimack River were analyzed.

Wind data from Logan Airport, Boston MA, were obtained through the National Climatic Data Center. These data were rotated into the coordinate system of the coast north of Cape Ann by subtracting 30°, and resolved into across and alongshore stresses using the algorithm of Large and Pond (1981).

Shellfish toxicity data were made available by the Department of Environmental Quality Engineering (MA), and the Department of Marine Resources (ME). Data from Lumbos Hole, Spurwink River and Little River (ME), and Gloucester and Scituate (MA) were processed for analysis. Differences in PSP analysis sensitivities between Maine and Massachusetts necessitated conversion of the toxicity data to binary time series: 1=toxicity present, 0=no measurable toxicity. This conversion allows comparison of the different data sets without the confounding influences of assay sensitivity and shellfish species sampled.

Nine cruises were made during 1987, 12 in 1988, and 11 in 1989. These cruises spanned the toxic dinoflagellate bloom season, from April to September, with the majority of the cruises from early May to late June. Only those cruises which occurred during the initial stages of a bloom will be described below.

RESULTS

DENSITY AND FLUORESCENCE DISTRIBUTIONS, 1988

The data of 1988 appear to represent typical May-June conditions along the southwestern coast of the Gulf of Maine, and thus are presented in detail in Figure 4-2 and 4-3. A strongly-sloping pycnocline was seen from at least May 27 to June 9 (Figure 4-2). This pycnocline intersected the bottom inshore and the surface offshore, giving a pattern typical of a water mass front. The lack of a well-mixed region inshore indicates that this was not a tidally-generated front. The pycnocline slopes in the wrong direction for a wind-driven upwelling front, while a wind-driven downwelling system would be expected to show a horizontal region of the pycnocline offshore.

The fluorescence contours (Figure 4-2) show isolated regions of high fluorescence offshore of the front. There was a gradual decline in fluorescence from May 14 to June 3, followed by a sudden increase on June 9. The fluorescence peak on May 14 was associated with spring-bloom diatoms of the genera *Thalassiosira*, *Stephanopyxis*, *Nitzschia*, and *Fragilaria*. The extremely high fluorescence values seen on June 9 and June 16 were related to a bloom of a diatom of the genus *Eucampia*. This bloom appears to have been separated from the inshore waters by the front. The depth of the peak fluorescence values increased by about 1 m d^{-1} from June 3 to June 16, possibly due to sinking of the diatoms.

The temperature contours (Figure 4-3) can be seen to parallel the density contours, with warmer water inshore. Surface temperatures of ~8°C increased rather slowly with time, until a strong warming period between June 9 and June 16. The horizontal surface temperature gradient was 2-3°C from inshore to offshore for most cruises, with the maximal gradient between Stations 1 and 3.

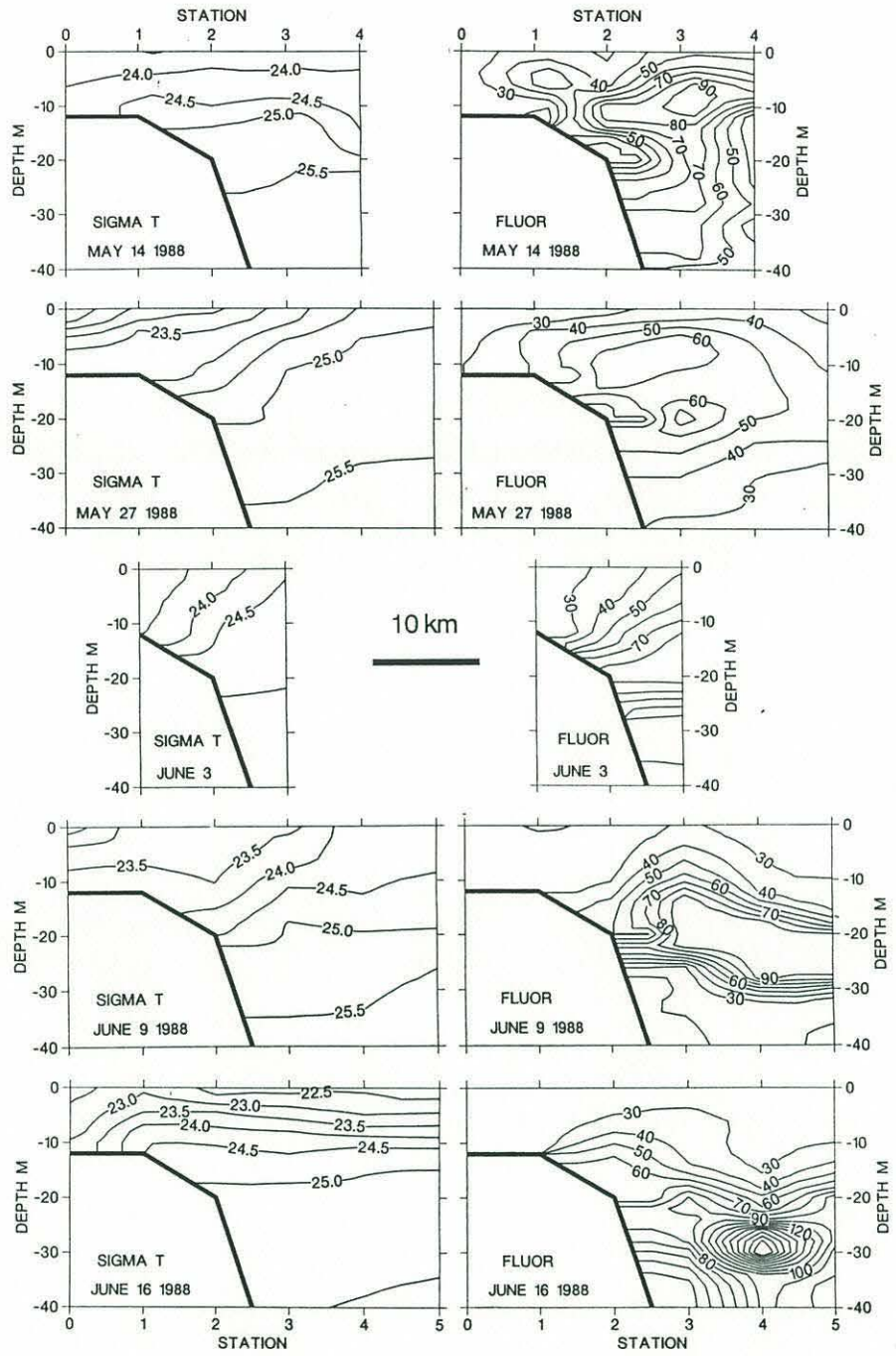

Figure 4-2. A time series of contour plots of sections of σ_T (left panels) and *in situ* fluorescence (right panels) from the regular cruise track in 1988. The cruise date is shown at the bottom left of each panel. The thick black line indicates the bottom profile. Stations 1 to 5 are ~7 km apart, while Station 0 is in Portsmouth Harbor.

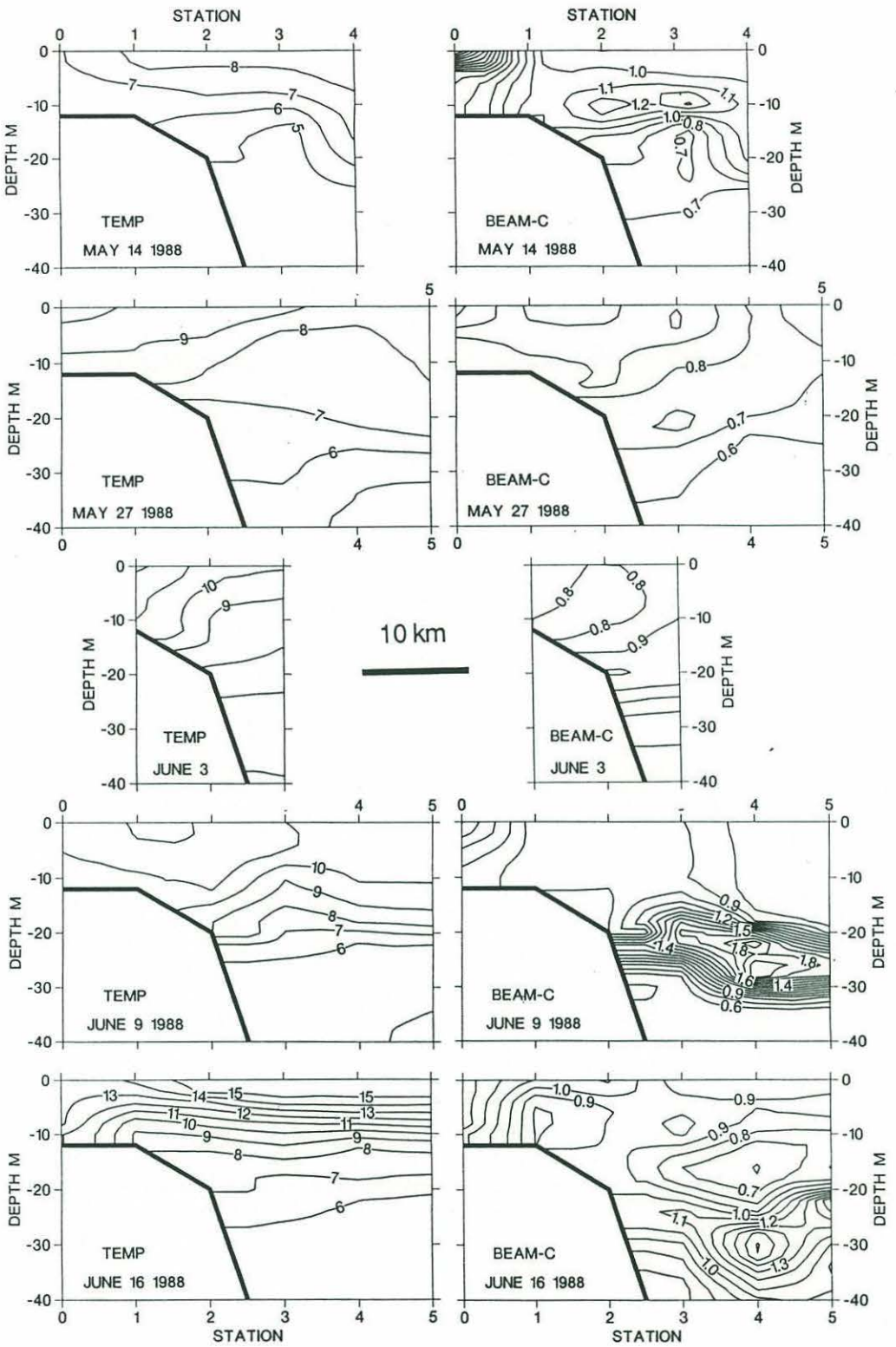

Figure 4-3. Same as Figure 4-2, but sections of temperature (left panels, °C) and beam c (right panels, m^{-1}) for 1988.

The beam-c fields (Figure 4-3) were almost identical to the fluorescence fields, indicating that most of the beam attenuation was associated with living phytoplankton. For the most part, the beam-c field maps the distribution of diatoms. As with the fluorescence, the highest beam-c values were found offshore of the front.

SALINITY AND *A. TAMARENSE* DISTRIBUTIONS, 1987-1989

The salinity fields of 1987 showed weak stratification, with approximately 1 psu (practical salinity unit) difference from the surface to 40 m (Figure 4-4). The isohalines were relatively horizontal, with little structure except near the surface on June 5. The temperature and σ_T fields showed identical structure (not shown). The *Alexandrium tamarense* cell concentrations were unusually low during 1987, reaching maximum values of ~150 cells l^{-1} after May 27. The cells were found in an isolated patch inshore, associated with the pycnocline. Almost no cells were found offshore of Station 3.

In striking contrast to the 1987 data, the 1988 salinity fields were similar to the temperature and σ_T fields, and show strongly-sloping isohalines, with salinity differences of up to 3 psu from the surface to 40 m (Figure 4-5). The sloping isohalines were most apparent on May 27, June 3 and June 9. Surface salinities of less than 30.5 psu were measured in inshore waters from May 14 to June 3, after which slightly more saline waters of 31 psu were seen inshore. The deeper waters were about 0.5 psu saltier in 1988 than 1987. During the initial stages of the bloom (May 14, May 27, June 3 1988), the *Alexandrium tamarense* cells were found mainly in waters of <31.5 psu (Figure 4-5). On May 27, in particular, the cells were strongly restricted to the inshore, low salinity water mass. After June 3, high concentrations of *A. tamarense* were measured offshore of the front, in areas which had previously shown cell concentrations of <1000 cells l^{-1}.

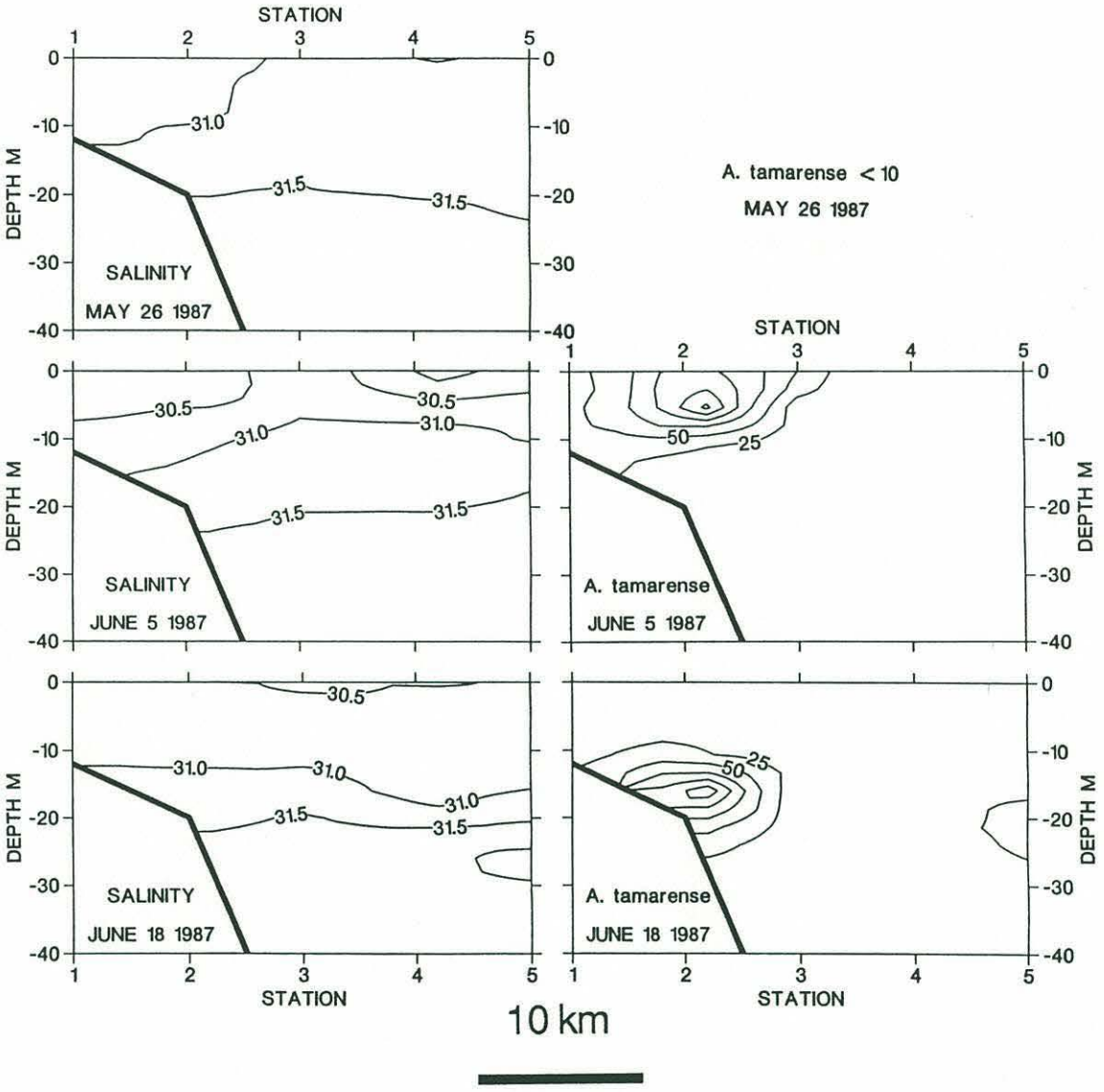

Figure 4-4. Same as Figure 4-2, but sections of salinity (left panels, psu) and *Alexandrium tamarense* cell concentrations (right panels, cells l^{-1}) for 1987.

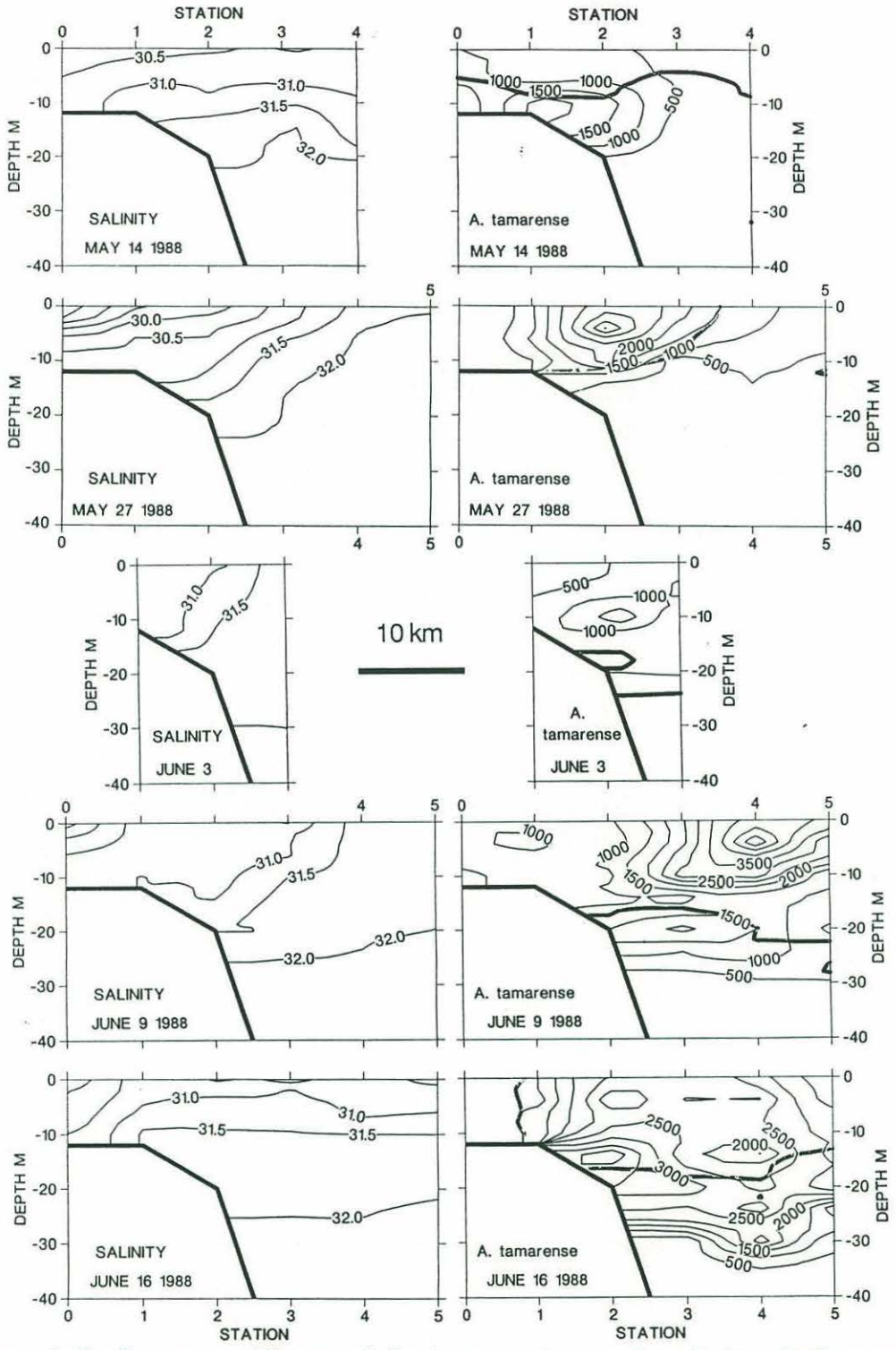

Figure 4-5. Same as Figure 4-2, but sections of salinity (left panels, psu) and *Alexandrium tamarense* cell concentrations (right panels, cells l^{-1}) in 1988. The heavy line on the *A. tamarense* plots is the 0.5 µg-at N l^{-1} contour of nitrate+nitrite.

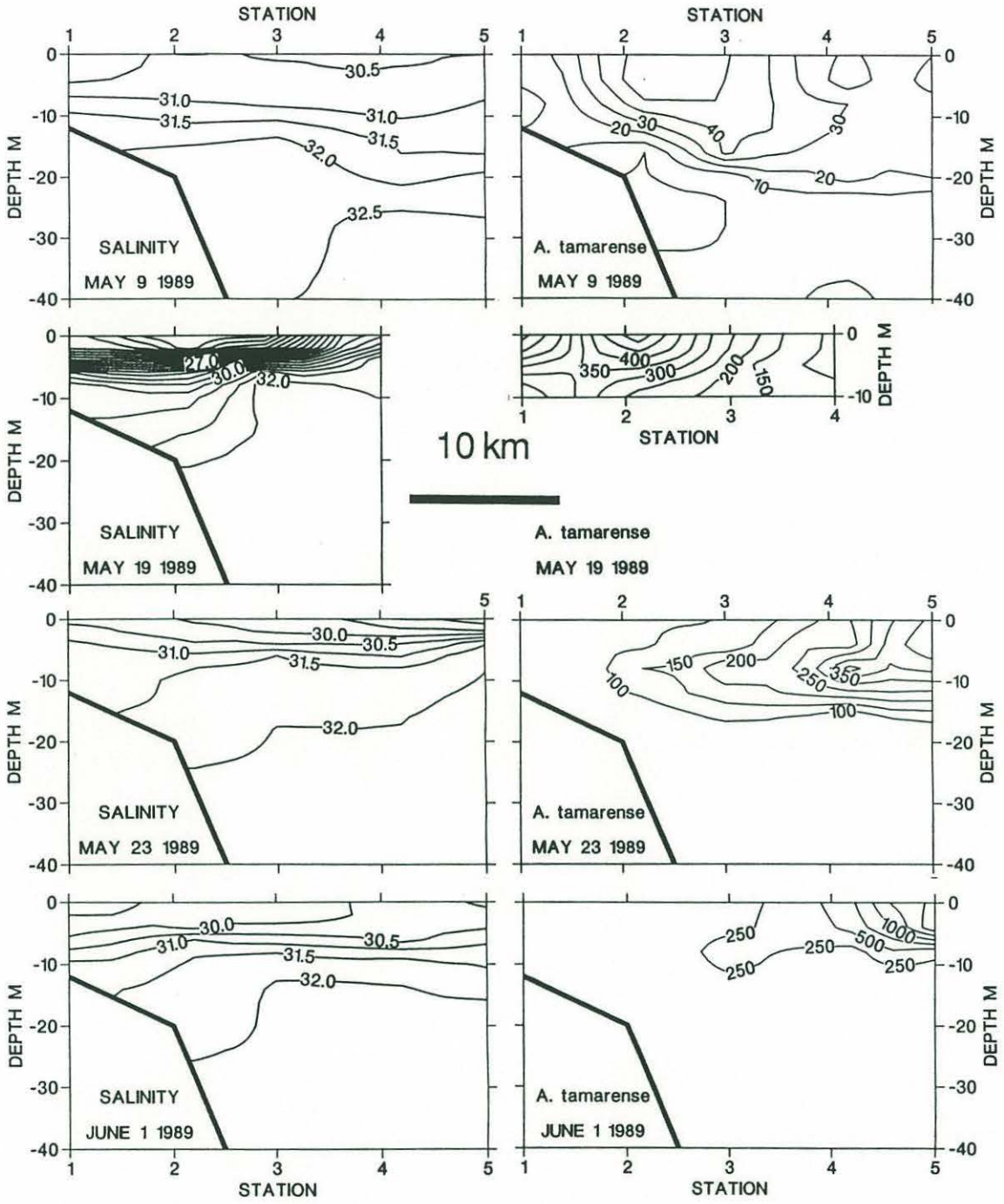

Figure 4-6. Same as Figure 4-2, but sections of salinity (left panels, psu) and *Alexandrium tamarense* cell concentrations (right panels, cells l^{-1}) for 1989. The May 19 panels are results from a C/V Unity cruise, and thus include cell counts from the surface and 10 m only.

The vertical salinity gradients during 1989 were similar to, or greater than, those measured during 1988 (Figure 4-6). Surface salinities as low as 23 psu were seen on May 19, the first C/V Unity cruise. These unusually low values were caused by extremely high flow rates of the Androscoggin and Kennebec Rivers in the week prior to this cruise, as will be discussed below. In general, the salinity contrast from the surface to 40 m was 2-3 psu. As with 1988, in 1989 the highest *Alexandrium tamarense* cell concentrations were associated with water <31.5 psu. However, the location of the low salinity water was quite variable: on May 19 it formed a 5 m thick lens which intersected the coast, whereas on May 9, May 23 and June 1 it was found offshore. On May 23, in particular, it formed an isolated offshore lens, with a pycnocline which sloped downwards and offshore. The *A. tamarense* cells show the same distributions as the low salinity water: on May 19 the cells are found in inshore surface waters, while on May 23 and June 1, the cells formed restricted patches in offshore waters. The cell concentrations were almost an order of magnitude lower than the same time of year in 1988.

The association of *Alexandrium tamarense* cells with low salinity water is also apparent in the alongshore surface distribution from the data of the C/V Unity cruise on May 19, 1989 (Figure 4-7). The 23-25 psu water shown in Figure 4-6 can be seen to extend in a band alongshore, throughout the region sampled. A band of *A. tamarense* cells with concentrations greater than 300 cells l^{-1} coincided with the 23-25 psu water distributed alongshore. An area of very fresh water at the mouth of the Merrimack River contained no *A. tamarense* cells. Similarly, very few cells were found in Portsmouth Harbor, which is the mouth of the Piscataqua River.

THE PLUME

The fresh inshore water in 1988 was warmer than the more saline offshore waters (Figures 4-3 and 4-5), suggesting that the alongshore extent of the low salinity water should be visible in

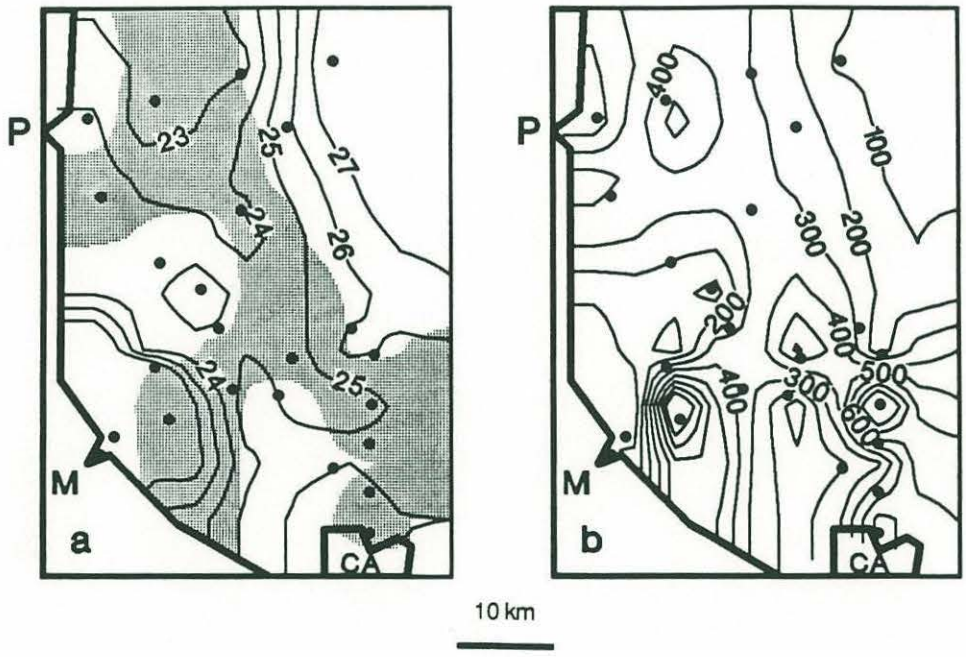

Figure 4-7. (a) surface (1 m) salinity field (psu) for May 19, 1989. The locations of the stations are shown in Figure 4-1. The coastline is shown by the heavy black line, with the north shore of Cape Ann to the bottom of the plot. The shaded area denotes the region of >300 cells l^{-1} of *Alexandrium tamarense*. (b) surface cell concentrations (cells l^{-1}) of *Alexandrium tamarense*. P=Portsmouth Harbor, M=Merrimack River estuary, CA=Cape Ann.

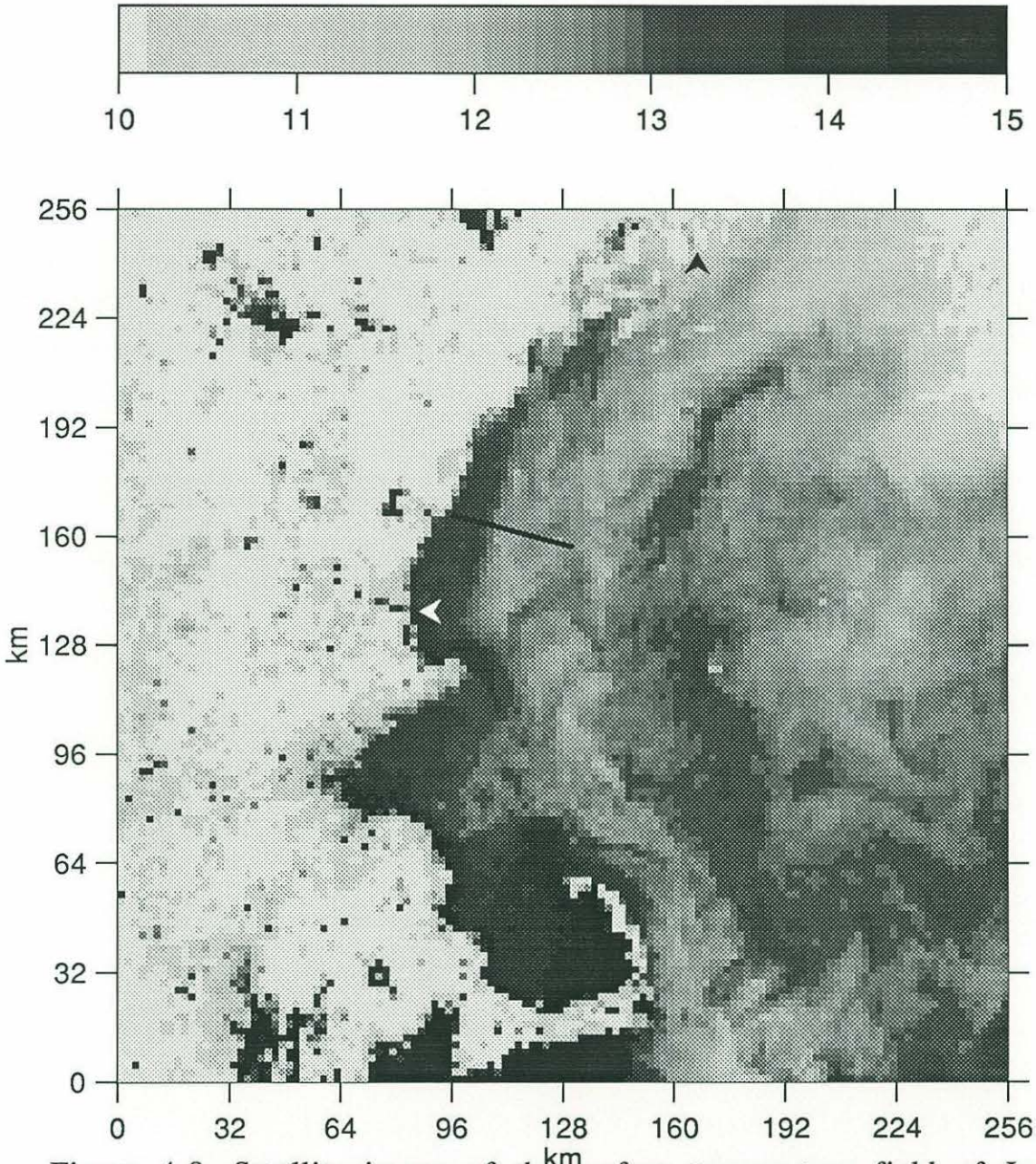

Figure 4-8. Satellite image of the surface temperature field of June 8, 1988. The heavy black line denotes the regular cruise transect (Figure 4-1). The black arrow indicates the approximate region of discharge of the Androscoggin and Kennebec Rivers, while the white arrow indicates the mouth of the Merrimack River. Cape Ann and Cape Cod are clearly seen in this image. Note that the temperature scale is not linear. Data courtesy of NORDA.

infra-red satellite images. The image shown in Figure 4-8, for June 8, 1988 (one of the only cloudless images from early May until mid-June, 1988) shows a distinct band of warm water extending from the Casco Bay area of Maine in the north of the image, southward into Cape Cod Bay. The heavy black line shows the regular cruise transect; the warm water front crosses the transect between Stations 2 and 3. The temperature contrast across the front in the image is ~2°C. This can be compared to the temperature section from June 9, 1988 (Figure 4-3), which shows a similar horizontal surface temperature gradient from Station 1 to Station 3. It appears that the nearshore buoyant plume of low-salinity water extended from Casco Bay in Maine to Cape Cod Bay in Massachusetts, a distance of ~250 km alongshore.

RIVER FLOW

The strong salinity gradients which formed the plume in 1988 and 1989 suggest that the temporal dynamics of the plume should correlate with variations in freshwater input to the coastal Gulf of Maine, in particular river flow. The Androscoggin, Kennebec, and Merrimack rivers are the three largest rivers between the Penobscot area in Maine, and Cape Cod (Figure 4-8). The flows of these rivers are plotted in Figures 4-9, 4-10 and 4-11 from April to July, 1987, 1988 and 1989. Also plotted are rough estimates of A_{FW}, the amount of fresh water (0 psu) present in any given cruise transect. This value was calculated by first finding the average salinity ($\overline{S}_i$) between the surface (z=0) and the depth of the 32 psu isohaline (h_{S32}):

$$\overline{S}_i = \frac{1}{h_{S32}} \int_0^{h_{S32}} S(z)\, dz. \qquad (4\text{-}1)$$

The fraction of fresh water, α_i, in that depth interval at the ith station was found according to

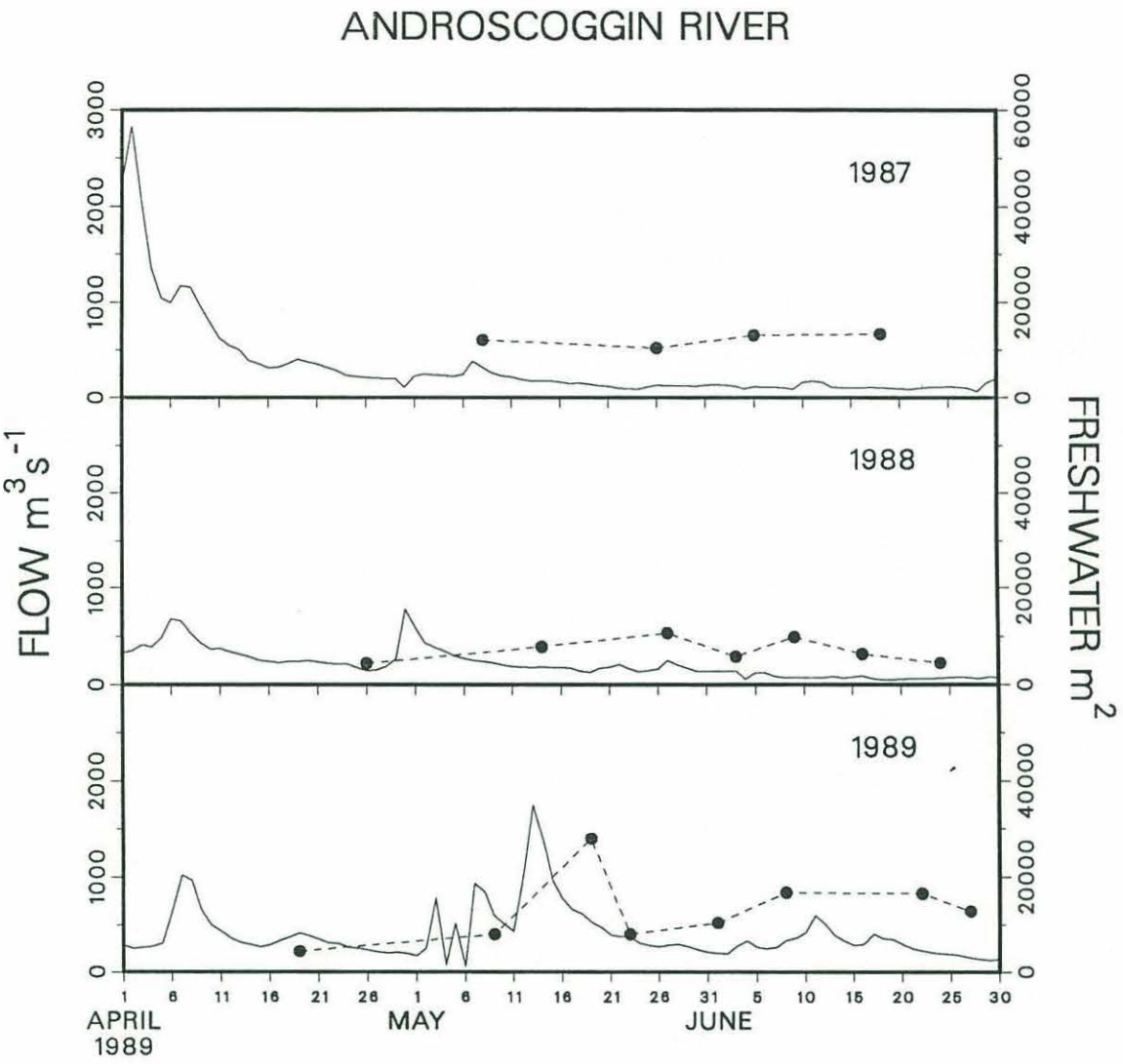

Figure 4-9. Discharge ($m^3 s^{-1}$) of the Androscoggin River for April to July of 1989 (bottom panel), 1988 (middle panel) and 1987 (top panel). The closed circles and dashed lines indicate A_{FW}, the area of fresh water which would have to be mixed into water of 32 psu to obtain the salinity distribution measured on that date.

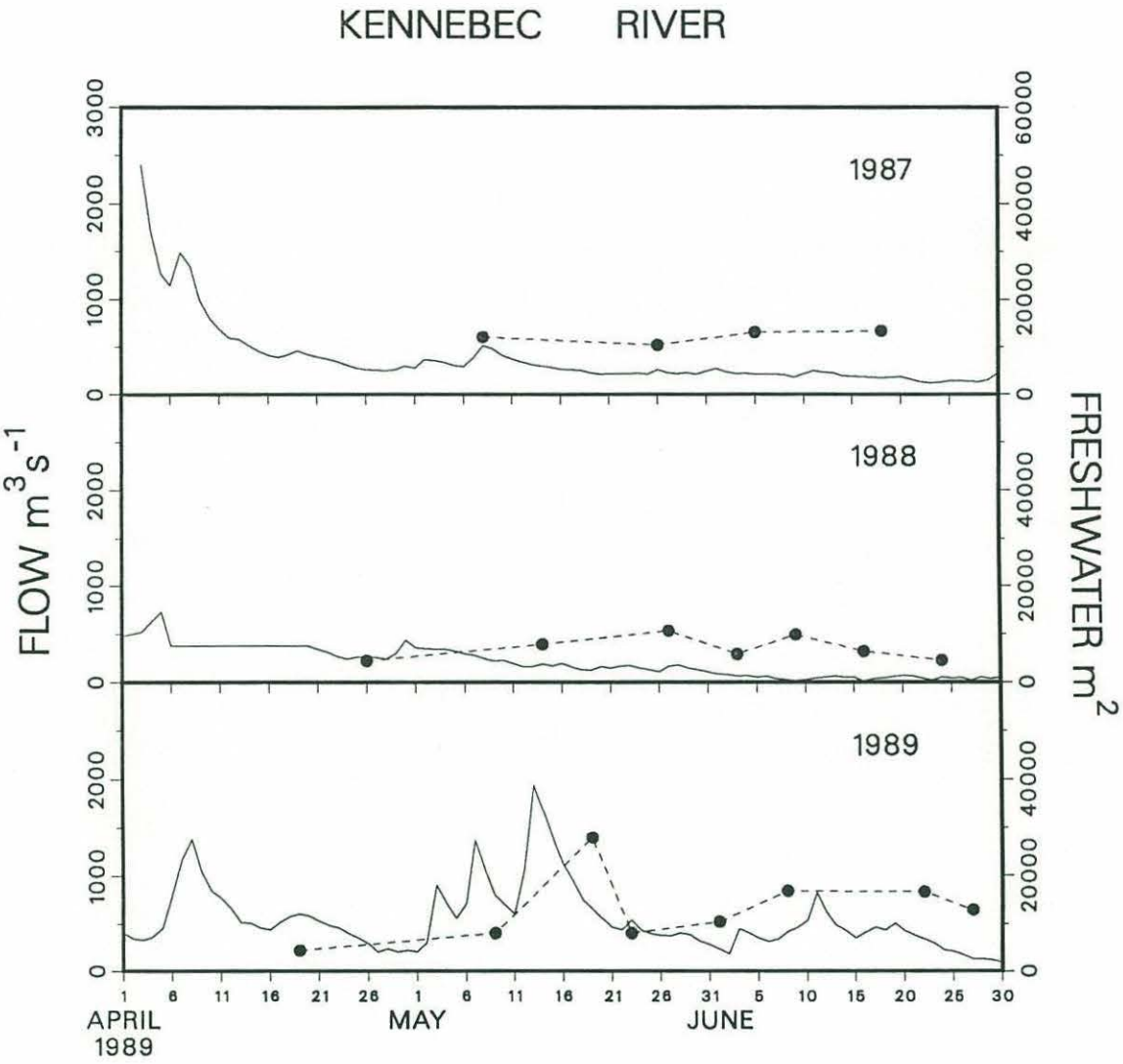

Figure 4-10. As Figure 4-9, but for the Kennebec River. The flat portion of the curve from April 7-19, 1988, indicates a time when no data were available.

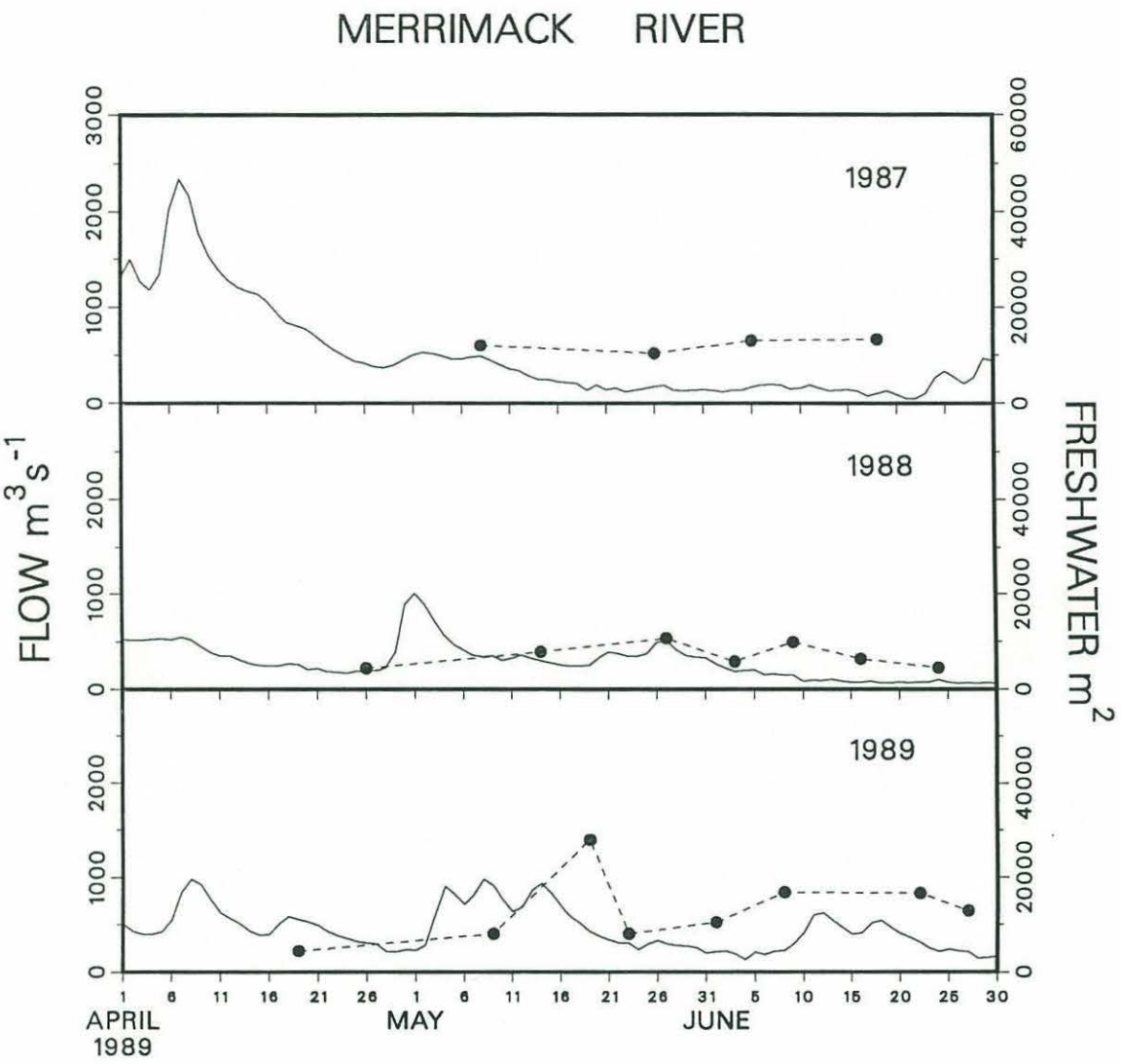

Figure 4-11. As Figure 4-9, but for the Merrimack River.

$$\alpha_i = \frac{32 - \bar{S}_i}{32}. \qquad (4\text{-}2)$$

The areal amount of fresh water, A_{FW}, in the region bounded by the surface, the depth of the 32 psu isohaline (h_{S32}), the coast, and the farthest offshore station (n) can then be found from:

$$A_{FW} = \sum_{i=1}^{n} (\alpha D h_{S32})_i. \qquad (4\text{-}3)$$

Here the sum is over n stations, with the *i*th station having an across-shelf scale D_i (m) based on the half-way points between adjacent stations. The value A_{FW} thus represents the area of a transect cross section that would contain fresh water sufficient to dilute 32 psu water to the observed salinities.

Given our hypothesis that the fresh water plume originates from rivers to the north of the study area, we expect to see a correlation of changes in A_{FW} with changes in the volume of river discharge. From Figures 4-9, 4-10 and 4-11 it can be seen that such a correlation exists: in 1987, the river flows were low, and relatively constant, which is reflected in the constant A_{FW} values. In 1988 there was an increase in A_{FW} after a peak in the river flows in late April. The strongest correlations are seen in 1989, when the unusually high flows during early May led to very high proportions of fresh water in the transect. The highest amount of fresh water was seen on May 19, 1989, the C/V Unity cruise (Figures 4-6, 4-7). The values of A_{FW} were generally much higher in 1987 than 1988 or 1989.

Changes in A_{FW} are most strongly related to changes in the flow rates of the Androscoggin and Kennebec Rivers, and less well correlated with changes in the flow of the Merrimack River. This is not surprising, as we expect the river flow to turn to its right after leaving the estuary. Thus the Merrimack River, which empties into

the Gulf of Maine to the south of the study area, should not have a significant effect on the salt balance along the transect (Stations 0-5, Figure 4-1). The Androscoggin and Kennebec Rivers, however, empty to the north of the transect, and should have a significant impact on the amount of fresh water measured in the hydrographic surveys.

The river flow patterns were quite similar to each other, but varied considerably from year to year. A peak in the flow rate typically occurrs in early April, in response to the spring thaw. This early peak was particularly pronounced in 1987, when the flow rates reached record levels. The early April peak is usually followed by a peak in early May, reflecting rainfall at that time. Such a peak was absent in 1987, but was particularly well-developed in 1989.

WIND PATTERNS

The winds measured at Logan airport, Boston, are shown in Figure 4-12 for 1987, 1988 and 1989, from May 1 to June 15. In a coastal ocean, the across-shelf water motions are controlled by the alongshore wind stresses. In 1987, the alongshore wind stress was weak, but mainly upwelling-favourable (generally positive alongshore stresses in Figure 4-12). Several events appear to dominate the signal, as discussed in Chapter 3, for example around May 15 and May 22. However, each of the cruises in May and early June of 1987 was preceded by weak or downwelling-favourable winds.

During 1988 the situation was somewhat different than 1987, as the alongshore wind stress time series shows several strong downwelling-favourable events (May 19, June 2). The May 14 cruise was preceded by a very strong upwelling-favourable wind (up to 0.15 Pa). The May 27 cruise showed only weak upwelling-favourable winds during a short interval prior to the cruise. The June 3 and June 9 cruises were preceded by strong downwelling-favourable wind stresses.

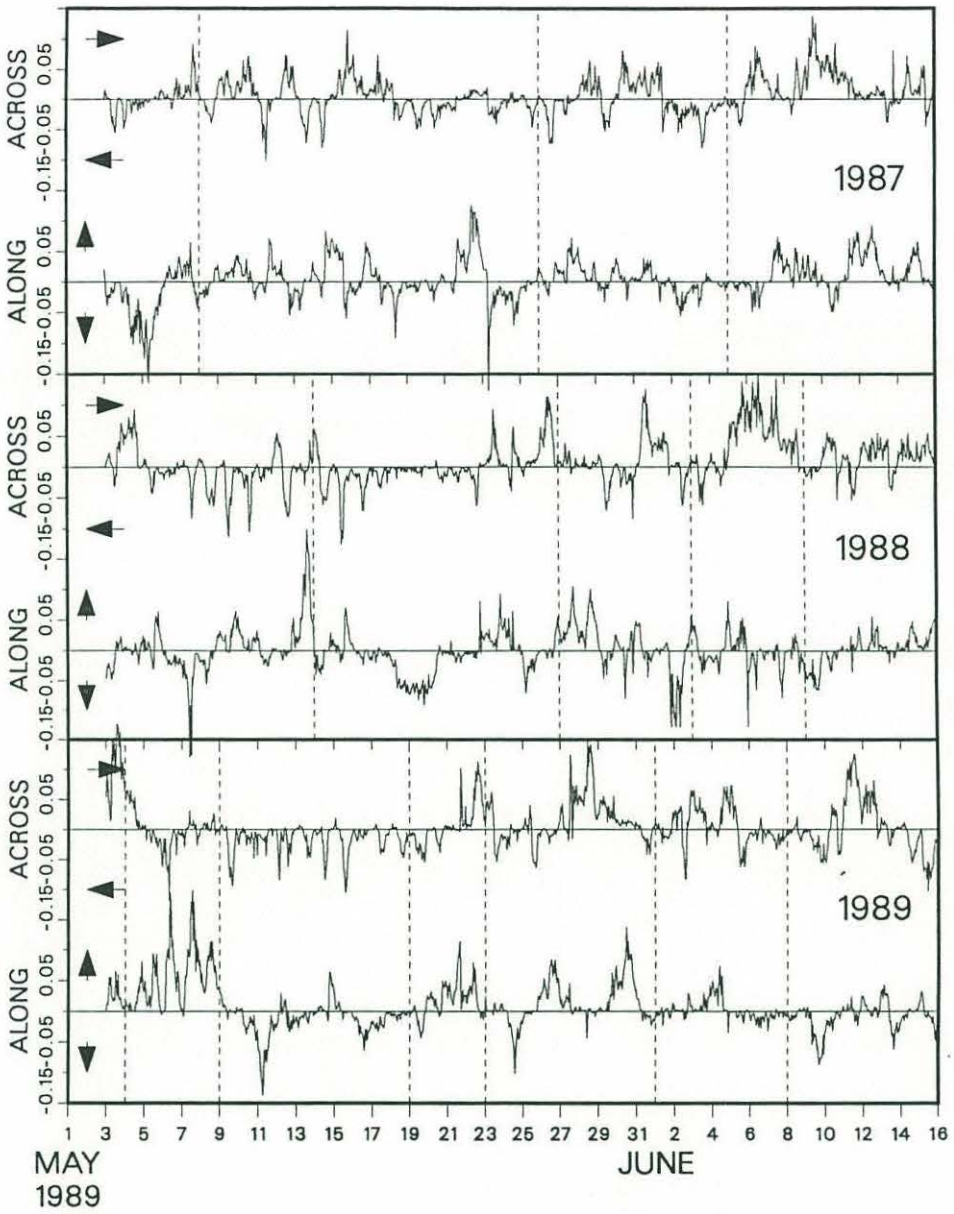

Figure 4-12. Wind data from Logan Airport, Boston, for May to June, 1987 (top panel), 1988 (middle panel) and 1989 (bottom panel). These data have been rotated into the coordinate system of the coast, so that the coastline runs vertically. The alongshore (ALONG) and across-shore (ACROSS) wind stresses (Pa) are plotted, with the arrows to the left of the plot indicating the direction the stress would act relative to the assumed coastline which is up/down along ordinate. Thus a positive alongshore stress acts to the north (upwelling-favourable). The dashed lines indicate the cruise dates.

In 1989 the May 9, May 23, and June 1 cruises were preceded by strong upwelling-favourable winds of long duration. Of the cruises shown in Figure 4-6, only the May 19 (C/V Unity) cruise took place after a period of relative calm. The alongshore wind stresses during May and early June of 1989 were predominantly upwelling-favourable.

In 1988 and 1989, cruises which were preceded by strong upwelling-favourable wind events showed flat pycnoclines, or pycnoclines which sloped downwards and offshore (e.g. May 14, 1988; May 9, May 23 and June 1, 1989; Figures 4-4, 4-5 and 4-6). Cruises preceded by strong downwelling-favourable winds showed steep fronts sloping downwards and onshore (e.g. June 3, 1988). Cruises preceded by weak wind stresses (May 27, June 9, 1988; May 19, 1989) showed fronts sloping downward and onshore, with a broader horizontal extent than was seen after downwelling winds. Cruises during 1987 were generally preceded by weak winds, yet showed nearly horizontal pycnoclines.

TOXICITY

The binary toxicity time series for five stations along the coasts of Maine and Massachusetts have been plotted in Figure 4-13 for the years 1987, 1988 and 1989. These time series show considerable variation from year to year. In 1987, toxicity was first detected in late April at the Maine stations. However, no toxic samples were found at any Massachusetts stations during 1987, for the first time since 1972. In 1988, the initiation of toxic outbreaks occurred in a north-to-south pattern, the first toxic sample being recorded in Lumbos Hole on April 25. Toxicity was then detected at Gloucester on May 8, and at Scituate on May 26. The large sampling interval at Spurwink River early in the year makes it difficult to know the exact date of initiation of toxicity.

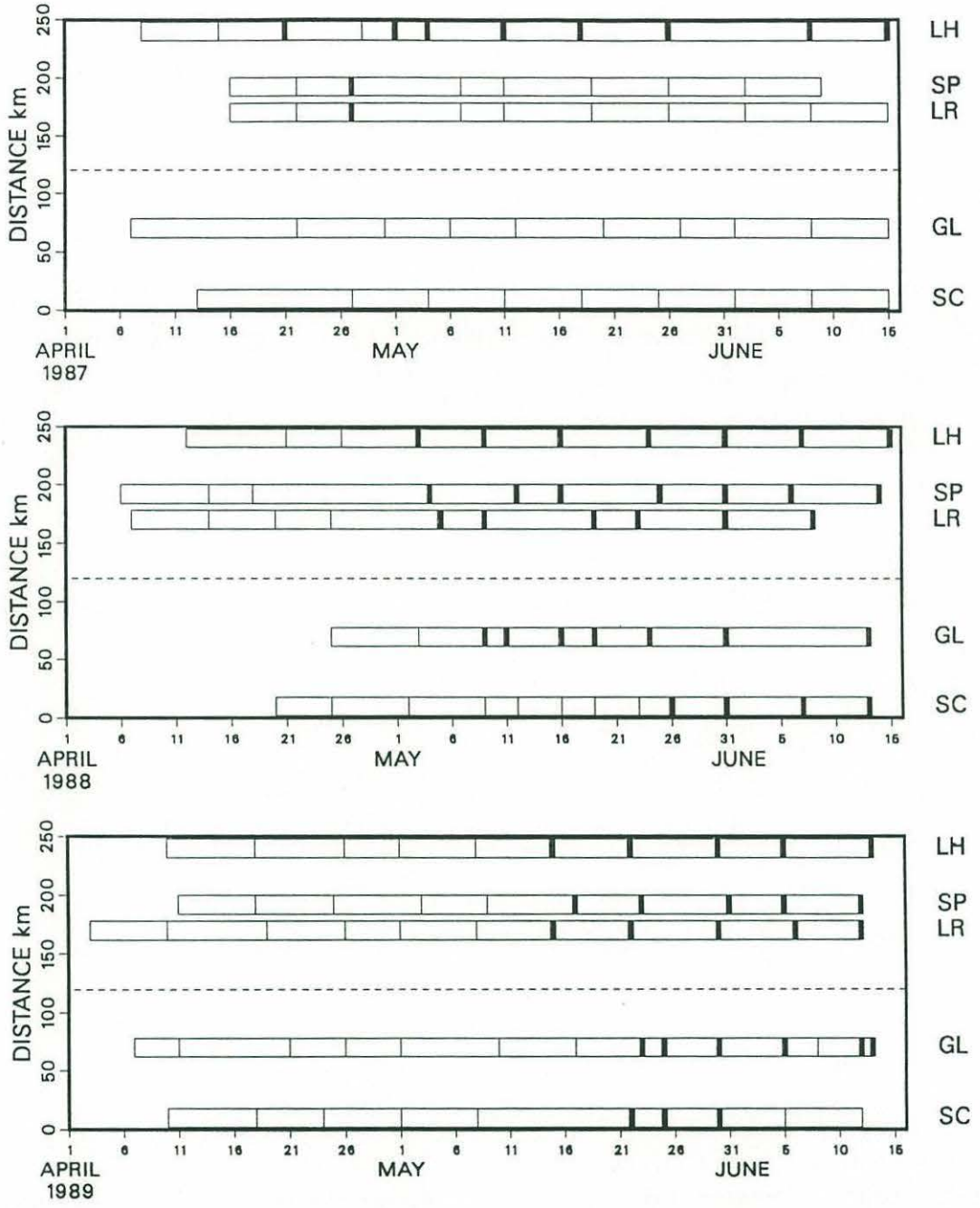

Figure 4-13. Time series of binary toxicity at the five stations shown in Figure 4-1, for 1987 (top panel), 1988 (middle panel) and 1989 (bottom panel) LH=Lumbos Hole, SP=Spurwink River, LR=Little River, GL=Gloucester and SC=Scituate. The alongshore distances of the stations relative to Scituate are shown on the vertical axis. The vertical bars indicate the sampling dates; heavy vertical bars indicate that the sample was toxic.

In 1989, the toxicity began much later than in 1987 or 1988, the first toxic sample being recorded at Lumbos Hole on May 15. As in 1988, the spread of toxicity showed a north-to-south pattern, although the time between the initiation of toxicity at Lumbos Hole and at Scituate was only about 7 d. The interval between samples is approximately the same as the transit time of toxicity along the coast; this could cause problems for our interpretation of patterns of initiation of toxic events.

From the river flow data of Figures 4-9, 4-10 and 4-11, it can be seen that the initial toxic outbreaks are preceded by a peak in the flow of the Androscoggin River. The isolated, patchy toxicity in Maine during 1987 followed a record early April runoff, followed by low flow during the rest of the season. For the first time since 1972, toxicity was absent from Massachusetts waters. In 1988 and 1989, large-scale spread of toxicity followed flow peaks in early May. In 1988 the relatively low peak flow preceded a slow spread of toxicity from north-to-south. In 1989 the very high flow rates of early May preceded a very rapid southward spread of toxicity.

DISCUSSION

In a region of complex coastal hydrography, measurements of a suite of physical and biological parameters for three years document the initial association of cells of *Alexandrium tamarense* with a buoyant plume along the southwestern coast of the Gulf of Maine. The cell distributions followed the distribution of low salinity water, which in turn was influenced by the surface wind stress and topography. The salinity balance of the plume suggests that the sources of this low salinity water were the Androscoggin and Kennebec Rivers, which show peak flows prior to the detection of toxicity along the coast. These results do not rule out the possibility of *in situ* growth as a major source of cells in the toxic outbreaks; however the alongshore advection of established populations in a coastally trapped buoyant plume can account for many of the

observed patterns of dinoflagellate abundance and PSP toxicity in the study area.

Cell Distributions and Density Structure

The patterns of *Alexandrium tamarense* cells and low salinity water in 1988 and 1989 were very different from 1987. In 1988 and 1989, isolated patches of cells were associated with patches of low salinity (<31.5 psu) water during May, regardless of the location of that water. This relationship of *A. tamarense* cells with low salinity water was also apparent alongshore, as data from the C/V Unity cruise on May 19, 1989, demonstrate (Figure 4-7). In 1987, low salinity water was found throughout the transect, but only low concentrations of *A. tamarense* were measured, late in the bloom season. These cells were found nearshore, within the pycnocline.

The lack of *Alexandrium tamarense* in 1987 despite significant fresh water nearshore is likely related to the timing of a massive river flow in early April of that year. This huge flux of fresh water caused a freshening of the surface waters of the Gulf of Maine. In our transects this was visible as a thick layer of low salinity water at all stations. It is also seen in the high proportion of fresh water, A_{FW}, that year (Figures 4-9, 4-10 and 4-11). The usual cyclonic circulation of the Gulf of Maine appears to have been disrupted in 1987, with negligible geostrophic alongshore currents for the greater part of the spring and summer (Brown and Irish, unpub. ms.) Due to low rainfall in early May, no subsequent peak was seen in the river flow, and no sloping pycnocline in the hydrographic surveys. Thus the alongshore transport mechanism of a coastally trapped buoyant plume was apparently weak or absent during the bloom season (May-August) of 1987, consistent with the lack of PSP toxicity in the south of our study area.

In 1988 and 1989, the strong association of the *Alexandrium tamarense* cells with the low salinity water mass suggests that the cells were being advected alongshore in this water mass, and that

they may have originated in or near the Androscoggin-Kennebec River estuary. As will be shown below, the plume probably had alongshore velocities of approximately 0.2 m s^{-1}. At this rate, the cells observed in the transect at Portsmouth, NH would have been at the Androscoggin-Kennebec estuary, approximately 120 km to the north, about 7 d earlier. If we assume that all the cells measured in the Portsmouth transect originated near the Androscoggin-Kennebec estuary, we can calculate the number of cells we would expect to find in that estuary 7 d earlier by balancing the salt budget and estimating a net growth rate. On May 14, 1988, for example, there were ~2.8 x 10^{11} cells in the waters above the 32 psu isohaline along our transect. Using equations (4-1) to (4-3), we can calculate the concentrations of these cells in a variety of parent water salinities. These values have been plotted in Figure 4-14 for a range of salinities and exponential growth rates of the cells. At an unrealistic extreme, had the cells originated in fresh, 0 psu water, and grown at 0.1 d^{-1}, we would expect concentrations of ~8000 cells l^{-1} in that water. If they originated in 25 psu water, the established population would have been only 2000 cells l^{-1}. The relatively high salinities and high cell concentrations of May 14, 1988, make these conservative estimates of the original cell concentrations. A similar calculation using the data of May 19, 1989, would yield much lower predicted cell concentrations since there was a higher proportion of fresh water and lower cell concentrations observed on that date (Figure 4-6).

Prakash (1967) measured the growth rate of a strain of *A. tamarense* (*Gonyaulax tamarensis*), isolated from the Bay of Fundy, over a salinity range of 7-40 psu at 10°C. Maximal growth rates of ~0.08 d^{-1} were achieved between about 17-23 psu. White (1978) performed more detailed experiments on a strain of *A. tamarense* (*Gonyaulax excavata*) isolated from the Cape Ann region of Massachusetts. He found a salinity of 30.5 psu to be optimal for growth at 10°C (0.25 d^{-1}), with very little change in growth rate between 27 psu to 35 psu. A similar experiment by Watras et al. (1982), performed using a salt-pond isolate of *A. tamarense*, showed

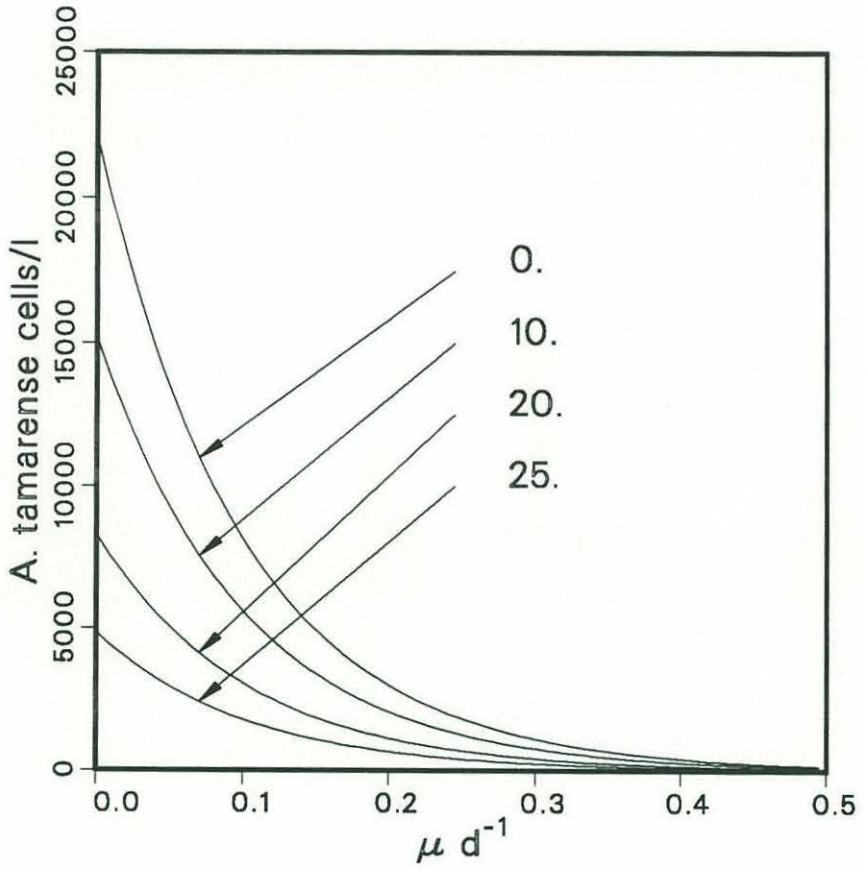

Figure 4-14. Predicted cell abundances in the Androscoggin-Kennebec estuary, given the growth rate on the horizontal axis, and the assumed parent salinities (psu) labelled with arrows. These calculations are based on the data from May 14, 1988.

the growth rate at 10°C and 25.5 psu to be ~25% higher than the growth rate at 32.5 psu (0.2 vs. 0.15 d^{-1}). From these experiments, we might expect *A. tamarense* to have grown up in water of 20-30 psu, with a growth rate of perhaps 0.2 d^{-1}. From Figure 4-14, this predicts a rough lower bound for the initial cell concentrations in the estuary of ~1000 cells l^{-1}. Incze and Yentsch (1981) performed a study in the Damariscotta estuary, just to the north of the Androscoggin-Kennebec estuary. They found *A. tamarense* concentrations of up to 10^5 cells l^{-1} during July of 1979, indicating that high concentrations of these cells can build up in the local estuaries. Thus the predicted cell concentrations of Figure 4-14 seem reasonable.

THE PLUME

A simple model can be used to estimate the buoyant plume flow rate. Given the slope of the pycnocline on May 27, 1988, a cruise which was preceded by weak winds, an estimate of the velocities of the upper (low salinity) layer can be made using Margule's equation. This equation assumes a geostrophic balance of forces, homogeneous layers, and a lower layer which is at rest:

$$v = -\zeta \frac{g}{f}\left(\frac{\rho' - \rho}{\rho}\right). \qquad (4\text{-}4)$$

Here v is the velocity of the upper layer (inshore water mass), ζ the slope of the pycnocline, g the acceleration due to gravity, f the Coriolis frequency, and ρ and ρ' the upper and lower layer densities, respectively. The slope of the 1024 kg m^{-3} (σ_T = 24) isopycnal on May 27 1988 gives $\zeta = 10^{-3}$. With g = 10 m s^{-2}, f = 10^{-4} s^{-1}, ρ = 1023.5 kg m^{-3} and ρ' = 1025.5 kg m^{-3}, we find v~0.2 m s^{-1}. Assuming alongshore uniformity to the plume (as suggested by the satellite image of Figure 4-8), this speed is equivalent to a displacement of ~17 km d^{-1} alongshore to the south. At this rate, the plume would travel from Lumbos Hole, ME, to Scituate, MA, a distance of 250 km, in ~15 d. The time between the initiation of

shellfish toxicity at the two stations was ~23 d in 1988, and ~10 d in 1989, in fair agreement with the calculated velocity.

We can calculate the transport of fresh water in the plume, T, from:

$$T = vA_{FW} . \qquad (4\text{-}5)$$

Using v=0.2 m s^{-1}, during 1988 the calculated flux was between 1000-2000 m^3 s^{-1}. From Figures 4-9 and 4-10, we can see that the average sum of the flows of the Androscoggin and Kennebec rivers was 500-1000 m^3 s^{-1} in the spring of 1988. Thus about half of the fresh water in the plume can be accounted for by the discharge from these two rivers by this simple calculation. However, there is probably a factor of two uncertainty in the estimate of the alongshore velocity, v, since we have assumed the lower layer to be at rest, and neglected the wind forcing, discharge rate of the river, shear, and other forces which may influence the alongshore velocities. Other methods of calculating the alongshore velocities (e.g. Appendix B), suggest that 100% of the fresh water in the plume derives from the Androscoggin and Kennebec Rivers.

The coastally trapped buoyant plume described above may have significant structure along its front. While the satellite image of Figure 4-8 suggests large-scale continuity of the thermal gradient alongshore, small-scale features can be discerned along the edge of the front. The model of James (1988) suggests that eddy formation should be a common occurrence across strong shear zones. The scalings of Flagg and Beardsley (1978) suggest that the plume front would be very unstable given the bottom slope and large density gradient. Thus we would expect eddy formation to be a significant mode of patch formation, and cross-frontal transfer of mass and cells.

WIND EFFECTS

It was suggested above that the presence of a lens of low salinity water at the surface, offshore, was a result of strong upwelling-favourable winds forcing the coastal plume offshore. Such behaviour has been reproduced in a three-dimensional primitive equation wind-forced model of a coastal plume (Chao, 1987). In this model, a 0.1 Pa upwelling-favourable wind stress was seen to cause detachment of buoyant water from the coast after less than two days (Figure 4-15). In cross-section, the detached water mass appears as a lens of fresh water, separated from the coast by more saline water, much as was seen on May 9 and May 23, 1989 after major upwelling-favourable wind events (Figures 4-6 and 4-12). The alongshore velocities of Chao's model plume were slowed by upwelling-favourable wind stresses, but the plume continued propagating alongshore against the prevailing wind.

Downwelling-favourable winds were seen to narrow the model plume, and enhance its propagation alongshore (Chao, 1987; Figure 4-15). In cross-section, the front forming the plume became steepened, and moved shoreward. This situation is analogous to the situation of June 3, 1988 (Figure 4-5), which shows a steep front nearshore after a strong downwelling-favourable wind event. Thus the model of Chao (1987) supports the inference that the across-shelf hydrographic structure of the plume was closely related to the prevailing wind stress. Strong upwelling-favourable wind stresses flattened the sloping front, or separated the plume from the coast and slowed its alongshore progression, while downwelling-favourable winds forced the plume into the coast and sped it alongshore.

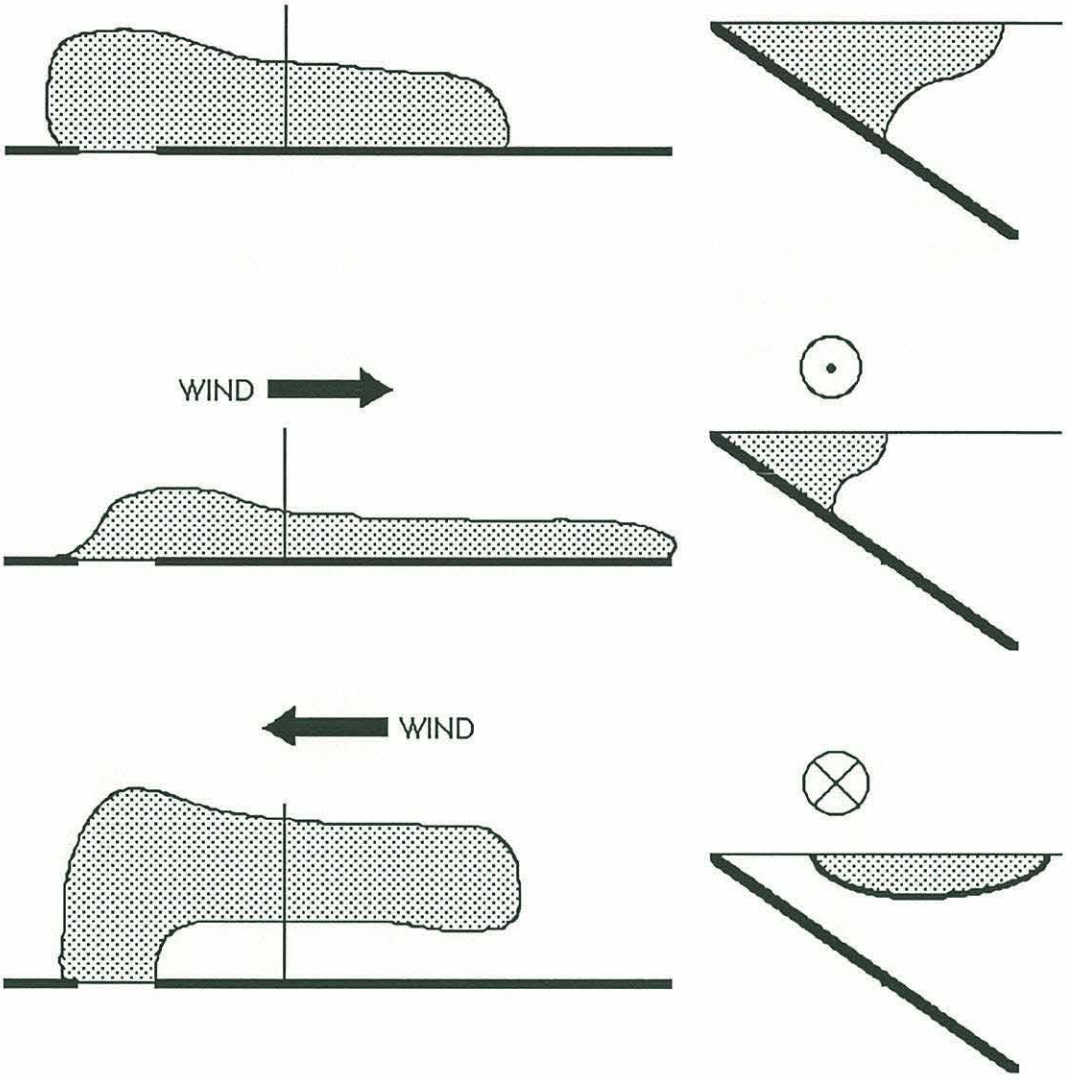

Figure 4-15. Surface (left-hand plots) and across-shelf (right-hand plots) salinity distributions for a buoyant plume (dark water) under no wind stress (top plots), downwelling-favourable wind stress (middle plots), and upwelling-favourable wind stress (bottom plots). Vertical line indicates transect for section plots on right. Adapted from Chao (1987).

CONCEPTUAL MODEL

The results discussed above suggest the following conceptual model for the development and spread of toxic dinoflagellates and concomitant shellfish toxicity in the study area:

1) SOURCE: A source population of cells to the north, possibly established and concentrated in the Androscoggin-Kennebec estuary.

We infer a source population of *Alexandrium tamarense* cells to the north of our study area based on the assumed southward alongshore movement of the plume waters. The fact that the flow of the Androscoggin and Kennebec Rivers can account for most of the flux of fresh water in the plume suggests that these two large rivers are the main source of plume waters and cells. Incze and Yentsch (1981) found concentrated populations of *A. tamarense* in an adjacent estuary of relatively low freshwater discharge. Thus the potential for seed populations exists in that area. Beds of concentrated cysts of *A. tamarense* have been shown to exist offshore, to the north-east of the Androscoggin-Kennebec estuary (Lewis et al., 1979). The outflow of fresh surface water from the estuary creates deep onshore flows (Graham, 1970) which could carry newly-germinated cells into the estuarine environment. Alternatively, the cysts may germinate from within the estuary, as described by Tyler et al. (1982) for the Chesapeake Bay system. Frontal systems of estuaries have been shown to be sites of dinoflagellate accumulation in a variety of locations (Tyler and Seliger, 1978; Tyler, 1984; Tyler et al., 1982; Incze and Yentsch, 1981). Furthermore, the large estuary (Penobscot) to the north of the Androscoggin-Kennebec estuary (Figure 4-1) has historically been devoid of PSP toxins (the "PSP sandwich"; Shumway et al., 1988). This again implies a source population of cells to the south of that estuary.

Alexandrium tamarense cells were generally undetectable in Portsmouth Harbor, the Merrimack River estuary, or offshore waters early in the bloom. It is possible that cysts in nearshore sediments seeded the coastal waters (e.g. Lewis et al., 1979; Anderson et al., 1982), which could then have been the site of localized blooms. However, these cells would still have been advected alongshore to the south in the plume. The timing and location of PSP outbreaks and inhomogeneous distribution of cells suggest a northerly source for the cells.

2) TIMING AND VOLUME OF OUTFLOW: A pulse of freshwater in May carries the growing *Alexandrium tamarense* population out of the estuary, causing initiation of toxic events alongshore.

It is likely that years with a large peak flow in May would show extensive alongshore spread of toxicity, with short transit times for initial detection of PSP along the coast. However, years of low flow in early May should show longer alongshore transit times, and a close relationship of toxicity patterns to the wind stress. Unusually high river flows early in April may remove the seed population from the estuary, reducing the risk of toxic outbreaks. In 1987, record river runoff in early April was followed by relatively low flow rates for the remainder of the season. A very early outbreak of toxicity in Maine (April 21, 1987) was followed by patchy toxicity, and little alongshore spread. The Massachusetts coast to the south was toxin-free. In 1988 and 1989, the pulse of freshwater in early May immediately preceded extensive toxic outbreaks along the coast.

3) WIND EFFECTS: Upwelling-favourable winds force the plume and cells offshore, potentially causing separation of the plume from the coast and a removal of cells from intertidal shellfish. Downwelling-favourable winds hold the plume to the coast, and speed it to the south.

Our data follow the predictions of Chao's (1987) model in the formation of offshore lenses, and influence of the surface wind stress on the frontal slope. Major changes in *Alexandrium tamarense* cell distributions and concomitant shellfish toxicity followed wind events in a predictable manner. The occurrence of toxicity in 1988 at Scituate, MA, the southernmost station shown in Figure 4-13, followed a strong downwelling-favourable wind stress (Figure 4-12, May 18-May 20, 1988) which would have accelerated the plume and cells alongshore to the south. In 1989, the wind events were primarily upwelling-favourable, however, the large freshwater flux at that time may have overcome the predominantly northward wind stresses. An alongshore wind stress should generate an alongshore current velocity given approximately by (Janowitz and Pietrafesa, 1980):

$$v = \frac{\tau}{\rho r}\left(1 - \exp\left(-\frac{r\,t}{h}\right)\right) \qquad (4\text{-}6)$$

where r is given by,

$$r = \frac{1}{40}\left(\frac{|\tau|}{\rho}\right)^{\frac{1}{2}} \qquad (4\text{-}7)$$

Thus a wind stress, τ, of 0.05 Pa, a water density, ρ, of 1024 kg m^{-3}, a water depth, h, of 20 m, and a 1 day duration, t, would produce v~0.15 m s^{-1}. This is slightly less than the 0.2 m s^{-1} calculated for the plume velocities using equation (4-4). In years of high river flow, the plume velocities might thus overcome the retarding effects of sustained upwelling winds, while in years of low flow, the wind-forced currents may dominate the plume advection. The relatively short time scale of wind events (~1 d) relative to changes in river flow (~20 d) also suggest that the plume should show a predominantly southward progression.

4) POST-INITIATION BLOOM STRUCTURE: Once delivered to the study area, the across-shelf distribution of the *Alexandrium tamarense* cells can change dramatically.

In 1988, the distribution of *A. tamarense* cells changed from an isolated patch restricted to low-salinity water, to an extensive population associated with the pycnocline and offshore waters. This change may have been due to a variety of mechanisms, including advection of cells across the front, or enhanced growth of populations in offshore waters. Such mechanisms are discussed below.

IMPLICATIONS AND SPECULATIONS

The conceptual model described above provides specific hypotheses that can be tested. These include: the presence of a population of *Alexandrium tamarense* in the Androscoggin-Kennebec estuary in April; enhanced flow of the Androscoggin and Kennebec Rivers prior to outbreaks of toxicity along the coast; short transit times of initial detection of toxicity along the coast in years of high peak flow; and relatively strong influence of alongshore wind stress in years of low peak flow. These are site-specific hypotheses, and may not apply to the northern areas of the Gulf of Maine.

Similar mechanisms of bloom transport have been described elsewhere. A dramatic example of the advective potential of buoyant coastal currents was seen recently in the bloom of *Chrysochromulina polylepis* in the Skaggerak-Kattegat area in 1988 (Dundas et al., 1989). This bloom, which originated in the brackish waters of the Baltic Sea, was advected ~350 km along the coast of Norway in the Norwegian Coastal Current. In many respects this bloom was similar to those described in the present study, being advected alongshore over hundreds of kilometers and causing widespread economic damage. Tyler and Seliger (1978; Tyler, 1984) performed detailed studies on the transport of the dinoflagellate

Prorocentrum mariae-lebouriae by the currents of the Chesapeake Bay. They demonstrated a complicated interaction between the behaviour of the cells and the structure of the current systems, which allowed transport of the dinoflagellates over hundreds of kilometers.

We do not expect this model to explain the patterns of toxic outbreaks that occasionally occur in the fall in this region; it is likely that different mechanisms are acting such as the delivery of offshore populations to inshore waters. This mechanism would be consistent with the observations of Mulligan (1973, 1975) and Hartwell (1975), who suggested that local offshore populations were advected inshore during wind-driven upwelling. The present data show that a population of *Alexandrium tamarense* was present offshore of the front late in the summer (e.g. Figure 4-5). This population may have derived from the inshore population present in early May, and could provide the biomass for late-season toxicity.

The mechanisms causing the apparent cross-frontal transfer of the *Alexandrium tamarense* population after the initiation of toxicity in 1988 are worthy of some speculation. Prior to the appearance of *A. tamarense* in waters offshore of the front, several strong across-shelf wind events occurred (Figure 4-12) which were directed toward the offshore. Although others might argue that wind-forced surface currents do not have a strong downwind component, Madsen (1977) presented a theory for a turbulent Ekman spiral which predicted the near-surface (<1 m) currents to have a component 10° to the right of the wind. If this were the case, near-surface populations of *A. tamarense* could have been swept across the front into offshore waters, without breakdown of the front itself.

A second mechanism of cross-frontal transfer is the instability of the front itself. As discussed above, such instabilities are likely to occur, given the relatively flat bottom slope and high density contrast. Thus eddies originating at the front which carry

Alexandrium tamarense cells could dissipate in adjacent offshore waters, seeding those waters with large, established populations.

Biological effects must also be considered: there may not have been cross-frontal transfer so much as differential growth or death of cells in the two water masses. Although the offshore populations of June 9, 1988 (Figure 4-5) appear as an isolated patch, there are still high concentrations of *Alexandrium tamarense* in the inshore waters. It is possible that extensive growth took place in offshore waters after the spring warming, or that grazing pressure was significantly greater in the inshore waters.

Another mechanism is that the cells migrating vertically could pass through a horizontal pycnocline formed during upwelling wind events. As the front relaxed back to a sloping position when the wind stress weakened, cells below the pycnocline would find themselves in offshore waters. Thus vertical migration through the pycnocline could lead to seeding of offshore waters.

Finally, alongshore advection of patches of cells explain the changing offshore distribution along our transect through time. From Figure 4-7, it can be seen that the cells were not in a uniform band alongshore, but showed patchiness on the scale of our smallest sampling interval (~5 km). These patches could have been created through a myriad of biological and physical forcings, including differential growth or death, uneven river discharge, internal waves, wind effects, patchy mixing, and frontal instability.

SUMMARY

We have presented data linking the initial distribution of *Alexandrium tamarense* cells in our study area to the alongshore transport of a coastally trapped buoyant plume of water. Many of the implications and hypotheses raised by these data remain to be tested, but the conceptual model we have presented explains many of the observed features of blooms in different years, as well as the

temporal trends in shellfsih toxicity (Hurst and Yentsch, 1981; Martin and Main, 1981; Shumway et al., 1988). Our data cannot directly assess the relative importance of *in situ* growth of localized, nearshore populations as hypothesized by Mulligan (1973, 1975), or physical accumulation of dinoflagellates at frontal convergences (Tyler and Seliger, 1978; Tyler, 1984), but it does emphasize once again the importance of long-distance transport in the general phenomenon of dinoflagellate blooms and shellfish toxicity.

LITERATURE CITED

Anderson, D.M., D. Kulis, J. Orphanos and A. Cuervels. 1982. Distribution of the toxic dinoflagellate Gonyaulax tamarensis in the southern New England region. Estuar. Coastal Mar. Sci. 14:447-458.

Balch, W.M. 1986. Are red tides correlated to spring-neap tidal mixing?: use of a historical recored to test mechanisms responsible for dinoflagellate blooms. In, "Oceanography from Space", J.F.N. Gower (ed.). Plenum Press. NY. 303-312.

Brown, W.S. and J.D. Irish. 1990. The annual evolution of geostrophic flow in the Gulf of Maine. Unpublished manuscript submitted to J. Geophys. Res.

Chao, S.-Y. 1987. Wind-driven motion near inner shelf fronts. J. Geophys. Res. 92:3849-3860.

Dundas, I., O.M. Johannessen, G. Berge and B. Heimdal. 1989. Toxic algal bloom in Scadinavian waters, May-June 1988. Oceanography, 2:9-14.

Flagg, C.N. and R.C. Beardsley. 1978. On the stability of the shelf water/slope water front south of New England. J Geophys. Res. 83:4623-4631.

Garrett, C., J. Keeley and D. Greenberg. 1978. Tidal mixing versus thermal stratification in the Bay of Fundy and Gulf of Maine. Atm-Oc. 16:403-423.

Graham, J.J. 1970. Coastal currents of the western Gulf of Maine, ICNAF Res. Bull 7:19-31.

Greenberg, D. A. 1979. A numerical model investigation of tidal phenomena in the Bay of Fundy and Gulf of Maine. Mar. Geodesy 2:161-187.

Hartwell, A.D. 1975. Hydrographic factors affecting the distribution and movement of toxic dinoflagellates in the western Gulf of Maine. In, "Proceedings of the First International Conference on Toxic Dinoflagellate Blooms", V.R. LoCicero (ed.) Massachusetts Science and Technology Foundation, Wakefield, MA. 47-68.

Holligan, P.M., W.M. Balch and C.M. Yentsch. 1984. The significance of subsurface chlorophyll, nitrite and ammonium maxima in relation to nitrogen for phytoplankton groqth in stratified waters of the Gulf of Maine. J. Mar. Res. 42:1051-1073.

Hurst, J.W. and C.M. Yentsch. 1981. Patterns of intoxication of shellfish in the Gulf of Maine coastal waters. Can. J. Fish. Aquat. Sci. 38:152-156.

Incze, L. and C.M. Yentsch. 1981. Stable density fronts and dinoflagellate patches in a tidal estuary. Estuar. Coast. Mar. Sci. 13:547-556.

James, I.D. 1988. Experiments with a numerical model of coastal currents and tidal mixing fronts. Cont. Shelf Res., 8:1275-1297

Janowitz, G.S. and L.J. Pietrafesa. 1980. A model and observations of time-dependent upwelling over the mid-shelf and slope. J. Phys. Oceanogr. 10:1574-1583.

Large, W.S. and S. Pond. 1981. Open ocean momentum flux measurements in moderate to strong winds. J. Phys. Oceanogr. 11:324-336.

Levy G. and R.A. Brown. 1986. A simple, objective analysis scheme for scatterometer data. J. Geosphys. Res. 91:5153-5158.

Lewis, C.M., C.M. Yentsch and B. Dale. 1979. Distribution of *Gonyaulax excavata* resting cysts in the sediments of Gulf of Maine. In,

"Toxic Dinoflagellate Blooms", D.L. Taylor and H.H. Seliger (eds.) Elsevier, New York. 235-238.

Loder, J.W. and D.A. Greenberg. 1986. Predicted positions of tidal fronts in the Gulf of Maine region. Cont. Shelf Res. 6:397-414.

Madsen, O.S. 1977. A realistic model of the wind-induced Ekman boundary layer. J. Phys. Oceanogr. 7:248-255.

Martin, C. and J.M. Main. 1981. Toxic dinoflagellate blooms (red tides) and shellfish resources in Plum Island Sound and adjacent Massachusetts waters. Final report to the Town of Ipswich, MA, under UMass/Amherst OGCA Contract No. 80A613.

Mulligan, H. 1973. Probable causes for the 1972 red tide in the Cape Ann region of the Gulf of Maine. J. Fish. Res. Bd. Canada 30:1363-1366.

Mulligan, H. 1975. Oceanographic factors associated with New England red tide blooms. In, "Proceedings of the First International Conference on Toxic Dinoflagellate Blooms", V.R. LoCicero (ed.) Massachusetts Science and Technology Foundation, Wakefield, MA. 23-40.

Pingree, R., P. Pugh, P. Holligan and G. Forster. 1975. Summer phytoplankton blooms and red tides in the approaches to the English Channel. Nature 258:672-677.

Prakash, A. 1967. Growth and toxicity of a marine dinoflagellate, Gonyaulax tamarensis. J. Fish. Res. Bd. Can. 24:1549-1606.

Seliger, H., M.A. Tyler and K.R. McKinley. 1979. Phytoplankton distributions and red tides resulting from frontal circulation patterns. In, "Toxic Dinoflagellate Blooms", D.L. Taylor and H.H. Seliger (eds.) Elsevier, New York. 239-248.

Shumway, S., S. Sherman-Caswell and J.W. Hurst. 1988. Paralytic shellfish poisoning in Maine: monitoring a monster. J. Shellfish Res. 7:643-652.

Steidinger, K.A. and Ø. Moestrup. 1990. The taxonomy of *Gonyaulax, Pyrodinium, Alexandrium, Gessnerium, Protogonyaulax* and

Goniiodoma. In, "Toxic Marine Phytoplankton", E. Graneli, B. Sundstrom, L. Edler and D. Anderson (eds.) Elsevier, New York. 522-523.

Strickland, J.D.H. and T.R. Parsons. 1972. A practical handbook of seawater analysis. Fisheries Research Board of Canada. Ottawa. 310 pps.

Tyler, M.A. 1984. Dye tracing of a subsurface chlorophyll maximum of a red-tide dinoflagellate to surface frontal regions. Mar. Biol. 78:285-300.

Tyler, M.A., D. Coats and D.M. Anderson. 1982. Encystment in a dynamic environment: deposition of dinoflagellate cysts by a frontal convergence. Mar. Ecol. Prog. Ser. 7:163-178.

Tyler, M.A. and H.H. Seliger. 1978. Annual subsurface transport of a red tide dinoflagellate to its bloom area: water circulation patterns and organism distributions in the Chesapeake Bay. Limnol. Oceanogr. 23:227-246.

Watras, C., S. Chisholm and D. Anderson. 1982. Regulation of growth in an estuarine clone of Gonyaulax tamarensis Lebour: salinity-dependent temperature responses. J. Exp. Mar. Biol. Ecol. 62:25-37.

White, A.W. 1978. Salinity effects on growth and tozin content of *Gonyaulax excavata*, a marine dinoflagellate causing paralytic shellfish poisoning. J. Phycol. 14:475-479.

Yentsch, C. M., P. M. Holligan, W. M. Balch and A. Tvirbutas. 1986. Tidal stirring vs. stratification: microalgal dynamics with special reference to cyst-forming toxin producing dinoflagellates. In, "Lecture Notes on Coastal and Estuarine Studies, Vol. 17. Tidal Mixing and Plankton Dynamics", J. Bowman, M. Yentsch and W. T. Peterson (eds.). Springer-Verlag, Berlin. Pgs 224-252.

CHAPTER 5

TOXIC PHYTOPLANKTON BLOOMS IN THE SOUTHWESTERN GULF OF MAINE: TESTING HYPOTHESES OF PHYSICAL CONTROL USING HISTORICAL DATA

"Hallo, Pooh," said Rabbit.
"Hallo, Rabbit. Fourteen, wasn't it?"
"What was?"
"My pots of honey what I was counting."
"Fourteen, that's right."
"Are you sure?"
"No," said Rabbit. "Does it matter?"
"I just like to know," said Pooh humbly. "So as I can say to myself: 'I've got fourteen pots of honey left.' Or fifteen, as the case may be. It's sort of comforting."
"Well, let's call it sixteen," said Rabbit.

A.A. Milne
Winnie-the-Pooh

ABSTRACT

Blooms of the toxic dinoflagellate, *Alexandrium tamarense* have been nearly annual features along the coasts of southern Maine, New Hampshire and Massachusetts since 1972. Two hypotheses which have been used to explain the initiation of these blooms were tested using historical records of toxicity, wind, and river flow. The first hypothesis states that the blooms were initiated or advected to shore by wind-driven coastal upwelling. The second states that established blooms were advected from north to south alongshore in a coastally trapped buoyant plume of water. Of the eleven years examined, we found four cases inconsistent with the wind-driven upwelling hypothesis, and only one case (1985) which contradicts the plume-advection hypothesis. 1985 was an unusual year in many respects, and we suggest that some other mechanism was responsible for the toxic outbreaks. In addition, the wind-driven upwelling hypothesis could not explain the observed north-to-south progression of toxicity each year. The plume-advection hypothesis thus best explains the details of the timing and spread of shellfish toxicity. These include the variable north-to-south progression with time, the presence of a toxin-free zone south of Cape Ann, MA, the sporadic nature of toxic outbreaks south of Massachusetts Bay, and the apparently rare occurrence of toxicity well offshore on Nantucket Shoals and Georges Bank.

INTRODUCTION

Blooms of the toxic dinoflagellate *Alexandrium tamarense*[1] have caused nearly annual shellfish bed closures along the coasts of southern Maine, New Hampshire and Massachusetts since 1972. Shellfish which ingest this dinoflagellate can accumulate its potent neurotoxins, becoming vectors of paralytic shellfish poisoning (PSP). Monitoring programs set up by state agencies regularly sample coastal shellfish and test for PSP toxins using the mouse assay (e.g. Hurst, 1979; Hurst et al., 1985; Shumway et al. 1988). Such programs, combined with laboratory experiments, have demonstrated a clear relationship between the toxicity of the mussel, *Mytilus edulis*, and the presence of *A. tamarense* cells. Bricelj et al. (1990) have shown mussels to accumulate measurable toxin in as little as 24 hours after exposure to *A. tamarense* cells, while saturating levels of toxicity were achieved in 10-13 d. In the analyses below, we use the toxicity of *M. edulis*, and the clam, *Mya arenaria*, as surrogates for the presence or absence of *A. tamarense* in the field.

Blooms of *Alexandrium tamarense* generally begin in April or early May, causing PSP outbreaks which progress from Maine southward to Massachusetts. This spatial and temporal progression of toxic events, and presumably *A. tamarense* blooms, could be due to either local growth of the cells, or advection of cells along the coast.

The former type of bloom was first discussed by Mulligan (1973, 1975), Hartwell (1975), and Seliger et al. (1979) who

---

[1] *Alexandrium tamarense* and *Alexandrium fundyense* were formerly included in the genera *Protogonyaulax* or *Gonyaulax* but are now accepted as *Alexandrium* species (Steidinger and Moestrup, 1990). Both species bloom in the Gulf of Maine (Anderson, unpub. data), but since discrimination between them is impossible for large-scale field programs or when referring to shellfish toxicity, only the more familiar name *Alexandrium tamarense* will be used here.

hypothesized that the blooms were initiated by wind-driven upwelling in the southern Gulf of Maine. They suggested that populations of *A. tamarense*, growing at mid-depth in offshore waters were advected onshore into the coastal zone where they formed local blooms. This presumes a population of *A. tamarense* was growing just offshore, below the pycnocline. This hypothesis predicts that toxic outbreaks in intertidal shellfish should be preceded by wind-driven upwelling, and that the *A. tamarense* cells are of nearby, offshore origin.

In Chapter 4 it was hypothesized that the annual southward progression of toxicity was instead a result of alongshore advection of an *Alexandrium tamarense* population in a coastally trapped buoyant plume. The plumes were thought to be formed by enhanced outflow of the Androscoggin and Kennebec Rivers in Maine (Figure 5-1), following heavy spring rainfalls. The plumes carry the *A. tamarense* populations for hundreds of kilometers along the coast, delivering them to shellfish beds along the way. Alongshore winds were hypothesized to influence the motion of the plume: upwelling (northeastward) winds would slow the plume and possibly move it offshore, while downwelling (southwestward) winds would hold the plume to the coast and speed it alongshore to the southwest. This hypothesis predicts that PSP outbreaks are likely to follow a peak in the regional river flow, and that downwelling-favourable winds should speed the southward progression of PSP toxicity. Furthermore, in years of high river discharge, the timing of toxic outbreaks should be relatively independent of the wind, while in years of low discharge, the wind should have greater control over the toxicity patterns, due to the dependence of plume velocities on volume of river discharge.

The present study tested these two hypotheses, using historical records of shellfish toxicity, flow rates of the Androscoggin River, and wind records from Logan Airport, Boston. In analyzing data from eleven years (1979-1989) we found four cases which were not consistent with the upwelling hypothesis, and only one

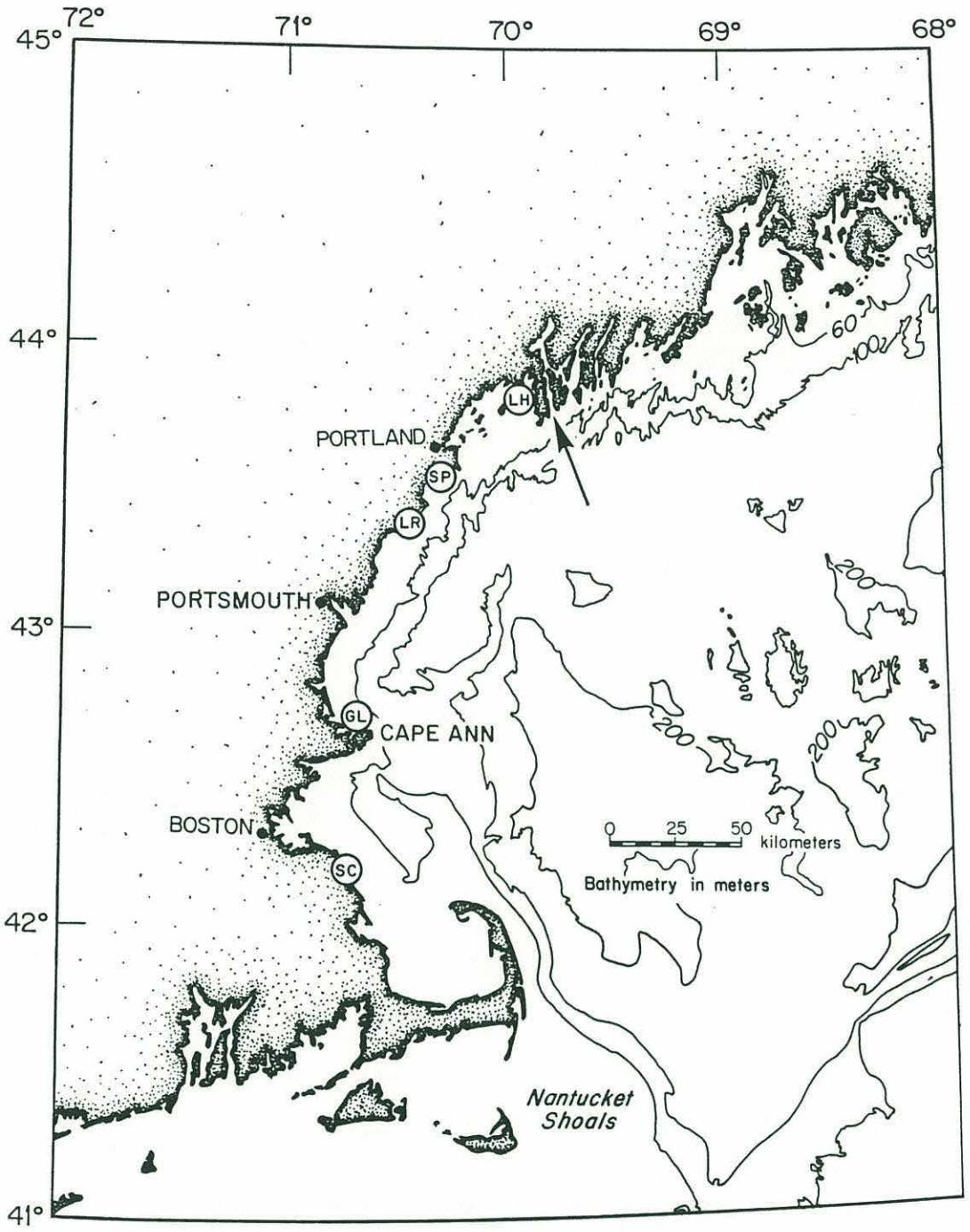

Figure 5-1. Map showing the region from Maine to Cape Cod, with the five sampling stations indicated: Lumbos Hole (LH), Spurwink River (SP), Little River (LR), Gloucester (GL), and Scituate (SC). The estuary into which the Androscoggin and Kennebec Rivers empty is indicated by the arrow.

case (1985) which rejected the plume-advection hypothesis. We believe that the plume-advection hypothesis best explains many details of the temporal and spatial distribution of PSP outbreaks for most years in the southern Gulf of Maine.

DESCRIPTION OF THE DATA SETS

Shellfish toxicity data were obtained through the Department of Marine Resources, Maine, and the Department of Environmental Quality Engineering, Massachusetts. Five stations were selected from the many which are regularly sampled. These stations were Lumbos Hole (LH), Spurwink River (SP) and Little River Kennebunkport (LR), all in Maine, and Gloucester (Annisquam Yacht Club; GL) and Scituate (Yacht Club; SC), Massachusetts (Figure 5-1). These stations were chosen for the completeness of their historical records, their geographic distribution along the coast, and their regular manifestation of shellfish toxicity.

Shellfish toxicity was measured using the mouse assay (AOAC, 1975). The different strains of mice used in Maine and Massachusetts showed different sensitivities to the dinoflagellate neurotoxins, giving different threshold responses for the two data sets (S. Sherman-Caswell, pers. comm.) In addition, different species of shellfish show different intoxication and depuration rates (Shumway et al., 1988). The mussel, *Mytilus edulis* becomes toxified very rapidly (Bricelj et al., 1990), and thus can be used as an indicator for the early exposure to toxic cells, and the onset of shellfish toxicity. The clam, *Mya arenaria*, which depurates the toxins fairly slowly, can be used to indicate the disappearance of the cells and the toxicity. The data from Maine have continuous records of toxicity in *Mytilus*, whereas the Massachusetts data reflect the mid-season switch from monitoring *Mytilus* to *Mya*, showing a discontinuity in the toxicity records. Thus the data for the initiation of toxicity are internally consistent (all *Mytilus*), while the data for the duration of toxicity are not (*Mytilus* or *Mya*). For these reasons, toxicity records were converted to a binary form: 1=measurable

toxicity (>58 μg/100 g shellfish meat (ME), >40 μg/100 g shellfish meat (MA)), 0=no measurable toxicity. Thus the magnitude of the toxicity is not considered in the present analyses.

The freshwater flow statistics for the Androscoggin River (indicated in Figure 5-1) were obtained through the United States Geological Survey. These data give the mean daily flow of the river, measured well inland of any tidal influence. The Androscoggin and Kennebec Rivers empty into the same estuary, and show the same temporal flow patterns and volumes (Chapter 4) Only the Androscoggin River flow rates are used here, but the importance of the Kennebec River should be recognized. The drainage basin of the Androscoggin River is ~8500 km^2, and the Kennebec is ~14000 km^2. The combined drainage areas are equivalent to 25% of the area of Maine.

The wind data were obtained from the National Climatic Data Center (National Oceanographic and Atmospheric Administration). These hourly observations of wind speed and direction at Logan Airport, Boston, Massachusetts, were rotated into the coordinate system of the coast by subtracting 30°. The data were resolved into across- and alongshore wind stresses (Pa), using the algorithm of Large and Pond (1981). The wind stresses were smoothed and gridded to points every three hours using the objective mapping routine of Levy and Brown (1986). This process smooths the spikes in the data, making them easier to visualize, and reduces the number of points to be manipulated. The weather patterns show the Boston data to be representative of a region from Cape Cod to southern Maine. For the present analyses, the wind patterns were considered to be identical throughout the study region.

Toxicity records were available for the years 1973-1989 from Massachusetts. However, regular sampling of stations did not become commonplace in both Maine and Massachusetts until 1979. For this reason the years to be analyzed extend only from 1979-

1989. No toxicity data were available for Gloucester or Scituate for 1984, and no data were found for Scituate, 1982.

OBSERVATIONS

TOXICITY

Figures 5-2 to 5-12 show the binary toxicity time series, flow rate of the Androscoggin River, and the alongshore and across-shelf wind stresses for the years 1979-1989. In the toxicity plots, the northern-most station, Lumbos Hole (LH), is at the top of the panel, and southern-most station, Scituate (SC), is at the bottom of the panel. The approximate alongshore distance between the stations is shown on the vertical axis. The time series of binary toxicity have been plotted so that toxic samples are heavy lines, and non-toxic samples are light lines. The sampling dates are shown by the vertical lines. An average trend of north-to-south movement of toxicity can be seen for all years (Figure 5-13a). For years such as 1979, the first samples taken in Maine were toxic, so we cannot specify the first occurrence of toxicity. In other years, the time between samples is large enough that the north-to-south trend could be an artifact of the sampling. However, the mean date of initiation of toxicity at Lumbos Hole, ME was significantly earlier ($P<0.05$) than the initiation of toxicity at Gloucester or Scituate, MA, despite being ~250 km farther north in presumably colder waters.

A weak trend toward later initiation of toxicity over the interval 1979-1989 suggested that the simple averages of Figure 5-13a may not give an accurate representation of the north-to-south progression. To account for this, the data for the first occurrence of toxicity at the five stations, T_i, were scaled by the time interval between the first occurrence of toxicity at Lumbos Hole and Gloucester, as follows:

$$T_i = \frac{T_i - T_{LH}}{T_{GL} - T_{LH}} . \qquad (5\text{-}1)$$

Here T_i is the time of initiation of toxicity at station i (i=LH, SP, LR, GL or SC). Thus Lumbos Hole scales to zero, and Gloucester to unity for each year, with the other stations distributed around zero and one. When the data are plotted in this way (Figure 5-13b), the north-to-south trend is enhanced. Spurwink River is found to show initiation of toxicity significantly later than Lumbos Hole ($P<0.05$), and Gloucester and Scituate are significantly later than the more northerly stations ($P<0.05$). The large confidence intervals on the Scituate data are due to the low number of data points; no toxicity was detected at Scituate in 1981, 1983 or 1987, and no data were available for 1982 or 1984. The data from 1985 weaken the apparent north-to-south trend since Little River was the first station to show toxicity in that year, giving a negative scaled time of PSP initiation.

The first measurable PSP toxin is usually detected in Maine between mid-April and mid-May. The one exception to this was the year 1985, when the first toxicity was seen in the last ten days of May (Figure 5-8). As we shall see below, 1985 was an unusual year in many respects, and presents the only case contradicting the plume-advection hypothesis.

Two temporal patterns of toxicity can be seen from Figures 5-2 to 5-12. In years such as 1980, 1985 and 1987, the toxicity showed a patchy temporal distribution, with several outbreaks of short duration at each station. In most other years, the toxicity persisted over several months. These patterns appear to be related to the volume of freshwater outflow (middle panels). Years with low flow during the summer show patchy toxicity, whereas years with high flow, particularly in early May, show sustained toxicity.

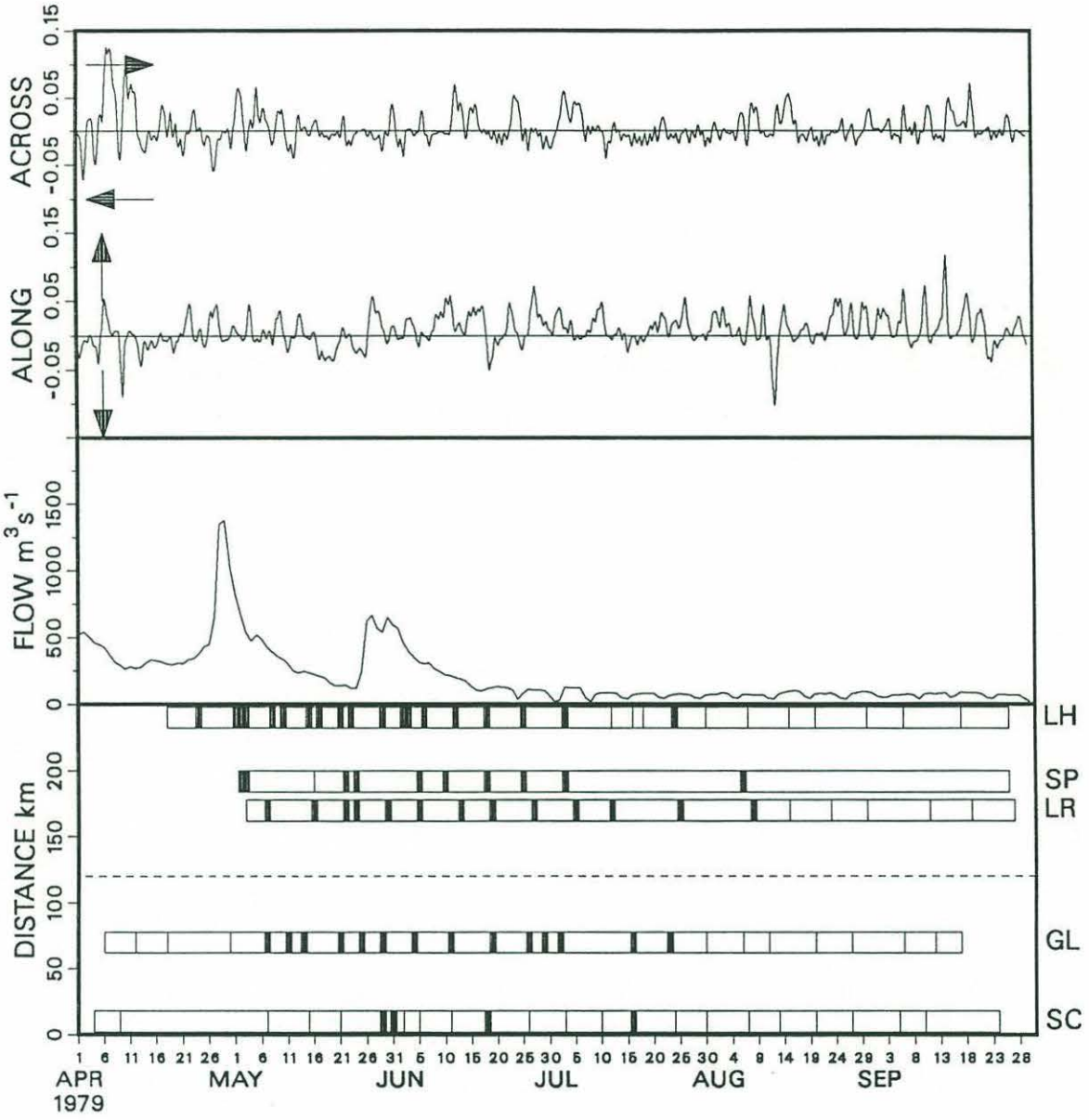

Figure 5-2. Lower panel: shellfish toxicity vs. time for 1979. Heavy vertical lines indicate toxic samples, while light vertical lines indicate non-toxic samples. The alongshore distance between stations is indicated on the vertical axis. Station abbreviations as in Figure 5-1. Middle panel: flow rate ($m^3\ s^{-1}$) of the Androscoggin River, for the dates indicated on the bottom horizontal axis. Top panel: alongshore (lower axis) and across-shelf (upper axis) wind stresses (Pa). The directions the stresses act are indicated by the arrows.

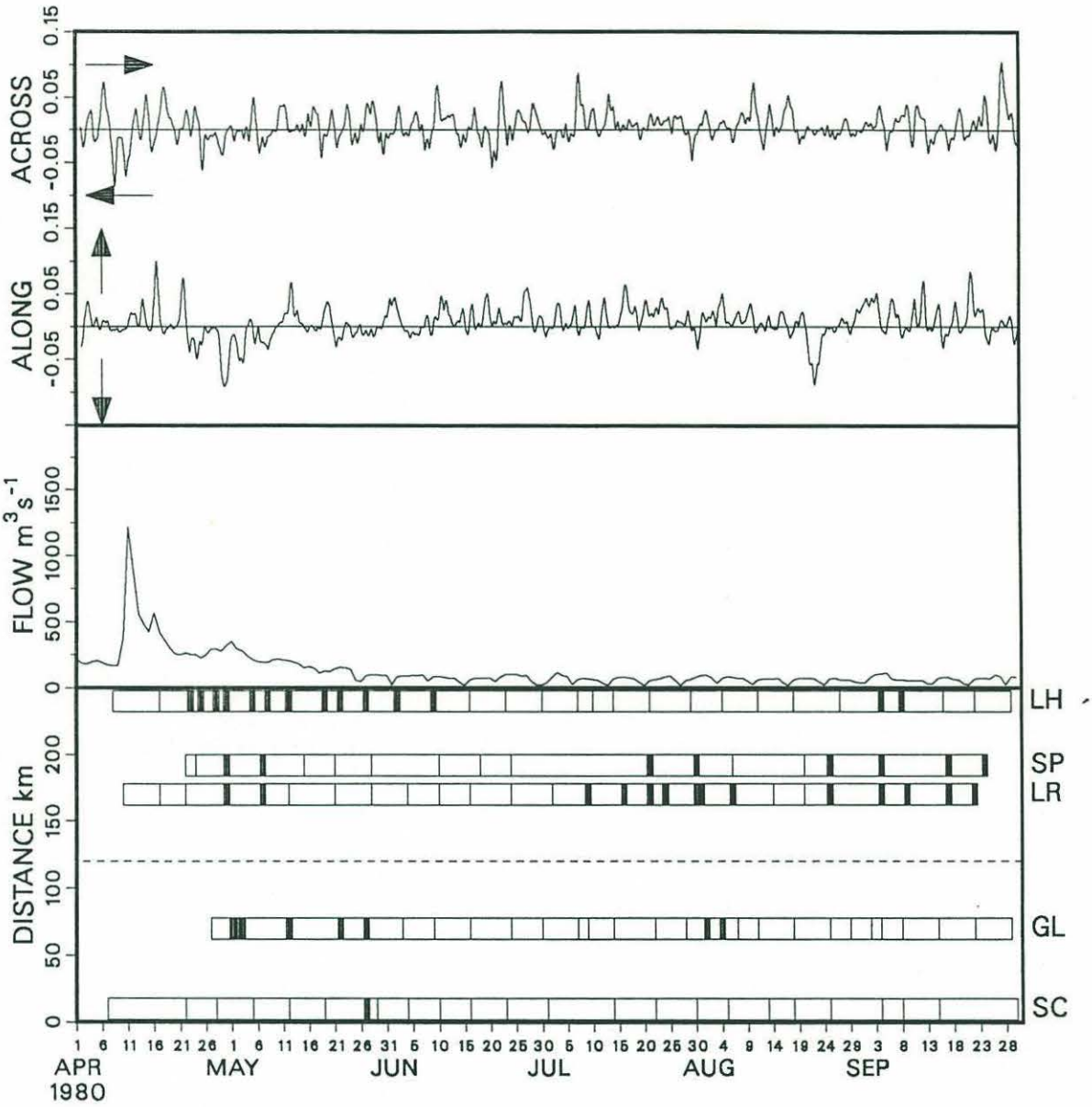

Figure 5-3. Legend same as Figure 5-2, but for the year 1980.

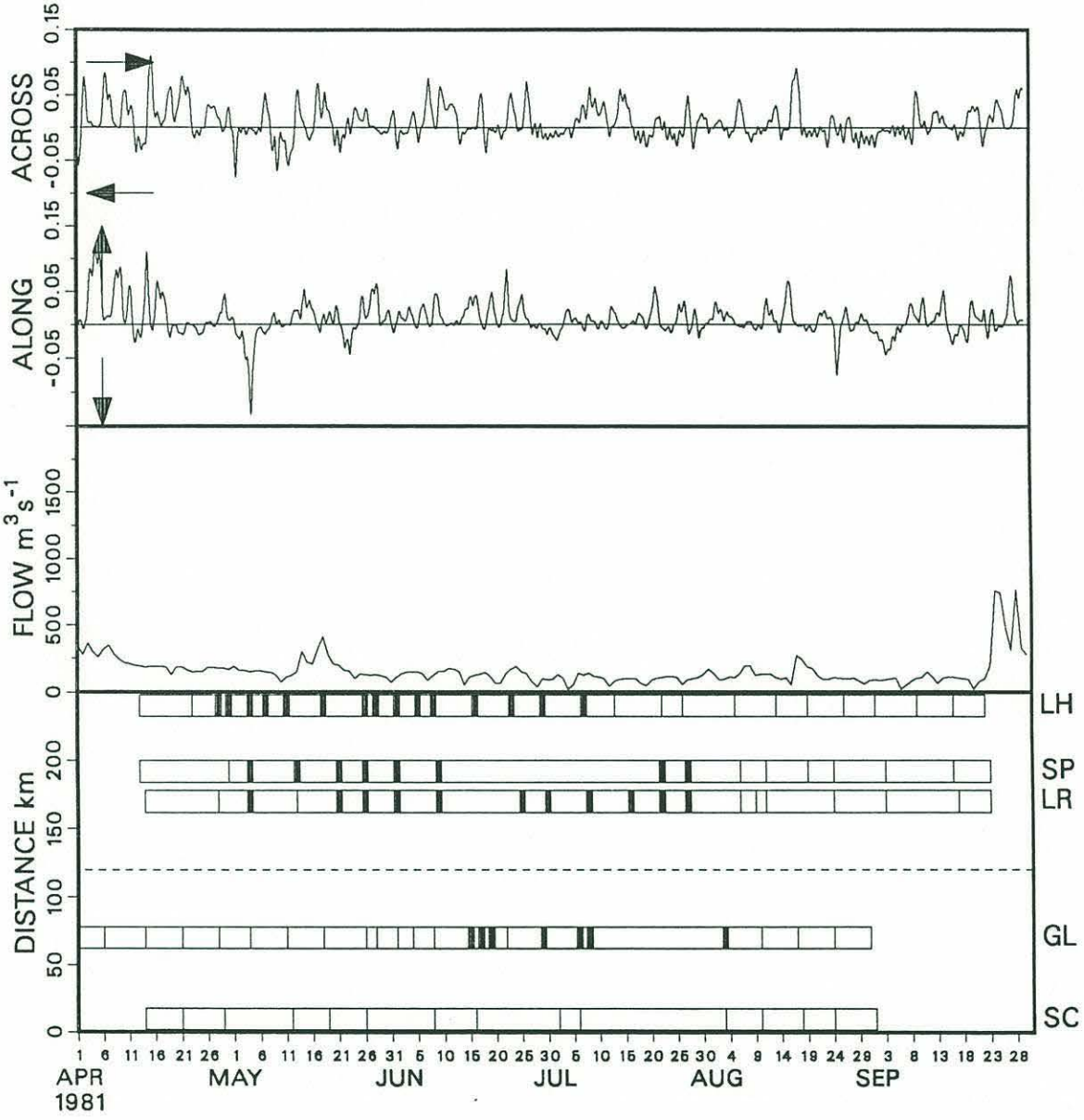

Figure 5-4. Legend same as Figure 5-2, but for the year 1981.

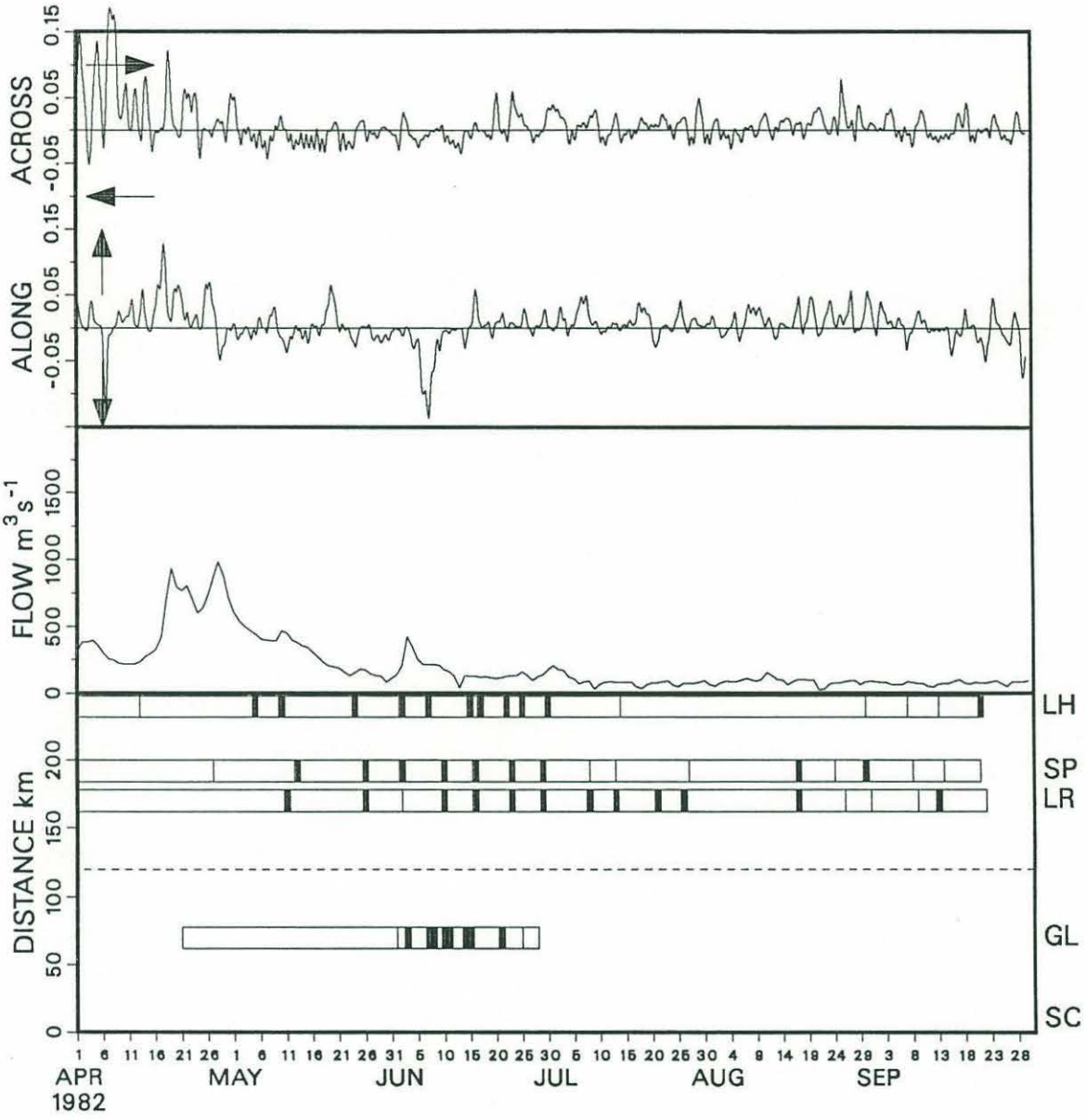

Figure 5-5. Legend same as Figure 5-2, but for the year 1982. No data were available for Scituate.

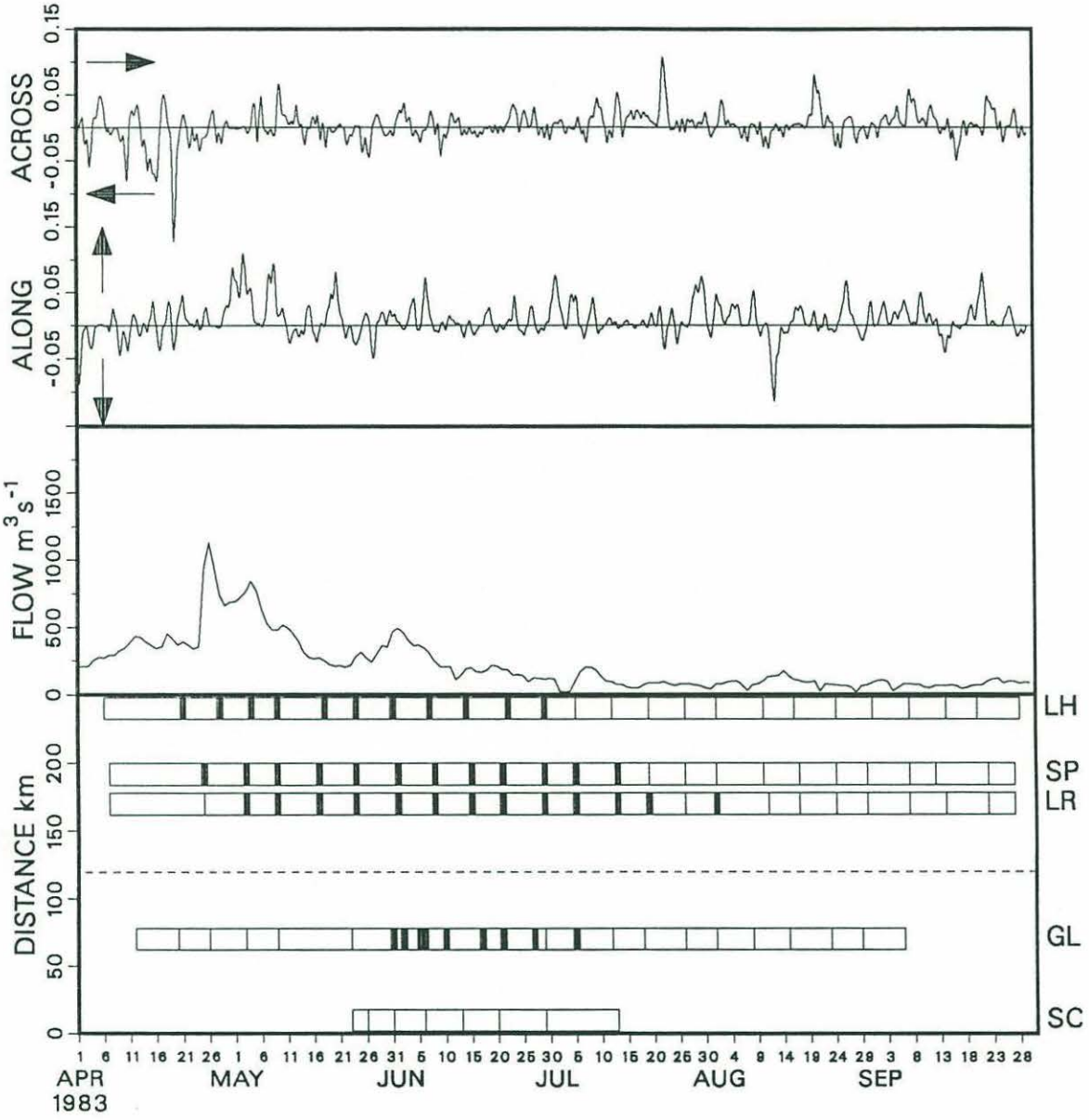

Figure 5-6 Legend same as Figure 5-2, but for the year 1983.

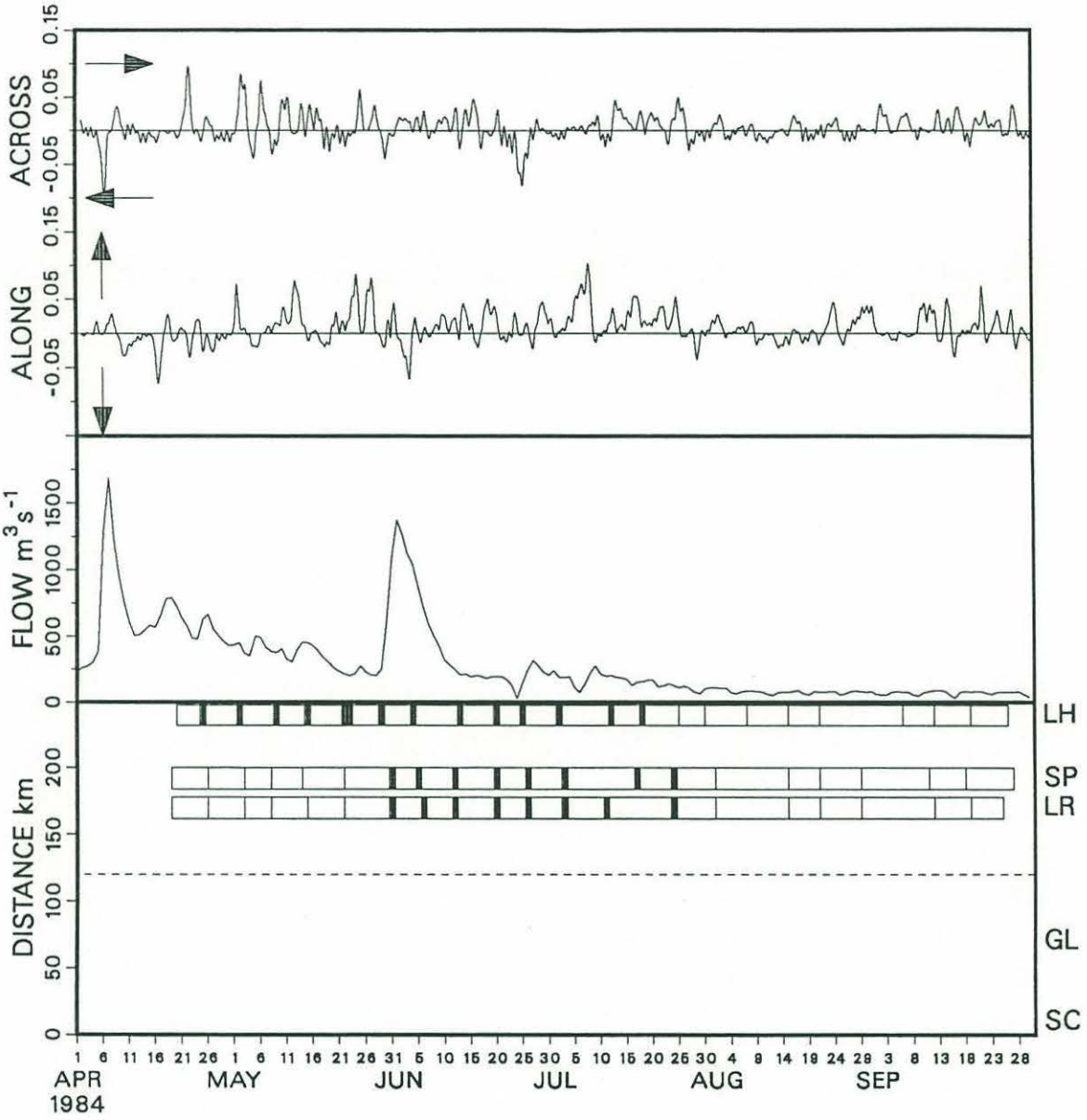

Figure 5-7. Legend same as Figure 5-2, but for the year 1984. No data were available for Gloucester or Scituate.

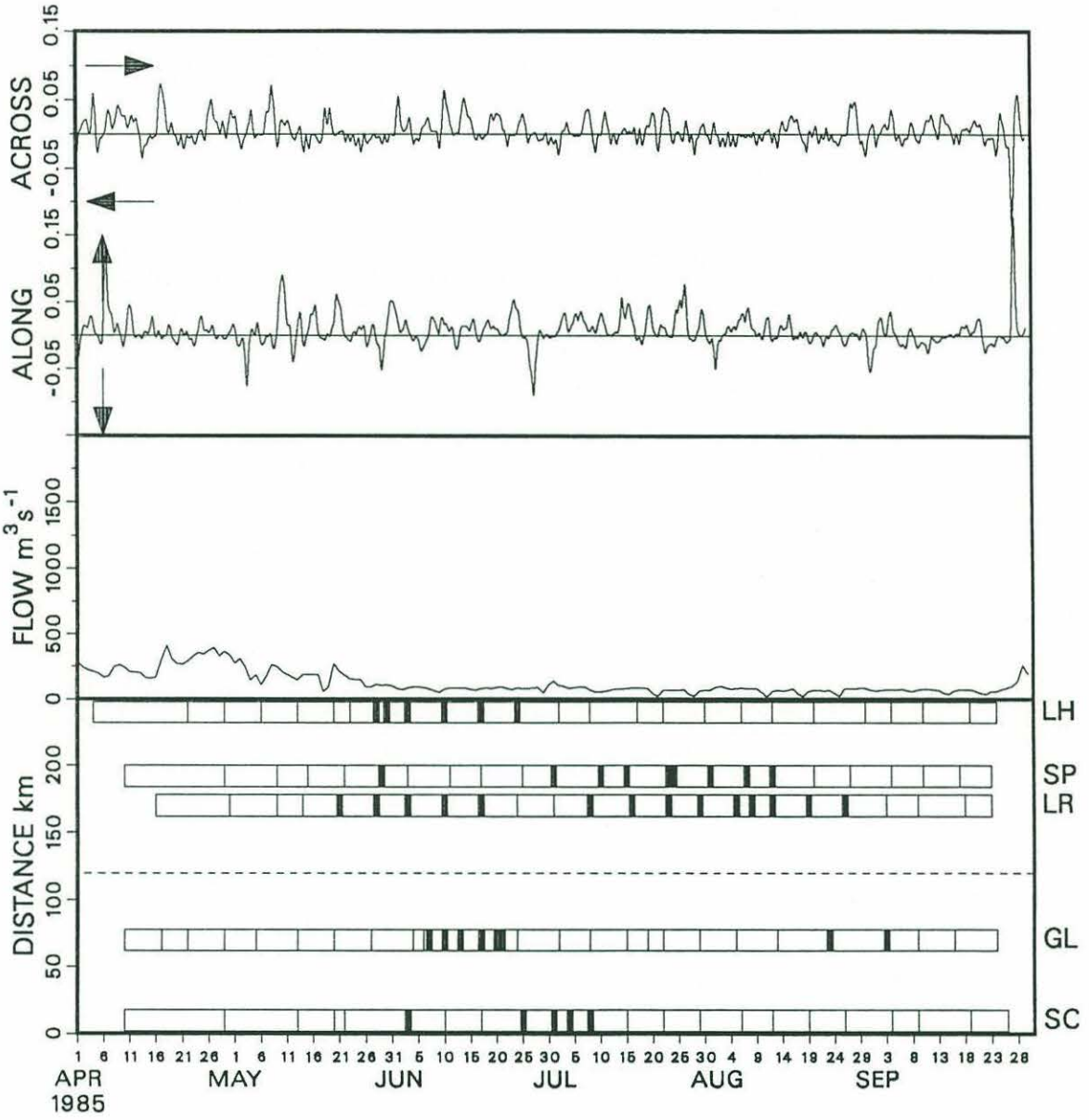

Figure 5-8. Legend same as Figure 5-2, but for the year 1985.

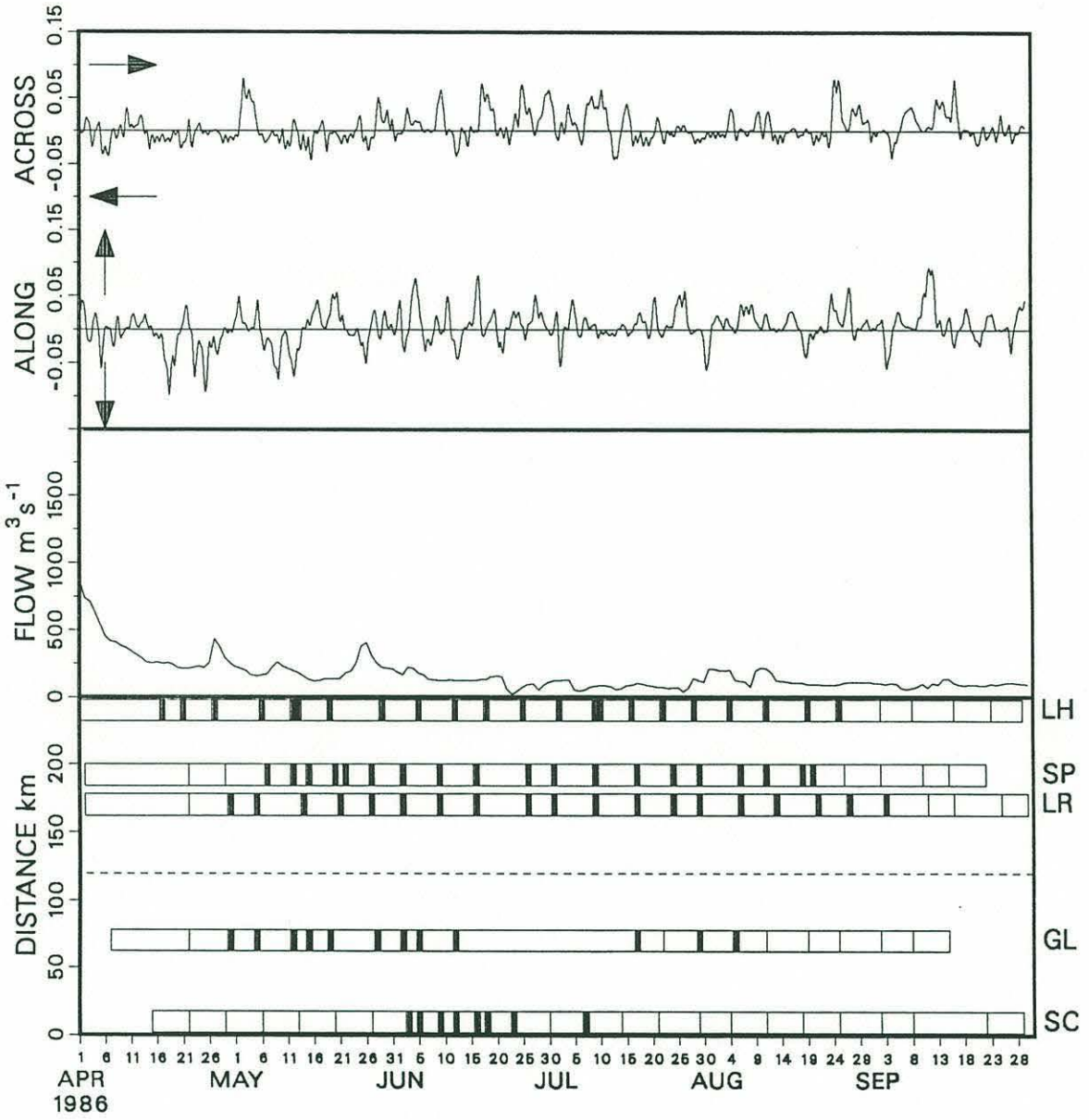

Figure 5-9. Legend same as Figure 5-2, but for the year 1986.

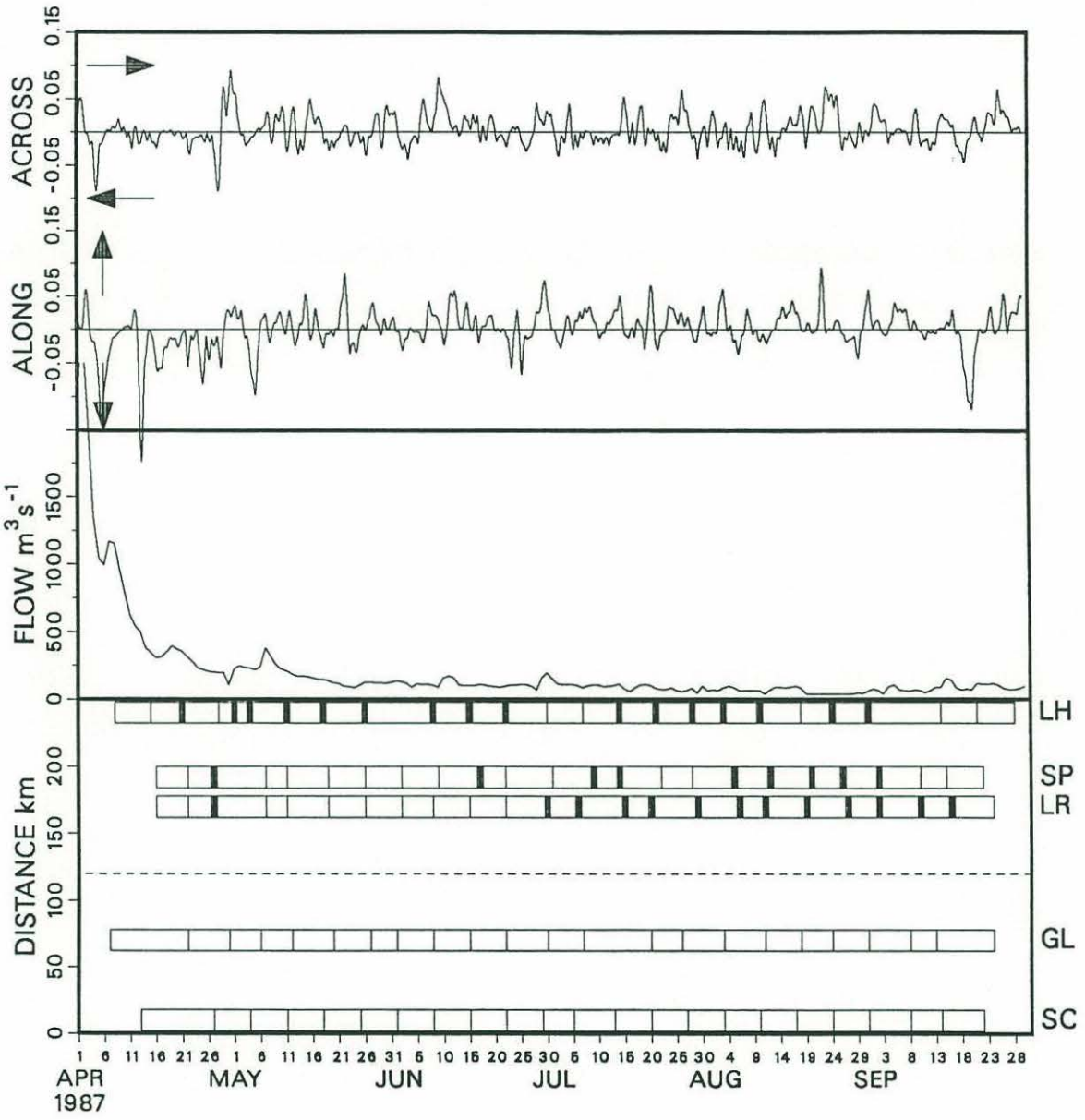

Figure 5-10. Legend same as Figure 5-2, but for the year 1987.

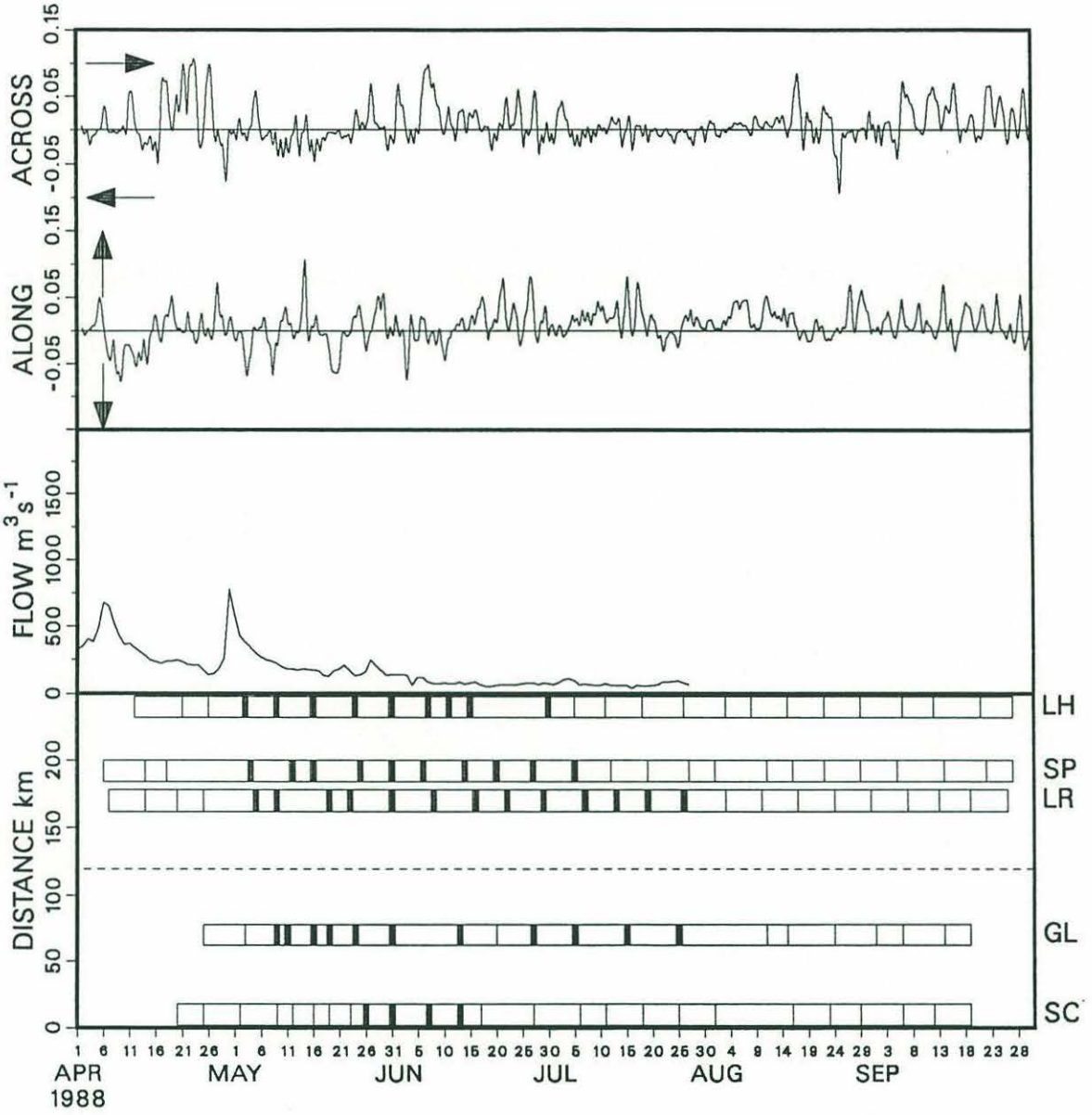

Figure 5-11. Legend same as Figure 5-2, but for the year 1988.

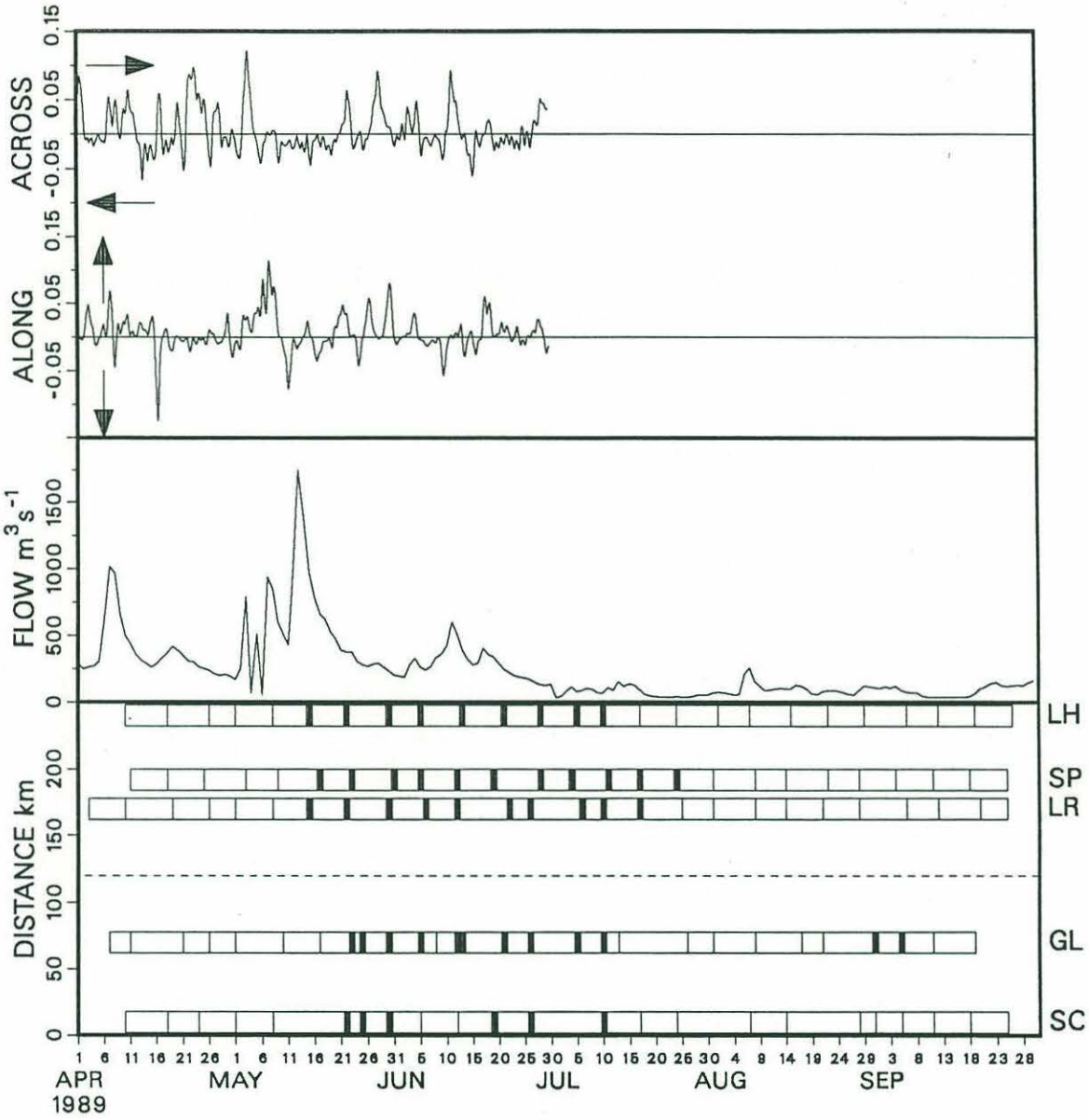

Figure 5-12. Legend same as Figure 5-2, but for the year 1989.

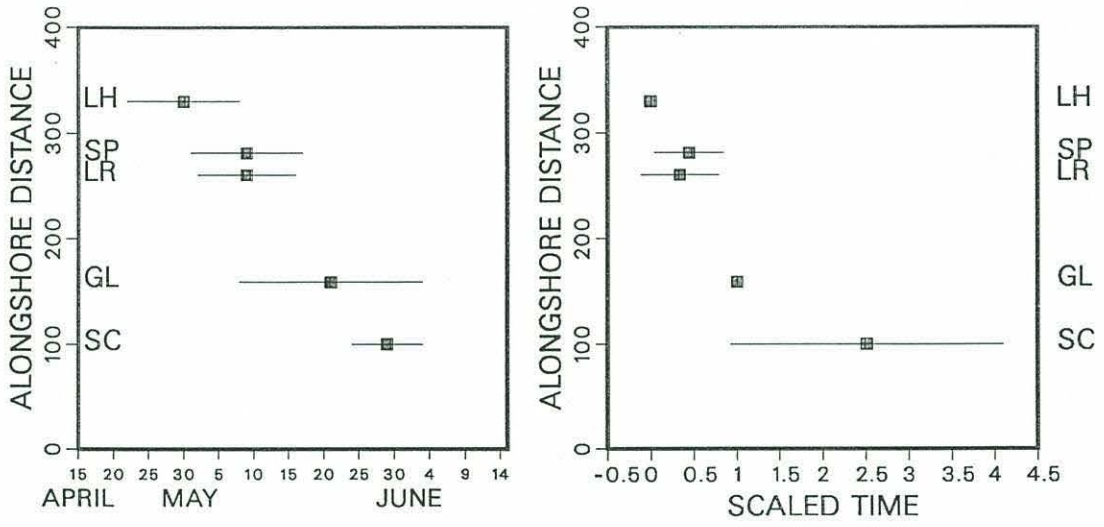

Figure 5-13. (a) Average time of initiation of toxicity at Lumbos Hole (LH), Spurwink River (SP), Little River (LR), Gloucester (GL), and Scituate (SC). (b) Scaled time lag of initiation of toxicity relative to Lumbos Hole. The error bars are 95% confidence intervals.

FRESHWATER FLOW

The outflow of the Androscoggin river generally shows two distinct peaks: the first in early April, driven by meltwater runoff, and the second in late April-early May, in response to rainfall. It can be seen that in every year, the first toxicity at Gloucester is preceded by a peak in the flow rate of the Androscoggin River. In years such as 1981, 1985 and 1986 this flow peak was low; it was absent in 1987, the only year since 1972 that shellfish toxicity was not detected in northern Massachusetts. This finding supports the plume-advection hypothesis, which states that the buoyant plume created by the enhanced freshwater outflow of the Androscoggin and Kennebec Rivers carries the toxic dinoflagellates alongshore to the south.

The plume-advection hypothesis predicts that years with high flow rates should show reduced transit times of toxicity along the coast. That is, the interval between the first occurrence of toxicity in Maine, and the initiation of toxicity at Gloucester should be smaller in years of large flow. Chao (1988) recasts some work of Kao et al. (1978) to give an equation relating the speed of a river plume along a coast (intrusion speed, v_i) with the volume of flow of the river:

$$v_i = (g' Q)^{1/3} \qquad (5\text{-}2)$$

where Q is the flow volume per unit width of the channel, and g' is the reduced gravity,

$$g' = g\frac{\rho' - \rho}{\rho'}. \qquad (5\text{-}3)$$

Here g is the acceleration due to gravity, ρ is the density of the freshwater, and ρ' is the density of the ambient offshore water. We can rearrange (5-2) to give the transit time, Δt, between points on the coast separated by a distance Δx:

$$\Delta t = \frac{\Delta x}{v_i} = \frac{\Delta x}{(g' Q)^{1/3}} . \qquad (5\text{-}4)$$

The parameter g' will tend to decrease over time as mixing reduces the density contrast of the plume. Using a constant g' and Δx in equation (5-4) will thus give estimates of Δt which are likely to be low, however our qualitative argument should hold: a plot of Δt versus Q should yield a shape similar to that of Figure 5-14a. To test this prediction, we have plotted the peak flow volume of the Androscoggin River in the interval preceding the first occurrence of toxicity ($\equiv$ Q), versus the time interval between the initiation of toxicity at Lumbos Hole ME, and at Gloucester MA ($\equiv \Delta t$) (Figure 5-14b). The points of Figure 5-14b show the same basic pattern as the curve of Figure 5-14a: large Δt for low flows, and low Δt for high peak flow volumes. There is a great deal of scatter of points about the predicted curve, however. The sources of this will be discussed below.

The shape of the curve in Figure 5-14a suggests that for low river flows, the time interval between toxic events along the coast, Δt, may vary considerably. For higher flows, Δt should be almost constant, varying only slowly with flow volume. This trend seems to be reflected in the data of Figure 5-14b: for low flows Δt varied from 9 to 53 days. For flows >1000 $m^3 s^{-1}$, Δt was between 8 and 13 days. From Figure 5-1, the distance between Lumbos Hole and Gloucester is ~170 km. Assuming Δt=10 d (high flow volume), v_i~0.2 m s^{-1}. This is the same as the plume velocity calculated independently in Chapter 4, using hydrographic data and Margule's equation. For low flow rates, we might expect plume velocities of v_i~0.02 m s^{-1}. At this rate, the plume would take ~85 d to cover the distance from Lumbos Hole to Gloucester. Note that in 1987, a low flow year, shellfish toxicity was not measurable at Gloucester or Scituate, despite its occurrence at stations to the north in Maine. From Figure 5-13a, the average progression rate of toxic events along the coast is given by the slope of the regression line fit to the

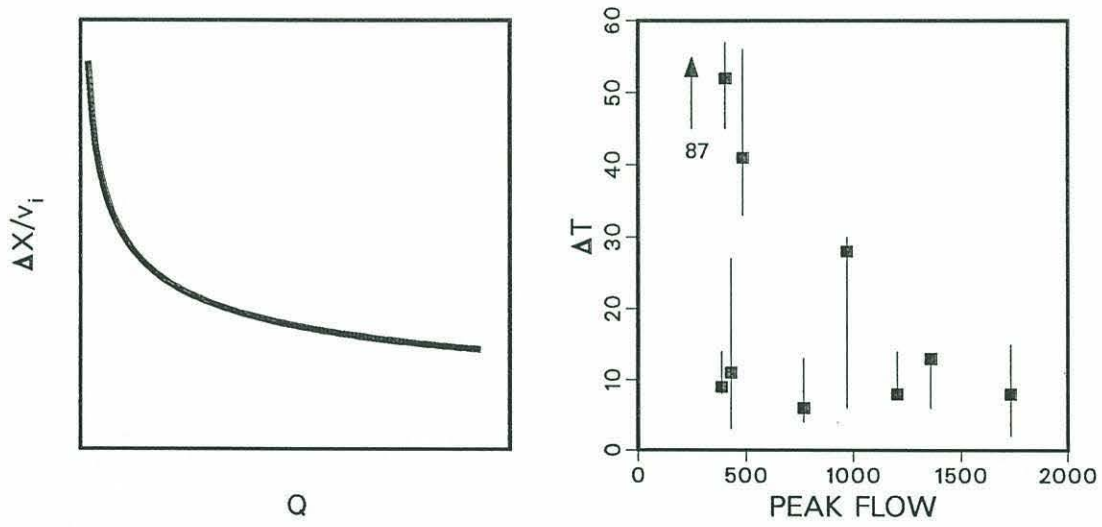

Figure 5-14. (a) Predicted relationship of transit time of toxicity alongshore ($\Delta x/v_i$), to flow rate of the river (Q). (b) time interval between initiation of toxicity at Lumbos Hole and Gloucester (Δt, days), plotted versus the peak flow volume of the Androscoggin River (Peak Flow, $m^3\ s^{-1}$). The error bars indicate the uncertainty of the estimate of Δt due to the interval between the last non-toxic sample, and the first toxic sample. The year 1987 did not show toxicity at Gloucester, so Δt is effectively infinite.

mean values. This slope is 8.23 km d^{-1}, (R^2=0.983), or ~0.1 m s^{-1} to the south, in good agreement with the values calculated above.

The river flow data thus tend to support the plume-advection hypothesis: every toxicity event in the south of the study area was preceded by an increase in the flow rate of the Androscoggin River. Years of high flow tended to show small transit times, Δt, between the first occurrence of toxicity at Lumbos Hole, and at Gloucester. The advective speed of the plume for high flow rates, calculated from $\Delta x/\Delta t$, was the same as that calculated independently using the observed density of water masses from hydrographic surveys in the study area.

WIND EFFECTS

As discussed in Chapter 4 and by Mulligan (1973, 1975), Hartwell (1975) and Seliger et al. (1979), the wind could have an influence on the timing and location of toxic shellfish outbreaks. The latter authors predicted that toxic events should be preceded by upwelling-favourable winds, whereas my Chapter 4 predicted that downwelling-favourable winds should have the greater effect by holding the buoyant plume (and thus the toxic cells) to the coast, and advecting it southward. The plume-advection hypothesis also predicts that sustained upwelling-favourable winds in years of low flow may slow or halt the progression of the plume, and potentially halt the alongshore spread of toxicity. This would occur because winds from the south would force a weak plume northward and offshore.

The wind stresses of Figures 5-2 to 5-12 have been plotted so that positive alongshore stresses are upwelling-favourable (winds to the north), and positive cross-shore stresses act from the coast to the ocean (to the east). These data show diel fluctuations, with superimposed longer-term events. Because of the regular passage of weather systems, any toxicity event can be seen to be preceded by at least one upwelling-favourable wind event. However, this

qualitative approach cannot give information concerning the relative effects of any wind event.

To obtain more quantitative information on the effects of the wind, the time-dependent model of Janowitz and Pietrafesa (1980) was employed. This very simple time-dependent model gives a solution for the wind-induced quasi-geostrophic motion of interior fluid (independent of surface and bottom boundary layers), given rigid lid, Boussinesq and hydrostatic approximations. The rigid lid approximation assumes that vertical motions of the sea surface are negligible. The Boussinesq approximation allows the use of a constant density over a region, except where vertical gradients of density enter the equation (i.e. buoyancy effects). The hydrostatic approximation assumes that the vertical gradient of pressure is dependent only on the vertical gradient of density, i.e. vertical accelerations, vertical Coriolis accelerations and vertical stress gradients are neglected. Alongshore variation is assumed negligible.

The alongshore momentum equation was integrated vertically, so that changes in the alongshore flux balance of the surface alongshore wind stress, $\tau^y(t)$, and the bottom frictional stress. If a linear bottom stress is used, an equation for the alongshore velocity, v, is obtained:

$$v = \frac{1}{\rho h} \int_0^t \tau^y(t') \exp[-fd(t-t')/h]\, dt'. \qquad (5\text{-}5)$$

The linear bottom stress, τ^B, was parameterized as

$$\tau^B = \rho c_1 v(-h,t) \qquad (5\text{-}6a)$$

$$d = c_1/f \qquad (5\text{-}6b)$$

with $c_1=2.5 \times 10^{-4}$ m s^{-1}, and the Coriolis frequency, $f=1 \times 10^{-4}$ s^{-1}. The water depth, h, was set at a constant 20 m, and 1024 kg m^{-3} was used for the water density, ρ. The model described by equation

(5-5) indicates that the alongshore velocity of the interior fluid is the result of an exponential weighting of the present and past alongshore wind stresses.

The forcing of the alongshore current occurs through the Coriolis deflection of the cross-shelf currents which were set up by the alongshore wind stress. The shallow water depths near the coast force an alongshore jet at the coast. According to Janowitz and Pietrafesa (1980), several criteria must be met for the model to be applicable. The first is that d/h«1. From equation (5-6b), we calculate d/h~0.1, so this condition is met. Secondly, the relationship of the nonlinear to time-dependent terms requires:

$$\frac{v h_x}{f h} \ll 1. \qquad (5\text{-}7)$$

The across-shelf bottom slope, h_x in this region is ~0.004. With v=0.2 ms^{-1}, the left-hand side of this equation is about 0.4. Thus this criterion is approximately met. The horizontal mixing terms will be small compared to the time-dependent terms if

$$40 A_H \left(\frac{|\tau|}{\rho}\right)^{-1/2} \frac{h_x^2}{h} \ll 1, \qquad (5\text{-}8)$$

where A_H is the eddy diffusivity, and τ is an average wind stress. Using A_H=10 $m^2 s^{-1}$ (Okubo, 1971) and τ=0.05 Pa, the left-hand side of equation (5-8) is approximately 0.05, suggesting that horizontal mixing may be safely neglected for this analysis.

Finally, for baroclinic effects to be small, we require:

$$g \frac{|\rho_z|}{\rho} \frac{h_x^2}{f^2} \ll 1. \qquad (5\text{-}9)$$

The vertical gradient of density, ρ_z, was approximately 0.05 kg m^{-4}, making the left-hand side of equation (5-9) about 0.8. This value

indicates that we may be ignoring some possibly important baroclinic effects. However, the calculations of Clarke and Brink (1985) indicate that waters respond barotropically on wide, gently-sloping shelves, and that even in baroclinic cases flow over the shelf tends to be barotropic. In applying model equations (5-5) and (5-6), we will be ignoring any alongshore advection due to a plume. If a plume were present, it would contribute a southward component to the displacements plotted in the figures below. Thus, the alongshore positions of a water particle, as described below, are inaccurate by some unknown factor. We recognize this limitation, and will use the results of this model mainly to indicate directional trends, rather than as a predictive tool for the alongshore velocity structure. The alongshore direction of motion of a particle as predicted by this model is probably accurate for upwelling and downwelling-favourable wind stresses.

The model was applied to the data by calculating the wind-driven alongshore displacement of water at the coast (y=0), which was initially at rest at Lumbos Hole on the date of the first measurable toxicity. The results of these calculations can be seen in Figures 5-15, 5-16 and 5-17 for the years 1979-1989. The dates of the first measured toxicity at each of the five stations along the coast are also plotted.

The upwelling hypothesis predicts toxicity at each station should be preceded by an upwelling-favourable wind event. In Figures 5-15, 5-16 and 5-17, a sustained upwelling event would appear as northward motion of the water particle through time, i.e. the solid curve would show a positive slope as was observed for 1979, 1981, 1983, 1984 and 1985. However, the data of 1980, 1986, 1987, 1988 and 1989 all show downwelling prior to the occurrence of toxicity. In contrast, the plume-advection hypothesis predicts that southern-most toxicity events are likely to follow downwelling events (negative slope of the curve). This prediction is supported by the data of 1979, 1980, 1982, 1986, 1988 and 1989.

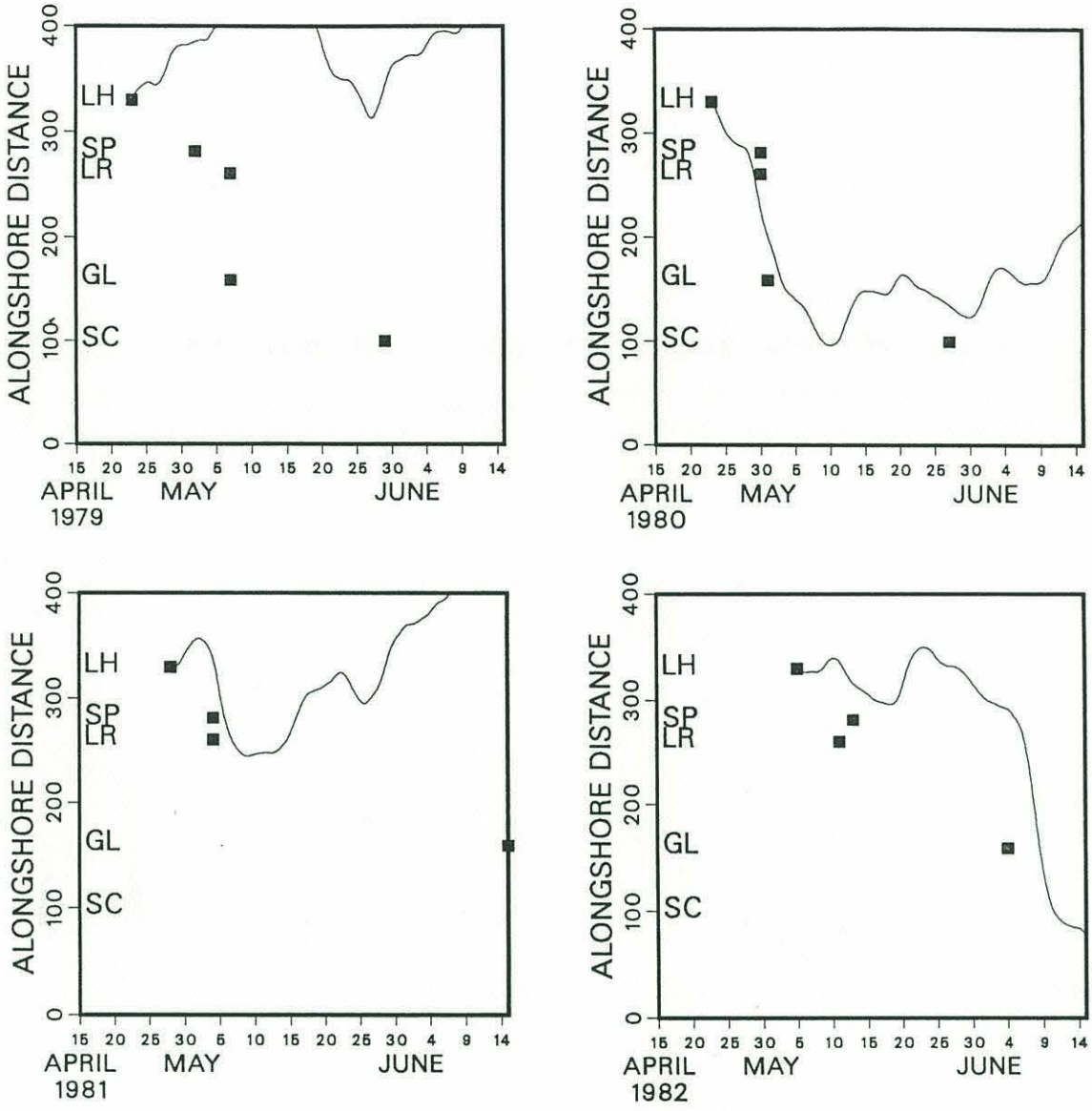

Figure 5-15. The points indicate the date of initiation of toxicity at the station indicated to the left (LH, SP, LR, GL and SC) for the years 1979-1982. The solid curve gives the predicted alongshore position of a water parcel initially at rest at Lumbos Hole (LH), under the influence of wind (equations (5-5) and (5-6)). The alongshore distance between the stations is shown on the vertical axis. The year is shown at the lower left of each plot.

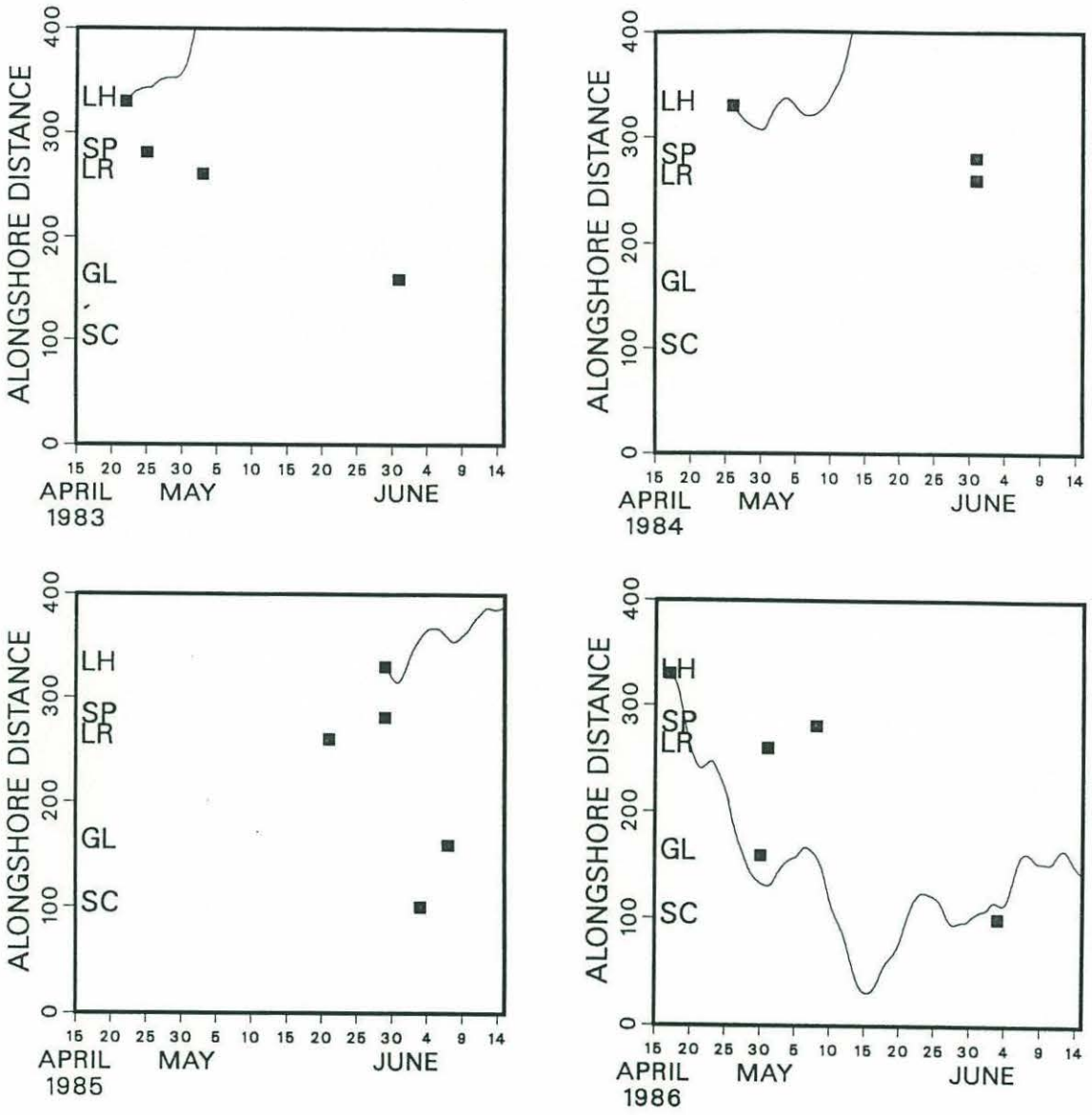

Figure 5-16. Legend same as Figure 5-15, but for the years 1983-1986.

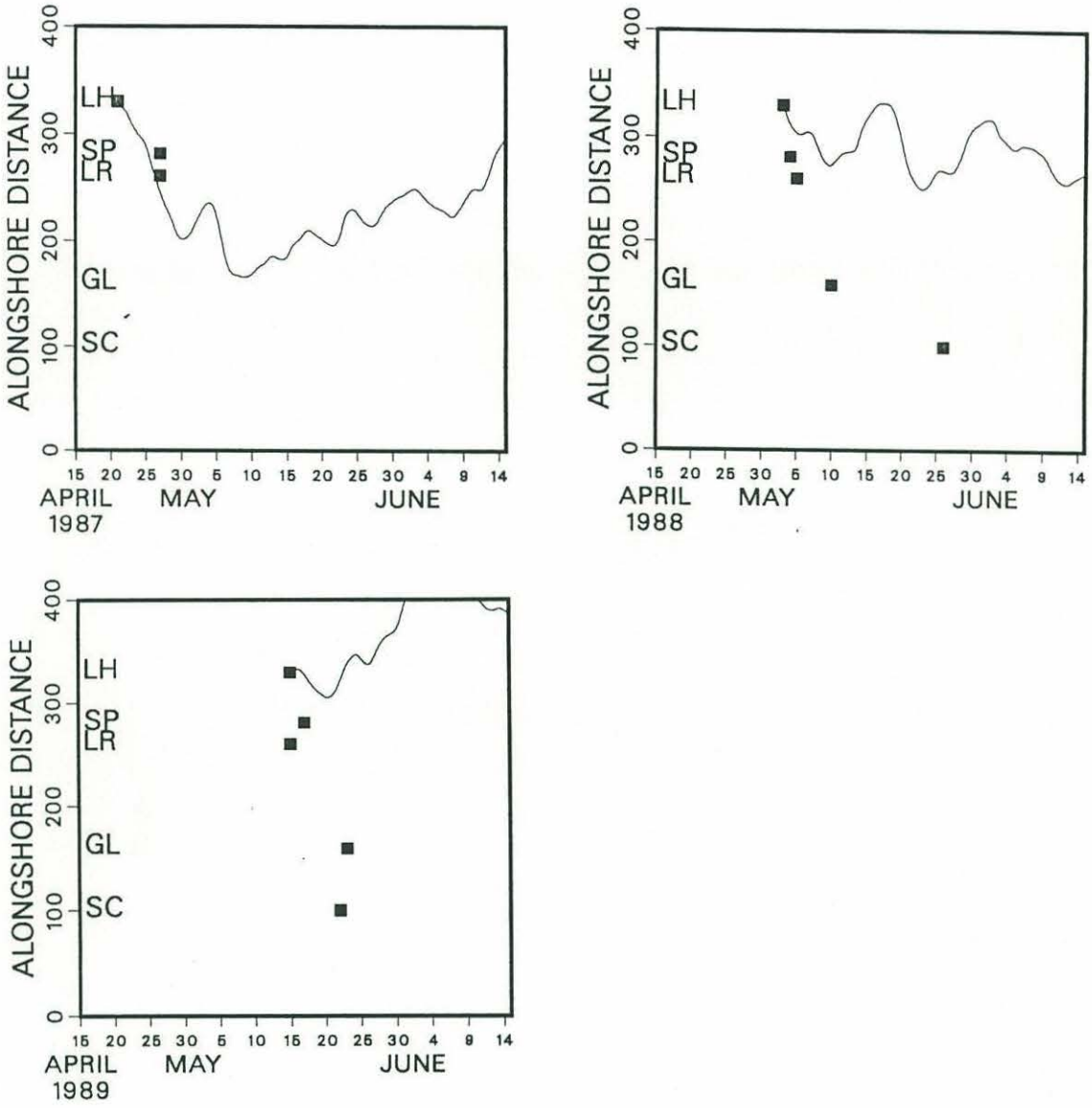

Figure 5-17. Legend same as Figure 5-15, but for the years 1987-1989.

The analyses described above assumed a point source of toxicity at Lumbos Hole, ME. Seliger et al. (1979) suggest that the *Alexandrium tamarense* cells were distributed alongshore in offshore waters. Thus we might expect upwelling-favourable winds to cause PSP outbreaks simultaneously over large regions of coastline. This does not appear to be the case in any year when upwelling-favourable winds preceded toxicity events. Thus it appears that neither upwelling nor downwelling-favourable winds are sufficient mechanisms to explain the spatial and temporal toxicity patterns.

The plume-advection hypothesis predicts that in years of high river runoff, the alongshore advection of the plume should largely control the spread of toxicity, with only slight moderation by wind. From Figures 5-2 to 5-12, we see that 1979, 1980, 1982, 1983, 1984, 1988 and 1989 were all years of high peak river flow, and in all cases the toxicity spread from north to south, even though in many cases the wind forced model (Figures 5-15 to 5-17) predicted an opposing northward flow direction (1979, 1983, 1984, 1988 and 1989). Thus the dominance of river flow over wind effects is evident in years of high flow.

The plume-advection hypothesis also predicts that in years of low flow, winds should have more impact on the spread of toxicity, since the plume velocities would be weak. From Figures 5-2 to 5-12, we find 1981, 1985, 1986 and 1987 to have been years of low river flow. Except for 1985, in years of low flow and weak or sustained upwelling-favourable winds toxicity was either delayed or absent from the southern stations. In 1987 neither Gloucester nor Scituate showed measurable toxicity; in 1981, Scituate was free from toxin; in 1986 toxicity at Scituate lagged Gloucester by over a month. These years showed weak or predominantly upwelling-favourable winds, in support of this hypothesis.

DISCUSSION

The wind-driven upwelling hypothesis of Mulligan (1973, 1975), Hartwell (1975), and Seliger et al. (1979), and the plume-advection hypothesis of Chapter 4 were tested using historical records of shellfish toxicity, river flow, and wind stress. The north-to-south pattern of toxicity events was seen for every case examined (1979-1989). Every toxic outbreak in Massachusetts was preceded by an outbreak in Maine, and by an increase in the flow rate of the Androscoggin River, as predicted by the plume-advection hypothesis. We found four cases which are inconsistent with the hypothesis of wind-driven upwelling as the factor initiating a toxic outbreak, and only one case, 1985, which suggests rejection of the plume-advection hypothesis.

The north-to-south trend of PSP toxicity cannot be explained by the wind-driven upwelling hypothesis, but is entirely consistent with the plume-advection hypothesis. Furthermore, transit times of toxicity along the coast were found to agree with the plume-advection model, and it was shown that sustained winds opposing the direction of motion of the plume had little effect in years of high peak river flow. Thus the wind-mediated motion of a coastally trapped buoyant plume is a consistent and sufficient explanation for the spatial and temporal patterns of coastal shellfish toxicity.

The wind-driven upwelling hypothesis and the plume-advection hypothesis are not mutually exclusive. It is likely that at different times of the year, different mechanisms will dominate in controlling toxic phytoplankton blooms. The wind-driven upwelling hypothesis was based mainly on data from late summer PSP events. The data of Chapter 4 combined with the present analysis suggest that the *Alexandrium tamarense* populations responding to wind-driven upwelling in the late summer may have derived from populations advected alongshore in early spring. It appears from the present study that the patterns of PSP detection in the spring along the southwestern coast of the Gulf of Maine are best explained by

alongshore advection of established *Alexandrium tamarense* populations in a coastally trapped buoyant plume.

The 1985 data appear to be the only exception to the dominance of plume-advection effects. That year was unusual in the lateness of the onset of toxicity, and it is possible that some mechanism other than advection within a buoyant plume was operating. The near-simultaneous occurrence of toxicity over a wide region of coastline, following several upwelling wind events, lends support to the wind-driven upwelling hypothesis. It is possible that late-blooming local populations of *Alexandrium tamarense* were advected from offshore waters to the shellfish beds by upwelling-favourable winds.

During June 1987, a low river flow year, it was observed in chapter 4 that low concentrations (<150 cells l^{-1}) of *Alexandrium tamarense* occurred in inshore waters, in an area free from measurable shellfish toxicity. In spite of the presence of this population and the persistent upwelling-favourable winds at the time, there was no toxicity detected along the Massachusetts coast that year. It is possible that the unusual conditions during 1987 (record river runoff in early April, followed by a dry summer) kept the local populations of *A. tamarense* at levels too low to cause detectable toxicity. However, the presence of some cells suggests that small, local populations of *A. tamarense* may occur late in the bloom season, in the absence of strong alongshore advection, and that other localized environmental factors might then stimulate a late-season outbreak of toxicity, as occurred during 1985.

Martin and Main (1981) proposed a dual mechanism for PSP outbreaks at Ipswich, MA, a tidally-flushed estuary to the north of Cape Ann. The first mechanism was a restricted bloom of cells from local populations which occasionally caused a slight increase in shellfish toxicity. The second was alongshore advection of a population from Maine which was swept into the estuary, and caused sudden increases in the toxicity levels of the bivalves during

early summer. This scenario agrees with the hypothesis of Chapter 4, where the alongshore transport mechanism was identified as a coastally trapped buoyant plume.

The alongshore advection of toxic *Alexandrium tamarense* cells in a buoyant plume can explain many details of the spread of PSP toxicity along the coasts of Maine and Massachusetts. The north-to-south motion is a result of the balance of forces which controls the plume: the Coriolis force deflects the plume to its right as it exits the estuary, and keeps it coastally trapped. We have explored the wind effects on the alongshore flow, and have shown that the wind has less influence over the plume dynamics in years of high flow. This was particularly apparent during 1989, when the winds were predominantly upwelling-favourable (to the north), while the huge runoff during May forced the cells alongshore to the south through the study area in a matter of days. The upwelling-favourable winds may not have been strong enough to stop the alongshore advection of the plume, however they did alter the across-shelf distribution of the low-salinity water and its cells (Chapter 4).

A coastally trapped buoyant plume should also show predictable behaviour at sharp topographic features such as Cape Ann. Butman (1976) describes the dynamics and hydrographic signature of a buoyant plume crossing Massachusetts Bay, south of Cape Ann, during May, 1973. A feature which is of particular interest here is that the plume separated from the coast south of Cape Ann, crossed the bay in open water, and rejoined the coast south of Boston, near Scituate (Figure 5-18). Had there been toxic cells in this plume, they would have bypassed the Boston Harbor area, leaving a PSP-free zone from just south of Cape Ann to Scituate (see Figure 5-1). This appears to be the general case, as only three occurrences of toxic mussels have ever been recorded from this zone: July 1979, June 1986, and May 1988. These events were each preceded by weak winds from the southeast which may have forced the plume into the coast south of Cape Ann, precipitating PSP outbreaks. However, it is surprising, given this scenario and the

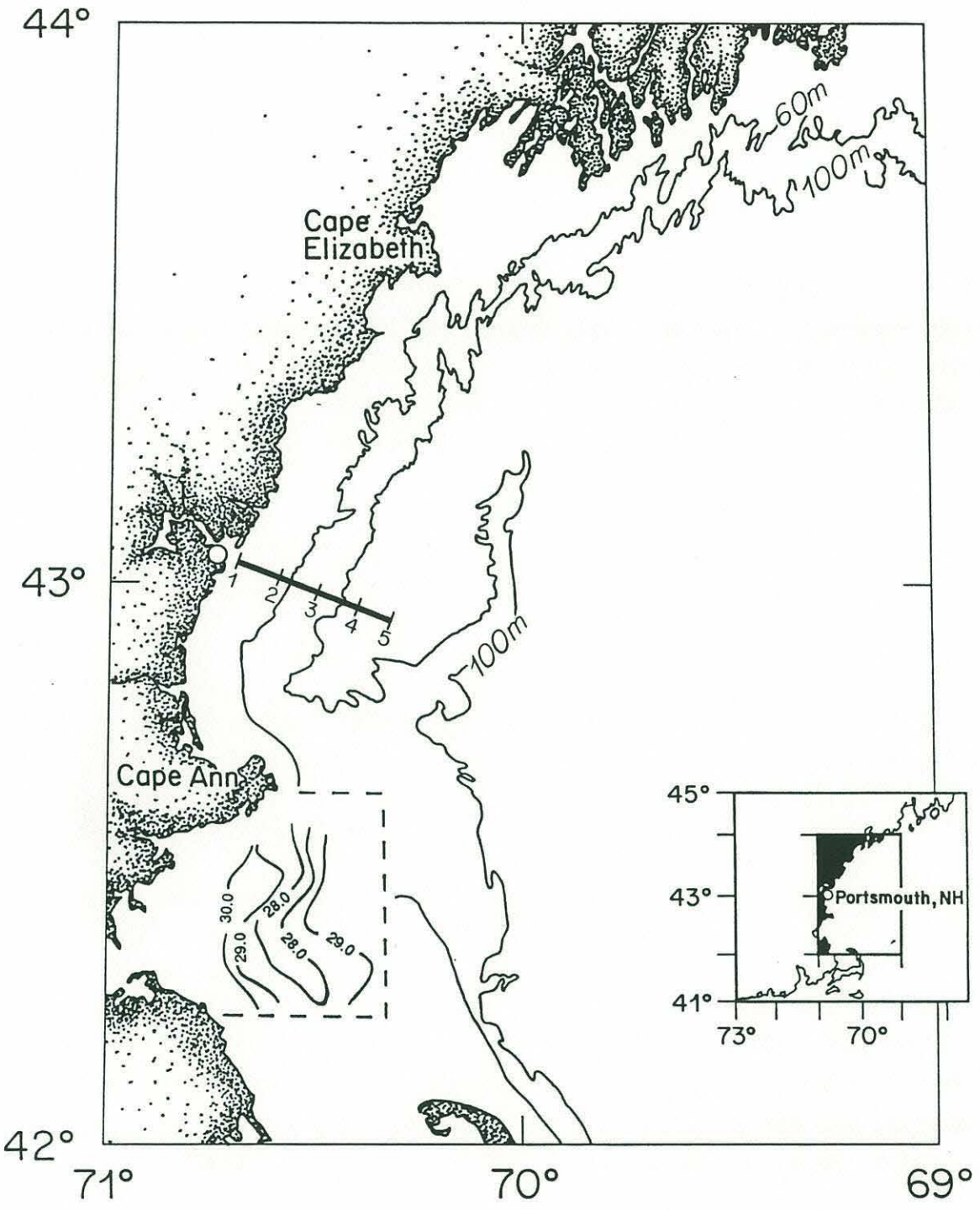

Figure 5-18. A plume of low salinity water crossing Massachusetts Bay, recorded May 5-6, 1973 by Butman (1976). Redrawn from Butman (1976).

frequent occurrence of toxicity at Scituate, that toxic outbreaks do not occur more frequently between Cape Ann and Scituate.

Bormans and Garrett (1989) suggested that a criterion for the separation of a current from a coast at a sharp topographic feature is given by the Rossby number, R_o:

$$R_o = \frac{v}{fr_c}. \qquad (5\text{-}10)$$

The alongshore velocity, v, is compared to the product of the Coriolis frequency, f, and the radius of curvature of the coast, r_c. If R_o is less than unity, the Coriolis force should dominate, and the plume should remain coastally trapped. When R_o is greater than unity, the inertial forces dominate, and the current should separate from the coast. For Cape Ann, r_c~2.5 km. Using a surface velocity for the plume suggested in Chapter 4, v~0.2 m s^{-1}, and f=10^{-4} s^{-1}, we find R_o~0.8. This suggests that separation of the plume from the coast may occur during situations in which the velocity is slightly increased, e.g. high volume of flow, or a southward wind stress. Note that these calculations of the plume velocity do not include the contribution of the Merrimack River, which lies just to the north of Cape Ann. This extra freshwater input would likely accelerate the plume, increasing the likelihood of separation from Cape Ann. This is consistent with the absence of toxicity along the south shore of Cape Ann.

The separation of the plume from the coast at Cape Ann may also explain the sporadic nature of PSP outbreaks along the south shore of Massachusetts, from Scituate to Plymouth. Once the plume is in open water, it is easily influenced by the wind. A wind which would be upwelling-favourable north of Cape Ann would tend to force a plume in Massachusetts Bay towards the east, or offshore. Thus we would expect that in years of persistent upwelling wind stress during the spread of toxicity, PSP outbreaks south of Cape Ann would be less likely. From Figures 5-15 to 5-17, we find 1981, 1983, 1984, 1985, and 1987 to have been years with persistent

upwelling-favourable winds. From Figures 5-2 to 5-12, we see that 1981, 1983, and 1987 were toxin-free years for Scituate, and no Scituate toxicity data were available for 1982 or 1984. Thus, except for 1985, which was an "unusual" year, the data support this hypothesis.

If the plume were forced offshore by upwelling-favourable winds as it crossed Massachusetts Bay, it would tend to flow around the tip of Cape Cod, and southward along its east coast. In doing so, it would advect toxic *Alexandrium tamarense* cells toward Nantucket, and possibly onto Georges Bank or into Long Island Sound. The year 1989 showed very high river discharge and persistent upwelling-favourable winds after the initiation of toxicity from Maine to Massachusetts (Figures 5-12, 5-17). Subsequently, toxicity was detected on Nantucket Shoals, an unusual event, and toxicity of surf clams (*Spisula*) and scallops (*Placopecten*) on Georges Bank was recorded by National Marine Fisheries.

Thus the predictions of the plume-advection hypothesis of Chapter 4 are supported, both in general and in detail, by the historical records of river flow, wind, and PSP toxicity. The predicted relationship of river flow volume to transport time of the toxicity alongshore was shown to hold. The predicted influence of the wind stress on plumes of varying strengths was supported for all years but 1985, which was shown to be an unusual year in other respects. The generally toxin-free region between Cape Ann and Scituate can be explained through the separation of the plume from the coast at Cape Ann, an occurrence which has been independently documented. Finally, the rare occurrence of PSP toxins in shellfish of Nantucket Shoals and Georges Bank might be linked to the unusual combination of extremely high river discharge and persistent upwelling-favourable winds that would force the plume offshore of Cape Cod.

While *in situ* growth of the dinoflagellates may occur near each site of shellfish toxicity, we would expect the patterns of

initiation of locally-derived PSP outbreaks to correlate with factors such as warming of local waters and show a south-to-north progression. If winds were relatively coherent along the coast of the study region, we would expect nearly simultaneous initiation of toxicity alongshore. However, we have demonstrated a north-to-south trend of toxicity, which implies that alongshore advection of toxic cells is of equal or greater importance than *in situ* growth in determining the patterns of shellfish toxicity.

LITERATURE CITED

Association of Official Agricultural Chemists. 1965. Paralytic shellfish toxin, biological methods. (18). In, "Official Methods Analysis, 10th ed.", A.O.A.C., Washington, D.C. pp 282-284.

Bormans, M. and C. Garrett. 1989. A simple criterion for gyre formation by the surface outflow from a strait, with application to the Alboran Sea. J. Geophys. Res. 94:12637-12644.

Bricelj, M., J.H. Lee, A.D. Cembella and D.M. Anderson. 1990. Uptake of *Alexandrium fundyense* by *Mytilus edulis* and *Mercenaria mercenaria* under controlled conditions. In, "Toxic Marine Phytoplankton", E. Graneli, B. Sundstrom, L. Edler and D. Anderson (eds.) Elsevier, New York. 269-274.

Butman, B. 1976. Hydrography and low-frequency currents associated with the spring runoff in Massachusetts Bay. Mem. Soc. R. Sci. Liege 6(X):247-275.

Chao, S.-Y. 1988. River-forced estuarine plumes. J. Phys. Oceanogr. 18:72-88.

Clarke, A.J. and K.H. Brink. 1985. The response of a stratified, frictional flow of shelf and slope waters to fluctuating large-scale, low-frequency wind forcing. J. Phys. Oceanogr. 15:439-453.

Hartwell, A.D. 1975. Hydrographic factors affecting the distribution and movement of toxic dinoflagellates in the western Gulf of Maine. In, "Proceedings of the First International Conference on Toxic Dinoflagellate Blooms", V.R. LoCicero (ed.) Massachusetts Science and Technology Foundation, Wakefield, MA. 47-68.

Hurst, J.W. 1979. Shellfish monitoring in Maine. In, "Proceedings of the First International Conference on Toxic Dinoflagellate Blooms", V.R. LoCicero (ed.) Massachusetts Science and Technology Foundation, Wakefield, MA. 23-40.

Hurst, J.W., R. Selvin, J.J. Sullivan, C.M. Yentsch and R.L. Guillard. 1985. Intercomparison of various assay methods for the detection of shellfish toxins. In, "Toxic Dinoflagellates", D.

Anderson, A. White and D. Baden (eds.) Elsevier, New York. 427-432.

Janowitz, G.S. and L.J. Pietrafesa. 1980. A model and observations of time-dependent upwelling over the mid-shelf and slope. J. Phys. Oceanogr. 10:1574-1583.

Kao, T., H.-P. Pao and C. Park. 1978. Surface intrusions, fronts, and internal waves: a numerical study. J. Geophys. Res. 83:4641-4650.

Large, W.S. and S. Pond. 1981. Open ocean momentum flux measurements in moderate to strong winds. J. Phys. Oceanogr. 11:324-336.

Levy G. and R.A. Brown. 1986. A simple, objective analysis scheme for scatterometer data. J. Geophys. Res. 91:5153-5158.

Martin, C. and J.M. Main. 1981. Toxic dinoflagellate blooms (red tides) and shellfish resources in Plum Island Sound and adjacent Massachusetts waters. Final report to the Town of Ipswich, MA, under UMass/Amherst OGCA Contract No. 80A613.

Mulligan, H. 1973. Probable causes for the 1972 red tide in the Cape Ann region of the Gulf of Maine. J. Fish. Res. Bd. Canada 30:1363-1366.

Mulligan, H. 1975. Oceanographic factors associated with New England red tide blooms. In, "Proceedings of the First International Conference on Toxic Dinoflagellate Blooms", V.R. LoCicero (ed.) Massachusetts Science and Technology Foundation, Wakefield, MA. 23-40.

Okubo, A. 1971. Oceanic diffusion diagrams. Deep-Sea Res. 18:789-802.

Seliger, H., M.A. Tyler and K.R. McKinley. 1979. Phytoplankton distributions and red tides resulting from frontal circulation patterns. In, "Toxic Dinoflagellate Blooms", D.L. Taylor and H.H. Seliger (eds.) Elsevier, New York. 239-248.

Shumway, S., S. Sherman-Caswell and J.W. Hurst. 1988. Paralytic shellfish poisoning in Maine: monitoring a monster. J. Shellfish Res. 7:643-652.

Steidinger, K.A. and Ø. Moestrup. 1990. The taxonomy of *Gonyaulax, Pyrodinium, Alexandrium, Gessnerium, Protogonyaulax* and *Goniiodoma*. In, "Toxic Marine Phytoplankton", E. Graneli, B. Sundstrom, L. Edler and D. Anderson (eds.) Elsevier, New York. 522-523.

CHAPTER 6

SUMMARY, CONCLUSIONS AND SUGGESTIONS FOR FURTHER STUDY

"Is that it?" said Eeyore.
"Yes," said Christopher Robin.
"Is that what we were looking for?"
"Yes," said Pooh.
"Oh!" said Eeyore. "Well, anyhow — it didn't rain," he said.

A.A. Milne
Winnie-the-Pooh

Several studies concerning the interactions of dinoflagellates with physical processes in the coastal ocean have been described. The general review of Chapter 2 suggested that, even though dinoflagellate blooms were often found at fronts, the cross-frontal length scale of the bloom was not generally correlated with the scale of the front. The implications of this mismatch were that either (1) they should have been correlated and some processes were acting to decorrelate them, or (2) they should not have been correlated, and processes uncorrelated with the scale of the front were influencing the bloom. An example of a decorrelating mechanism was a mismatch of the timescales of frontal development and phytoplankton growth. Physical processes which might influence dinoflagellate production and are uncorrelated with the frontal scale include diffusion, and cross-frontal mixing. These possibilities were explored in some detail.

In Chapter 3, a simple one-dimensional time-dependent model was used to explore the factors controlling a bloom of *Ceratium longipes* offshore of Portsmouth, New Hampshire. The model suggested that the spatial and temporal distribution of the bloom could be explained through population-density dependent growth, and along-isopycnal diffusion of an offshore assemblage. The long-term changes in cell concentration appeared to be linked to variations in the amount of incident sunlight, measured as minutes of sunlight per day at Boston, Massachusetts. The specific growth rates, μ, which were calculated using the model agreed well with growth rates found in the literature, but were half the maximal net population growth rates, r, calculated from changes in the cell concentrations in the field. This difference can be accounted for by the along-isopycnal diffusion of cells, which created enhanced net population growth rates inshore. It is of note that this model assumed no alongshore variability. As discussed in Chapter 4, the absence of a freshwater plume in 1987 resulted in a significant reduction in alongshore advective processes.

The work of Chapter 4 demonstrated the association of *Alexandrium tamarense* populations with coastally trapped buoyant plumes. These plumes appeared to have been formed by the outflow from the Androscoggin and Kennebec Rivers in southwestern Maine, had a duration of about a month, and extended alongshore for hundreds of kilometers. Most importantly, the plumes provided a vehicle for the alongshore transport of toxic cells, and a mechanism for the initiation of toxic events alongshore. The effects of wind and topography on the plume dynamics were explored, and were found to explain many of the details of the *A. tamarense* distributions and toxicity outbreaks. A conceptual model, the "plume advection hypothesis", was formulated to explain the initiation and spread of toxic dinoflagellate blooms and concomitant shellfish toxicity in the study area:

1) A source population of cells to the north, possibly established and concentrated in the Androscoggin-Kennebec estuary.
2) A pulse of fresh water in May to carry the growing *A. tamarense* population out of the estuary, initiating toxic events alongshore. Years of high peak flow in May show extensive alongshore spread of toxicity, with short transit times along the coast. Years of low flow in early May show longer alongshore transit times, and a close relationship of the toxicity patterns to the wind stress.
3) Upwelling-favourable winds force the plume and cells offshore, potentially causing separation of the plume from the coast. Downwelling-favourable winds hold the plume to the coast, and speed it to the south.
4) Once delivered to the study area, the across-shelf distribution of the *A. tamarense* cells can change dramatically.

The important predictions from this model are:

1) the toxicity patterns should show a north-to-south progression,
2) the transit time of toxicity along the coast should be positively correlated with the volume of flow of the Androscoggin and Kennebec Rivers,
3) upwelling-favourable winds should slow or stop the progression of the plume and concomitant toxicity, and

4) downwelling-favourable winds should speed the plume and toxic cells alongshore.

Tests of these predictions using historical records of shellfish toxicity, wind speed and direction, and river flow were described in Chapter 5. It was found that the data from 1979-1989 supported the plume-advection hypothesis, both in general and in detail. One year, 1985, was found to contradict the model. It was noted that this year was unusual in many respects, and a different mechanism may have been acting to control the spread of PSP toxicity.

The work described above provides testable hypotheses for the control of phytoplankton production at fronts, the along-isopycnal growth and diffusion of a bloom of *Ceratium longipes*, and the alongshore transport of a bloom of the toxic dinoflagellate *Alexandrium tamarense* in a coastally trapped buoyant plume. The latter hypothesis, in particular, adds significantly to our understanding of the mechanisms controlling PSP outbreaks along the coast of the Gulf of Maine. Like most hypotheses, however, those described above generate as many new questions as they answer old ones. Thus suggestions for further study include:

1) measurements of the dissipation rate of turbulent kinetic energy at a variety of fronts to better understand the mechanisms promoting phytoplankton production there. In particular it is important to gain understanding into the spatial and temporal inhomogeneities of turbulent mixing in, and around a front.

2) measurements of *in situ* growth rates of phytoplankton confined to the pycnocline, coincident with hydrographic measurements. Such measurements should help in understanding the contributions of diverse processes leading to the distribution of cells along a density surface, and enable a test of the model described in Chapter 3.

3) tests of the various predictions of the plume-advection hypothesis, including:

   a) location of source population, and factors influencing its growth and distribution

b) more detailed measurements of plume structure and dynamics, including current meter measurements and satellite images

c) testing of the conceptual model with time-dependent wind-driven models of buoyant plumes coupled with models of toxic dinoflagellate growth and behaviour

d) exploration of the factors controlling the fall toxic outbreaks along the coast

e) study of the factors controlling the across-shelf distribution of *Alexandrium tamarense* cells after initiation of toxicity

f) testing of the predictions of the plume-advection hypothesis through independent means, such as a comparison of the genotypes of cells along the coast.

APPENDIX A

SAMPLING COASTAL DINOFLAGELLATE BLOOMS: EQUIPMENT, STRATEGIES AND DATA PROCESSING

PETER J.S. FRANKS AND DONALD M. ANDERSON

Biology Department, Woods Hole Oceanographic Institution
Woods Hole, MA USA 02543

PUBLISHED IN:

BIOLOGY, EPIDEMIOLOGY AND MANAGEMENT OF *PYRODINIUM* RED TIDES.

G. HALLEGRAEFF AND J. MACLEAN (EDS.)

ICLARM CONFERENCE PROCEEDINGS 21, 286 P.
FISHERIES DEPARTMENT, MINISTRY OF DEVELOPMENT,
BRUNEI DARUSSALAM,
AND
INTERNATIONAL CENTER FOR LIVING AQUATIC RESOURCES MANAGEMENT,
MANILA, PHILIPPINES

Sampling Coastal Dinoflagellate Blooms: Equipment, Strategies and Data Processing

PETER J.S. FRANKS
DONALD M. ANDERSON
Biology Department
Woods Hole Oceanographic Institution
Woods Hole, MA, USA 02543

FRANKS, P.J.S. and D.M. ANDERSON. 1989. Sampling coastal dinoflagellate blooms: equipment, strategies and data processing, p. 235-256. *In* G.M. Hallegraeff and J.L. Maclean (eds.) Biology, epidemiology and management of *Pyrodinium* red tides. ICLARM Conference Proceedings 21, 286 p. Fisheries Department, Ministry of Development, Brunei Darussalam, and International Center for Living Aquatic Resources Management, Manila, Philippines.

Abstract

Brief descriptions of a variety of low-cost systems for sampling dinoflagellate populations are given, together with sampling schemes for the field, and the factors which will affect the sampling program. Methods of data collection and reduction are discussed, and a brief introduction to methods of data interpretation is made.

Introduction

Dinoflagellates are important constituents of the coastal phytoplankton community throughout the world. Under conditions which are still poorly understood, certain species can dominate the phytoplankton community, creating a visible coloration of the water: a "red tide". The ability of these organisms to swim may contribute to the formation of such dense blooms by allowing the dinoflagellates access to deep reservoirs of nutrient-rich water. However, swimming creates particular problems in sampling dinoflagellates and in interpreting their vertical and horizontal distributions.

It is becoming increasingly apparent that much of the large-scale variability in dinoflagellate distributions can be explained by the advection and diffusion of blooms by physical processes. These processes include wind-driven, buoyancy-driven and tidally-generated motions of the water column, coupled with seasonal cycles of temperature and freshwater runoff. At a minimum, dense CTD (Conductivity, Temperature and Depth) coverage in time and space is necessary to understand the forcings and resultant motions. These samples should be coincident with biological sampling to provide maximum insight into the couplings of the physical and biological systems.

Many questions arise: what is sufficient coverage, what types of samples should be taken, and when should they be collected? Here we offer some insights based on our experience in sampling coastal dinoflagellate populations in the Gulf of Maine, USA. First we describe sampling methodologies: the choice and construction of sampling gear, the types of samples to take, and the interfacing of different types of instruments. We then describe sampling strategies: the selection of stations in both time and space, and data reduction and interpretation. We hope this information will be useful to those designing field programs in coastal areas, and that our guidelines will lead to sufficient and interpretable data sets that can be compared to similar data sets from other regions.

Sampling Methodologies

Dinoflagellate populations normally show a great deal of vertical structure in natural waters. In many situations this structure is intimately linked to the hydrography, the cells being found within the seasonal pycnocline or zone of maximum vertical density change. In other cases, the cells may accumulate quite independently of the hydrography due to their ability to swim. Sampling gear must be capable of sufficient vertical resolution to distinguish these possibilities. This often requires biological sample spacing of 5m or less in the vertical. Here we will describe a variety of sampling systems which are capable of dense vertical resolution for a range of field situations.

Pumping Systems

In shallow (<5m) embayments, a simple integrating tube sampler may be the most appropriate sampling device. These samplers consist of a length of 6.25-cm internal diameter (i.d.) PVC

·.pe, fitted with a cork attached to a line threaded through the pipe to a handle at the top (Fig. 1). A short foot at the bottom keeps the sampler from being pushed into the benthos. The sampler is slid vertically into the water until the foot rests on the bottom. Once the depth to the bottom is known, the tube is raised and moved to a new location nearby, and lowered until the foot is just off the bottom. This procedure prevents the water column samples from being contaminated with resuspended material. The line is then pulled to seal the tube with the cork. The tube is emptied by pouring from the top, since pouring from the bottom causes spillage around the cork. The integrated vertical sample can be poured into a carboy or bucket for further subsampling (see below). The advantages of this type of sampler are: 1) low cost; 2) ease of construction; 3) one sample integrates any vertical heterogeneity of the organism; and 4) ease of deployment. The disadvantages include: 1) no vertical resolution; 2) relatively small volume; and 3) no real-time vertical information.

In shallow areas, and relatively calm seas, the tube sampler described by Lindahl (unpub. ms.) may be the most appropriate sampling device. This low-cost sampler consists of lengths of 2-cm i.d. PVC pipe or garden hose, linked with valves and easily-separated connectors (Fig. 2). The length of a section determines the vertical

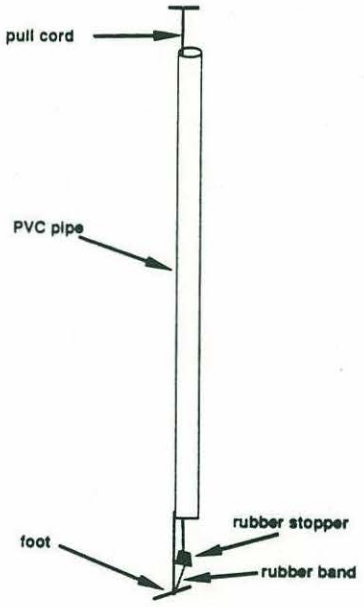

Fig. 1. The tube sampler. When the cord is pulled at the top, the cork seals the bottom of the tube. The rubber band keeps the cork oriented properly until the cord is pulled.

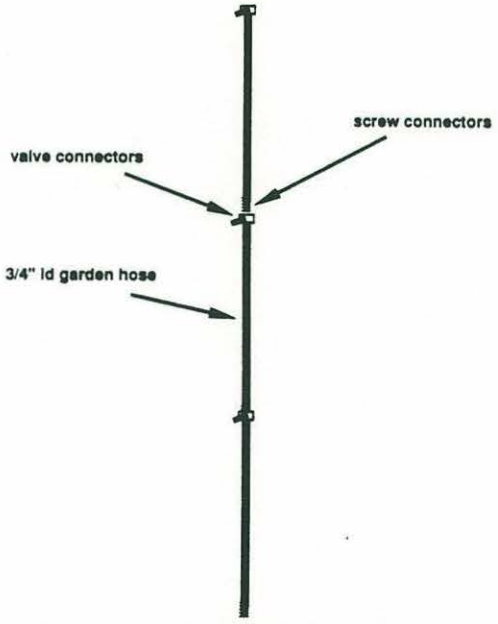

Fig. 2. The hose sampler. Lengths of hose are joined by valves and connectors. All valves must be open during deployment, and the surface valve closed upon recovery. A valve must be closed before the section of hose above it is removed, or the sample will be lost.

resolution of sampling. The sampler is slowly lowered with all valves open until the hose is filled. The top valve is then closed, and the hose raised until the next valve down can be closed. The upper section can now be removed, and its water drained. This procedure can be repeated until the whole length of hose has been raised. Hydrostatic forces within the hose will hold the water within the hose while it is being raised. Thus a small-volume vertical profile of the water column is obtained. The advantages of this sampler are similar to those of the tube sampler described above, although vertical resolution is obtained. The disadvantages are: 1) small volume; 2) no real-time vertical information; and 3) smearing of vertical structure within the pipe due to its narrow diameter.

Most vertical areas are dynamically complicated, requiring detailed coverage of both the biology and the hydrography. The samplers described above can be useful, but are nevertheless somewhat limiting due to their small volume and inability to provide continuous vertical profiles. We suggest the use of a pump profiling system. These systems have the advantages of: 1) high volume, permitting sampling of a number of variables; 2) continuous vertical profiles; and 3) the possibility of real-time observations of vertical features. The disadvantages are: 1) relatively high cost (generally < US$200); 2) they are more difficult to deploy than the sampler described above; and 3) they require an AC or DC power source for the pump and associated instruments.

The pump profiling system at its simplest is a pump and a length of hose. Aspects of the system design which must be evaluated include the position of the pump (at surface or at depth), the insertion of various flow regulators and a bubble trap, and the inclusion of subsidiary sampling devices such as fluorometers, autoanalyzers, etc. Here we describe the configuration used in our laboratory, with justification for each of the features. This configuration is certainly not exclusive of other arrangements; we hope that readers will use the information here in designing pump profiling systems specific to their own needs.

The central feature of the pump profiler is the pump. We use a "Lil' Giant" submersible pool pump (available from swimming pool supply companies, and scientific supply houses). This pump requires AC power, as would another alternative, the submersible well pump (available from dealers who drill wells for drinking water). Another feasible pump is a boat bilge pump which can run on DC power (available from marinas and boat supply companies).

The pump need not be submersible, but it should be able to withstand being soaked in salt water. If a deck pump is used, it should be self priming: priming the pump is the most difficult aspect

of the deployment of the Lil' Giant system. The pump can be suspended either just below the surface or at the bottom of the hose. The consideration here is the formation of bubbles due to cavitation within the pump. The surface pump is likely to cavitate if the hose below is too long. We use 40 m of 2-cm i.d. garden hose, the maximum length useable with this pump. Placing the pump at the base of the hose solves the cavitation problem, but generates a new problem with the length of electrical wire over the side of the vessel. Kinks in the hose and the tangling of wires are the most serious deployment problems after the flow has started.

Since the Lil' Giant pump is not self-priming, the hose must be completely filled with water before the pump is plugged in. After much trial and error, we found that putting the hose over the side of the vessel until it is fully submerged is the best way to fill it: this means that all our vertical profiles are taken as the hose is raised. The hose must be deployed carefully, as it has a tendency to twist and kink. Kinks are fatal to a profile. The most common location of kinking is where the hose attaches to the wire. To ease the strain here, we use a dual thickness of radiator hose, clamped to the wire with hose clamps, with a screw connector for the garden hose at the other end (Fig. 3). This is a particularly convenient arrangement, since the hose may be unscrewed at any time if the wire is required

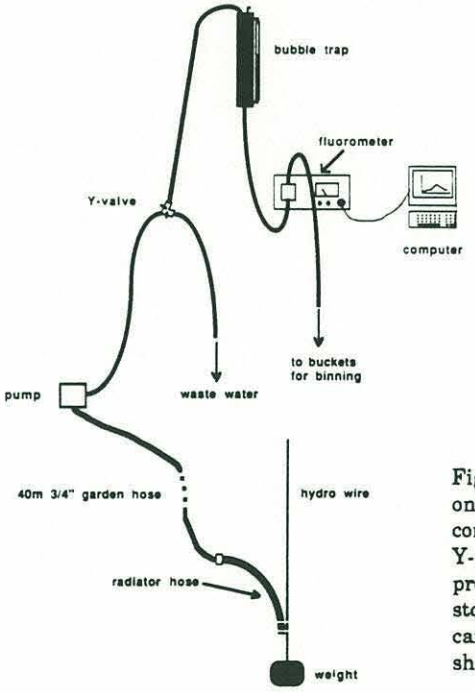

Fig. 3. The pump profiling system. This is only one of a variety of possible configurations. The flow is regulated at the Y-valve. The radiator hose at the wire prevents the hose from kinking and stopping the flow. A variety of instruments can be included in-line; a fluorometer is shown here as an example.

for something else, without having to remove the radiator hose and hose clamps. Any reasonably stiff length of hose can be substituted for radiator hose, so long as it will not kink. It is also useful to have duct tape handy: it can be used as a hose wrap should the hose kink or fail. Note also that a heavy weight is required to keep the hose as vertical as possible. We use a 30 kg weight attached to the wire (never to the hose itself).

The hose leading out of the pump brings the water on deck. A Y-valve is necessary for dividing the flow into the portion to be sampled, and the waste, which is pumped overboard. This Y-valve is critical to maintaining a steady flow to the instruments. Steady flow is achieved by adjusting the amount of waste water, not by adjusting the flow of water to the instruments. The valve to the instruments should always be wide open to avoid bubble formation.

Bubbles within the hose can be a serious problem with certain instruments such as fluorometers and autoanalyzers. To mitigate the problem, we include a bubble trap between the Y-valve and the instruments (Fig. 4). The bubble trap consists of a 1-m length of 10-cm i.d. acrylic pipe, fitted with stoppers and hose connectors at the top and bottom. A small chimney tube at the top allows air to escape. A length of clear tubing joined to the top and bottom with right-angled connectors allows visualization of the water level within the pipe. A 20-cm length of hose extends from the top hose connector into the bubble trap. The level of water within the bubble trap should

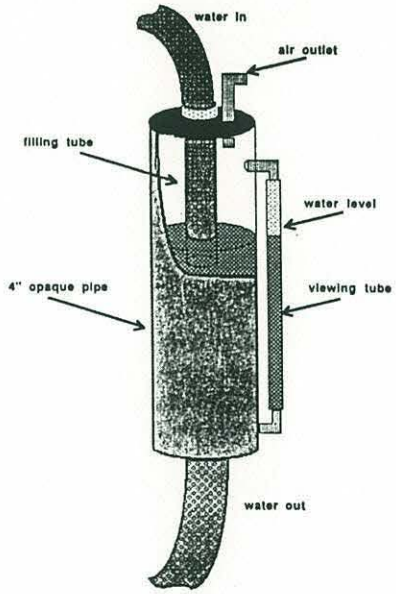

Fig. 4. Cut-away view of the bubble trap. This should be made of opaque material so that the phytoplankton are not over irradiated. The water level should be kept above the end of the inlet hose so that no new bubbles are created. The level of water is shown by the clear tube on the side of the bubble trap.

always be kept above the level of this hose so that no more bubbles are created. The bubble trap itself should be located at the highest point of the pumping system, so that all bubbles within the system may escape. The height of the bubble trap will largely be determined by the head of the pump and the geometry of the ship.

From the bubble trap, the flow feeds by gravity into the attached instruments, and back to the deck. The water may be collected in carboys to obtain samples integrated over any desired depth interval as the hose is raised or lowered. For certain analyses (e.g., productivity or chlorophyll) the sample containers should be opaque or acid-washed, although a seawater rinse is sufficient for species counts.

The protocol for sampling with the pump profiling system is complicated by the residence time of the water within the hose. Thus the water which is being pumped on deck was obtained from the depth the hose inlet occupied some time ago. The method we use to correct for this requires measurement of the residence time. This was done using a flow-through fluorometer to detect a spike of chlorophyll introduced at the hose inlet. Simple coloured dye would work, as long as it is visible to the eye or to a spectrophotometer after passage through the hose. The calculated transit time should be at the first appearance of the dye at the end of the hose: smearing within the hose will cause an initial spike to be spread over a considerable distance within the hose.

Once the transit time within the hose is known, the procedure for performing a vertical profile is relatively easy. The variables which must be decided before the profile is begun (and preferably before the cruise begins) are: 1) the rate of rise of the hose; and 2) the flow rate. The former will depend mostly on the winch being used. We have found that a rate of 2 m/min. gives reasonably dense vertical coverage. However, most winches will not raise that slowly. Our protocol is thus to raise the hose 1m every 30 seconds, and pause at that depth. The hose inlet usually takes 5 or 6 seconds to rise 1 m. Thus the profile is taken in a series of steps. Water from 5-m intervals is collected in individual buckets for subsampling. Clearly, it is important to time the raising of the hose and the bucket collection carefully so that a representative sample is collected that integrates over the 5-m interval.

In order to know the depth from which the water that arrives on deck was pumped, the winch operator and the person handling the hose must work independently. At the start of the profile, both persons should start their stop watches. The winch operator keeps his going, raising the hose 1 m every 30 seconds, beginning 30 seconds after the start signal. The person handling the hose waits an amount

of time equal to the transit time of the water in the hose, at which time the water being pumped on deck is water for the first interval. At that time, the hose handler should restart his stopwatch, to time the filling of the bucket. For example, to integrate over 5 m, the hose handler would place the hose outlet into a bucket for 2.5 min. (if the hose is being raised at 2 m/min.). Continuing this process will give samples binned into 5-m intervals. The winch operator must pause at the surface so that the hose handler can "catch up". The hose inlet must not break the surface, or the pump's prime will be lost.

Various strategies for binning or integrating of samples will be described below. Subsampling from the bins depends on the information needed. We sieve one liter from each bin through 20-mm Nitex mesh (epoxied onto a cylinder of 8-cm PVC pipe) and preserve it in 5% formalin for cell counts. An additional 500 l is filtered through GF/A filters. The filters are used for chlorophyll analyses and the filtrate is frozen for nutrient analyses. The flow rate should be adjusted at the Y-valve so that sufficient water is obtained for all these analyses, as well as for the auxiliary, on-line instruments.

Auxiliary Instruments

A variety of auxiliary instrumentation is available for interfacing with the pump profiling system, depending on the needs of the project and the available budget. Many of the instruments are relatively costly (> US$5000), and so may not be available to smaller laboratories.

Our particular pumping system includes an in-line fluorometer (Turner Designs Model 10-00R with flow-through cell and chlorophyll *a* filter set). This fluorometer is interfaced to a portable personal computer (NEC APC IV Powermate Portable) through an A/D (analog/digital) board (Metrabyte Dash-8; Metrabyte Corp., 440 Myles Standish Blvd., Taunton MA, 02780 USA) following the instructions in the fluorometer manual. The excellent software supplied with the A/D board was modified to plot fluorescence on the computer screen in real time, and to store the data to disk. The screen plot allows visual location of the fluorescence maximum, and can be used in real time to modify sampling and "binning" procedures. We have found the vertical fluorescence profiles to be an invaluable tool in our phytoplankton field studies, even though the dinoflagellates of interest are seldom the dominant source of fluorescence.

Alternative in-line devices could include an autoanalyzer (e.g., Technicon AutoAnalyzer II, available through scientific supply companies) to obtain detailed nutrient profiles. A transmissometer

could be included in-line to obtain turbidity data. Some sort of flow chamber must be designed for the transmissometer which is especially sensitive to bubbles. We suggest using a submersible transmissometer, located below the hose inlet.

The A/D board may have additional available channels. These can be used to digitize the signal from a light meter or pressure sensor attached near the hose inlet. Once again, these instruments require additional wires, which can cause tangling and kinking of the hose.

As mentioned above, we consider it essential to obtain coincident hydrographic and biological information. It is somewhat unfortunate that most dinoflagellate blooms are associated with strong signals in salinity: salinity is much harder to measure than temperature. Temperature is sometimes a useable surrogate for salinity, but not reliably. In dynamically simple areas such as shallow embayments, salinity can be measured adequately with a hand-held, relatively inexpensive refractometer. This device has an accuracy of about 0.2 ppt, which is reasonable for most coastal situations. If no more sophisticated instruments are available, temperature readings, measured with a thermometer, and salinity values, measured with a refractometer, should be taken at least at 0.5 m intervals. These measurements can be made on water exiting the hose.

Inexpensive battery-operated temperature/conductivity probes, such as those manufactured by InterOcean Systems Inc. (3540 Aero Ct., San Diego, CA 92123 USA) can be lowered to learn details of water column structure, but accuracy is limited. A more sophisticated system might include an in-line thermosalinograph (available through InterOcean Systems, Inc.). This instrument may also be interfaced to the computer, allowing rapid data aquisition and storage. The quality and durability of such instruments is of paramount importance: nothing is more frustrating than trying to collect data with unreliable instruments. Always try to test an instrument in the field before purchase, and talk to others who have used the instrument.

The instrument we recommend is a CTD (Conductivity, Temperature, Depth) profiler. We use the "Sea Cat Profiler" (Sea Bird Electronics, 1808-136th Pl. NE, Bellevue WA, 98005 USA). This small CTD stores data internally during a cast, thus no extra electrical wires are required over the side of the vessel. The data can be subsequently transferred to a personal computer using the various programs supplied with the CTD. The instrument itself is practically indestructible and foolproof. We generally mount our CTD below the hose inlet, with the sensors pointing upward in order to take data as the instrument is raised through the water.

Station Selection: Spatial

The decision of when and where to locate stations can be overwhelming. Coastal areas have notoriously complicated physical systems, requiring relatively dense spatial coverage. The main forcing over much of the year is the wind, which varies on time scales of hours and days. What is the best strategy for dealing with these problems, without spending your whole life at sea?

The first suggestion we make is to plan as dense CTD coverage as possible. Hydrographic data are an absolute necessity for interpretation of any data concerning biological distributions in the ocean. One criterion for deciding on CTD station spacing is the internal Rossby radius of deformation, Ri. This length scale is the natural length scale for most physical features in the ocean: the width of frontal zones, the size of eddies, the width of river plumes, etc. (Franks, 1990, in press). It is calculated from the thickness of the surface layer, h, the densities of the upper and lower layers, r and r', the acceleration due to gravity, g, and the Coriolis frequency, f:

$$R_i = \frac{gh\,(\rho' - \rho)}{f}$$

This length scale is typically < 5 km in most coastal regions. Hydrographic station spacing of this order or less will allow resolution of features such as fronts and river plumes. Since most dinoflagellate blooms are associated with such features, it is important to be able to resolve them with some confidence.

One of the main factors contributing to the complicated dynamics of coastal regions is the physical barrier formed by the coast. This feature will tend to align physical systems (e.g., wind-driven upwelling, coastal currents and river plumes) parallel to the coast. This means that hydrographic variables will tend to show greater changes across shore than along shore. For this reason, it is important to obtain good cross-shore coverage. We suggest sampling to at least 5Ri from the coast, in order that coastal features be adequately sampled.

Most physical systems in coastal areas tend to follow bathymetric contours. At areas where the curvature of the coast is very sharp, a physical feature such as a coastal current will separate from the coast and move into open water. The criterion for this separation is roughly given by the Rossby number, R_o:

One of the main reasons for recommending a CTD profiler is that it may be used without the hose pumping system. A vertical profile

with the pumping system may take half an hour, whereas a CTD cast need only take a few minutes. Thus dense CTD coverage may be obtained in an area with more sparse biological profiles. The variations in hydrography can be used to explain details of the biological distributions and dense CTD coverage will always make data interpretation easier. An additional advantage of many CTD profilers is that they may be expanded to include *in situ* fluorometers, transmissometers, light meters, O2 sensors, etc. These instrument packages are easily deployed even in fairly rough seas, when deployment of a pumping system may be impossible. They also allow dense sampling of a variety of fields.

One final word on sampling equipment: always plan for the worst. Bring spares of all pieces of equipment: hose, pumps, valves, connectors, radiator hose, hose clamps, etc. A supply of duct tape is a necessity. Always make contingency plans if any aspect of the sampling program should fail at sea, e.g., if the pump loses its prime, the computer fails, or the fluorometer breaks. Planning ahead for such emergencies will help to make the best out of a bad situation, and may prevent the waste of a lot of time and money.

Sampling Strategies

Here we describe various factors to consider when designing a sampling program. We examine certain physical parameters which merit consideration, and suggest some biological features which may influence timing and location of stations. Finally we describe some standard techniques of data reduction and interpretation.

$$R_o = \frac{u}{fr_c}$$

Here u is the velocity of the current, f is the Coriolis frequency for that latitude, and rc is the radius of curvature of the coast (or the bathymetry). If this number can be calculated, and it is greater than 1, the coastal current is likely to separate from the coast and move offshore. The sampling scheme should be adjusted accordingly, and more offshore samples taken. The orientation of the transects may also be adjusted: they should, in general, be oriented perpendicular to the feature being sampled. Near a sharp bend in the coast, the transects may be oriented almost parallel to the coast in order to obtain good hydrographic coverage of a coastal current (see Fig. 5).

If multiple transects are to be run, it is preferable that they be oriented parallel to each other. This will give even data coverage,

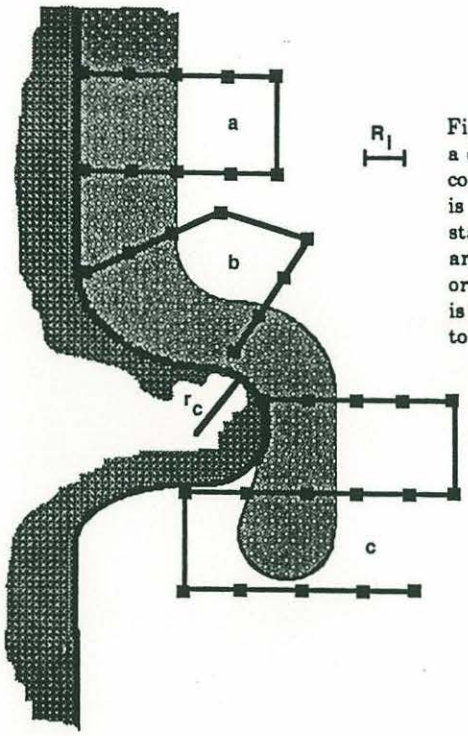

Fig. 5. An example of a sampling scheme for a coastal current which separates from the coast at a cape. In section a, where the coast is straight, the legs are parallel, and the stations evenly spaced. In section b, the legs are oriented perpendicular to the coastline or the bathymetry. More offshore coverage is made in areas where the feature is likely to separate from the coast such as section c.

with no poorly sampled areas. It may be more efficient, in terms of the ship, to orient the transects into a Z shape. However, relatively large gaps in coverage occur at the top and bottom of the Z. A more even coverage is obtained with an E-shaped cruise pattern. This will be found to be important when trying to contour the data and make surface maps of features.

In the vertical, dense coverage is always preferable. Some workers advocate binning of samples into three categories: below the thermocline, within the thermocline, and above the thermocline. We do not suggest using this procedure for several reasons: 1) the thermocline may not correlate with the dinoflagellate peak or the nutricline; 2) the sample resolution is low; 3) the variable depth of the thermocline will make data reduction and interpretation difficult; and 4) unexpected features may be missed. Rather, we recommend obtaining as many evenly-spaced samples as is feasible given sample processing time. The even spacing allows for quick and easy plotting of data, with good resolution of most vertical features. We use a binning interval of 5 m, and recognize that this spreads the cell concentrations and nutrients out vertically. Thus, a feature which is

1-m thick in the *in situ* fluorescence becomes 5-m thick in the cell counts.

We also stress obtaining coincident CTD data. These data will help to resolve binning problems by giving a detailed picture of the vertical structure of the water column. The more different types of data obtained in vertical profiles, the easier will be the interpretation of the data. For example, we have found transmittance to be a good inverse tracer for *in situ* fluorescence. Since they are obtained by very different methods (transmittance via submerged instrument, fluorescence via the hose), we are confident that the strong correlation between the fields is real. Thus the transmittance gives an independent check on the hose profiling system.

Station Selection: Temporal

Considerations for the timing of sampling are numerous. Physical factors such as wind, rain, tides and sunlight have all been shown to affect dinoflagellate distributions. Seasonal considerations are also important, as dinoflagellates often show fairly restricted periods of extensive growth.

The linkage of dinoflagellate distributions with hydrographic features is strong in both space and time. Forcing such as the wind and tides will have effects on both the hydrography and the dinoflagellate distributions and should be taken into account when planning cruises. However, for most sampling programs the size of the ship is the main consideration in timing cruises: a small vessel cannot be used in heavy seas and deployment of a pump profiling system may be impossible in even moderate swell. This causes aliasing with respect to the wind: cruises are only made in light seas. Our solution to this has been to make multiple cruises, as often as possible, and to interpret the CTD data with reference to continuous wind data obtained nearby.

Tides are more predictable, the semi-diurnal and fortnightly tides being the most prominent. A good knowledge of the local tides is important in deciding whether tidal advection or mixing will be a serious problem. In small embayments, the tides may be the predominant mode of forcing, while in shallow coastal areas, strong tides may create fronts which accumulate phytoplankon. If possible, samples should be taken at the same phase of the tide each time. For large-scale features, the tides may be relatively unimportant. At the very least, the phase of the semi-diurnal tide should be recorded at each station, in order that any aliasing be taken into account during data reduction.

Tides are also important when sampling continuously at a single station, for example when performing vertical migration studies. For this reason, samples should be taken at an interval of 3 hours or less, in order that all phases of the semi-diurnal tide be resolved. This may lead to a large number of samples to process, but the data will be less subject to misinterpretation.

Over a season the frequency of cruises depends largely on the organism being sampled and its suspected distribution. In general, though, at least one cruise should be taken before the particular dinoflagellate blooms, in order that the initial conditions of the water masses are known. When studying the distribution of a particular dinoflagellate, it is best to concentrate cruises early in the bloom. This will allow good resolution of the physical systems mediating bloom distribution as the bloom develops. In particular, numerous cruises can help distinguish between in situ growth, and alongshore advection, a particularly difficult problem in much dinoflagellate research.

If the dinoflagellate being studied is toxic, the local shellfish or fish monitoring programs can provide valuable information for planning the location and timing of cruises. We rely heavily on the state-run shellfish toxicity monitoring program for planning cruises: the timing of toxicity indicates how often cruises should be taken, while the spread of toxicity determines the extent and location of a given cruise. As the bloom spreads, we alternate between cruises along one transect, gathering detailed vertical information, with cruises having extensive alongshore coverage (in the E pattern), but less vertical resolution. In the latter instance, we are able to sample 25 stations (continuous CTD profiles, 2 bottle casts for cell counts at each station) from a fast (18 kt) 10-m vessel in 8 hours. Our single transect with more detailed data at each station covers only 5 stations in the same time from a 15-m ship.

In the absence of a monitoring program, there are some environmental cues which correlate well with dinoflagellate blooms. Most dinoflagellate blooms are found in the pycnocline of a well-stratified water column. This stratification can be caused either by salinity differences or by heating. Thus strong rains or several sunny days in a row can be important in bloom formation. Keeping a close eye on the weather is important when sampling for dinoflagellates.

Data Reduction: Smoothing, Plotting and Interpretation

The detailed vertical coverage obtained by a pump profiling system with a CTD is both a boon and a bane: the large amount of

data provides an excellent picture of the vertical distributions, but data processing can be tedious and time-consuming.

One of the main problems in using a variety of instruments is the diverse nature of the data sets generated. Merging these data sets into a single visualizable data set can be a difficult task. The techniques of data smoothing and interpolation become indispensable at this stage. Data smoothing is generally necessary to remove instrument spikes and noise. A variety of tools exists for smoothing data; we recommend the use of cubic splines. An excellent book, "Numerical Recipes" (Press et al. 1986) describes the use of a variety of splines, and gives computer codes for their implementation. A useful offshoot of the smoothing process is that the smoothed data are easily interpolated. Thus vertical profiles obtained with a variety of instruments can be interpolated onto the same vertical grid, and merged into a single data file.

Data gathered via the pumping system (e.g., fluorescence) will generally be stored as a time series, whereas CTD data are plotted versus depth. To merge a time series with a depth profile, some simple manipulations of both data sets may be necessary. First, the CTD data and the time series data must be converted to the same sampling rate. Thus, if the CTD samples at 0.5-second intervals but the fluorometer samples at 2-second intervals, every four CTD data points should be averaged. The unwanted portions of each data set should then be removed (i.e., the CTD up- or downcast data and the fluorescence data up to one hose-transit-time from the start of the profile). The two data sets can then be merged, line for line, creating a single data set. This data set can then be smoothed and interpolated onto a vertical grid for plotting depth profiles.

Discrete data such as cell counts, chlorophyll samples, or nutrient data can be smoothed and interpolated in the same manner as the CTD data. However, the low vertical resolution makes this an unreliable method of data manipulation. We prefer plotting such data as histograms in a vertical profile (Fig. 6). This method leaves no ambiguity as to sample location and lets the readers draw their own conclusions as to adequacy of sampling. Fig. 6 demonstrates another useful property of cubic splines: they can be used for calculating gradients of quantities. Once the coefficients for the spline are known, it is easy to differentiate them to find the slope of a property. This process is described in Press et al. (1986) and computer codes are given for implementation. In the case of Fig. 6, we have calculated the Brünt-Väisälä, frequency, or vertical gradient of density, N^2:

$$N^2 = -\frac{g}{\rho}\,\frac{\partial \rho(z)}{\partial z}$$

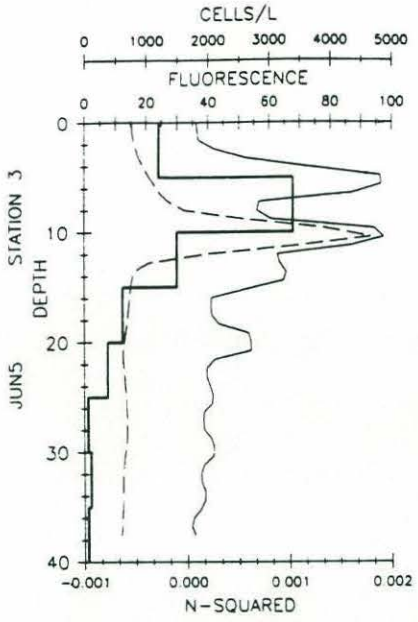

Fig. 6. Vertical profiles of cell concentration (*Ceratium longipes*, cells/l, heavy solid line), *in situ* fluorescence (dashed line), and N^2 (light solid line). As described in the text, maxima in N^2 correspond to maximum gradients in density (pycnoclines). The cell counts, binned into 5-m intervals, show a maximum coincident with the peak of *in situ* fluorescence, and the deeper pycnocline.

Here g is the acceleration due to gravity, r(z) the vertical density profile, and z the vertical coordinate. This quantity will show a maximum where the density gradient is strongest (i.e., the pycnocline). Thus it is very useful for assessing correlations between the density and other fields. As can be seen in Fig. 6, the maximum cell concentrations are found at the maximum gradient in density.

Plotting data is an art in itself. Numerous plotting packages exist for personal computers which allow quick and easy visualization of data. However, many of these packages will not allow plotting in the standard oceanographic format: a decreasing vertical axis. One way around this is to manipulate the data so that the depth is negative, with the surface being zero. This is not a very elegant solution, but cannot be avoided in many cases.

Plotting the vertical profiles of several properties on a single set of axes is a very useful means of visualizing the vertical correlations of various fields. Such a plot is shown in Fig. 7, where the raw and smoothed data sets are shown for comparison. The strong correlation between the phytoplankton fluorescence and the water density becomes obvious. This plot also shows some of the problems associated with smoothing data. These data were smoothed using an objective mapping routine after Levy and Brown (1986). The main problems associated with smoothing appear at the boundaries of the data set, in this case the surface and the bottom. In Fig. 7 it can be

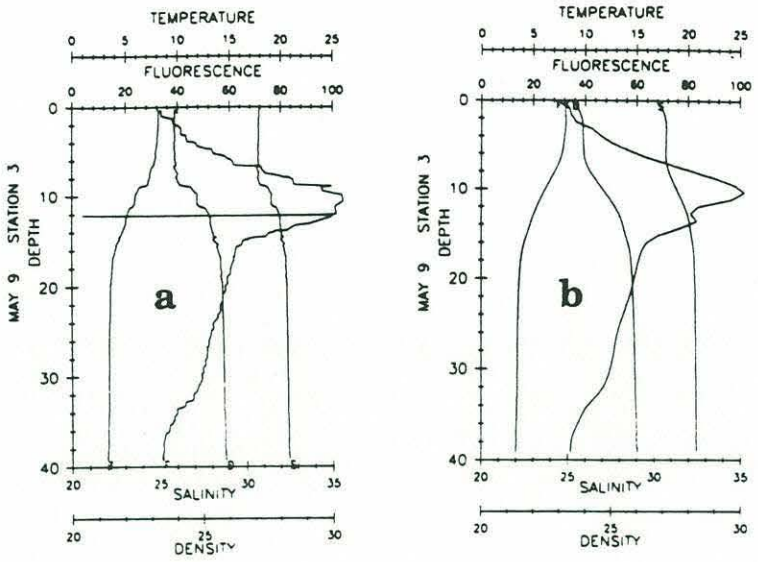

Fig. 7. Plots of the vertical profiles of temperature (°C), salinity (ppt), density (σT), and in situ fluorescence (relative units). Panel a shows the raw data (approximately 500 points in each profile), while panel b shows the smoothed profiles (50 points per curve). The small letter at the top or bottom of the profile indicates the property being plotted (T,S,D or F). Note that the smoothed salinity and density profiles tail off at the surface, while the raw data are vertical. This is an artifact of the smoothing program used.

seen that the smoothed data set shows a gradient at the surface, whereas the raw data show no such slope. This occurs because of the low number of data points near boundaries. Cubic splines can overcome some of these problems, but it is important to check the smoothed data against the raw data before conclusions are drawn. The second point where the smoothing program fails is in removing the instrument spike in the fluorescence at 12 m. Since we know that this spike was due to the instrument changing scales, and was not a real feature, we could manually remove the spike from the raw data before smoothing.

If many vertical profiles have been generated, it may prove fruitful to examine horizontal variations in properties. In this case we recommend contouring of data. Contouring of vertical profiles is a surprisingly difficult and frustrating task. If the stations were not evenly spaced, some interpolation scheme must be available for mapping onto a regular grid. If the depths of profiles vary because of bathymetry, some method should be available for masking out the bottom. Without this, the contouring program will generally create its own data in this region.

Given these caveats, contouring is still an extremely powerful tool in oceanographic research. A series of contour plots of some of our own data are shown in Fig. 8. The strong correlations of the diverse fields are immediately apparent from this type of plot, and the vertical variability is easily visualized.

The highlighting of vertical variations between stations is the most important aspect of contour plots. Most of this variability is caused by physical forcings; different types of forcings will show characteristic patterns in the cross-shore hydrography (Franks, in press). With experience, recognition of the particular physical system becomes more routine. Fig. 8 shows a river plume front, with an associated population of *Alexandrium tamarense*. The salinity gradient indicates the presence of the river plume, and the slope of the pycnocline suggests that it is moving towards the reader. The

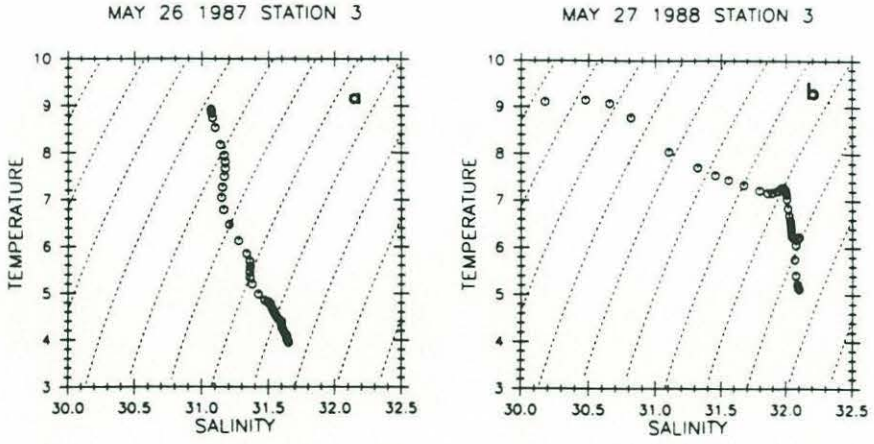

Fig. 8. Temperature/salinity plots from the same location, one year apart. The dashed lines are curves of constant density. Panel a shows a profile with a thermocline, while panel b shows a profile with a halocline. Note that the temperature range in the two panels is the same, but the salinity range is much less in a than b. The profile in b covers a much wider range of density.

magnitude of the slope allows an estimate of the current speed: ~10 cm/second. An introductory physical oceanography text will explain how these calculations are made.

Much information about dinoflagellate populations can be obtained by identification of water masses. This is most easily done using temperature/salinity (T/S) plots. The convention in oceanography is to make temperature the vertical axis, and salinity

the horizontal axis. Plotting a vertical profile on such axes makes individual water masses readily apparent: deep water masses are cold and salty, thermoclines and haloclines will point at right angles to each other, and the surface water will be warm, fresh or both. Thus water below the pycnocline will cluster toward the lower right of the plot, while surface water will be toward the top or the left, depending on whether the pycnocline is due to temperature or salinity, respectively. In Fig. 9, two T/S plots are shown from the same location a year apart. Fig. 9a shows a typical profile with a thermocline, while Fig. 9b shows a profile with a halocline. The differences between these are obvious and demonstrate the variability possible in the hydrography of coastal regions. Such plots

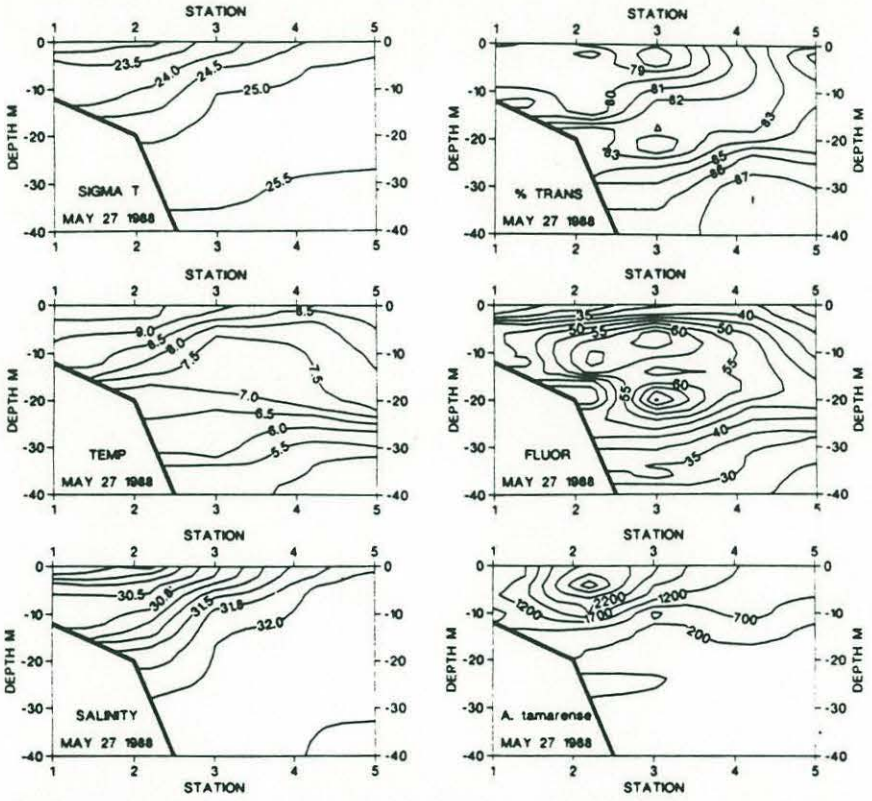

Fig. 9. A series of contour plots of data gathered in the Gulf of Maine. Clockwise from the upper left: density (σT), % transmittance, in situ fluorescence, cell concentration (Alexandrium tamarense, cells/l), salinity (ppt), and temperature (°C). The thick line at the bottom left of each panel is the bottom. The maximum depth is 40 m, the length of our hose. The stations are ~7 km apart; station 5 is 30 km offshore. Note the strong, sloping pycnocline created by the salinity gradient. The cells are found mainly within the fresher water and the pycnocline.

also bear strongly on the distributions of cells: in Fig. 9a, the pycnocline is formed by heating, so we might expect the cells to be horizontally uniform. In Fig. 9b the pycnocline is formed by a salinity gradient, indicating the presence of a river plume. We might expect considerable horizontal variability in cell concentrations due to their association with the river plume front.

Numerous other tools exist for visualizing data. Plotting a profile versus density rather than depth can be a useful way to assess correlations with the hydrography. Three-dimensional plots of density surfaces can lead to insights into the local dynamics. An introductory physical oceanography text, taking physical oceanography courses, or obtaining the help of a local expert for interpreting complicated hydrographic data are useful steps.

Of all the points made above, none can be stressed more than the importance of obtaining coincident hydrographic and biological samples. It is only with a good knowledge of the local physical dynamics that confident interpretations of biological patterns can be made.

Acknowledgements

Development of these methods and the preparation of this paper were supported in part by the Office of Naval Research (Grant No. N00014-89-3-1111) and by NOAA Sea Grant College Program Office, Department of Commerce under grant no. NA86AA-D-S6090 (R/B-76) to Woods Hole Oceanographic Institution. Contribution No. 7172 from the Woods Hole Oceanographic Institution.

References

Franks, P.J.S. Dinoflagellate blooms at fronts: Patterns, scales and forcing mechanisms. *In* L. Ford (ed.) Proceedings of the Fourth International Conference on Modern and Fossil Dinoflagellates, L. Ford (ed.) Amer. Assoc. Stratigraphic Palynologists Contr. Ser. (In press)

Levy, G. and R.A. Brown. 1986. A simple, objective analysis scheme for scatterometer data. J. Geophys. Res. 91:5135-5158.

Press, W.H., B.P. Flannery, S.A. Teukolsky and W.T. Vetterling. 1986. Numerical Recipes. Cambridge University Press, New York. 818 p.

APPENDIX B

CALCULATION OF PLUME VELOCITIES USING THE THERMAL WIND EQUATION

PREAMBLE

The thermal wind equation allows an estimate of the baroclinic component of the horizontal velocity perpendicular to the line joining two vertical profiles of density. The thermal wind equations are derived from the equations for geostrophic flow as follows. Having assumed steady flow at low Reynolds number, with negligible frictional effects, the equations for horizontal velocities u and v in a geostrophic balance are:

$$-fv = -\frac{1}{\rho}\frac{\partial p}{\partial x} \tag{B1a}$$

$$fu = -\frac{1}{\rho}\frac{\partial p}{\partial y}. \tag{B1b}$$

Here ρ is the reference density, f the Coriolis frequency, and p the pressure at any given depth. Differentiating (B1a) and (B1b) with respect to z, we have

$$-\frac{\partial}{\partial z}(\rho fv) = -\frac{\partial^2}{\partial x \partial z}p \tag{B2a}$$

$$\frac{\partial}{\partial z}(\rho fu) = -\frac{\partial^2}{\partial y \partial z}p. \tag{B2b}$$

Assuming the pressure to be hydrostatic (i.e. $\frac{\partial p}{\partial z} = -\rho g$), we find

$$\frac{\partial}{\partial z}(\rho v) = -\frac{g}{f}\frac{\partial \rho}{\partial x} \tag{B3a}$$

$$\frac{\partial}{\partial z}(\rho u) = \frac{g}{f}\frac{\partial \rho}{\partial y}. \tag{B3b}$$

Equations (B3a,b) are the thermal wind equations, describing the vertical gradient of horizontal velocities set up by a horizontal gradient in density. These equations may be integrated vertically to give

$$v = -\frac{g}{\rho f} \int_{0}^{-h} \frac{\partial \rho}{\partial x} \, dz \qquad \text{(B4a)}$$

$$u = \frac{g}{\rho f} \int_{0}^{-h} \frac{\partial \rho}{\partial y} \, dz \; . \qquad \text{(B4b)}$$

In performing this last step, we have neglected a constant of integration, which is an unknown barotropic component of the horizontal velocity field. Several methods have been utilized to adjust for the unknown barotropic component. The most common is to assume that the velocities are negligible at some reference depth (the "depth of no motion"), and to normalize the calculated velocity profile to that depth. This method works well in areas where there is no horizontal shear at the reference depth. In areas of strongly sloping isopycnals, however, this may not be the case. In such a situation it has been suggested that an isopycnal surface be used as a "layer of no motion", rather than a reference depth. This assumes that flow is constant along an isopycnal surface. A third method, used for coastal regions, has been to integrate from the offshore, extending the isopycnals inshore along their last observed slopes or along the steric heights (Reid and Mantyla, 1976).

METHODS

The horizontal gradient of density was calculated from cubic splines (IMSL routines CSAKM and CSDER), fit to the densities at a given depth for Stations 1-5. The velocity at this depth and station was calculated using equation (B4b). The integrand was evaluated at each depth and summed vertically to calculate the velocity profile for each station. The velocity profile was then adjusted by either 1) subtracting the 20 m velocity from the profile, 2) subtracting the velocity at the 1025 kg m^{-3} isopycnal from the profile, or 3) making

the 20 m velocity at inshore stations equal to the 20 m velocity at Station 5.

RESULTS

Equation (B4b) was applied to the data from May 27, 1988. The hydrography showed a strongly sloping pycnocline, and the wind stress was fairly weak (Chapter 4, Figures 4-2, 4-12). The velocities calculated using the three methods of barotropic correction were practically identical. The velocity profiles using the method 1 and 2 corrections are shown with the density structure in Figure B-1. The surface waters of the plume show southward alongshore velocities 0.2 m s^{-1} greater than the offshore surface waters. A strong shear zone is evident near Station 2, the location of the maximum concentrations of *Alexandrium tamarense* (Figure B-1c).

DISCUSSION

Application of the thermal wind equations to the density structure seen May 27, 1988 indicated a strong southward surface jet of buoyant water. Velocities in this jet were 0.2 m s^{-1} greater than the ambient waters. These velocities agree well with those calculated using Margule's equation (Chapter 4). The location of the peak velocities coincided with the maximal concentrations of *Alexandrium tamarense*.

The hydrographic data from May 27, 1988 were chosen for this calculation because of the weak wind field at that time. Thus the velocities calculated are representative of the alongshore velocities of the buoyant plume with no wind stress. As discussed in Chapters 4 and 5, the alongshore wind stress can have a significant impact on the hydrographic structure, and presumably the velocity structure, of the plume. For density profiles such as were seen on May 23, 1989 (Chapter 4, Figure 4-6), the thermal wind equations

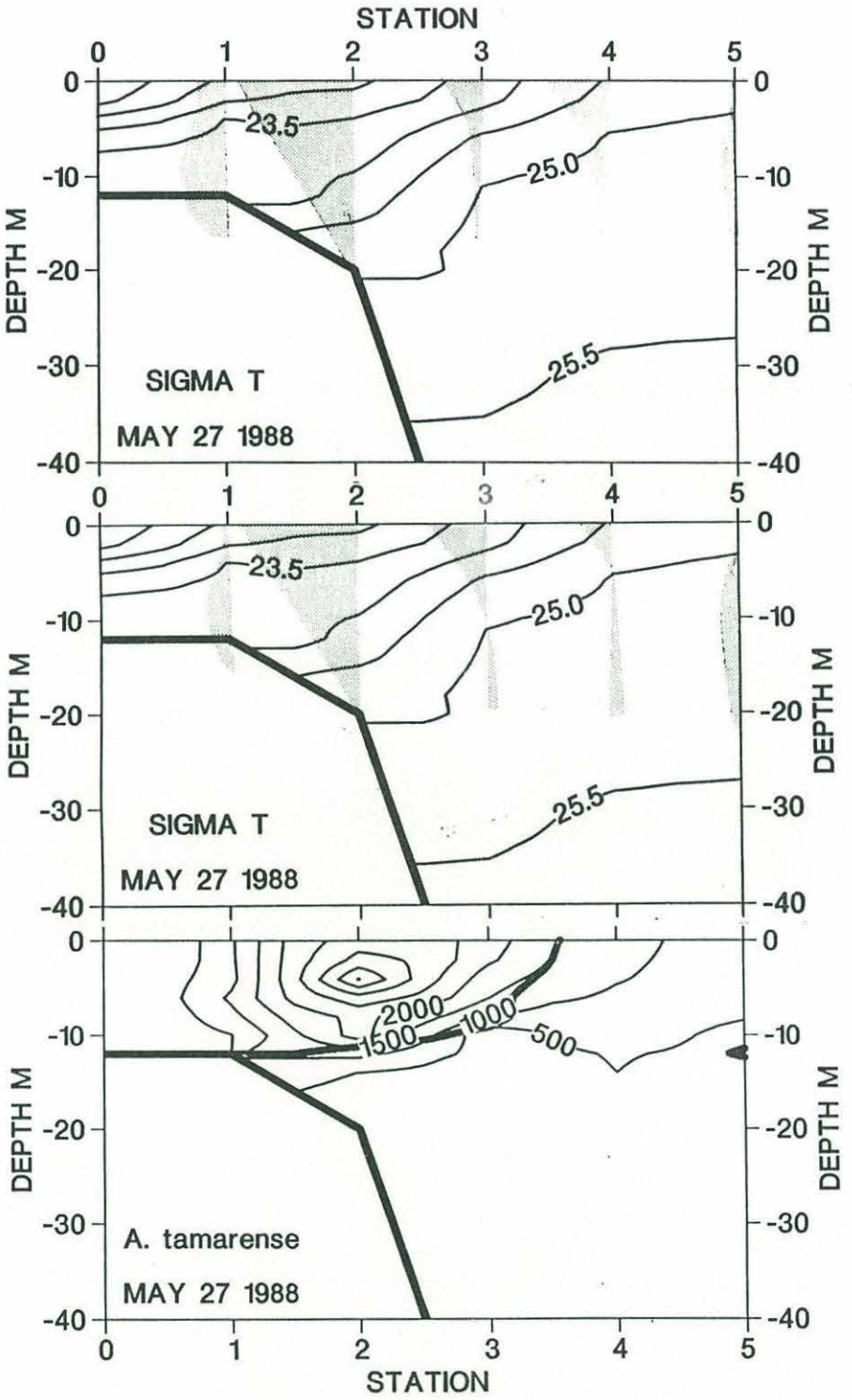

Figure B-1. σ_T sections from May 27, 1988 with vertical profiles of velocity (shaded areas) calculated by method 1 (top) and method 2 (middle). Bottom panel is section of *Alexandrium tamarense* cell concentrations (cell l^{-1}) from the same date. See text for explanation of methods.

would have given northward alongshore velocities. The model of Chao (1987) would suggest, however, that the plume was advecting slowly southward. Thus interpretation of the results of the application of equation (B4b) can be problematic. The computed velocity structure should be analyzed critically with consideration of the prevailing winds and knowledge of the local hydrographic conditions.

The velocities calculated above reinforce the hypothesis that the plume acts as a vehicle for the alongshore transport of toxic dinoflagellate populations. The association of the peak concentrations of *Alexandrium tamarense* with the peak alongshore velocities could be due to the cells originating in that water mass, or could be an artifact created by the shears within the plume. The lack of information on the alongshore distributions of the cells makes this a difficult point to address.

Integrating the velocities vertically gives an estimate of about 3×10^4 m^3 s^{-1} for the alongshore transport of the water in the plume. From Figure 4-9, the area of freshwater on May 27, 1988 was about 10^4 m^2, or a fraction of freshwater of 0.025. Thus the alongshore flux of 0 psu water was about 750 m^3 s^{-1} on May 27, 1988. This flux is almost exactly equal to the combined flows of the Androscoggin and Kennebec Rivers at that time. Thus all of the fresh water in the plume can be accounted for by the flows of these two rivers, using velocities calculated from the thermal wind equations.

LITERATURE CITED

Chao, S.-Y. 1987. Wind-driven motion near inner shelf fronts. J. Geophys. Res. 92:3849-3860.

Reid, J.L. and A.W. Mantyla. 1976. The effect of the geostrophic flow upon coastal sea elevations in the northern North Pacific Ocean. J. Geophys. Res. 81:3100-3110.

APPENDIX C

DATA FROM A THERMISTOR CHAIN MOORED NEAR STATION 2, MAY-JULY, 1988

PREAMBLE

One of the hypotheses we sought to test during the course of this study was the hypothesis of wind-driven control of the toxic dinoflagellate blooms. A convenient measure of wind-driven upwelling and downwelling motions in stratified coastal waters is the vertical fluctuation in temperature. Coastal upwelling should cause a decrease in inshore surface temperatures, and a possible homogenization of the inshore waters. Downwelling-favourable winds should cause a warming of the inshore waters and deeper waters as warm surface water is forced toward the shore. The data from a thermistor chain can give a continuous record of vertical temperature fluctuations; unfortunately, a single chain cannot resolve the changes into along- and across shelf components. Thus alongshore advection of different water masses cannot be conveniently distinguished from across-shelf advective motions.

The use of ancillary data sets can aid in interpreting the thermistor chain time series. Time series of surface wind stress, hydrographic data, and satellite images of sea surface temperature proved particularly useful in identifying dominant physical forcings. The major forcings identified were the M_2 tide, the alongshore wind stress, and surface heating.

METHODS

An Aanderaa Instruments TR-1 temperature recorder was moored with a 40 m, 12-thermistor chain as shown in Figure C-1. The last thermistor was doubled back to enhance the vertical resolution in the surface layer. The top thermistor was about 5 m from the surface, with nominally 3 m between adjacent thermistors.

The thermistor mooring was first deployed from the R/V Jere A. Chase on May 23, 1988, about 1 km northeast of Station 2, at LORAN coordinates 13642.5, 25939.17. The recorder was set to record at an interval of 15 min. A timed explosive bolt released the

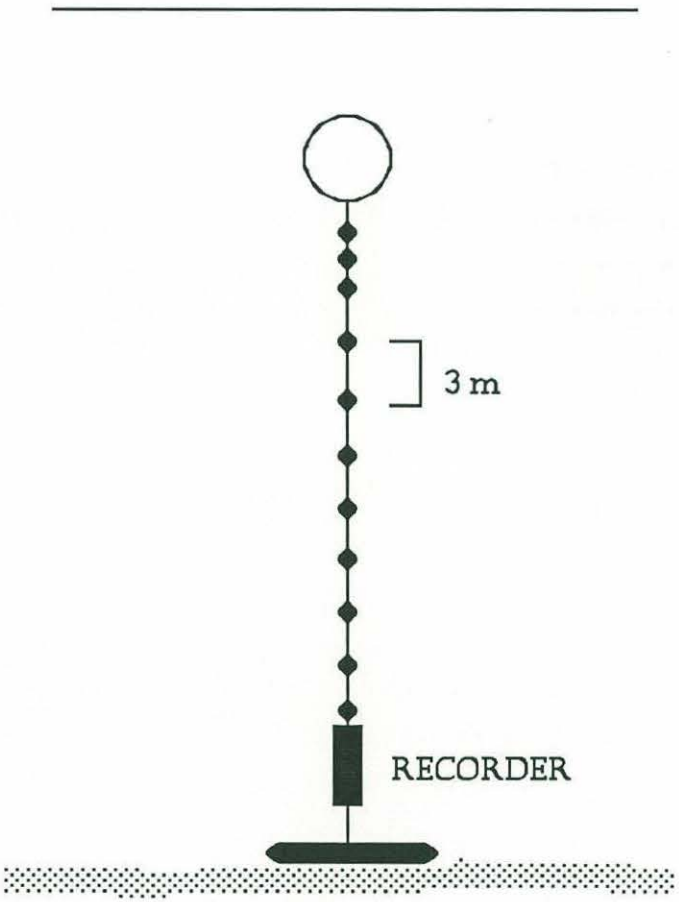

Figure C-1. Arrangement of the thermistor chain on the mooring. The recorded was attached near the explosive release, with the thermistors extending upward into the water column. The last thermistor was doubled over to obtain greater resolution in the near-surface waters.

mooring weights on June 29, 1988. The chain was redeployed on July 1, 1988, with a recording interval of 5 min. The mooring was finally retrieved on July 20, 1988.

The data were plotted as temperature vs. depth using the contouring routines of UNIMAP. Smoothing of the data to remove the tidal signal was done in the INTERPOLATION routines of UNIMAP.

RESULTS

The strongest signal seen in the data of Figures C-2 and C-3 is the M_2 tidally-forced fluctuation in temperature. The range of temperature at a given depth over a tidal cycle was sometimes as much as 3° C.

The smoothed temperature data of Figure C-2 and C-3 show several long-timescale events. A warming of the surface waters can be seen, particularly after Julian day 162 (June 10). A sudden cooling of the surface waters, and warming of the deeper waters on Julian day 154 (June 2), was reversed on day 155-156 (June 3-4).

DISCUSSION

The main signal seen in the thermistor chain records is fluctuations on the M_2 tidal frequency (semi-diurnal). These fluctuations are particularly strong after July 3 (Julian day 185; Figure C-3), probably in response to calm weather and a full moon at that time. The tidal amplitude in this region is approximately 2 m, thus some of the temperature fluctuation is caused by vertical motions of the pycnocline across the thermistors. However, the rather weak stratification at that time (Chapter 4, Figure 4-3) suggests that other mechanisms must be acting.

The data of Moody et al. (1984) indicate the tidal ellipse in this region to be elongate in the across-shelf direction, with an

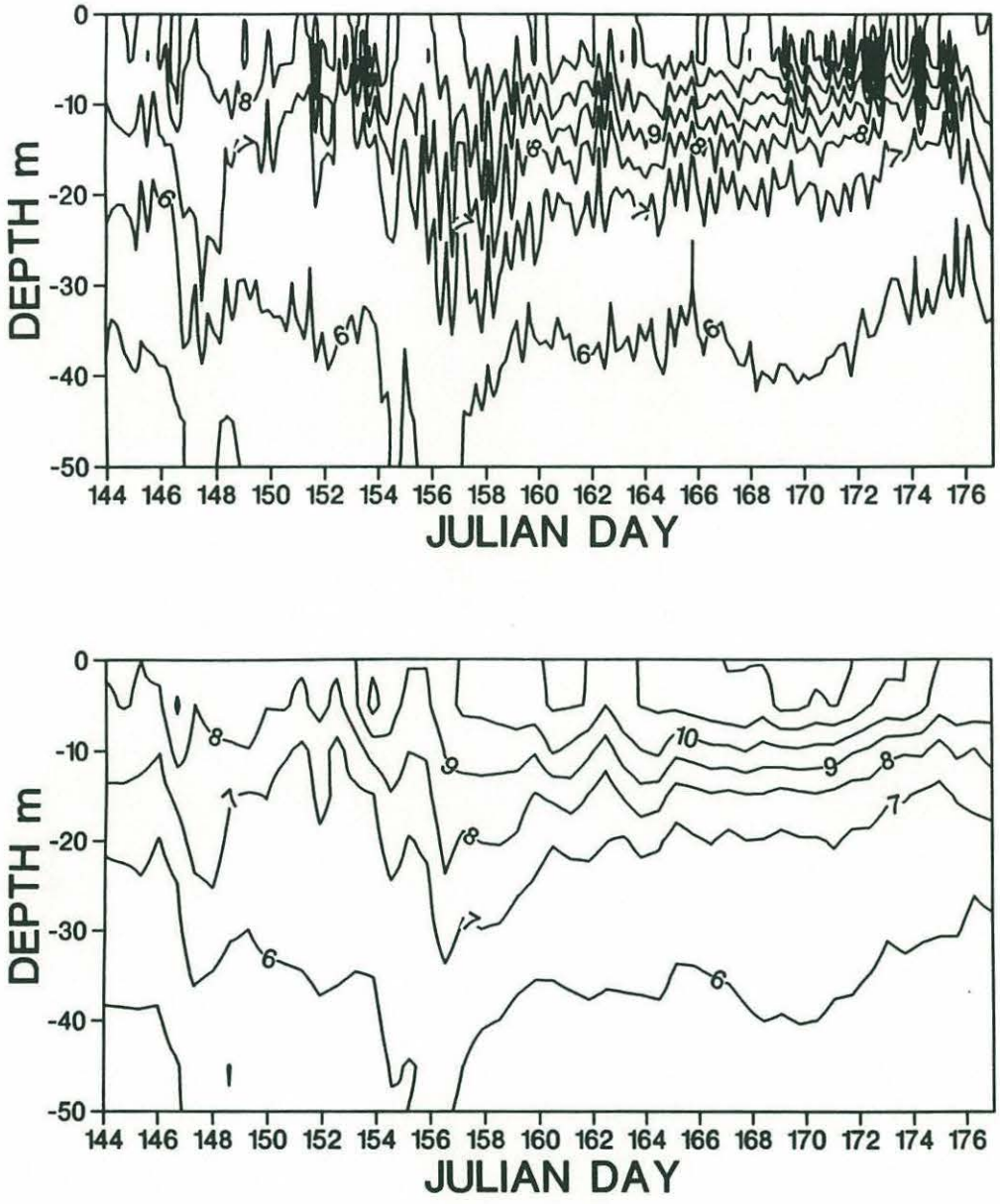

Figure C-2. Temperature vs. depth for the times (Julian day) indicated on the horizontal axis. Upper panel: unsmoothed time series. Lower panel: time series smoothed to remove tidal signal.

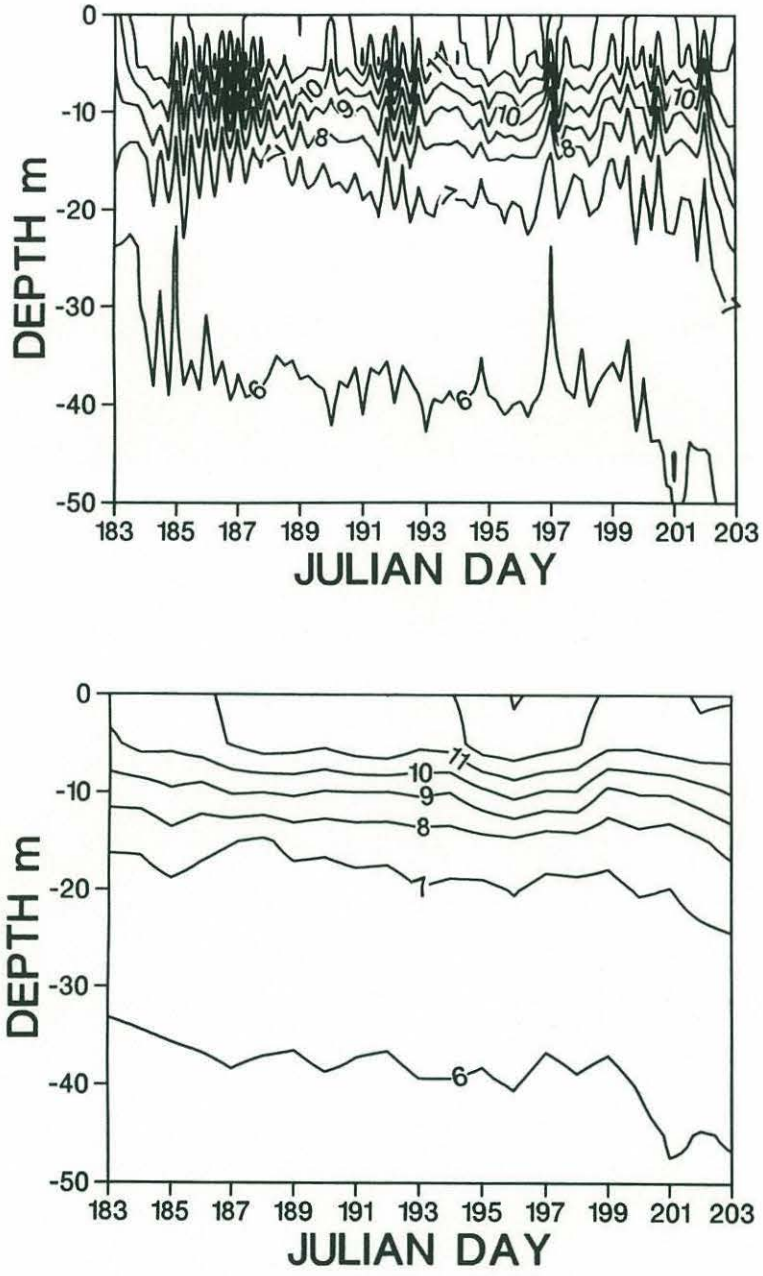

Figure C-2. Temperature vs. depth for the times (Julian day) indicated on the horizontal axis. Upper panel: unsmoothed time series. Lower panel: time series smoothed to remove tidal signal.

across-shelf tidal excursion of approximately 6 km. The horizontal advection of a sloping thermocline across the thermistor chain could account for much of the temperature fluctuation seen. It was the regularity, and long duration of this signal that first led us to investigate the hypothesis of a relatively stable front in the region.

The motion of a temperature front across the thermistor chain mooring can account for much of the variability in the temperature records. The sudden cooling of surface waters on June 2, followed by warming on June 3-4 can be explained through the effects of a strong downwelling-favourable wind event at that time (Chapter 4, Figure 4-12). With warm waters inshore, such a wind would bring cold offshore surface waters inshore. If the sloping front were to steepen, warmer inshore waters could be moved offshore, causing an increase in temperature at the deeper thermistors. The hydrographic data of May 27 and June 3, 1988 (Chapter 4, Figure 4-3) indicate that this was probably what happened.

A cooling of the temperatures on days 146-149 (May 26-28), and day 151 (May 30), was probably caused by the upwelling-favourable winds at those times (Chapter 4, Figure 4-12).

The long-term cooling of deep water after Julian day 160 (June 8; Figure C-2) is unexpected given the surface heating at that time. It is possible that by this time the fresh water flow was so low that the warm waters of the buoyant plume were no longer forcing the inshore pycnocline downward (Chapter 4, Figure 4-3, June 16). Thus cold offshore waters could have gradually moved nearer the surface as the pycnocline shoaled and relaxed to the horizontal.

The time series data from the thermistor chain were invaluable in explaining the hydrographic patterns recorded in this region. The data were consistent with the wind and tide-driven motions of a coastal front across the thermistor mooring. The strength and duration of the temperature signal gave considerable insight into the dynamics and duration of the buoyant plume. It was

these data, in fact, which initiated the formulation of the plume advection hypothesis (Chapters 4 and 5).

LITERATURE CITED

Moody, J.A., B. Butman, R.C. Beardsley, W.S. Brown, P. Daifuku, J.D. Irish, D.A. Mayer, H.O. Mofjeld, B. Petrie, S. Ramp, P. Smith and W.R. Wright. 1984. Atlas of tidal elevation and current observations on the northeast American continental shelf and slope. U.S. Geological Survey Bull. 1611.

APPENDIX D

SUMMARY OF HYDROGRAPHIC AND BIOLOGICAL DATA FOR CRUISES TAKEN NEAR PORTSMOUTH, NEW HAMPSHIRE, 1987-1989

PREAMBLE

A 30 km transect off Portsmouth, New Hampshire was sampled between April and September of 1987-1989. The sampling procedure is described in Appendix A. The station locations are shown in Figure 3-1 of Chapter 3. Their coordinates are:

Station 0:	43°04'28.1" N	70°42'37.5" W
Station 1:	43°03'30.2" N	70°39'57.7" W
Station 2:	43°02'52.3" N	70°35'15.9" W
Station 3:	43°02'05.6" N	70°30'09.8" W
Station 4:	43°00'54.9" N	70°24'15.7" W
Station 5:	43°00'00.2" N	70°18'56.6" W

The following unnumbered figures summarize the σ_T, salinity (psu), temperature (°C), beam-c (m^{-1}), fluorescence (relative units, may not be comparable between years), and cell concentrations (cells l^{-1}) for the dates indicated at the bottom left of each panel. No beam-c data were available for 1987, since we did not have a transmissometer. Some panels are missing as the data were not worked up.

The cruises were aboard the R/V Jere A. Chase, excepting the cruises on May 19, June 8 and June 27 1989, which were taken aboard the C/V Unity. No pumping system was deployed during these cruises, thus no fluorescence data were available. Only surface and 10 m samples were collected for cell counts. Not all stations were sampled on all cruises, and on some cruises the CTD data were lost. The following figures summarize the processed data.

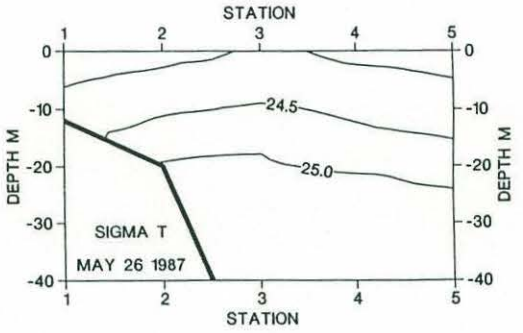
STATION
DEPTH M
24.5
25.0
SIGMA T
MAY 26 1987

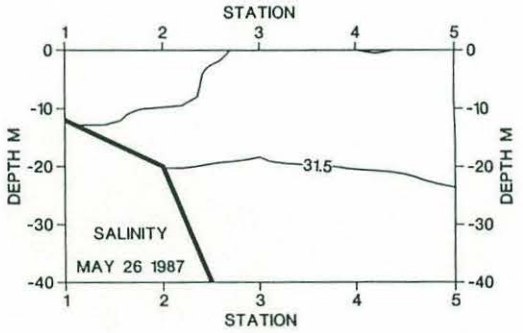
STATION
DEPTH M
31.5
SALINITY
MAY 26 1987

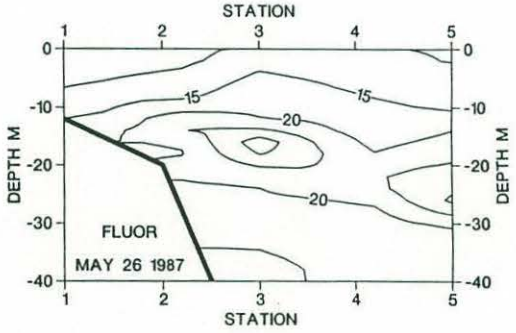
STATION
DEPTH M
15
20
FLUOR
MAY 26 1987

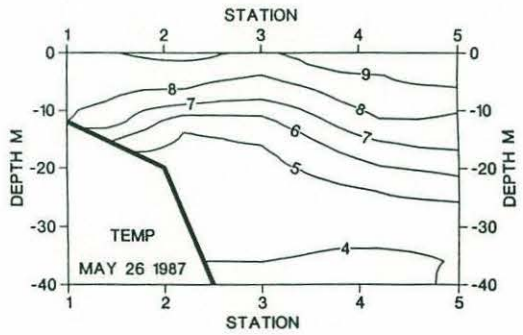
STATION
DEPTH M
9
8
7
6
5
4
TEMP
MAY 26 1987

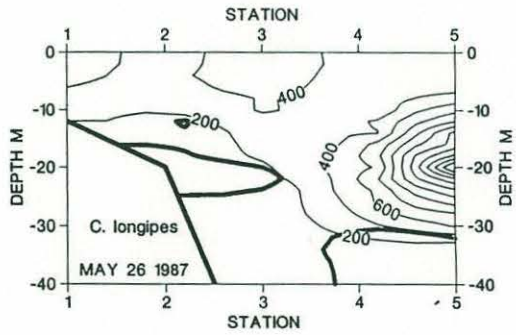
STATION
DEPTH M
400
200
600
C. longipes
MAY 26 1987

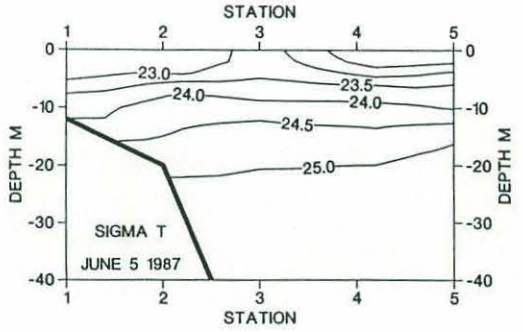
STATION
DEPTH M
23.0
23.5
24.0
24.0
24.5
25.0
SIGMA T
JUNE 5 1987
STATION

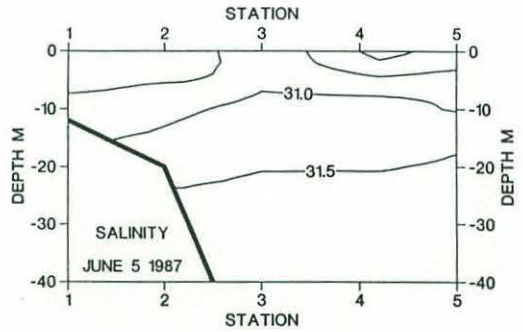
STATION
DEPTH M
31.0
31.5
SALINITY
JUNE 5 1987
STATION

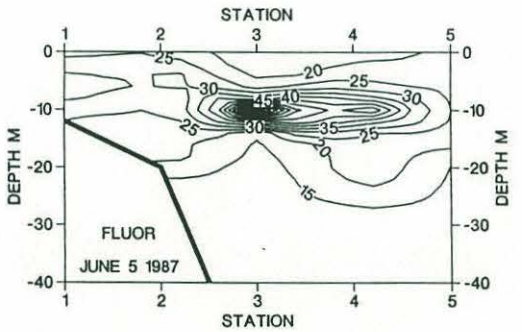
STATION
DEPTH M
25
20
25
30
45
40
30
30
25
35
25
20
15
FLUOR
JUNE 5 1987
STATION

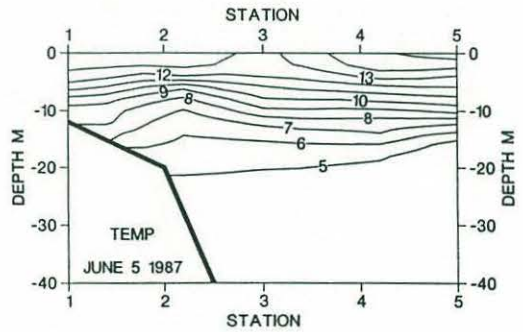
STATION
DEPTH M
12
9
8
13
10
8
7
6
5
TEMP
JUNE 5 1987
STATION

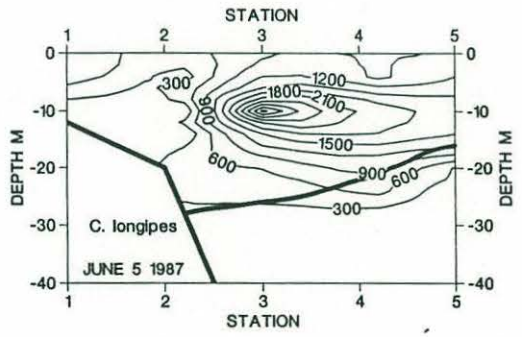
STATION
DEPTH M
300
900
1200
1800
2100
1500
600
900
600
300
C. longipes
JUNE 5 1987
STATION

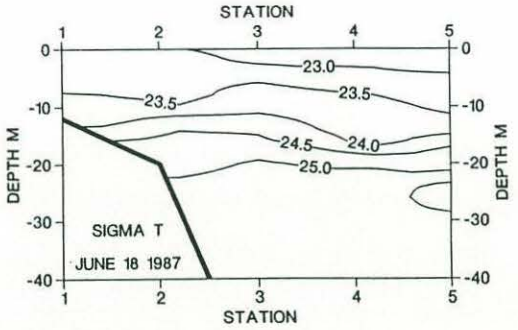
STATION
DEPTH M
SIGMA T
JUNE 18 1987
23.0
23.5
24.5
24.0
25.0

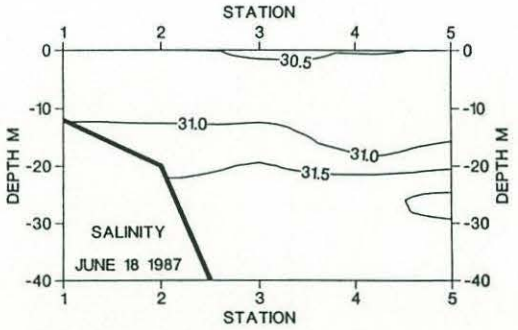
STATION
DEPTH M
SALINITY
JUNE 18 1987
30.5
31.0
31.5

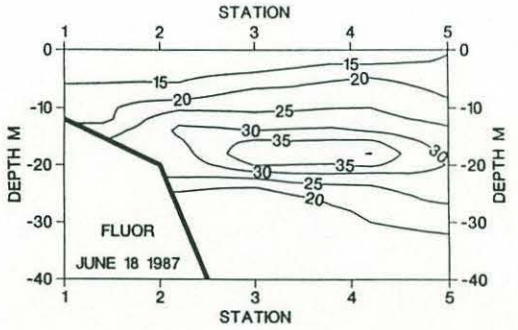
STATION
DEPTH M
FLUOR
JUNE 18 1987
15
20
25
30
35

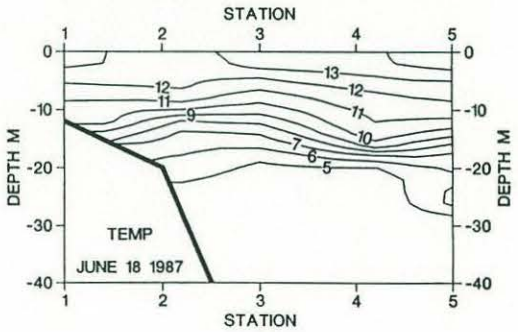
STATION
DEPTH M
TEMP
JUNE 18 1987
13
12
11
9
7
6
5
10

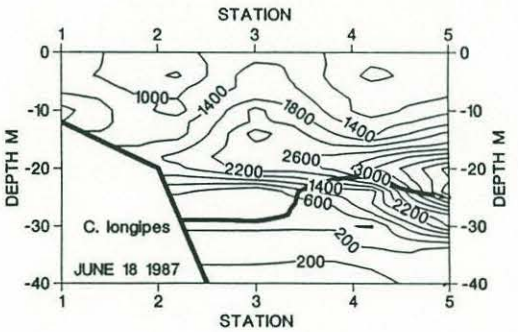
STATION
DEPTH M
C. longipes
JUNE 18 1987
1000
1400
1800
2600
2200
3000
600
200

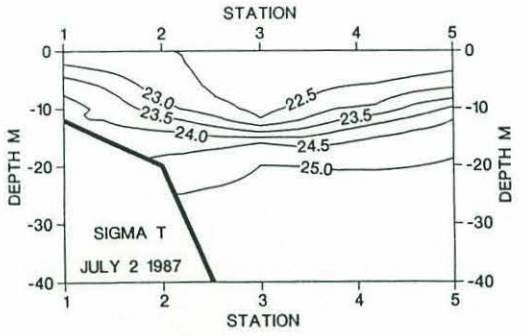
STATION
DEPTH M
SIGMA T
JULY 2 1987
23.0
23.5
24.0
22.5
23.5
24.5
25.0

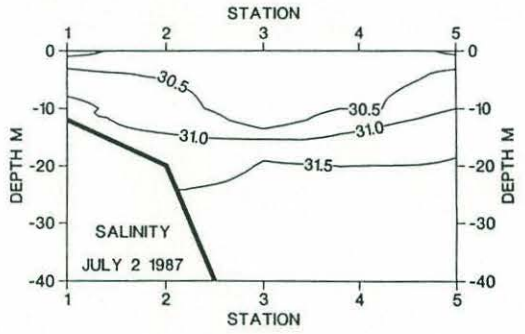
STATION
DEPTH M
SALINITY
JULY 2 1987
30.5
31.0
30.5
31.0
31.5

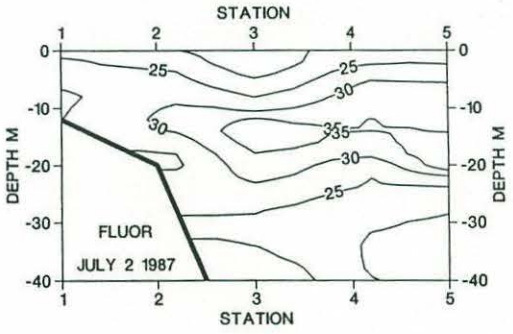
STATION
DEPTH M
FLUOR
JULY 2 1987
25
30
25
30
35
30
25

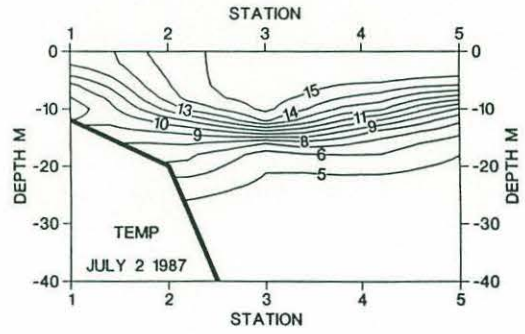
STATION
DEPTH M
TEMP
JULY 2 1987
15
13
14
11
10
9
9
8
6
5

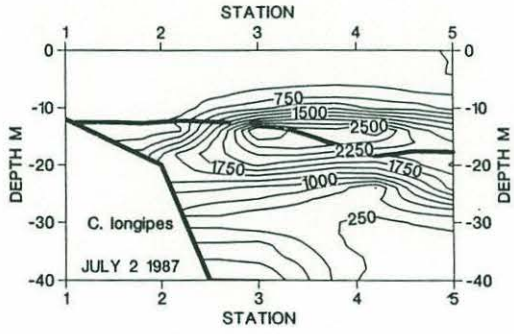
STATION
DEPTH M
C. longipes
JULY 2 1987
750
1500
2500
2250
1750
1750
1000
250

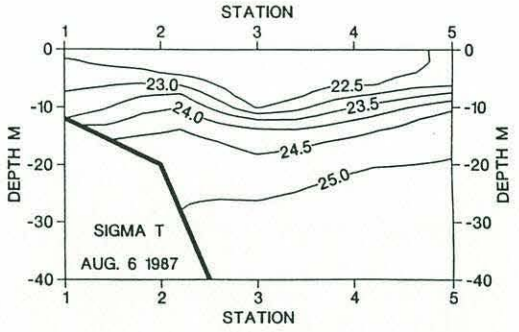
STATION
1
2
3
4
5
0
-10
-20
-30
-40
DEPTH M
23.0
22.5
24.0
23.5
24.5
25.0
SIGMA T
AUG. 6 1987
STATION

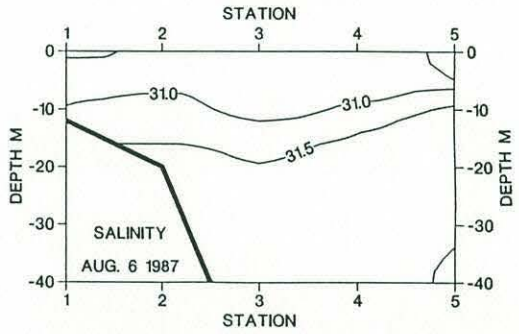
STATION
1
2
3
4
5
0
-10
-20
-30
-40
DEPTH M
31.0
31.0
31.5
SALINITY
AUG. 6 1987
STATION

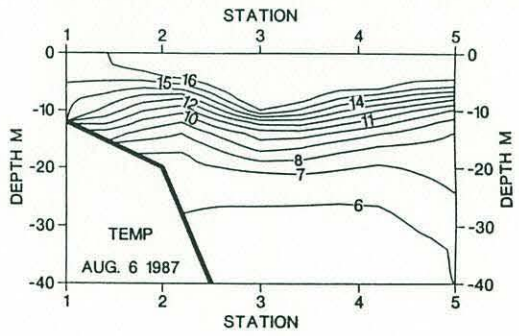
STATION
1
2
3
4
5
0
-10
-20
-30
-40
DEPTH M
15
16
12
10
14
11
8
7
6
TEMP
AUG. 6 1987
STATION

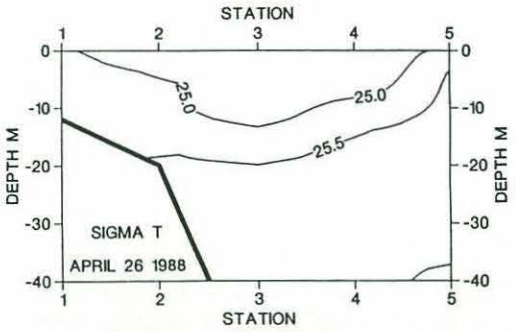
STATION
DEPTH M
SIGMA T
APRIL 26 1988
25.0
25.5

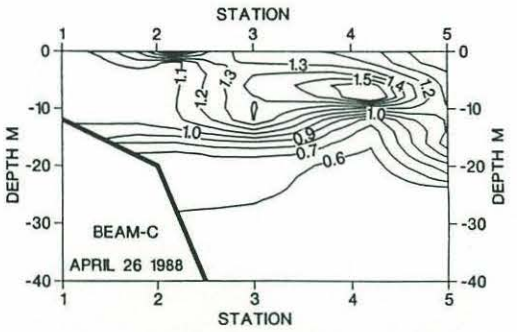
STATION
DEPTH M
BEAM-C
APRIL 26 1988

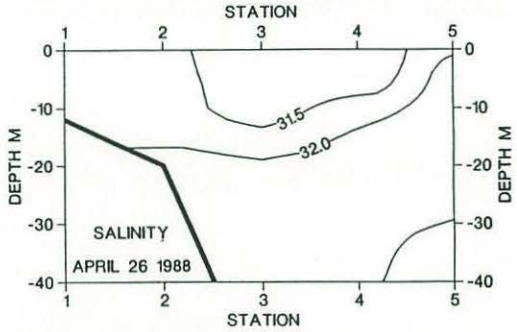
STATION
DEPTH M
SALINITY
APRIL 26 1988
31.5
32.0

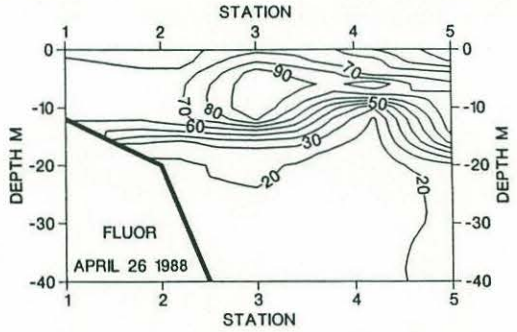
STATION
DEPTH M
FLUOR
APRIL 26 1988

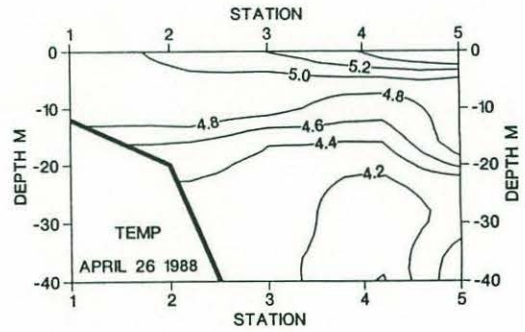
STATION
DEPTH M
TEMP
APRIL 26 1988
5.0
5.2
4.8
4.6
4.4
4.2

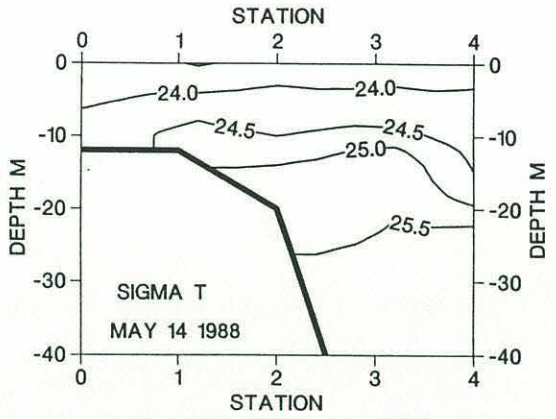
STATION
DEPTH M
SIGMA T
MAY 14 1988
24.0
24.5
25.0
25.5

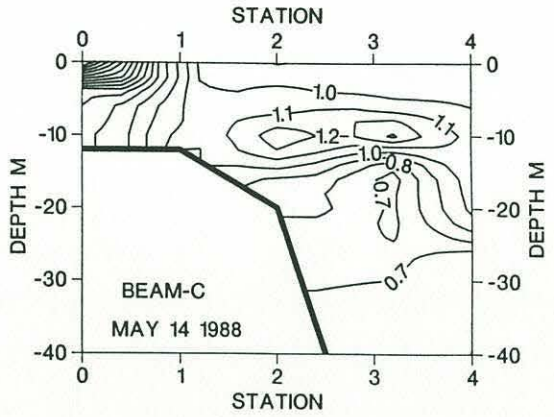
STATION
DEPTH M
BEAM-C
MAY 14 1988
1.0
1.1
1.2
0.8
0.7

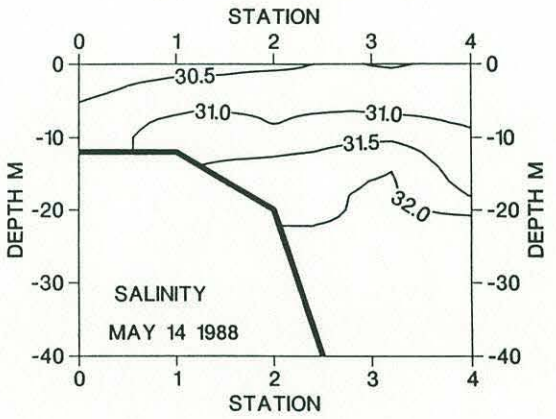
STATION
DEPTH M
SALINITY
MAY 14 1988
30.5
31.0
31.5
32.0

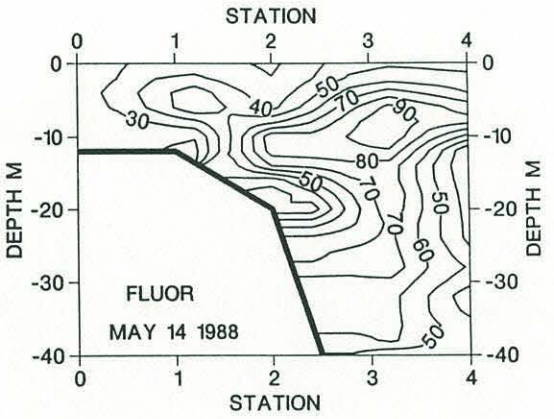
STATION
DEPTH M
FLUOR
MAY 14 1988
30
40
50
70
90
80
60

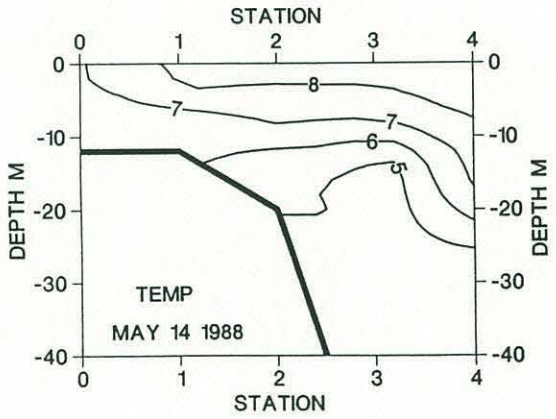
STATION
DEPTH M
TEMP
MAY 14 1988
8
7
6
5

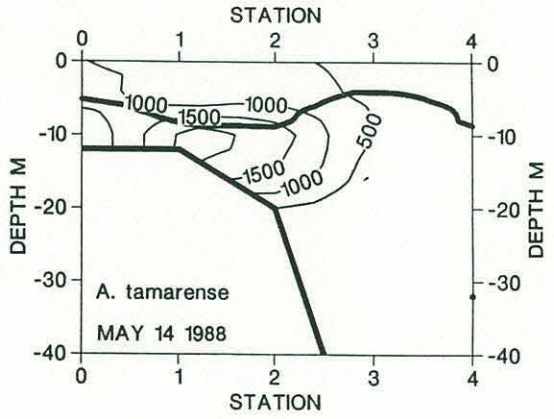
STATION
DEPTH M
A. tamarense
MAY 14 1988
1000
1500
500

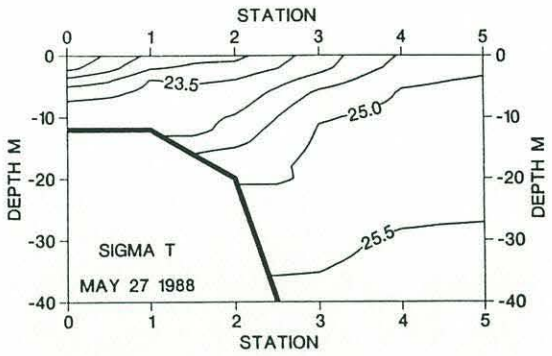
STATION
DEPTH M
23.5
25.0
25.5
SIGMA T
MAY 27 1988

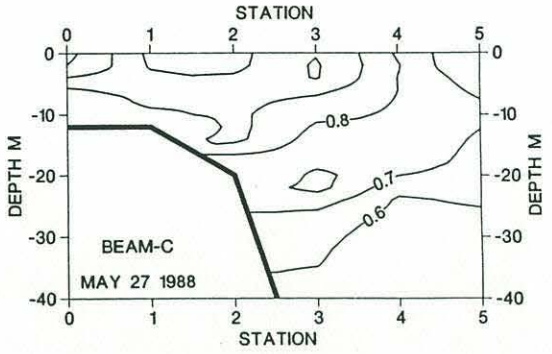
STATION
DEPTH M
0.8
0.7
0.6
BEAM-C
MAY 27 1988

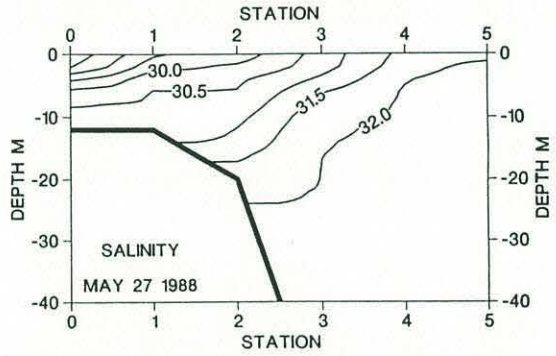
STATION
DEPTH M
30.0
30.5
31.5
32.0
SALINITY
MAY 27 1988

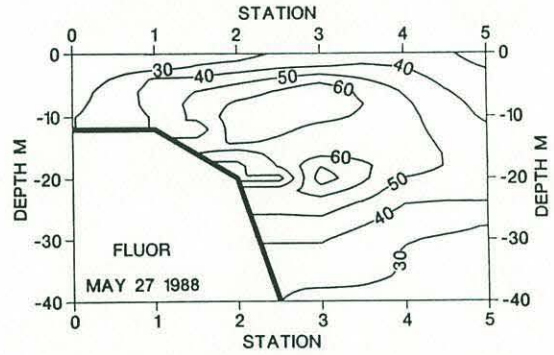
STATION
DEPTH M
30
40
50
60
FLUOR
MAY 27 1988

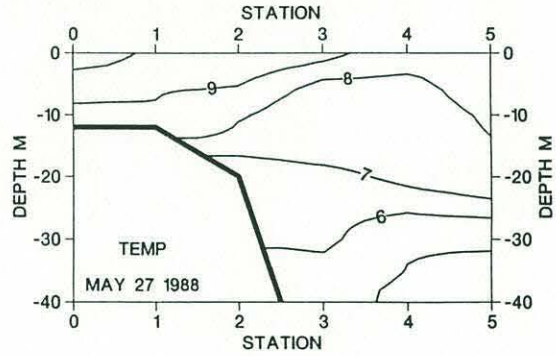
STATION
DEPTH M
9
8
7
6
TEMP
MAY 27 1988

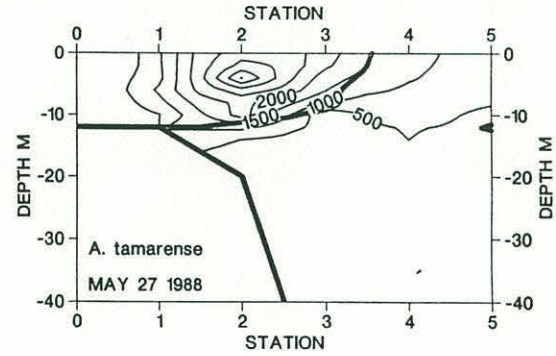
STATION
DEPTH M
2000
1500
1000
500
A. tamarense
MAY 27 1988

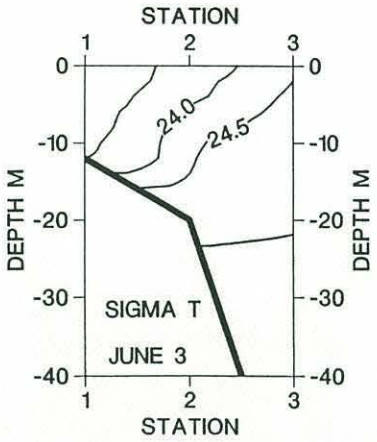
STATION
1
2
3
0
-10
-20
-30
-40
DEPTH M
24.0
24.5
SIGMA T
JUNE 3
STATION

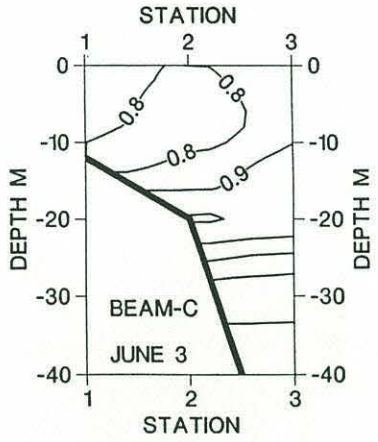
STATION
1
2
3
0
-10
-20
-30
-40
DEPTH M
0.8
0.8
0.8
0.9
BEAM-C
JUNE 3
STATION

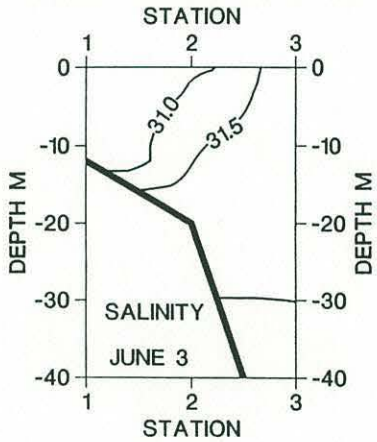
STATION
1
2
3
0
-10
-20
-30
-40
DEPTH M
31.0
31.5
SALINITY
JUNE 3
STATION

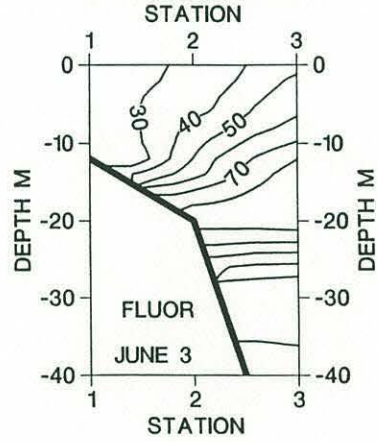
STATION
1
2
3
0
-10
-20
-30
-40
DEPTH M
30
40
50
70
FLUOR
JUNE 3
STATION

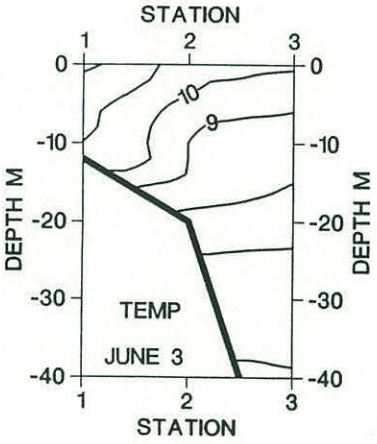
STATION
1
2
3
0
-10
-20
-30
-40
DEPTH M
10
9
TEMP
JUNE 3
STATION

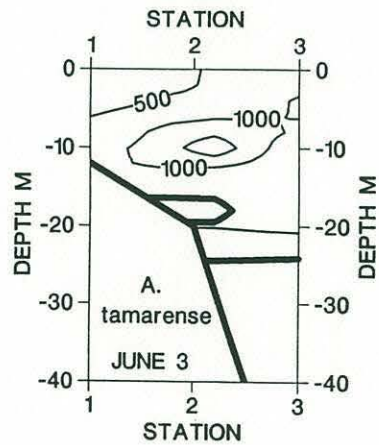
STATION
1
2
3
0
-10
-20
-30
-40
DEPTH M
500
1000
1000
A.
tamarense
JUNE 3
STATION

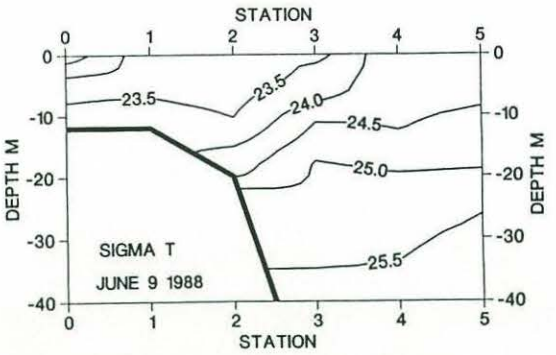
STATION
DEPTH M
SIGMA T
JUNE 9 1988
23.5
24.0
24.5
25.0
25.5

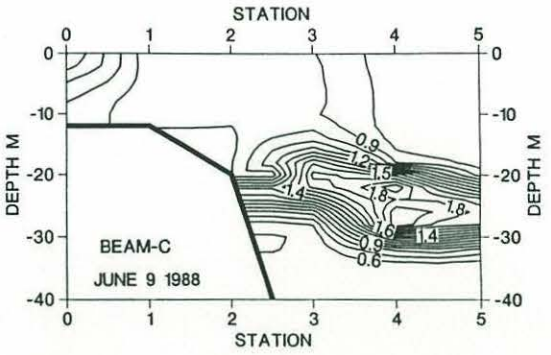
STATION
DEPTH M
BEAM-C
JUNE 9 1988
0.9
1.2
1.5
1.4
1.8
1.6
0.6

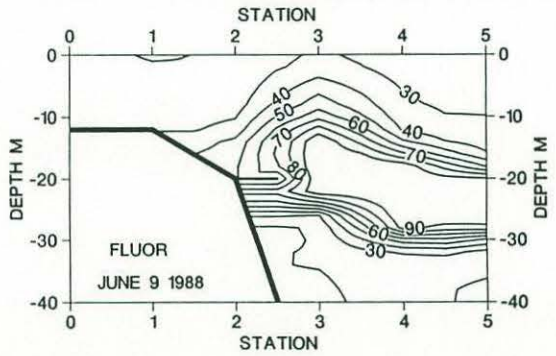
STATION
DEPTH M
FLUOR
JUNE 9 1988
40
50
70
60
80
30
90

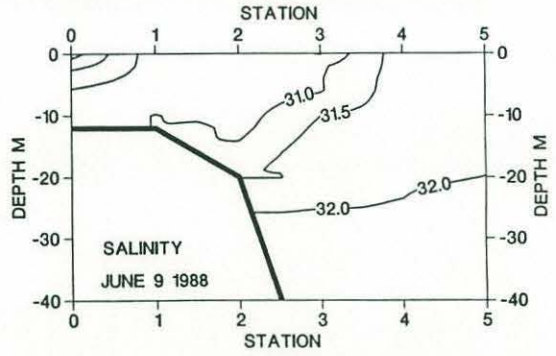
STATION
DEPTH M
SALINITY
JUNE 9 1988
31.0
31.5
32.0

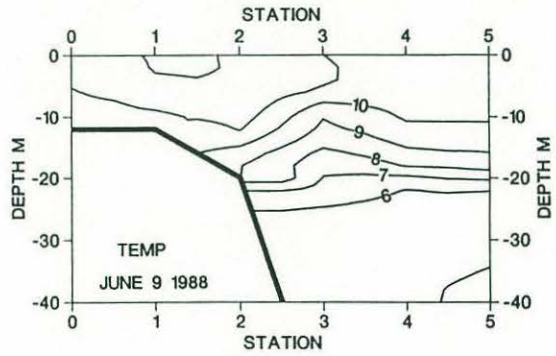
STATION
DEPTH M
TEMP
JUNE 9 1988
10
9
8
7
6

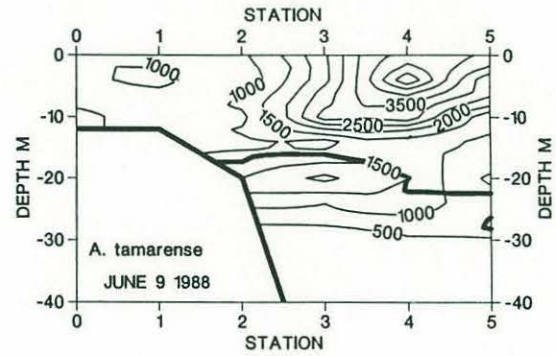
STATION
DEPTH M
A. tamarense
JUNE 9 1988
1000
1500
3500
2500
2000
500

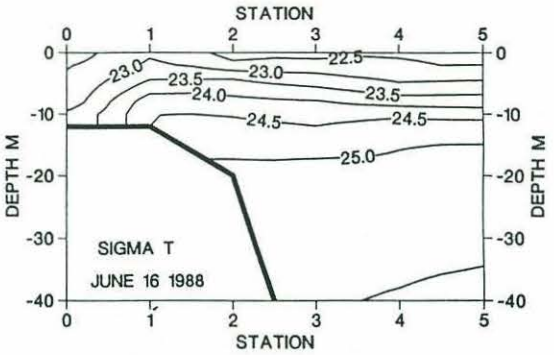
STATION
DEPTH M
SIGMA T
JUNE 16 1988

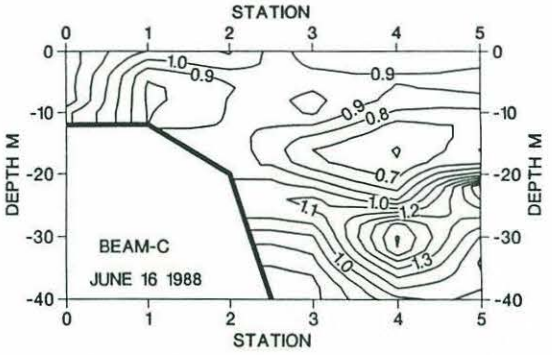
STATION
DEPTH M
BEAM-C
JUNE 16 1988

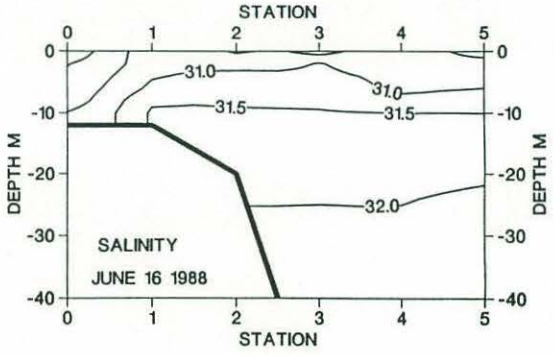
STATION
DEPTH M
SALINITY
JUNE 16 1988

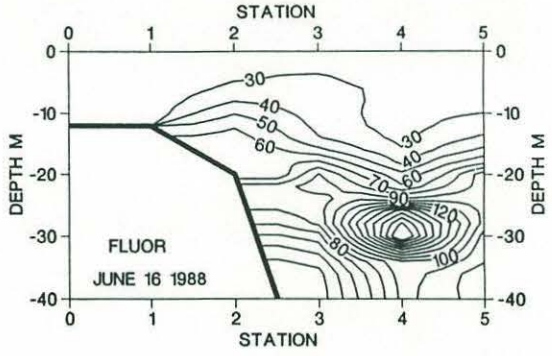
STATION
DEPTH M
FLUOR
JUNE 16 1988

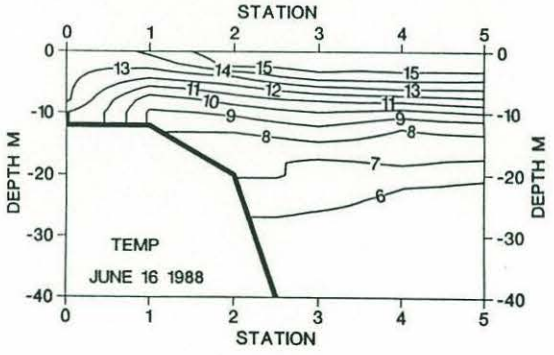
STATION
DEPTH M
TEMP
JUNE 16 1988

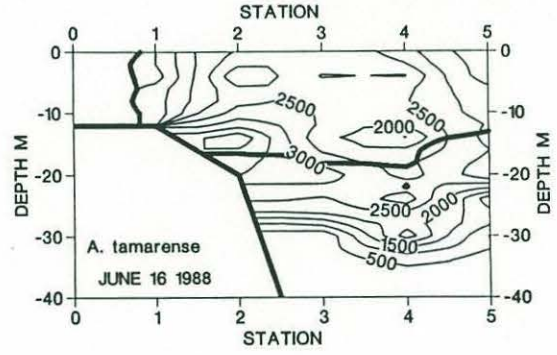
STATION
DEPTH M
A. tamarense
JUNE 16 1988

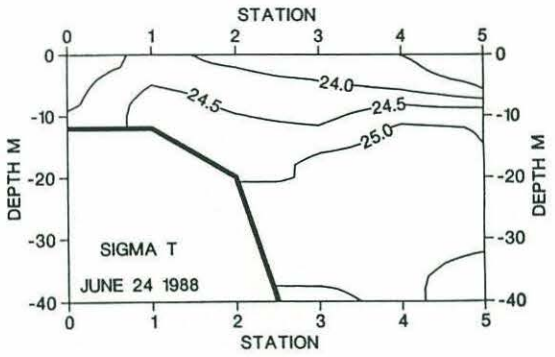
STATION
DEPTH M
24.0
24.5
24.5
25.0
SIGMA T
JUNE 24 1988
STATION

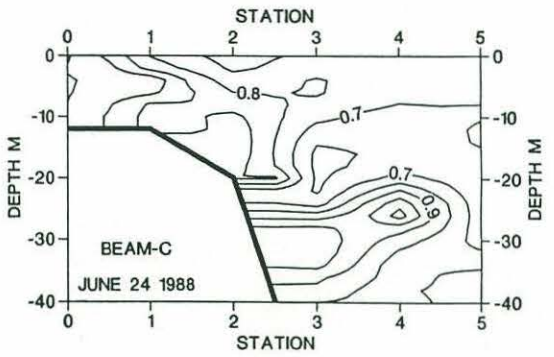
STATION
DEPTH M
0.8
0.7
0.7
0.6
BEAM-C
JUNE 24 1988
STATION

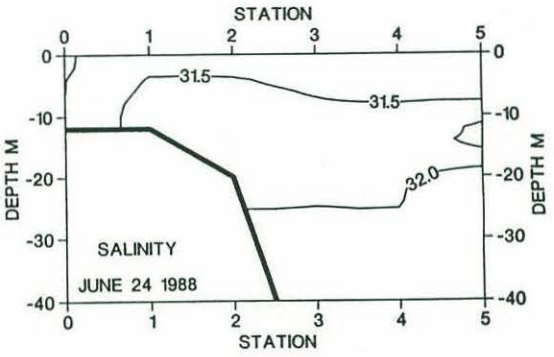
STATION
DEPTH M
31.5
31.5
32.0
SALINITY
JUNE 24 1988
STATION

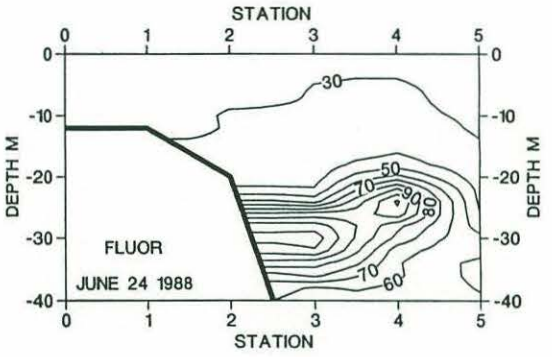
STATION
DEPTH M
30
50
70
90
80
70
60
FLUOR
JUNE 24 1988
STATION

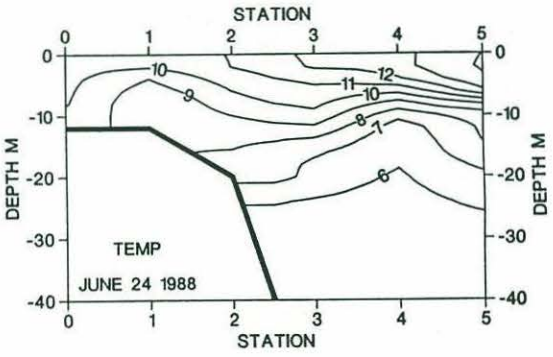
STATION
DEPTH M
10
9
11
12
10
8
7
6
TEMP
JUNE 24 1988
STATION

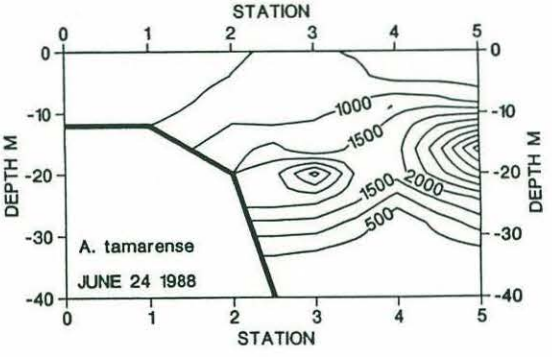
STATION
DEPTH M
1000
1500
1500
2000
500
A. tamarense
JUNE 24 1988
STATION

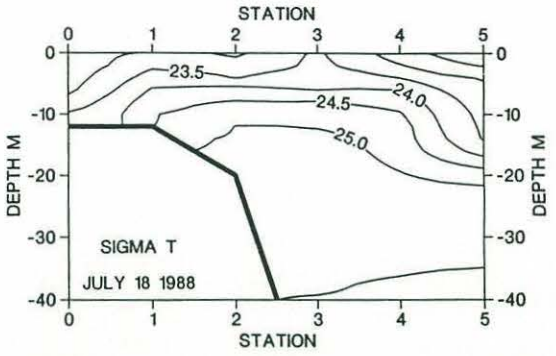
STATION
DEPTH M
23.5
24.0
24.5
25.0
SIGMA T
JULY 18 1988

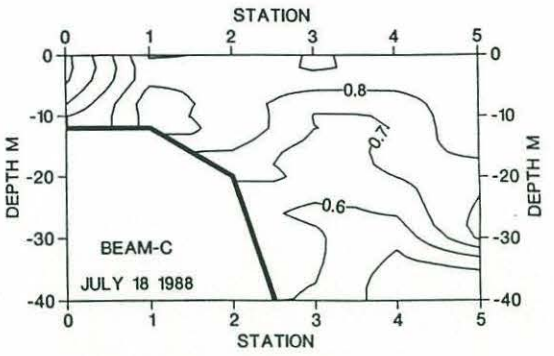
STATION
DEPTH M
0.8
0.7
0.6
BEAM-C
JULY 18 1988

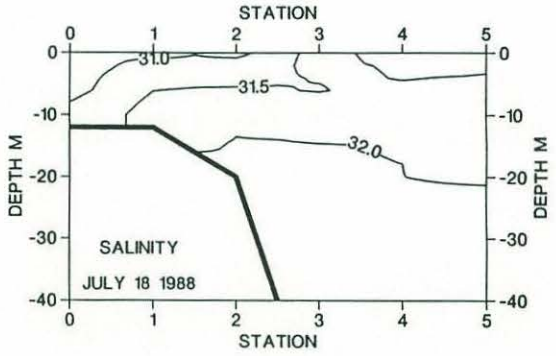
STATION
DEPTH M
31.0
31.5
32.0
SALINITY
JULY 18 1988

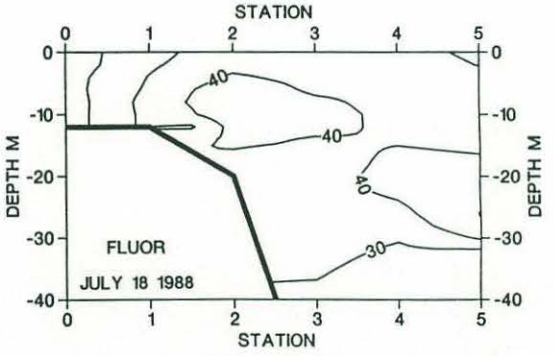
STATION
DEPTH M
40
40
40
30
FLUOR
JULY 18 1988

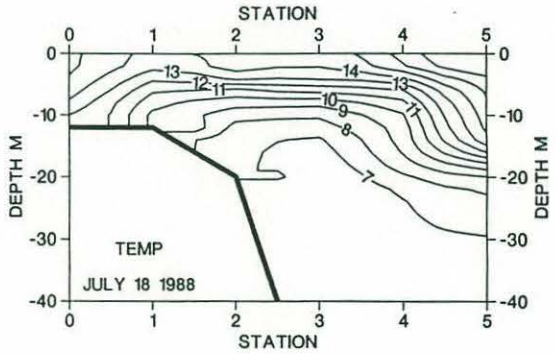
STATION
DEPTH M
13
12
11
14
13
11
10
9
8
7
TEMP
JULY 18 1988

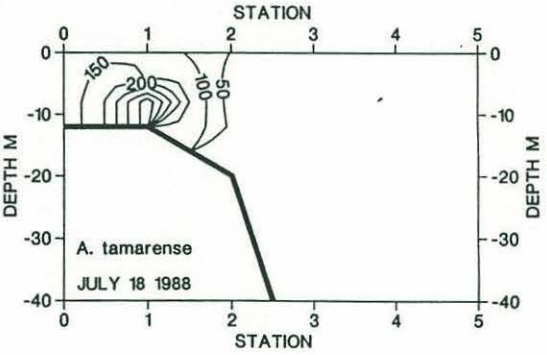
STATION
DEPTH M
150
200
100
50
A. tamarense
JULY 18 1988

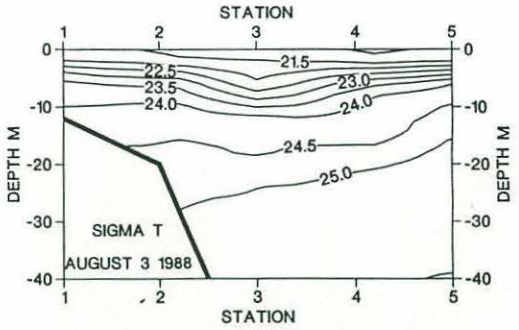
STATION
DEPTH M
SIGMA T
AUGUST 3 1988
STATION

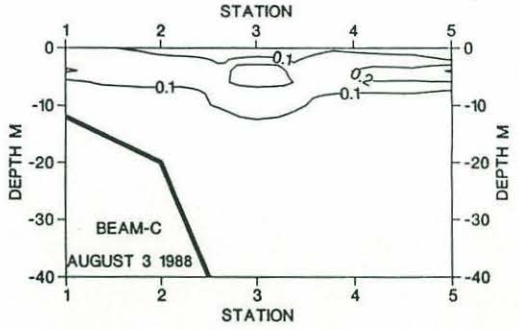
STATION
DEPTH M
BEAM-C
AUGUST 3 1988
STATION

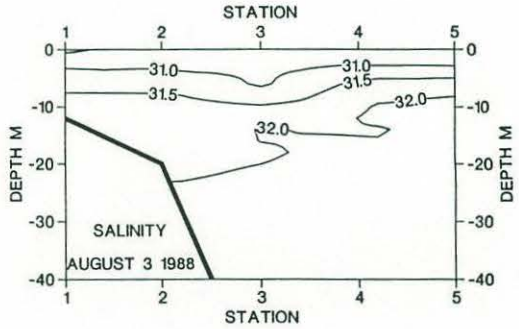
STATION
DEPTH M
SALINITY
AUGUST 3 1988
STATION

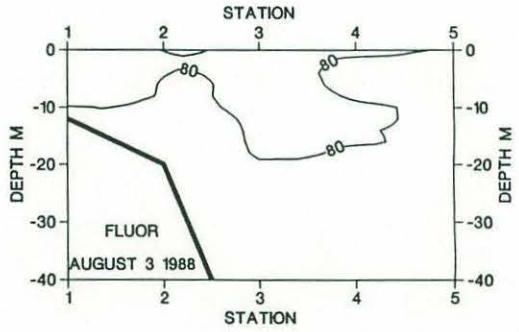
STATION
DEPTH M
FLUOR
AUGUST 3 1988
STATION

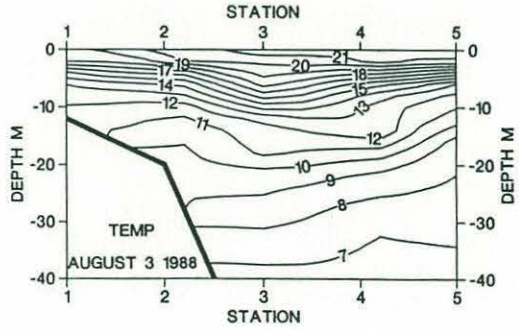
STATION
DEPTH M
TEMP
AUGUST 3 1988
STATION

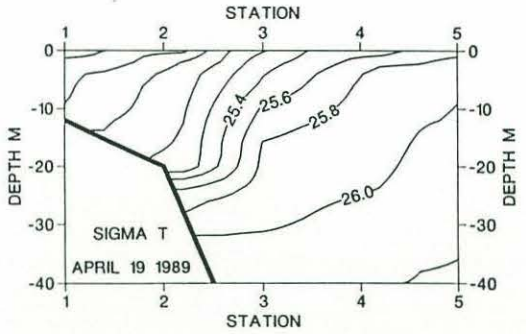
STATION
DEPTH M
SIGMA T
APRIL 19 1989
25.4
25.6
25.8
26.0

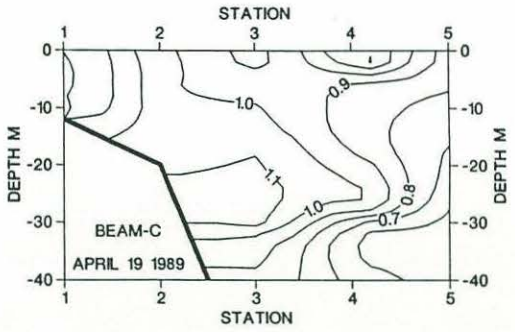
STATION
DEPTH M
BEAM-C
APRIL 19 1989
1.0
0.9
1.1
0.8
0.7

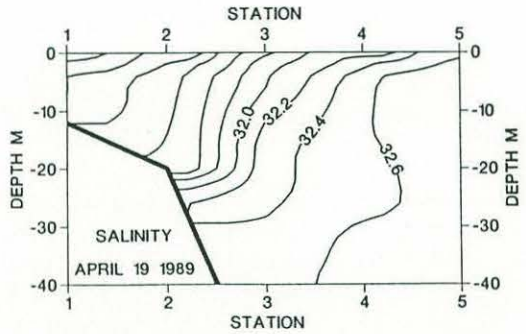
STATION
DEPTH M
SALINITY
APRIL 19 1989
32.0
32.2
32.4
32.6

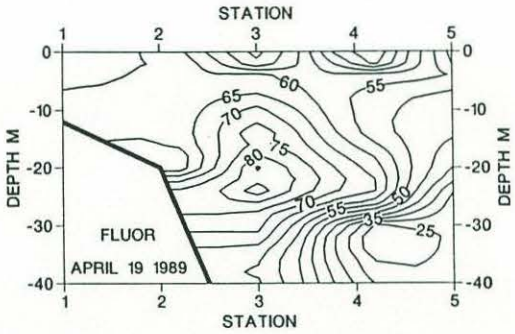
STATION
DEPTH M
FLUOR
APRIL 19 1989
65
60
55
70
75
80
50
35
25

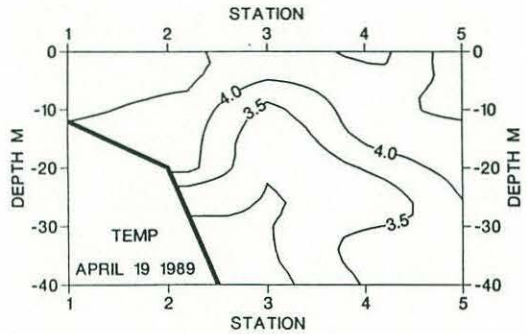
STATION
DEPTH M
TEMP
APRIL 19 1989
4.0
3.5
4.0
3.5

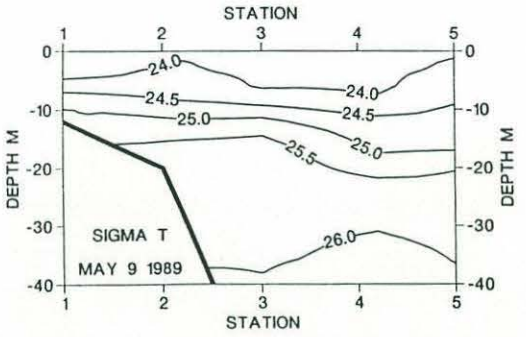
STATION
DEPTH M
SIGMA T
MAY 9 1989
24.0
24.5
25.0
25.5
26.0

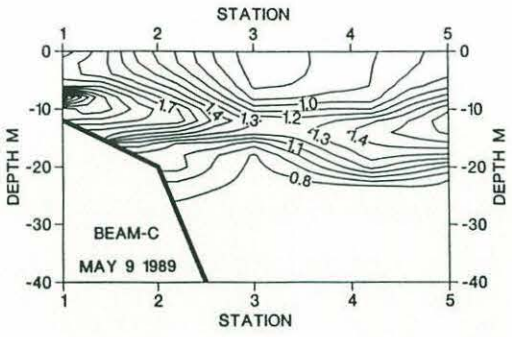
STATION
DEPTH M
BEAM-C
MAY 9 1989
1.7
1.5
1.3
1.2
1.0
1.1
1.3
1.4
0.8

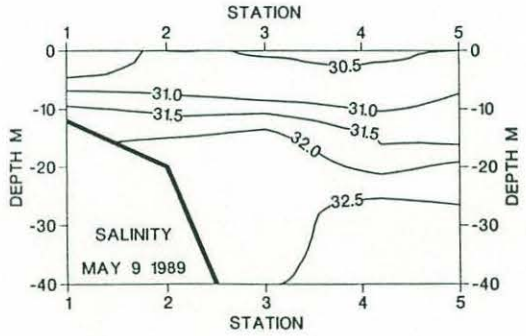
STATION
DEPTH M
SALINITY
MAY 9 1989
30.5
31.0
31.5
32.0
32.5

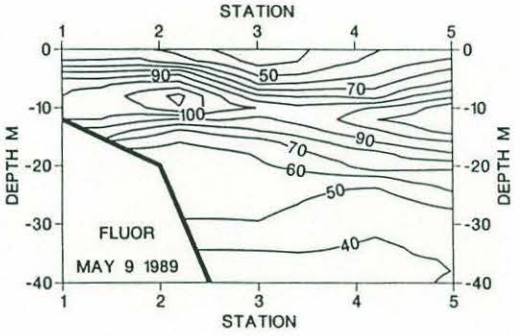
STATION
DEPTH M
FLUOR
MAY 9 1989
90
50
70
100
90
70
60
50
40

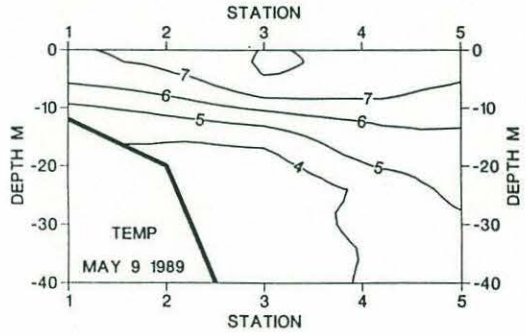
STATION
DEPTH M
TEMP
MAY 9 1989
7
6
5
4

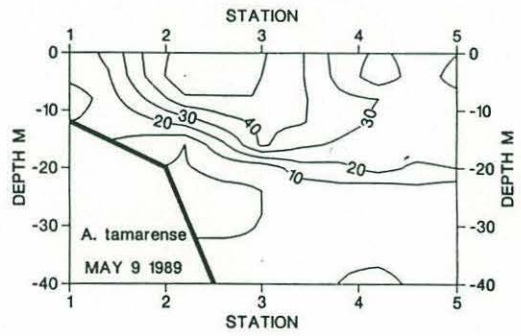
STATION
DEPTH M
A. tamarense
MAY 9 1989
20
30
40
30
20
10

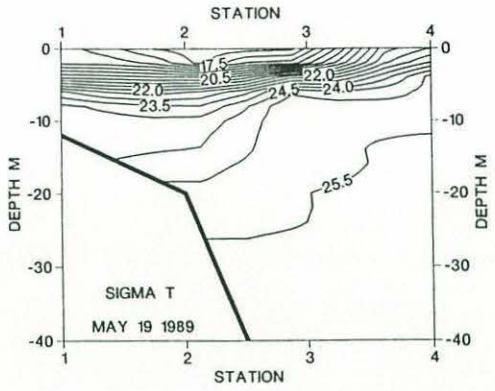

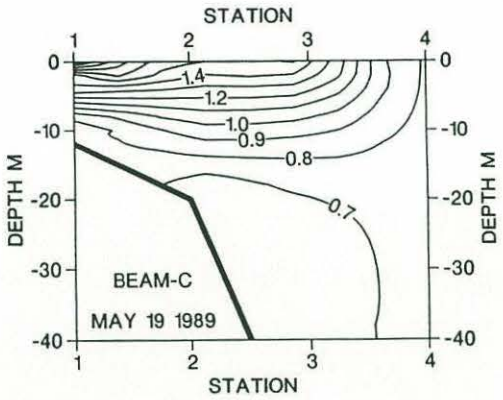

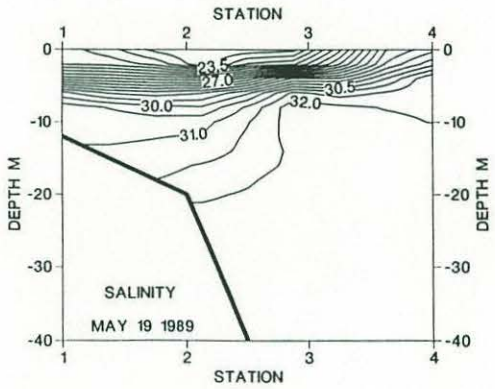

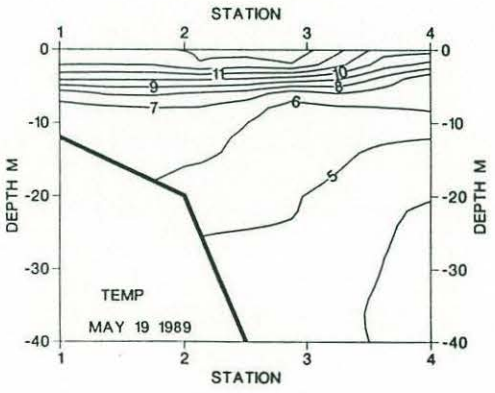

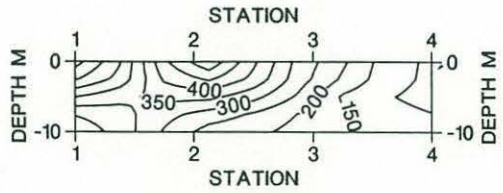

A. tamarense

MAY 19 1989

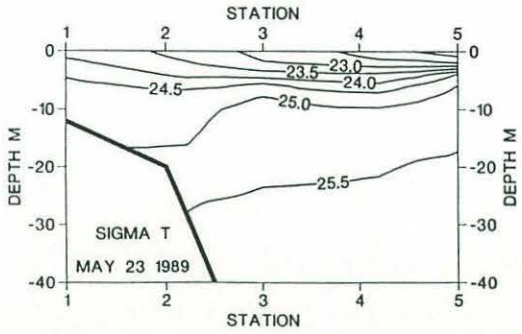
STATION
DEPTH M
SIGMA T
MAY 23 1989
23.0
23.5
24.0
24.5
25.0
25.5

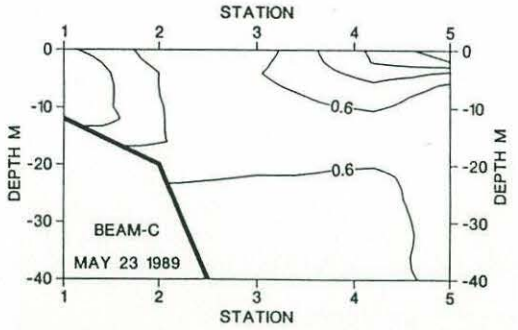
STATION
DEPTH M
BEAM-C
MAY 23 1989
0.6
0.6

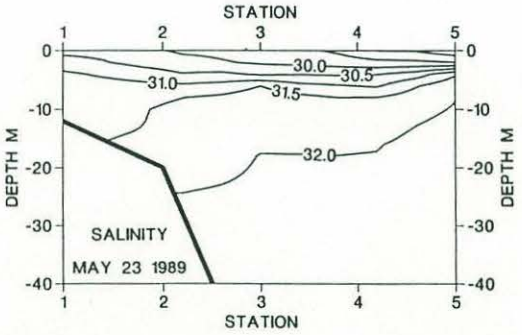
STATION
DEPTH M
SALINITY
MAY 23 1989
30.0
30.5
31.0
31.5
32.0

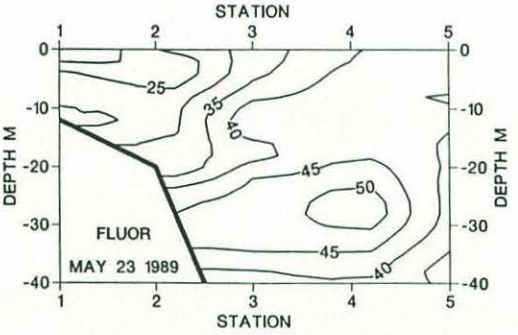
STATION
DEPTH M
FLUOR
MAY 23 1989
25
35
40
45
50
45
40

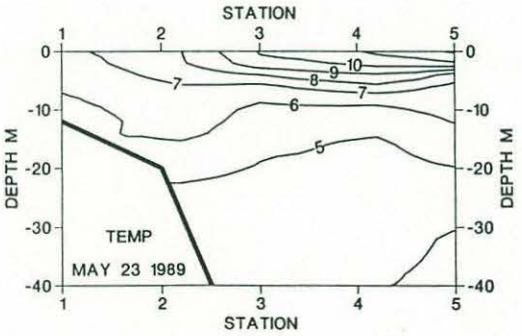
STATION
DEPTH M
TEMP
MAY 23 1989
7
8
9
10
7
6
5

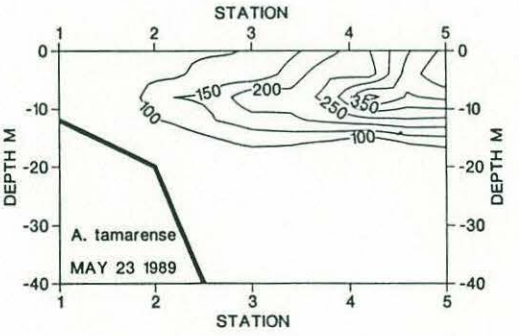
STATION
DEPTH M
A. tamarense
MAY 23 1989
100
150
200
250
350
100

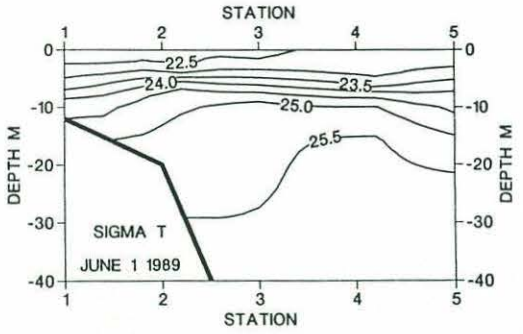
STATION
DEPTH M
22.5
24.0
23.5
25.0
25.5
SIGMA T
JUNE 1 1989

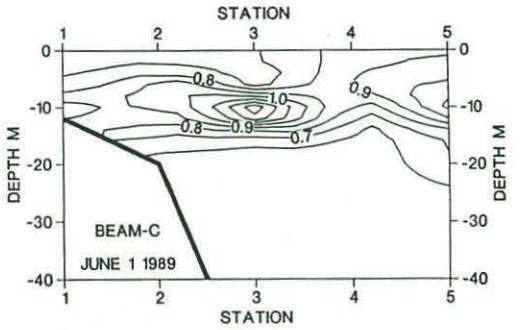
STATION
DEPTH M
0.8
1.0
0.9
0.8
0.9
0.7
BEAM-C
JUNE 1 1989

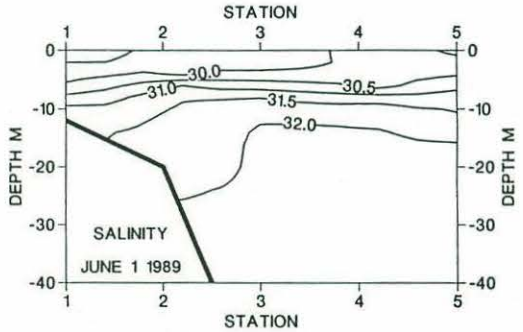
STATION
DEPTH M
30.0
31.0
30.5
31.5
32.0
SALINITY
JUNE 1 1989

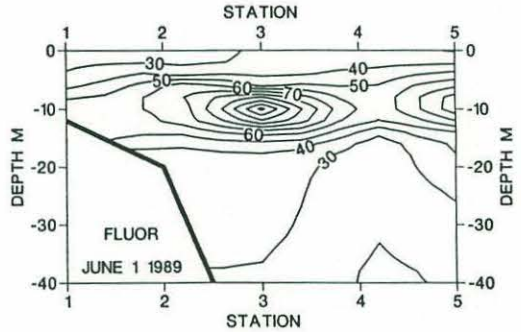
STATION
DEPTH M
30
50
40
60
70
50
60
40
30
FLUOR
JUNE 1 1989

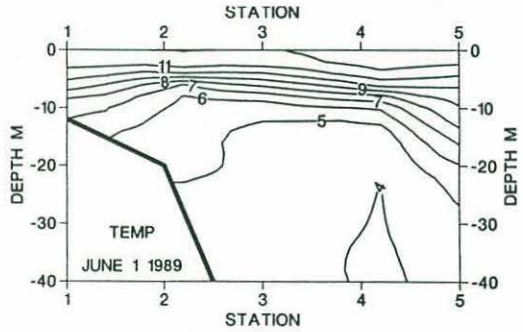
STATION
DEPTH M
11
8
7
6
9
7
5
TEMP
JUNE 1 1989

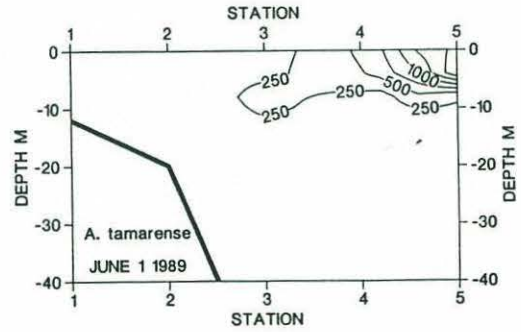
STATION
DEPTH M
250
250
250
500
1000
250
A. tamarense
JUNE 1 1989

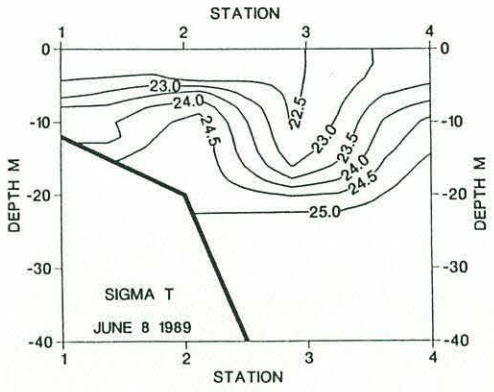

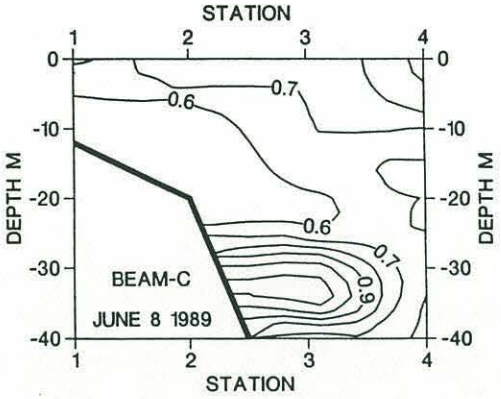

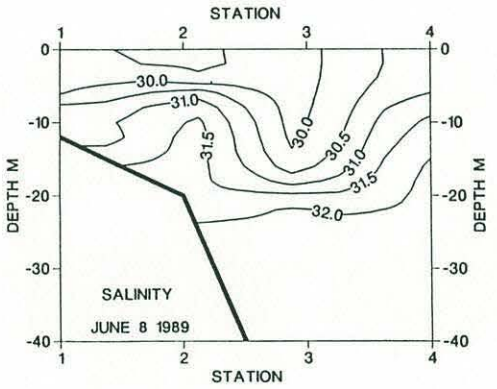

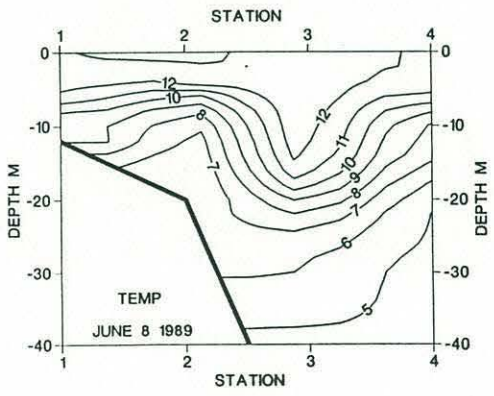

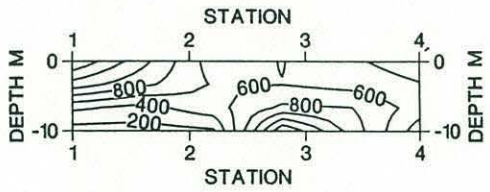

A. tamarense

JUNE 8 1989

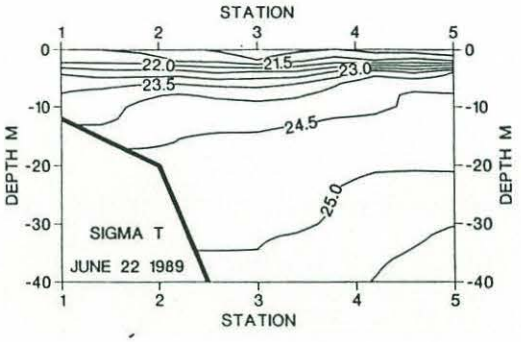
STATION
DEPTH M
22.0
21.5
23.0
23.5
24.5
25.0
SIGMA T
JUNE 22 1989

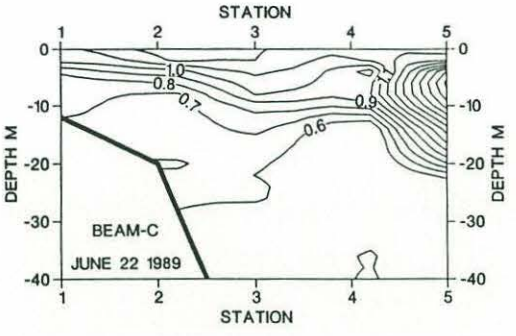
STATION
DEPTH M
1.0
0.8
0.7
0.9
0.6
BEAM-C
JUNE 22 1989

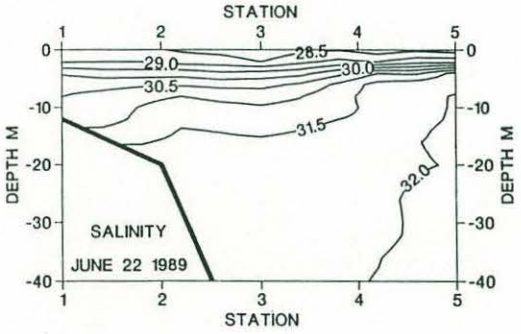
STATION
DEPTH M
28.5
29.0
30.0
30.5
31.5
32.0
SALINITY
JUNE 22 1989

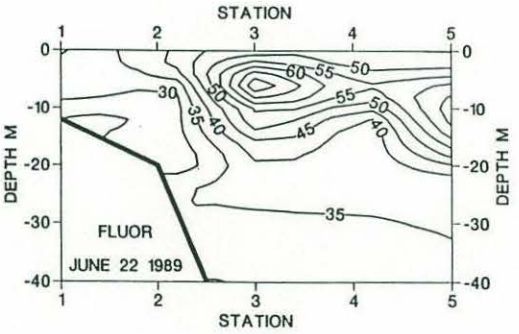
STATION
DEPTH M
60
55
50
30
35
40
45
35
FLUOR
JUNE 22 1989

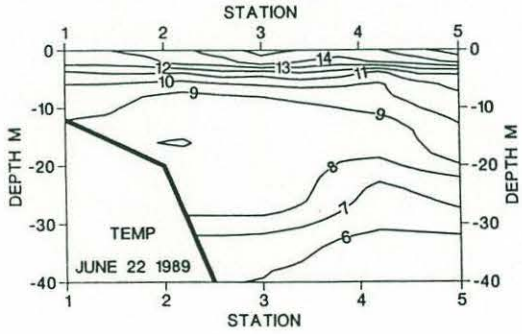
STATION
DEPTH M
12
13
14
11
10
9
8
7
6
TEMP
JUNE 22 1989

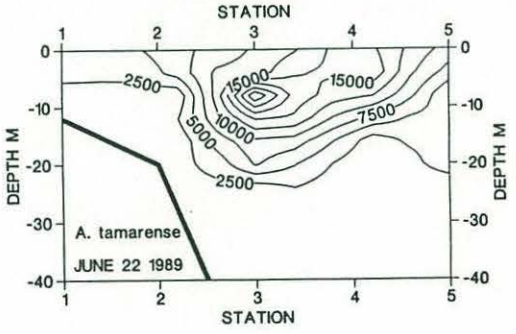
STATION
DEPTH M
2500
15000
10000
7500
5000
A. tamarense
JUNE 22 1989

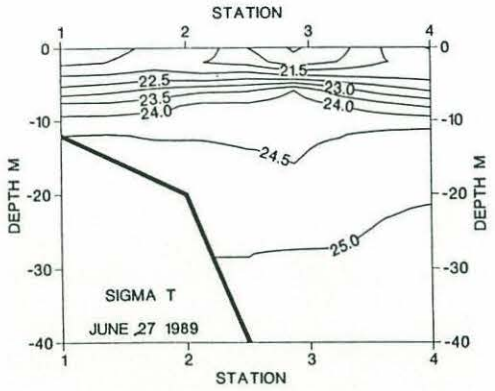
STATION
DEPTH M
22.5
23.5
24.0
21.5
23.0
24.0
24.5
25.0
SIGMA T
JUNE 27 1989
STATION

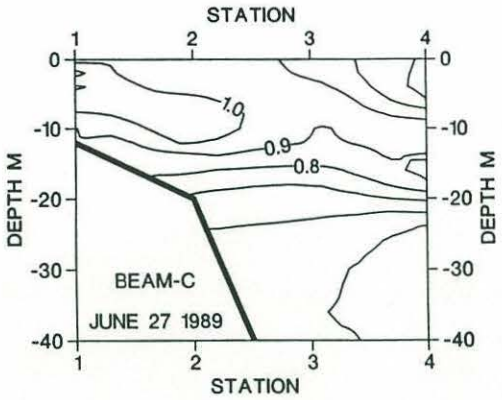
STATION
DEPTH M
1.0
0.9
0.8
BEAM-C
JUNE 27 1989
STATION

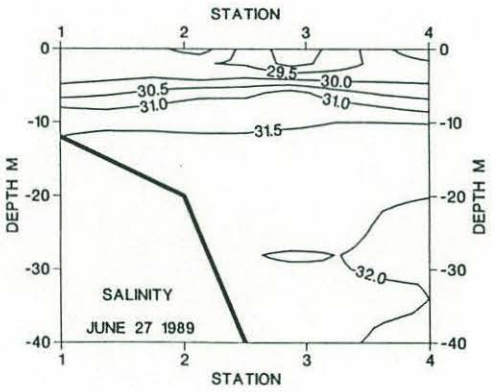
STATION
DEPTH M
30.5
31.0
29.5
30.0
31.0
31.5
32.0
SALINITY
JUNE 27 1989
STATION

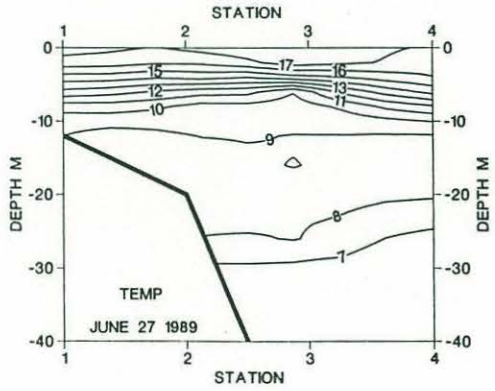
STATION
DEPTH M
15
12
10
17
16
13
11
9
8
7
TEMP
JUNE 27 1989
STATION

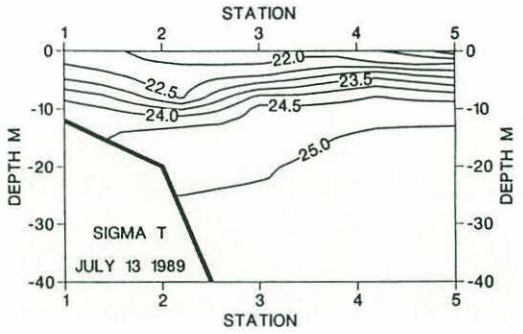
STATION
DEPTH M
SIGMA T
JULY 13 1989
22.0
22.5
23.5
24.0
24.5
25.0

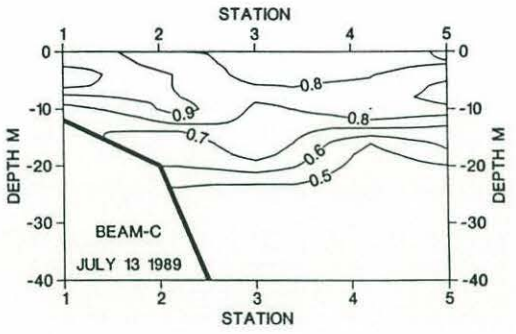
STATION
DEPTH M
BEAM-C
JULY 13 1989
0.8
0.9
0.7
0.6
0.5

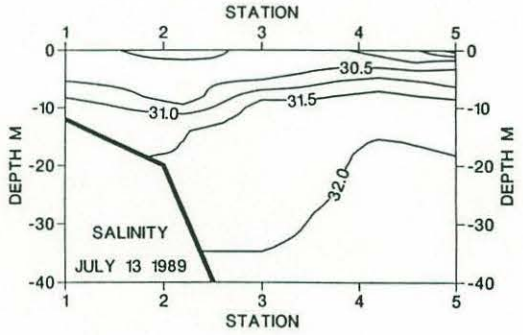
STATION
DEPTH M
SALINITY
JULY 13 1989
30.5
31.0
31.5
32.0

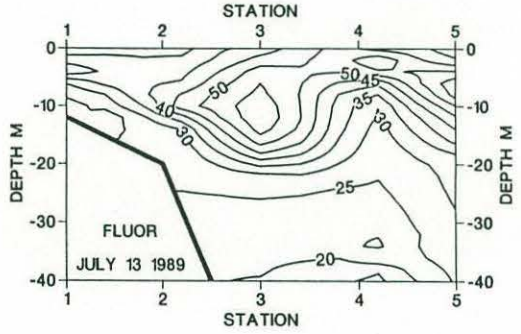
STATION
DEPTH M
FLUOR
JULY 13 1989
50
45
40
35
30
25
20

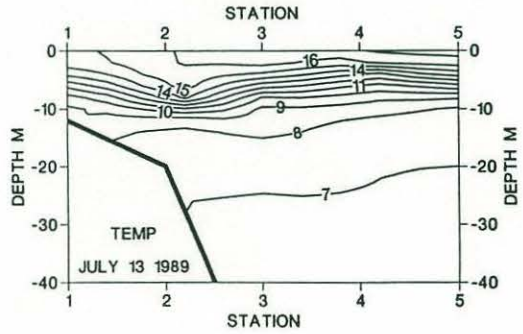
STATION
DEPTH M
TEMP
JULY 13 1989
16
14
15
11
10
9
8
7